

Influence of mutations at the type 1 copper site of a two-domain laccase: Biochemical and biophysical characterization

Inaugural-Dissertation

zur Erlangung des Doktorgrades
der Mathematisch-Naturwissenschaftlichen Fakultät
der Heinrich-Heine-Universität Düsseldorf

vorgelegt von

Anna Caroline Olbrich
aus Münster

Düsseldorf, Mai 2021

aus dem Institut für Biochemie
der Heinrich-Heine-Universität Düsseldorf

Gedruckt mit der Genehmigung der
Mathematisch-Naturwissenschaftlichen Fakultät der
Heinrich-Heine-Universität Düsseldorf

Berichterstatter:

1. Prof. Dr. Vlada B. Urlacher

2. Jun.-Prof. Dr. Ingrid Span

Tag der mündlichen Prüfung: 20. September 2021

Eidesstattliche Versicherung

Ich versichere an Eides Statt, dass die Dissertation von mir selbständig und ohne unzulässige fremde Hilfe unter Beachtung der „Grundsätze zur Sicherung guter wissenschaftlicher Praxis an der Heinrich-Heine-Universität Düsseldorf“ erstellt worden ist.

Die Dissertation wurde in der vorgelegten oder in ähnlicher Form noch bei keiner anderen Institution eingereicht. Ich habe bisher keine erfolglosen Promotionsversuche unternommen.

Düsseldorf, den _____

Anna Olbrich

Content

1	Abstract	IV
2	Zusammenfassung	VI
3	Introduction	8
3.1	Copper proteins	8
3.1.1	Cupredoxins and multicopper oxidases	9
3.1.2	Evolution of multicopper oxidases	12
3.1.3	Copper sites and their spectroscopic features	14
3.1.4	Electron transfer	16
3.1.5	Determinants of the T1 Cu reduction potential	18
3.2	Laccases.....	20
3.2.1	Reaction mechanism.....	21
3.2.2	Applications of laccases	24
3.2.3	The two-domain laccase Ssl1 from <i>Streptomyces sviveus</i>	25
3.3	Aim of the work	26
4	Manuscript 1: Correlation between the T1 copper reduction potential and catalytic activity of a small laccase.....	27
5	Manuscript 2: Influence of the T1 Cu axial ligand on kinetic, spectral, and structural properties of the laccase Ssl1 from <i>Streptomyces sviveus</i>	52
6	Ruthenation of Ssl1: First steps towards measurements of the T1 to TNC electron transfer kinetics	96
7	Conclusions	112
9	Abbreviations	113
10	References	115
11	Appendix	127
12	Danksagungen	130

1 Abstract

Laccases (EC 1.10.3.2) belong to the multicopper oxidase family and represent promising biocatalysts for various applications due to their ability to oxidize phenols, aryl amines, anilines, benzenethiols, and inorganic metal ions. They couple four one-electron oxidations of a substrate to the four-electron reduction of dioxygen to water which is the only by-product of the laccase catalyzed reaction. The active site of laccases contains four copper ions. The primary electron acceptor in laccases is a type 1 (T1) Cu and electrons are transferred through the protein over a distance of 13 Å to the trinuclear copper cluster (TNC), where dioxygen reduction occurs. In contrast to fungal laccases, bacterial laccases are often active at alkaline pH, and stable at elevated temperatures and in the presence of organic solvents but possess lower activities. The reduction potential E° of the T1 Cu is assumed to correlate with enzyme activity and therefore is a target of protein engineering efforts that increase E° and thereby the activity and substrate spectrum in bacterial laccases. As bacterial two-domain laccases have been discovered more recently they remain less investigated compared to well-studied three-domain laccases.

To identify molecular factors influencing the T1 Cu E° in the two-domain laccase Ssl1 from *Streptomyces sviveus*, a set of enzyme variants with mutated T1 Cu axial ligand was constructed and characterized. The hydrophobicity of the T1 Cu axial ligand was found to provide the major contribution to the reduction potential changes in the mutants. The highest E° was measured with the M295I mutant (467 mV compared to 375 mV in the wild-type), the lowest for M295A and M295T (<290 mV). Through additional mutations in the second coordination sphere of the T1 Cu E° increased up to 560 mV. A good correlation between E° and laccase activity was observed for substituted phenols. Additionally, Ssl1 variants with $E^\circ \geq 500$ mV were able to oxidize 4-methylphenol, 2-*tert*-butylphenol and 4-*tert*-butylphenol, which were not converted by the wildtype enzyme (375 mV), thus extending the substrate spectrum. However, there was no obvious correlation between E° and kinetic parameters for the oxidation of the low redox-potential syringaldazine. For the oxidation of two large dyes, alizarin red S and indigo carmine, a correlation was only observed for Ssl1 variants with $E^\circ > 470$ mV. These observations and further measurements of the T1 Cu reduction kinetics indicated that replacing the axial ligand methionine impacts all three factors that determine electron transfer rates: reduction potential, reorganization energy, and electronic coupling between the substrate and the T1 Cu.

Due to the large influence of the axial ligand, the structural and spectroscopic properties of the T1 Cu site of Ssl1 variants with various axial ligands were investigated. The Ssl1 variants M295A/V/I/Y/F/T displayed perturbed spectral features like those observed in four-coordinate T1 Cu sites with an axial oxygen ligand, e.g., a water molecule. The presence of a water ligand was confirmed in the crystal structures of the Ssl1 variants M295A/V/I/Y/F. The accompanying tetrahedral distortion of the coordination geometry suggests that the reorganization energy for the $\text{Cu}^{\text{II}}/\text{Cu}^{\text{I}}$ reduction increased.

To study the intramolecular electron transfer in Ssl1 a ruthenated variant with a [Ru(bipyridine)₂(imidazole)] complex bound close to the T1 Cu site was synthesized. Site-specific ruthenation required a single surface-exposed histidine accessible for the reaction and a Ssl1 H85Q/H132Q/ Δ C mutant was created for this purpose. Formation of the Ssl1-ruthenium complex was verified by fluorescence spectroscopy. Measurements of the intramolecular electron transfer were complicated by short fluorescence lifetimes that were observed for the ruthenated Ssl1 sample and other approaches for intramolecular electron transfer measurements were proposed.

2 Zusammenfassung

Laccasen (EC 1.10.3.2) gehören zur Familie der Multikupferoxidasen und sind vielversprechende Biokatalysatoren für verschiedene Anwendungen aufgrund ihrer Fähigkeit, Phenole, Arylamine, Aniline, Thiophenole und anorganische Metallionen zu oxidieren. Sie koppeln vier Ein-Elektronen-Oxidationen eines Substrats an die Vier-Elektronen-Reduktion von Sauerstoff zu Wasser, welches das einzige Nebenprodukt der Laccase-Reaktion ist. Das aktive Zentrum von Laccasen enthält vier Kupferionen. Der primäre Elektronenakzeptor in Laccasen ist ein Typ 1 (T1) Cu und die Elektronen werden über eine Entfernung von $\sim 13 \text{ \AA}$ durch das Protein zum dreikernigen Kupfercluster (TNC) übertragen, wo die Reduktion von Sauerstoff stattfindet. Im Gegensatz zu pilzlichen Laccasen sind bakterielle Laccasen oft bei alkalischem pH aktiv sowie stabil bei erhöhten Temperaturen und in Gegenwart von organischen Lösungsmitteln, besitzen aber geringere Aktivitäten. Es wird angenommen, dass das Reduktionspotential E° des T1 Cu mit der Enzymaktivität korreliert. Es ist daher ein Ziel von Proteinengineering, E° und damit die Aktivität und das Substratspektrum von bakteriellen Laccase zu erhöhen. Da bakterielle Zwei-Domänen-Laccasen erst in jüngerer Zeit entdeckt wurden, sind sie im Vergleich zu Drei-Domänen-Laccasen noch viel weniger untersucht.

Um molekulare Faktoren zu identifizieren, die das T1 Cu E° in Zwei-Domänen-Laccasen beeinflussen, wurden Mutanten der kleinen Zwei-Domänen-Laccase Ssl1 aus *Streptomyces sviveus* konstruiert und charakterisiert. Es wurde festgestellt, dass die Hydrophobizität des axialen T1-Cu-Liganden, M295 in Wildtyp-Ssl1, den Hauptbeitrag zu den Veränderungen des Reduktionspotentials in den axialen Ligandenmutanten darstellt. Das höchste E° wurde für die M295I-Mutante gemessen (467 mV im Vergleich zu 375 mV im WT), das niedrigste für M295A und M295T ($< 290 \text{ mV}$). Durch zusätzliche Mutationen in der zweiten Koordinationssphäre des T1 Cu stieg E° auf bis zu 560 mV. Eine gute Korrelation zwischen E° und Laccaseaktivität wurde für substituierte Phenole beobachtet. Zusätzlich waren Ssl1-Varianten mit $E^\circ \geq 500 \text{ mV}$ in der Lage, 4-Methylphenol, 2-tert-Butylphenol und 4-tert-Butylphenol zu oxidieren, die vom Wildtyp-Enzym (375 mV) nicht umgesetzt wurden, wodurch das Substratspektrum erweitert wurde. Für die Oxidation von Syringaldazin gab es keine offensichtliche Korrelation zwischen E° und den kinetischen Parametern. Für die Oxidation von zwei Farbstoffen, Alizarinrot S und Indigokarmin, wurde eine Korrelation nur für Ssl1-Varianten mit $E^\circ > 470 \text{ mV}$ beobachtet. Diese Beobachtungen und weitere Messungen der Kinetik der T1 Cu-Reduktion deuteten darauf hin, dass der Austausch des axialen Liganden Methionin alle drei Faktoren beeinflusst, die die Elektronentransferraten bestimmen: Reduktionspotential, Reorganisationsenergie und elektronische Kopplung zwischen dem Substrat und dem T1 Cu.

Aufgrund des großen Einflusses des axialen Liganden wurden die strukturellen und spektroskopischen Eigenschaften des T1-Kupferzentrums in Ssl1-Varianten mit verschiedenen axialen Liganden untersucht. Die Ssl1-Varianten M295A/V/I/Y/F/T zeigten veränderte spektrale Eigenschaften, wie sie in vierfach koordinierten T1 Cu-Zentren mit einem axialen Sauerstoffliganden, z. B. einem

Wassermolekül, beobachtet werden. Die Anwesenheit eines Wasserliganden wurde in den Kristallstrukturen der Ssl1-Varianten M295A/V/I/Y/F bestätigt. Die damit einhergehende tetraedrische Verzerrung der Koordinationsgeometrie deutet darauf hin, dass die Reorganisationsenergie für die $\text{Cu}^{\text{II}}/\text{Cu}^{\text{I}}$ -Reduktion erhöht wurde.

Zur Untersuchung des intramolekularen Elektronentransfers in Ssl1 wurde eine rutheniierte Variante mit einem $[\text{Ru}(\text{Bipyridin})_2(\text{Imidazol})]$ -Komplex hergestellt, der nahe des T1-Cu-Zentrums gebunden ist. Die ortsspezifische Ruthenierung erforderte ein einzelnes exponiertes Histidin an der Proteinoberfläche, das für die Reaktion zugänglich ist. Zu diesem Zweck wurde eine Ssl1 H85Q/H132Q/ Δ C-Mutante erzeugt. Die Bildung des Ssl1-Ruthenium-Komplexes wurde durch Fluoreszenzspektroskopie nachgewiesen. Messungen des intramolekularen Elektronentransfers wurden durch kurze Fluoreszenzlebensdauern erschwert, die für die rutheniierte Ssl1-Probe beobachtet wurden, und es wurden andere Ansätze für Elektronentransfermessungen vorgeschlagen.

3 Introduction

3.1 Copper proteins

Metal ions play a crucial role in biology. Almost half of all known proteins are metalloproteins containing at least one metal ion like magnesium, zinc, iron, manganese, calcium, cobalt, molybdenum, tungsten, or copper¹. Metalloproteins are responsible for important biological processes, e.g. photosynthesis, water oxidation, reduction of molecular oxygen, nitrogen fixation, and respiration². Metalloproteins exploit the physicochemical properties of metal ions for their function supported by diverse contributions from the protein. Contributions of the protein to metalloprotein function include mediation of allosteric interactions between the active sites of different subunits, the organization of metal sites for directional electron transfer (ET), providing superexchange pathways for ET, the formation of surface recognition sites, substrate binding pockets and substrate access channels leading to the active site, creation of a hydrophobic environment, activation of substrates, charge and H-bonding residues to assist catalysis, and imposing a defined geometry on the metal site to activate it for reactivity³⁻⁴.

While some metal ions facilitate catalysis by activation of reacting species and/or stabilization of intermediates based on their Lewis acidity, others are used for redox catalysis. Copper sites in proteins are exclusively used to mediate redox catalysis with copper occurring in the oxidation states Cu^I and Cu^{II}^[1]. There are several types of copper sites (Figure 1) which are involved in a variety of functions such as electron transfer (ET) processes, binding, activation, and reduction of molecular oxygen, nitrite and nitrous oxide reduction, and substrate activation⁵.

Copper sites have been classified into several types. The type 1 (T1) Cu is a mononuclear site with a Cu that is always coordinated by three strong ligands in an approximate trigonal plane: two histidine imidazole nitrogens (N(His)) and one cysteine thiolate (S(Cys)) (Figure 1a). Additionally, a methionine or glutamine can occupy the axial position of the Cu ion as a fourth ligand. The T1 Cu is involved in electron transfer processes. The type 2 (T2) Cu has a square planar coordination, e.g., by three N(His) ligands in copper nitrite reductase (CuNiR) (Figure 1b). At the T2 Cu of CuNiR nitrite is reduced to nitric oxide. A T2 Cu also forms a trinuclear cluster (TNC) with a pair of type 3 (T3) Cu ions in multicopper oxidases. The T3 Cu ions are each coordinated by three histidine residues (Figure 1c) with a bridging oxygen moiety. The TNC is responsible for the reduction of molecular oxygen to water. These copper types are present in multicopper oxidases and will be discussed in detail in the following chapters.

Further types of copper sites are the Cu_A, Cu_B, and Cu_Z centers. Cu_A sites are found in cytochrome *c* oxidase and nitrous oxide reductase (N₂OR) where they are responsible for electron transfer. The Cu_A site is a binuclear center with Cu coordination by two histidine and one methionine residues, a protein backbone carbonyl oxygen, and two bridging cysteine residues (Figure 1d). In cytochrome *c* oxidase the

Cu_A accepts electrons from cytochrome *c* and passes them to the heme *a* prosthetic group. The electrons are then further transferred to the Cu_B /heme *a*₃ binuclear center where O_2 is reduced to H_2O . The Cu_B atom is coordinated by three histidine residues in trigonal pyramidal geometry. In N_2OR electrons are transferred from the binuclear Cu_A center to a tetranuclear Cu_Z catalytic center where N_2O is reduced to N_2 . The four copper ions are coordinated by seven histidine residues and bridged by a sulfur atom (Figure 1f)⁶.

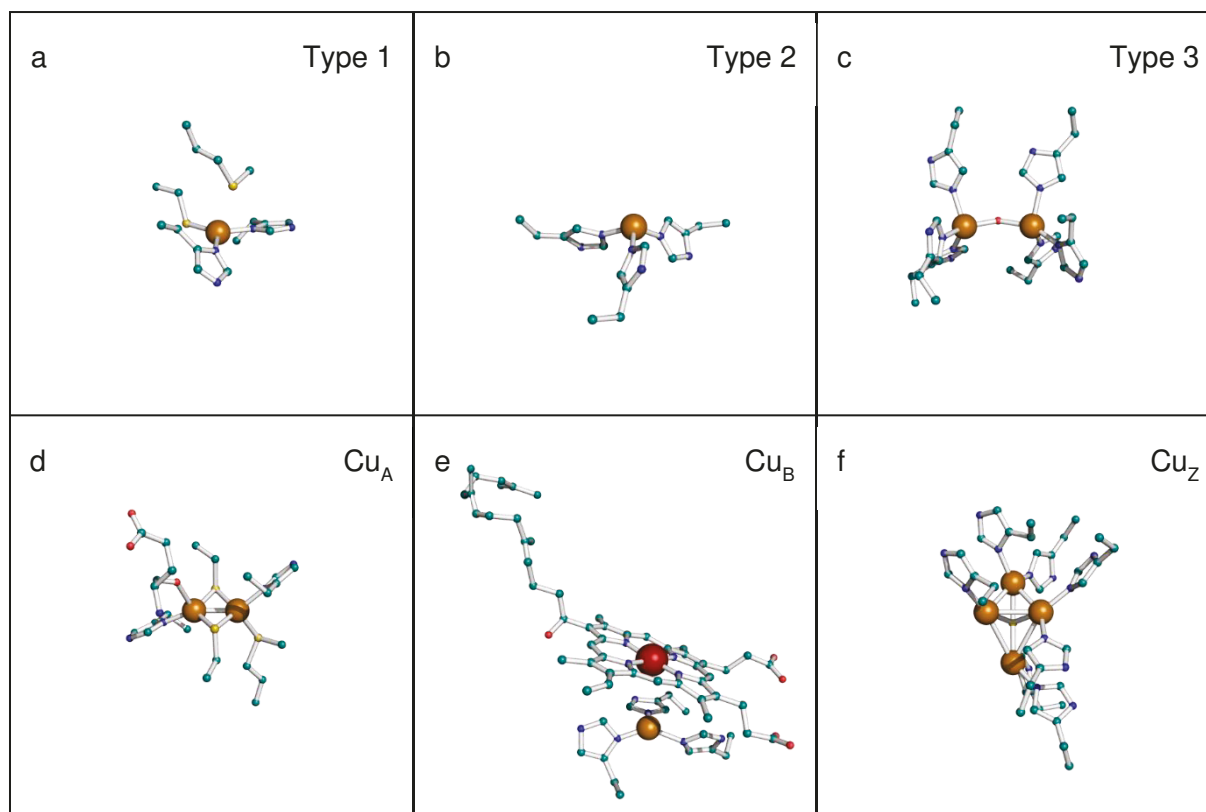


Figure 1: Copper sites in proteins. (a) T1 Cu site of *Pseudomonas aeruginosa* azurin (PDB code 4AZU); (b) T2 Cu site of nitrite reductase from *Alcaligenes faecalis* (PDB code 5F7B); (c) T3 Cu pair of ascorbate oxidase from zucchini (*Cucurbita pepo* var. *melopepo*) (PDB 1AOZ); (d) binuclear Cu_A site of cytochrome *c* oxidase from *Bradyrhizobium japonicum* (PDB code 4W9Z); (e) Cu_B and heme *a*₃ site of bovine heart cytochrome *c* oxidase (PDB code 1OCC); (f) Cu_Z site of nitrous oxide reductase from *Paracoccus denitrificans* (PDB code 1FWX). Copper ions are highlighted as orange spheres. The heme iron is shown as dark red sphere. Metal ligands are colored by element. Oxygen: red; Nitrogen: blue; Carbon: teal; Sulfur: yellow.

3.1.1 Cupredoxins and multicopper oxidases

Cupredoxins are relatively small one-domain copper proteins (e.g., azurin, plastocyanin, pseudoazurin, rusticyanin, stellacyanin, and amicyanin) that generally function as electron mediators and contain a T1 Cu. The cupredoxin-fold domains contain two β -sheets with seven β -strands arranged in a Greek-key β -barrel. This motif differs slightly from other Greek-key β -barrels. While the classic Greek-key motif contains only antiparallel strands (Figure 2a), the first and third strand in the cupredoxin-fold form parallel connections to their β -sheets and strands two and three are part of different sheets (Figure 2c)⁷. The T1 Cu site of cupredoxins is located at the connecting bend between strands seven and eight while one of the coordinating histidines is located 50-70 residues closer to the N-terminus⁸. The T1 Cu

coordinating cysteine residue is located at the C-terminal end of strand seven. The axial ligand, a methionine in azurin, is the first residue of strand eight (Figure 2b and c).

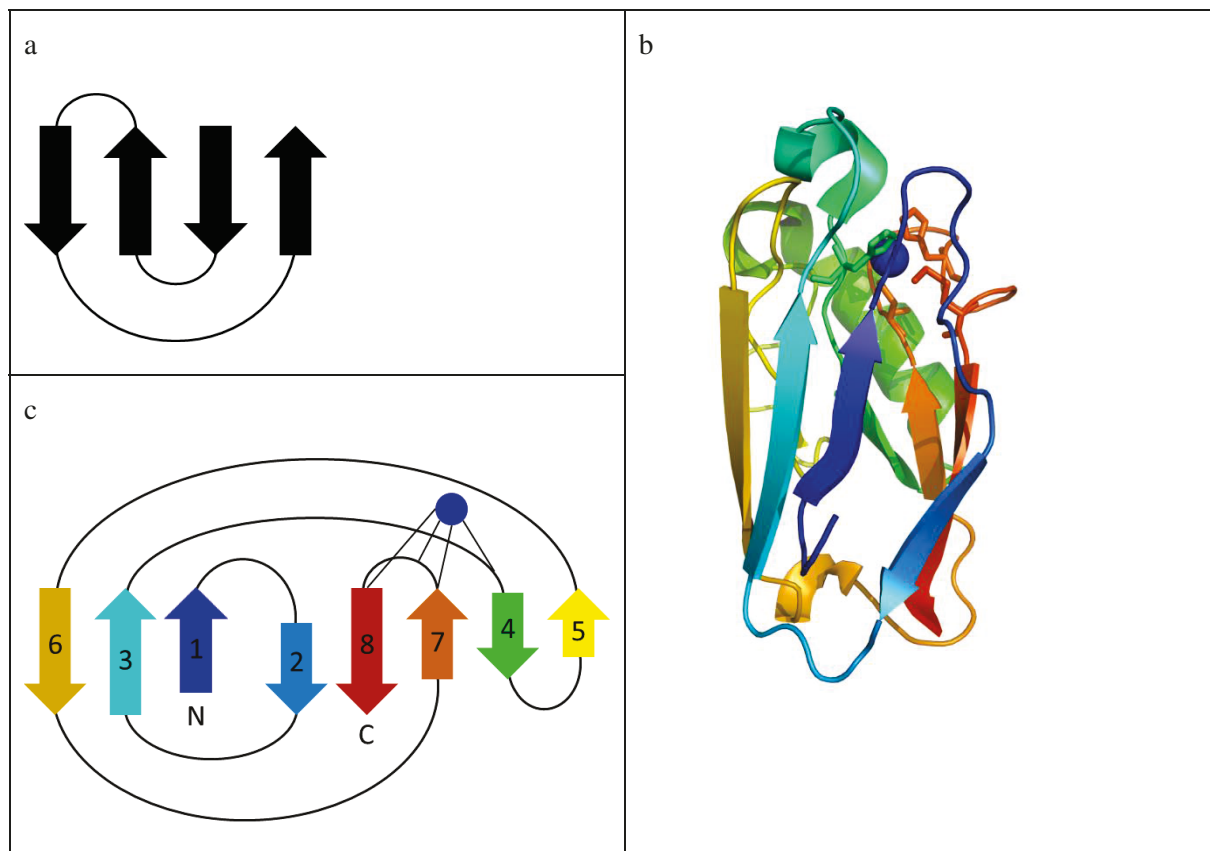


Figure 2: (a) Greek key motif consisting of four antiparallel strands. (b) Structure of the single cupredoxin domain protein azurin (PDB code 4AZU), and (c) a schematic representation of its topology. The T1 Cu is depicted as a blue sphere.

Multicopper oxidases (MCOs) contain two, three, or six of these cupredoxin-fold domains and additional copper sites. They are ubiquitous in nature and are present in all three kingdoms of life. They have a variety of functions, including lignin degradation in white rot fungi, denitrification in archaea, cuticle tanning in insects, metal homeostasis in bacteria, yeast, and mammals (see Table 1).

Table 1: Origin, structural features and functions of MCOs and closely related proteins.⁹

MCO	Origin	Structure	Function
Nitrite reductase	<i>Alcaligenes faecalis</i> S-6	2 domains, trimer, one T1 and one T2 per monomer	Dissimilatory reduction of nitrite
Laccase SLAC	<i>Streptomyces coelicolor</i>	2 domains, trimer, TNC at interface between chains	Putatively involved in lignin degradation ¹⁰
Phenol oxidase EpoA	<i>Streptomyces griseus</i>	2 domains, trimer, TNC at interface between chains	Stimulation of morphogenesis ¹¹
Bilirubin oxidase	<i>Myrothecium verrucaria</i> MT-1	3 domains	Laccase with high activity for oxidation of bilirubin ¹²
Laccase CotA	<i>Bacillus subtilis</i>	3 domains, one T1 Cu and one TNC at domain interface	Spore coat pigmentation and protection against UV light and hydrogen peroxide ¹³
Laccases	<i>Trametes versicolor</i>	3 domains, one T1 Cu and one TNC at domain interface	Degradation of lignin ¹⁴
McoP	<i>Pyrobaculum aerophilum</i>	3 domains structure solved ¹⁵	Role in the denitrification pathway ¹⁶
Laccase 2A	<i>Tribolium castaneum</i>	3 domains (accession no. Q49I41)	Cuticle sclerotization and pigmentation ¹⁷⁻¹⁸
Copper efflux oxidase CueO	<i>Escherichia coli</i>	3 domains, one T1 and one TNC, additional fifth regulatory copper ¹⁹⁻²⁰	Oxidation of Cu ^I , copper tolerance in <i>E. coli</i> ²¹
Ascorbate oxidase	<i>Cucurbita pepo</i>	3 domains, dimer ²²	Putatively involved in plant growth ²³
Ferroxidase Fet3p	<i>Saccharomyces cerevisiae</i>	3 domains, monomer, one T1 in domain 3, TNC between domains 1 and 3 ²⁴	Oxidation of Fe ^{II} , related to Fe ^{II} transport ²⁵⁻²⁶
Laccase PcoA	<i>Escherichia coli</i>	3 domains	Part of plasmid encoded copper resistance system in <i>E. coli</i> ²⁷⁻²⁸
Laccase CumA	<i>Pseudomonas putida</i> GB-1	3 domains	Mn ^{II} oxidation ²⁹

Table 1 continued.

Phenoxazinone synthase phsA	<i>Streptomyces antibioticus</i>	3 domains low activity dimers and high activity hexamers and a fifth copper atom in a type 2 center ³⁰	Oxidative coupling of substituted o-aminophenols to produce phenoxazinones, spore pigmentation in <i>Streptomyces antibioticus</i> ³¹
Dihydrogeodin oxidase	<i>Aspergillus terreus</i>	3 domains, homodimer ³²	Biosynthesis of (+)-geodin ³²
Sulochrin oxidase	<i>Penicillium frequentans</i>	homodimer ³³	Biosynthesis of bisdechlorogeodin from sulochrin ³⁴
Ceruloplasmin	Vertebrate	6 domains, 3 T1 Cu, one TNC ³⁵	Oxidation of Fe ^{II} , various functions e.g. in iron metabolism ³⁶
Hephaestin	Vertebrate	6 domains high sequence similarity to ceruloplasmin, contains C-terminal putative transmembrane domain ³⁷	Ferroxidase, may be involved in copper transport and homeostasis, iron homeostasis, mediation of iron efflux ³⁷⁻³⁸

3.1.2 Evolution of multicopper oxidases

Multicopper oxidases have evolved from the single domain cupredoxins through duplication and domain insertion events, and creation and losses of Cu binding sites. In 2003 Nakamura *et al.*³⁹ identified two-domain multicopper oxidase sequences that contain the required characteristics of the hypothetical common ancestors for three- and six-domain cupredoxins and proposed the model presented in Figure 3. The first cupredoxin domain duplication event was also previously proposed by other groups^{7,40}. Nakamura's model includes three different types (named A, B, C) of two-domain cupredoxins that form functional homotrimers and harbor a T1 Cu and an interdomain trinuclear center.

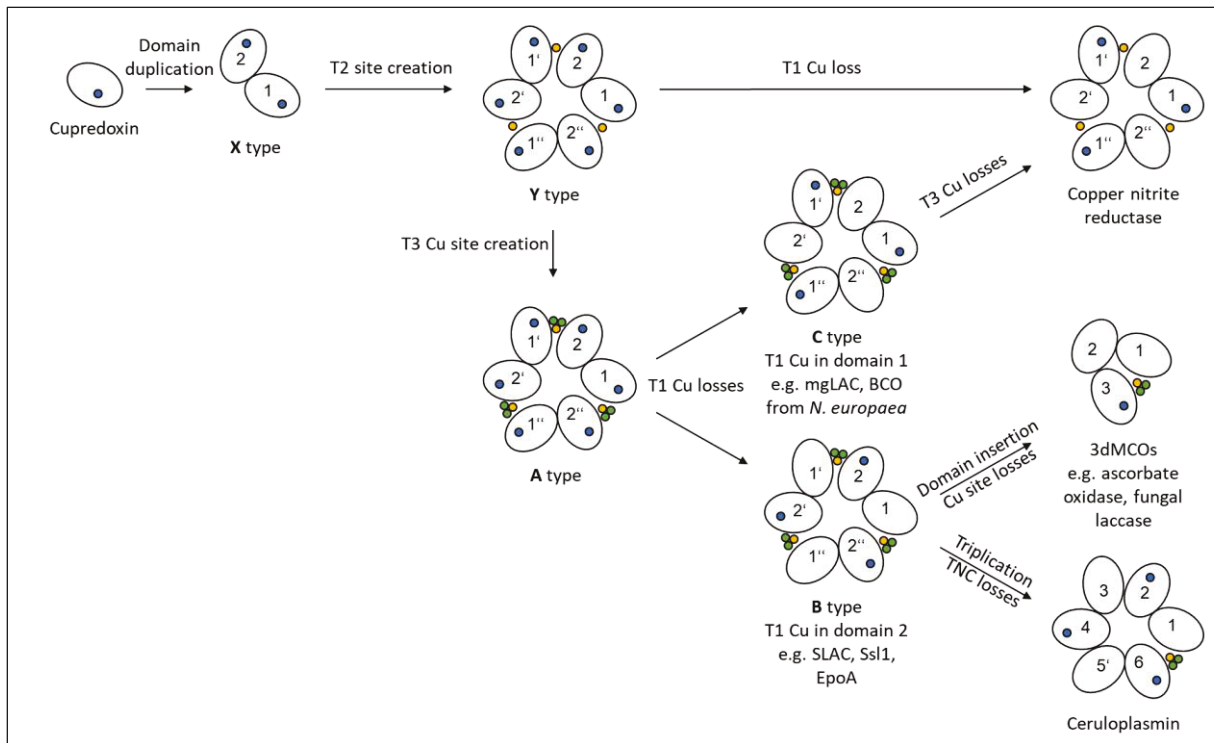


Figure 3: Domain architecture and proposed mechanism for the evolution of multicopper oxidases that includes domain duplication and insertion events, as well as loss of and creation of copper sites. mgLAC⁴¹ and BCO from *N. europaea*⁴² represent C type MCOs, SLAC⁴³⁻⁴⁴, Ssl1⁴⁵, and EpoA¹¹ are representatives of B type MCOs. Blue circles are T1 Cu, yellow circles T2 Cu, and green circles T3 Cu ions. Adapted from Nakamura *et al.*³⁹

From 2002 on several multicopper oxidases belonging to the C and B type groups of two-domain MCOs (2dMCOs) have been described, like an extracytoplasmic phenol oxidase (EpoA) from *Streptomyces griseus*. EpoA is active as a homotrimer and a representative of the type B group¹¹. The laccase SLAC from *Streptomyces coelicolor*, another type B 2dMCO, was described first by Machczynski *et al.*⁴³ in 2004 and later became one of the first 2dMCOs whose structure was solved⁴⁴. Around the same time structures of two other 2dMCOs were published, both belonging to the group of type C 2dMCOs: blue copper oxidase (BCO)⁴² from *Nitrosomonas europaea* and mgLAC⁴¹, that was derived from a metagenomic database.

For CuNiR two possible evolutionary pathways were suggested. In contrast to other MCOs CuNiR only has an interdomain mononuclear T2 Cu coordinated by three histidine residues and is lacking the T3 Cu pair. They have either evolved from a type A ancestor by T1 Cu loss or from type C MCOs by T3 Cu loss. Since the domain arrangement of the type C 2dMCO BCO is more like in three-domain MCOs (3dMCOs) than in CuNiRs, Lawton *et al.*⁴² proposed that it diverged from type A 2dMCOs and CuNiRs evolved before the TNC acquisition event.

Three-domain MCOs like ascorbate oxidase and fungal laccase have a T1 Cu site in the third domain and a TNC between the first and third domain. Despite also being a cupredoxin domain, the second domain of 3dMCOs has no copper binding site. In contrast to 2dMCOs these MCOs can function as monomers.

Another type of MCO is represented by ceruloplasmin. It has a complex structure, with six cupredoxin domains and a total of six copper ions. A trinuclear cluster is located between domains one and six, and domains two, four, and six each contain a T1 Cu site. The T1 Cu ions in domains four and six are coordinated by two histidine ligands, a cysteine, and a methionine ligand. The third T1 Cu in domain 2 lacks the axial methionine and a leucine is present in this position instead³⁵.

3.1.3 Copper sites and their spectroscopic features

The copper sites occurring in MCOs were historically classified into three different types based on their spectroscopic features. The T1 Cu^{II} or blue copper displays a characteristic intense ($\epsilon = 2000\text{--}6000\text{ M}^{-1}\text{ cm}^{-1}$) absorption at around 600 nm in the ultraviolet-visible (UV/Vis) spectrum and a small parallel hyperfine coupling constant in electron paramagnetic resonance (EPR; $A_{\parallel} = 40\text{--}90 \times 10^{-4}\text{ cm}^{-1}$; Figure 4)⁴⁶. These characteristics originate from the unusual geometry and ligation of the T1 Cu. To facilitate fast ET the T1 Cu site evolved to undergo minimal structural changes upon oxidation/reduction resulting in a T1 Cu coordination intermediate between that preferred by Cu^{II} (square planar) and Cu^I (tetrahedral)⁴⁶⁻⁴⁷.

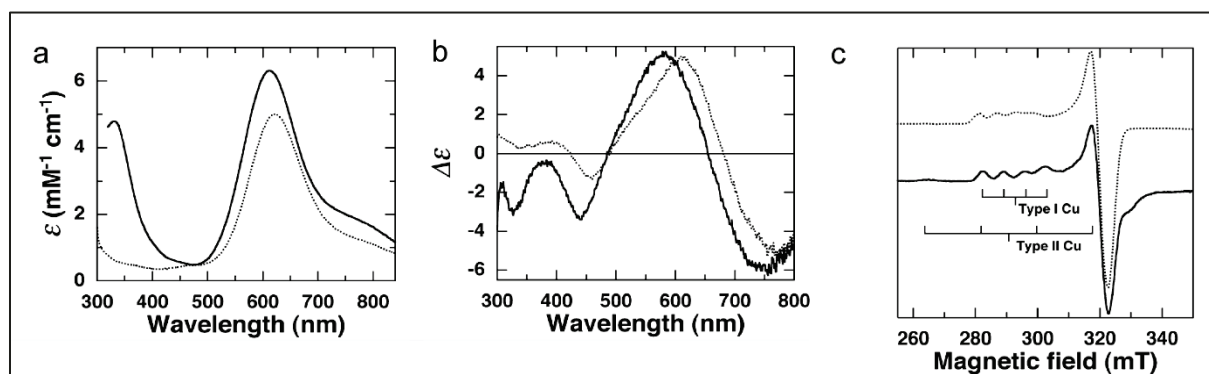


Figure 4: (a) Absorption, (b) circular dichroism (CD), and (c) EPR spectra of CueO (solid line) and azurin (dotted line). Reprinted by permission from Springer Nature: Springer Cellular and Molecular Life Sciences, Structure and function of type I copper in multicopper oxidases, T. Sakurai et al.⁴⁸, COPYRIGHT (2021). License #5070680126731. Modified for layouting purposes.

Differences in the ligands sets observed in the variety of T1 Cu containing proteins arise solely from the presence or absence of axial interactions above or beneath the plane. A commonly present axial ligand is a methionine thioether sulfur (S(Met)) above the plane as in the laccase CotA from *Bacillus subtilis* (Figure 5). A glutamine amide group is the axial ligand in stellacyanin. In fungal laccases this position is occupied by non-coordinating leucine or phenylalanine leaving both axial positions uncoordinated. In addition to the axial methionine, azurin has a second axial ligand beneath the plane, a backbone amide oxygen.

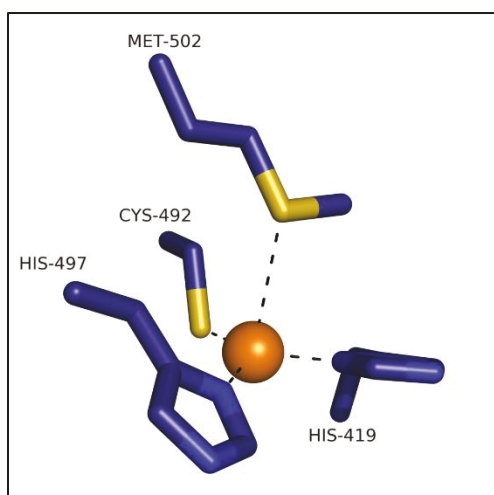


Figure 5: T1 Cu coordination in *B. subtilis* CotA (PDB code 1GSK).

The Cu^{II}-S(Cys) bond is highly covalent (ground state wavefunction with only 41% copper 3d_{x₂-y₂} character⁴) providing strong electronic coupling into the protein for rapid long-range electron transfer⁴⁹⁻⁵⁰. The high covalency accounts for the unusual spectroscopic characteristics of the T1 Cu compared to other copper complexes. Cu^{II} has nine d-electrons leaving an unpaired electron in the d_{x₂-y₂} orbital. This is oriented perpendicular to the Cu^{II}-S(Met) bond and close to the S(Cys) and 2N(His) plane in the ground state⁴. The large overlap of the S(Cys) p_π and the Cu 3d_{x₂-y₂} orbitals results in an intense absorption of the respective ligand-to-metal charge transfer (LMCT) at 600 nm. In addition to this strong S(Cys) p_π → Cu^{II} LMCT there is also a weak S(Cys) p_σ → Cu^{II} LMCT. The electronic structure and consequently the spectral features of the Cu^{II}-S(Cys) bond are anisotropic, switching from π- to σ-types through the interaction of the T1 Cu site with the protein environment⁵¹⁻⁵³. Geometric changes of the T1 Cu site induced by the protein can lead to a rotation of the ground state wavefunction from π to σ bonding, changing the color of the T1 Cu from blue to green due to the strong S(Cys) p_σ → Cu^{II} LMCT at ~450 nm^{52,54}.

The remarkably small parallel hyperfine coupling constant of the blue copper is also a result of the high covalency and the concomitant delocalization of the electron from the metal onto the ligand. This reduces the electron spin coupling to the nuclear spin on the Cu⁴. Since the nuclear spin of copper is 3/2 there is a hyperfine splitting into four lines (Figure 4c).

The trinuclear cluster (TNC) contains one T2 Cu and a T3 Cu pair coordinated by a total of eight histidine residues from two different domains (Figure 6). These domains can be part of the same peptide chain as in the 3dMCO CotA from *B. subtilis* or originate from different peptide chains as in 2dMCOs. The latter require trimerization to form a functional TNC. The T2 Cu is coordinated by two histidine residues and a water molecule⁵⁵. It gives a “normal” EPR spectrum with A_{||} = 150-201 × 10⁻⁴ cm⁻¹ (Figure 4c) but has no absorption features. Studies using pulsed EPR experiments show that both coordinating histidine residues are equivalent and have low anisotropy (10% or less)⁵⁶. The T3 Cu pair is antiferromagnetically coupled. Consequently, it does not give a signal in EPR, but it contributes to

the UV/Vis absorption spectrum with a charge transfer (CT) transition from the bridging OH⁻ ligand at ~330 nm (Figure 4a). Six N_ε atoms of histidine side chains serve as ligands for the T3 Cu pair in 2dMCOs. This is different in 3dMCOs, where five N_ε atoms and one N_δ atom coordinate the T3 Cu's.

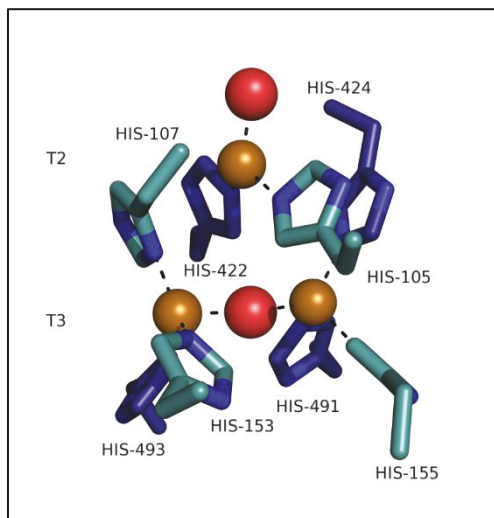


Figure 6: TNC of *B. subtilis* CotA (PDB code 1GSK). Copper ions are depicted as orange spheres. Red spheres represent H₂O bound to the T2 and the T3 bridging OH moiety, respectively⁵⁵. Blue colored histidine residues are in domain 3 and teal colored histidine residues in domain 1.

All three copper ions in the TNC have an open coordination position oriented into the cluster. This coordination unsaturation is necessary for the bridged intermediates in reduction of O₂ to H₂O (see also Chapter 3.2.1 and Figure 7)⁵⁷. Quintanar *et al.*⁵⁶ did extensive spectroscopic studies on the TNC in *Rhus vernicifera* laccase using a T1 mercury-substituted derivative. They concluded that the T2 Cu is coordinated by a hydroxide at all pH's and the coordination unsaturation of the resting TNC is stabilized by the protein matrix.

3.1.4 Electron transfer

The T1 Cu in cupredoxins and MCOs participates in electron transfer processes. It is responsible for electron shuttling between the substrate molecule and the TNC in MCOs and therefore is both acceptor and donor in two different ET steps. Two important properties of electron transfer proteins are the rates of ET and their reduction potential⁴. The ET rate (k_{ET}) in MCOs can be described by the following semi-classical expression for non-adiabatic ET between a donor (D) and an acceptor (A) at fixed distance (Equation 1).⁵⁸

$$k_{ET} = K_A S \sqrt{\frac{4\pi^3}{h^2 \lambda k_B T}} |H_{DA}|^2 \exp\left(-\frac{(\Delta G^\circ + \lambda)^2}{4\lambda k_B T}\right) \quad \text{Equation 1}$$

In equation 1 h and k_B are the Planck and Boltzmann constants. The steric term S represents the fraction of the complex competent for ET and K_A is the equilibrium constant for the electron donor-acceptor complex.⁵⁹ Three parameters that regulate k_{ET} for the ET from the T1 to the TNC are the free energy

difference (ΔG°), the reorganization energy (λ), and the electronic coupling matrix element H_{DA} ⁵³. These parameters will be discussed in more detail in the following.

The free energy difference (ΔG°) for electron transfer in MCOs directly derives from the reduction potential (E°) of the T1 Cu⁶⁰ (all potentials mentioned in this work are potentials vs. standard hydrogen electrode (SHE) unless explicitly given otherwise). A higher T1 Cu E° reduces the driving force for the intramolecular electron transfer (IET). Comparison of *T. versicolor* laccase (780 mV) and *R. vernicifera* laccase (430 mV) demonstrated that the increase in E° by 350 mV reduced the driving force for IET by 8 kcal/mol. The rate-determining step in the catalytic cycle changed from T1 Cu reduction to the first IET step⁶¹. The main determinants of the T1 Cu reduction potential will be discussed in chapter 3.1.5.

In addition to the electronic driving force ΔG° , the reorganization energy λ is an important parameter influencing k_{ET} for the intermolecular ET from substrate to the T1 Cu⁶⁰. It combines inner (λ_{IN}) and outer sphere (λ_{OUT}) contributions, associated with changes in the first coordination sphere of the metal ion and changes in the rest of the protein, the solvent, and the substrate, respectively^{58,60,62-63}. ET is fast if the structures before and after the reaction are similar and therefore λ is small⁶⁴. In fact, λ_{IN} in blue copper proteins is in the range of 0.5-0.8 eV and thus remarkably smaller than λ of a representative copper tetraammine complex which has a λ of ~ 1.4 eV⁶⁴⁻⁶⁵. The reorganization energy is similar for copper sites of different proteins because the first coordination sphere component dominates λ ^{60,64,66}. This underlines the role of the protein coordination that facilitates long range electron transfer with a relatively small release of free energy. The protein creates a balance between the driving force, the reorganization energy, and the adequate electronic coupling between distant redox centers which is represented as H_{DA} in equation 1⁶⁷.

The electron transfer rate is proportional to H_{DA}^2 . H_{DA} is the electronic coupling matrix element and reflects the orbital overlap and depends on the covalency of the ligand-metal bond, the anisotropy in this covalency, and electron tunneling through the protein ligand^{4,60}. In MCOs the highly covalent Cu-S(Cys) bond, its anisotropy as well as the Cys-His superexchange pathway contribute to a large H_{DA} for intramolecular ET⁶⁰. It was shown that H_{DA} values for superexchange pathway in MCOs do not change significantly between proteins^{4,53,61}. In computational studies a direct correlation between the Cu-S(Cys) bond covalency (% S character) and H_{DA} as well as between the anisotropy of this bond (π vs σ overlap) and H_{DA} was demonstrated⁵³. The importance of the electronic coupling has been also shown for the substrate to T1 Cu electron transfer in the yeast ferroxidase, Fet3p. Mutation of E185 that is both part of the Fe^{II} binding site and the electron-transfer pathway from the substrate Fe^{II} to the T1 Cu decreased H_{DA} and therefore k_{ET} ⁶⁸.

H_{DA} decays exponentially with increasing distance between acceptor and donor. This is expressed in the distance decay constant β ⁶⁹. β was experimentally determined to be 1.1 \AA^{-1} for the Ru \rightarrow Cu tunneling along a β -strand in ruthenated azurins ([Ru(2,2'-bipyridine)₂(imidazole)(His)]-azurin) with Ru-Cu distances between 15.9 and 26 \AA ⁷⁰. This was in agreement with previously calculated values for β ⁷¹. The

mechanism of this intraprotein ET is superexchange tunneling⁶⁷. Studies on the intramolecular ET between a fifth copper and the T1 Cu site in *E. coli* CueO also demonstrated that a decrease of the distance improved the electrocatalytic kinetics of the respective CueO variants⁷². Another factor for improvement identified in the same study was an increase in the localized structural stability of the fifth copper site which influences the reorganization energy⁷².

3.1.5 Determinants of the T1 Cu reduction potential

The reduction potential of the T1 Cu^{II}/Cu^I redox couple is often significantly higher than the reduction potential of the aqueous Cu^{II}/Cu^I redox couple (<200 mV). This is a result of the coordination by the protein derived ligands, the protein environment, and the solvent⁷³⁻⁷⁴. Although the structures of different T1 Cu sites are very similar E° varies over a range of ~800 mV, from 184 mV in *R. vernicifera* stellacyanin⁷⁵ up to >1000 mV in domain 2 of ceruloplasmin^{35,76}. The reduction potentials are adapted to the function of the protein. For example, plastocyanin, shuttling electrons from cytochrome f (340 mV) to P700+ in photosystem I (490 mV), has a reduction potential of 370 mV which is right between those of its interaction partners⁷⁴. Several determinants of the T1 Cu E° were identified by comparison of different T1 Cu sites, mutational studies, and computational methods: hydrophobic or desolvation effects, metal-ligand interactions, hydrogen bonding to Cu coordinating sulfur atoms, protein constraints, and intraprotein electrostatic interactions.

The T1 Cu sites are located in a hydrophobic environment that stabilizes the less charged Cu^I over Cu^{II} and thereby raises the reduction potential of the Cu ion⁷⁷⁻⁷⁸. The comparably high E° of *Thiobacillus ferrooxidans* rusticyanin (680 mV)⁷⁹ can be attributed to its remarkable hydrophobicity as shown in NMR studies⁸⁰. Mutational studies on *Pseudomonas aeruginosa* azurin also demonstrated that incorporation of a hydrophobic residue in the second coordination sphere of the T1 Cu increased the redox potential⁸¹. Similar effects of a more hydrophobic T1 Cu environment were also observed in the small laccase Ssl1 from *Streptomyces sviveus* when methionine and threonine residues in the otherwise hydrophobic core of domain 2 were replaced with leucine⁴⁵.

Although differences in the T1 Cu axial ligation alone cannot explain the complete range of observed T1 Cu reduction potentials in nature, its influence has been extensively studied. Olsson and Ryde⁸² performed density functional calculations and demonstrated that the Cu-S(Met) bond length variations can only account for reduction potential changes of up to 70 mV, in contrast to previous studies⁸³ from the Solomon group. These suggested a reduction potential increase by more than 1000 mV due to elongation of the Cu-S(Met) bond⁸³. Even when axial ligand exchange and the presence or absence of a back-bone amide ligand were considered the possible variations were limited to 140 mV⁸². This is also what has been mostly observed in experimental mutation studies.

Introduction of methionine as axial ligand in *Botrytis aclada* laccase lowered the reduction potential by 140 mV from 720 mV to 580 mV in the L499M mutant⁸⁴. Similar effects were observed with *Trametes villosa* laccase, where phenylalanine occupies the axial position in the wildtype enzyme. The reduction potential of 790 mV decreased by 50 mV and 110 mV in the F463L and F463M mutants, respectively⁸⁵. Substitution of the wildtype methionine by non-bonding amino acids can also increase the reduction potential, e.g., in *P. aeruginosa* azurin or *B. subtilis* CotA. In azurin, methionine to isoleucine, leucine, or valine mutations increased the reduction potential by 112-138 mV⁸⁶. Even though phenylalanine is present in high reduction potential fungal laccases, substitution of the axial methionine in CotA (455 mV) with phenylalanine led to a smaller increase (+60 mV) than substitution with leucine (+93 mV)⁸⁷. Stellacyanin from *Cucumis sativus* has a comparably low T1 Cu reduction potential (260 mV) attributed to its glutamine axial ligand⁸⁸. Mutation of this glutamine led to comparably large potential increases, +160 mV in the Q99M⁸⁸ and +320 mV in the Q99L⁴⁹ mutant. The reverse mutation, M510Q, in *E. coli* CueO decreased the reduction potential by 130 mV⁸⁹. This also demonstrates that the effect of an axial ligand mutation varies between proteins. In *Myceliophthora thermophila* laccase introduction of an axial ligand in the L513H mutant decreased the potential by 30 mV⁹⁰ whereas substitution of one coordinating residue with another coordinating residue in azurin was able to induce a much larger potential decrease of ~100 mV⁹¹. The major determinant for the effect of the amino acid in the axial position of the T1 Cu is the hydrophobicity of its side chain. This has been nicely demonstrated in *P. aeruginosa* azurin where this was systematically probed using also unnatural amino acids⁹²⁻⁹³.

The next determinant to consider is hydrogen bonding to the copper coordinating sulfur which has been addressed in mutational studies on azurin, pseudoazurin, and amicyanin. The F114P mutation in azurin removes an H-bond between the F114 backbone amide and the C112 ligand⁹⁴. This resulted in a 90 mV decrease of the reduction potential which was attributed to the greatest part to the change in H-bonding, but the authors also state that there are possibly other contributions. Mutations introducing a hydrogen bond to the cysteine ligand in *Alcaligenes faecalis* pseudoazurin⁹⁵ and *Paracoccus denitrificans* amicyanin⁹⁶ increased the reduction potential. Due to the presence of a homologous serine in rusticyanin⁹⁷ with its very high reduction potential, Marshall *et al.*⁹⁸ created a N47S mutant of azurin. They observed a 130 mV increase in E° attributed to changes in the hydrogen bonds between the protein backbone and the cysteine copper ligand⁹⁸.

The role of protein constraint on the reduction potential remains controversial. The presence of an entatic state in blue copper proteins was first proposed by Vallee⁹⁹ in 1968. Later Solomon and coworkers⁸³ found that only the Cu-S(Met) bond is constrained by the protein and Olsson and Ryde⁸² provided evidence that axial ligands have only small effects on the T1 Cu reduction potential and concluded that there is no strain and therefore no entatic state. Quantum mechanical calculations on small structural models however led Li *et al.*⁷⁸ to the conclusion that protein constraint is a major determinant of the T1

Cu reduction potential though previous experimental¹⁰⁰⁻¹⁰¹ and theoretical¹⁰²⁻¹⁰⁴ studies did not support protein constraint on the T1 Cu site. Hurd *et al.*¹⁰⁵ also concluded from their quantum mechanics/molecular mechanics (QM/MM) calculations that there is strain on the blue copper site and therefore an entatic state. All this has been reviewed recently by Wilfred R. Hagen¹⁰⁶ who pointed out that the major problem of the entatic state/induced rack theory is that there is no consensus on testable (experimental or computational) criteria for the presence/absence of an entatic state yet.

The T1 Cu reduction potential is also influenced by intraprotein electrostatic interactions^{78,107-109}, solvent effects¹¹⁰⁻¹¹², and π - π interactions^{77,94,113-115}. Through combination of mutations that act on different aspects of the T1 Cu site, e.g., the axial ligand or H-bonding, it was possible to create azurin mutants covering the complete range of reduction potentials observed in cupredoxins⁹⁸. Using nickel substituted azurin variants the reduction potential range was extended even further to cover the full range of physiologically relevant potentials from -1 V to 1 V¹¹⁶.

3.2 Laccases

Laccases (EC 1.10.3.2) belong to the multicopper oxidase family and couple the one-electron oxidation of electron rich substrates at the T1 Cu site to the four-electron reduction of molecular oxygen to water at the TNC. They are widely distributed in nature¹¹⁷ (see also Table 1) and abundant in white rot fungi, where they participate in lignin degradation. The laccase from the lacquer tree *Toxicodendron vernicifluum* (formerly *R. vernicifera*) was first described in 1883¹¹⁸.

Common reducing substrates are phenols, aryl amines, anilines, benzenethiols, and inorganic metal ions^{14,119-120}. The one electron oxidation of aromatic substrates yields radicals which then undergo diverse non-enzymatic reactions, e.g. formation of covalent C-C, C-O, and C-N bonds leading to dimerization, oligomerization or polymerization, degradation of polymers, or aromatic ring cleavage^{117,121}. The catalytic activity of laccases and the substrate spectra correlate with the difference in half reduction potentials between the substrate and the T1 Cu^{120,122-123} and laccases can be classified as low, medium, and high-potential laccases based on the reduction potential of the T1 Cu. Low-potential laccases commonly have an axial methionine ligand and reduction potentials between 340 and 490 mV. Medium-potential laccases with reduction potentials in the range between 470 and 710 mV usually have a non-coordinating leucine residue in the axial position. In high potential laccases (720 to 780 mV) usually a non-coordinating phenylalanine residue occupies the axial position¹²⁴.

The exact discrimination of laccases from other MCOs is difficult. There have been efforts to find definitions based on the primary sequence or alternatively focusing on the enzyme activity and presence of the canonical copper sites. The following four conserved sequence regions L1-L4 were derived from fungal and plant laccase sequences¹²⁵.

- L1: H-W-H-G-X₉-D-G-X₅-QCPI
- L2: G-T-X-W-Y-H-S-H-X₃-Q-Y-C-X-D-G-L-X-G-X-(FLIM)
- L3: H-P-X-H-L-H-G-H
- L4: G-(PA)-W-X-(LFV)-HCHI-DAE-X-H-X₃-G-(LMF)-X₃-(LFM)

MCOs can have both laccase and metallo-oxidase activity. The metallo-oxidase McoA from *Aquifex aeolicus* was subjected to mutagenesis and the evolved 2B3 variant was then designated as a laccase due to its 10-fold higher catalytic activity towards the laccase substrate 2,2'-azino-bis(3-ethylbenzthiazoline-6-sulfonic acid) (ABTS) than for Cu^I oxidation¹²⁶. *E. coli* CueO is also referred to as both laccase⁷² and cuprous oxidase¹²⁷ with laccase activity that can be increased through mutagenesis¹²⁷. Metallo-oxidases often have specific substrate binding sites such as E185, D283, and D409 in the ferroxidase Fet3p^{68,128}. The specificity for organic substrates is a consequence of the shape of the substrate-binding cleft and an interaction between the substrate molecule and an amino acid residue adjacent to the T1 Cu coordinating histidine⁹.

The first three-dimensional structure of a laccase, a T2 depleted form of *C. cinereus* laccase, was published more than 20 years ago¹²⁹. Since then, the number of available structures continuously increased and in 2009 the first structures of two-domain laccases became available^{41-42,44}. At the time of writing, the latest depositions of laccase structures in the Protein Data Bank (PDB) were *Zea mays* laccase 3 (PDB codes 6KLG, 6KLI, 6KLJ)¹³⁰ and a laccase from *Thermus thermophilus* HB27 in two different conformations (PDB codes 6TYR and 6Q29).

Several laccase-substrate complex structures are available in the PDB. From the analysis of the respective electron density maps Hakulinen and Rouvinen¹³¹ concluded that the electron densities not always allowed the determination of the substrate's identity and exact position. Nevertheless, the authors concluded that the observed compounds are always bound between the first and second domain close to the T1 Cu and H-bonded to one of the T1 Cu ligating histidine residues, which is part of the putative substrate-T1 Cu electron transfer pathway⁶⁰. To date there are no structures of two-domain laccase with bound substrate available. For SLAC from *S. coelicolor* it was proposed that the substrate binding pocket is formed by one tyrosine and two methionine residues⁴⁴. These residues have been subjected to mutagenesis and indeed effected the catalytic efficiency for 2,6-dimethoxyphenol oxidation¹³².

3.2.1 Reaction mechanism

The reaction mechanism of laccases involves four relevant states of the active site (Figure 7). In the resting oxidized (RO) state, all four copper ions are oxidized (Cu^{II}) with hydroxide-bridged T3 copper ions⁶⁰. The first step in the laccase reaction is an outer sphere ET from the substrate molecule to the T1 Cu¹³³. It is thought to be the rate-determining step in the laccase reactions⁶³ and determines which reducing substrates can be oxidized¹²². The electrons are then transferred from the T1 Cu to the TNC

and the fully reduced state with four Cu^{I} ions is formed. Molecular oxygen binds to the reduced TNC and is then reduced in two two-electron steps, forming the peroxide intermediate (PI) first and afterwards the native intermediate (NI)¹³⁴.

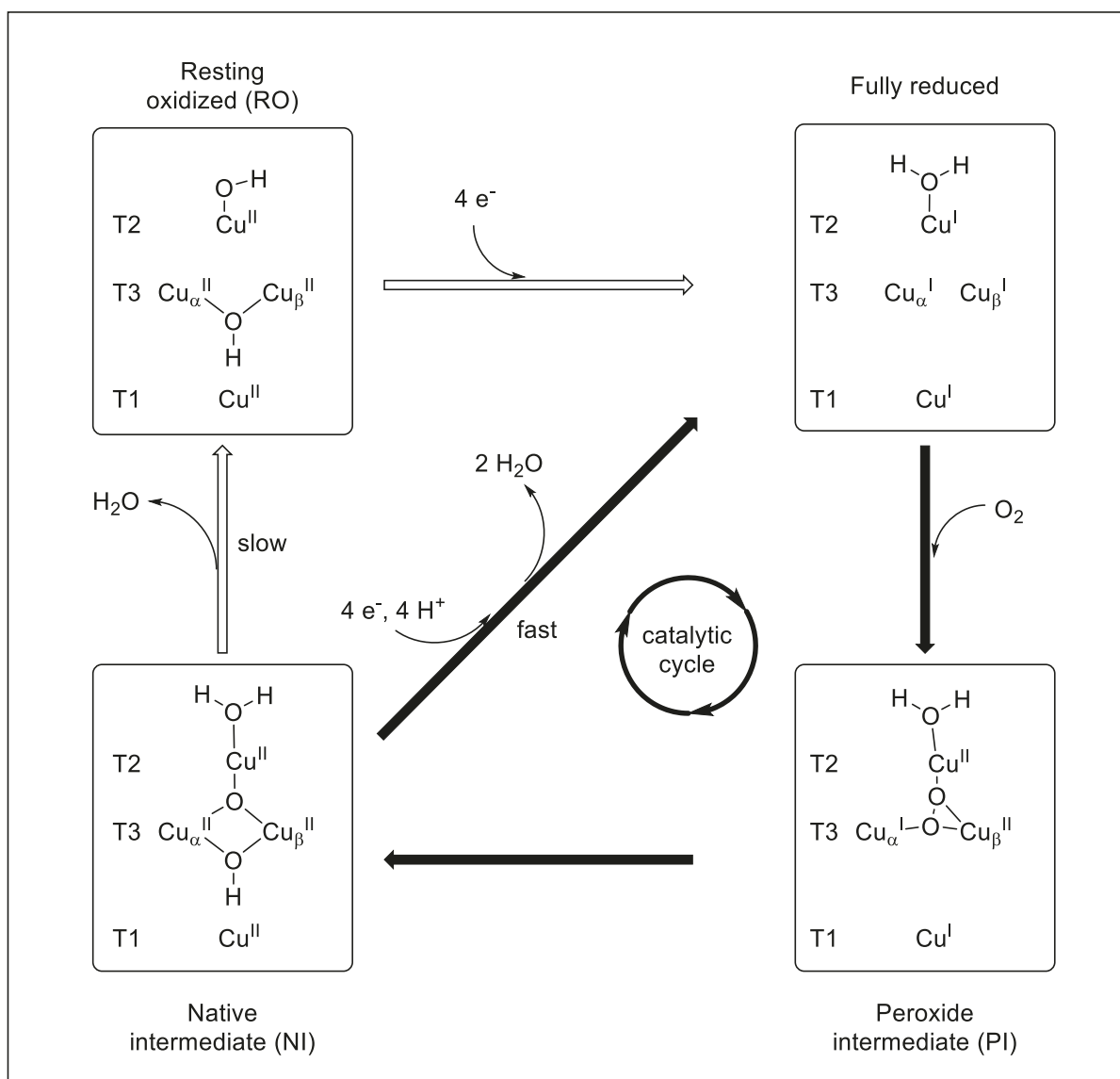


Figure 7: Reaction mechanism of laccases. Bold arrows show steps of the catalytic cycle. After dioxygen binding to the fully reduced enzyme and a two-electron reduction the peroxide intermediate (PI) is formed. Further reduction of the peroxide leads to the native intermediate (NI) which is the fully oxidized form of the enzyme relevant for catalysis. Additionally shown steps are the initial reduction of the resting oxidized (RO) form of the enzyme and the slow decay of NI to the RO state in the absence of substrates. Modified after Jones and Solomon⁶⁰. The T3 Cu ions are not equivalent and are designated as T3 α and T3 β as indicated by respective subscripts.

The peroxide in the PI is bound to all three Cu ions of the TNC as proposed by Solomon and coworkers⁶⁰ based on extended X-ray absorption fine structure (EXAFS) and QM/MM methods (Figure 7)¹³⁵. However, Ferraroni *et al.*¹³⁶ observed a peroxide moiety only bridging the T3 Cu pair. The two T3 Cu ions are not equivalent in O_2 reduction. Augustine *et al.*¹³⁷ created T1 Cu depleted variants of Fet3p with additional mutations of T3 coordinating histidine residues and observed that T2 and T3 β are necessary for the two-electron reduction of O_2 to the peroxide level while the other T3 Cu ion (T3 α) remains reduced.

The further two-electron reduction of the peroxide yields the NI where the enzyme is fully oxidized and O_2 is reduced to water-level products. These are bound as a μ_3 -oxo ligand bridging all three Cu ions of the TNC and a μ_2 -hydroxo ligand between the T3 Cu pair¹³⁸⁻¹³⁹. The μ_3 -oxo bridge enables electron delocalization over all three Cu ions⁵⁷. The NI was first shown to be the catalytically active, fully oxidized form in the low-potential *R. vernicifera* laccase RvL¹⁴⁰. Although the driving force for IET from the T1 to the TNC is smaller if the T1 Cu redox potential is higher, the NI is also the catalytically relevant intermediate in the high redox potential laccase from *T. versicolor*, since intramolecular ET is still faster than the decay of NI to RO⁶¹. In the absence of substrate molecules, the NI slowly decays to the RO form.

Two acidic residues are important for the reductive cleavage of the O-O bond, i.e., E487 and D94 in yeast Fet3p¹⁴¹⁻¹⁴², E506 and D116 in *E. coli* CueO¹⁴³, and E498 and D116 in *B. subtilis* CotA¹⁴⁴⁻¹⁴⁵. The Fet3p D94A mutant does not react with O_2 since it is required for deprotonation of the water ligand on the T2 Cu in the PI, which facilitates the O-O bond cleavage¹⁴². E487 is the protonable species responsible for acceleration of PI decay at low pH. Together with D94 it creates a flow of H^+ from the T3 side to the T2 side of the TNC and thereby drives the reductive O-O bond cleavage¹⁴¹.

The T1 Cu is connected to the TNC via a His-Cys-His motif. The cysteine residue is a T1 Cu ligand and the histidine residues are a ligands to one of the T3 Cu ions each (Figure 8). This superexchange bridge involves the bridge orbitals in the electronic coupling between donor and acceptor. It provides a pathway from the Cu-S(Cys) π bond at the T1 site to the Cu-N(His) σ bond at the T3 site through the protein backbone^{4,46,53,146}. There is an additional contribution to the electronic coupling between the two copper sites through an H-bond between the cysteine backbone carbonyl and a histidine nitrogen^{46,53}.

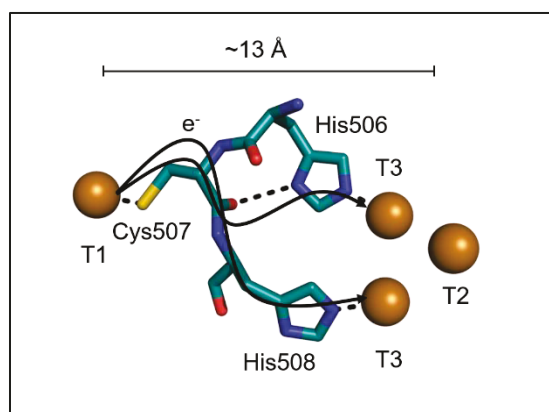


Figure 8: Schematic representation of the Cys-His pathways connecting the T1 and the T3 Cu ions in ascorbate oxidase (PDB code 1AOZ).

Kyritsis and coworkers¹⁴⁷⁻¹⁴⁹ performed theoretical calculations to determine the efficiency of the two different pathways in zucchini squash ascorbate oxidase (Figure 8). According to these, the C507 to H506 pathway which includes an H-bond is three times more efficient than the pathway to H508.

Extensive studies of the reaction mechanism have also been performed on the small laccase SLAC from *S. coelicolor*. This enzyme differs from other laccases as a redox-active tyrosine residue (Y108) participates in the catalytic cycle¹⁵⁰. This tyrosine residue is located ~5 Å away from the T2 Cu and it was proposed that by contributing an electron it can prevent the occurrence of reactive three-electron-reduced oxygen intermediates⁴⁴. As the tyrosine radical was also observed during turnover it may also play a role in the conversion of organic substrates¹⁵¹.

3.2.2 Applications of laccases

The ability to oxidize a wide variety of organic compounds using molecular oxygen as co-substrate makes laccases interesting enzymes for biotechnological applications. Furthermore, they do not require expensive co-factors and only produce water as a by-product. They are environmentally friendly catalysts and are so called “green” enzymes¹⁵².

Laccase preparations have already been commercialized with applications in the food, paper, and textile industries. They are used for brewing, color enhancement, cork modification, paper pulp delignification, pulp bleaching, and denim finishing and bleaching, respectively¹⁵³. Further research focuses on potential applications in medical diagnostics, organic synthesis, bioremediation, and production of biofuels and fuel cells¹⁵³⁻¹⁵⁶. A recent review of laccase related patents from the years 2009-2019 showed that patents covering laccase applications for lignin removal and modification were the most frequent¹⁵⁷. On the other hand, laccase application for bioremediation purposes was the topic with most scientific articles in a literature search from 2017¹⁵⁸. This suggests that the use of laccases for bioremediation or waste degradation purposes can be expected in the near future¹⁵⁷.

High-redox potential fungal laccases are of particular interest for biotechnological purposes due to their high activities and their ability to oxidize a wide range of substrates¹⁵⁸⁻¹⁵⁹. However, applications of these fungal enzymes are limited due to their high degree of glycosylation, their need for eukaryotic expression hosts, the restriction to acidic reaction conditions, and sensitivity to many inhibitors¹⁶⁰. To overcome these limitations, bacterial laccases including small two-domain laccases have gained research interest. SLAC from *S. coelicolor* was investigated as a potential biocatalyst and successfully applied for the synthesis of phellinisin A, a β - β caffeic acid dimer with antioxidative properties¹⁶¹. *Streptomyces cyaneus* is active towards lignin model compounds, suggesting its suitability for biomass degradation¹⁶². Since bacterial laccases possess lower activities than fungal laccases, protein engineering has been aiming to increase the T1 Cu reduction potential, and thus increase oxidation rates and extend substrate spectra^{45,87,89,132,163-164}.

3.2.3 The two-domain laccase Ssl1 from *Streptomyces sviveus*

Ssl1 is a two-domain laccase from the mesophilic soil bacterium *S. sviveus*. It was discovered by genome mining and characterized previously in our group¹⁶⁵. In contrast to many other laccases, especially fungal laccases, Ssl1 combines several properties beneficial for applications as a biocatalyst. Its pH optimum for oxidation of phenolic compounds lies in the alkaline region, its activity is not affected by detergents or organic co-solvents, and Ssl1 is stable at elevated temperatures ($T_{1/2, 60^\circ\text{C}} = 88 \text{ min}$)¹⁶⁵. It has been successfully applied in an enzymatic oxidation/Michael addition sequence¹⁶⁶.

According to a Conserved Domain Search¹⁶⁷, domain 1 of Ssl1 is related to nitrite reductases and has lost the T1 Cu binding site that is present in other two-domain laccases. Domain 2 belongs to the cupredoxin super family and contains a T1 Cu. Therefore, Ssl1 belongs to the type B 2dMCOs (see Chapter 3.1.2 and Figure 3). In 2014 the 3-dimensional structure of Ssl1 was published⁴⁵ confirming its homotrimeric structure with the TNC located at the interface of domain 2 and domain 1 of neighboring monomers (Figure 9). The T1 Cu is ligated by C285, H290, H228, and M295 in the axial position (Figure 9b) and lies $\sim 4 \text{ \AA}$ beneath the protein surface. The His-Cys bridge connects the T1 to the TNC via C285, H284, and H286. The TNC is connected to the central cavity that is covered with hydrophilic residues and lies between the three Ssl1 molecules. In addition, there are two solvent channels along the monomer interface connecting the TNC to the enzyme surface⁴⁵.

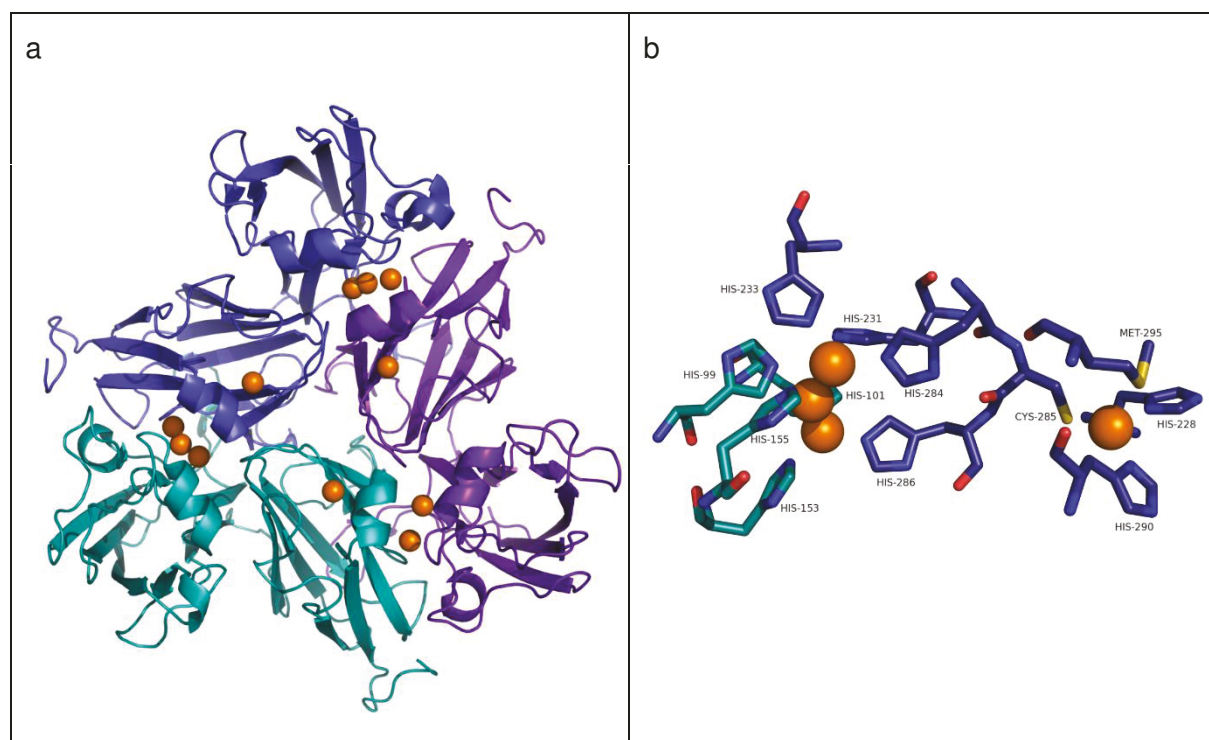


Figure 9: (a) Trimeric structure of Ssl1 and (b) coordination of the copper ions (PDB code 4M3H). Different monomers are colored differently (teal, blue, purple) and copper ions are depicted as orange spheres.

As expected for a T1 Cu with an axial methionine ligand the reduction potential of Ssl1's T1 Cu of 375 mV⁴⁵ is lower than that of fungal laccases, which have potentials reaching up to 800 mV¹²⁰. Mutational studies have been previously performed aiming to identify residues influencing the T1 Cu

reduction potential⁴⁵. These have confirmed the axial ligand of the T1 Cu and the hydrophobicity of the T1 Cu environment as determinants of the reduction potential. These findings, in combination with the feature of Ssl1 to be easily produced in *E. coli* and the convenient purification process via an N-terminal hexahistidine tag, make this laccase a suitable model to further investigate molecular factors influencing the reduction potential, the catalytic activity, and the spectroscopic characteristics of two-domain multicopper oxidases (2dMCOs).

3.3 Aim of the work

Implementation and optimization of biocatalytic processes need a multidisciplinary approach including process engineering, enzyme immobilization, and protein engineering¹⁶⁸. Tailored protein engineering relies on knowledge of the molecular determinants of the catalytic activity, stability, substrate spectrum, and the structure of an enzyme. Though there are already established industrial applications of laccases (see chapter 3.2.2), there is no natural laccase that combines all desirable features for their application, namely stability and activity over a broad range of temperatures and pH values, a high reduction potential which is associated with high activities and a broad substrate spectrum, halide/hydroxide tolerance, and cost-effective production¹⁵⁹. One approach to overcome some of these limitations is protein engineering of bacterial laccases to combine their beneficial properties with the high oxidative activity and broad substrate spectrum observed in fungal laccases. Due to the low reduction potential of bacterial laccases and its impact on the activity, increasing the reduction potential is a promising approach.

- 1) To identify molecular factors contributing to the T1 Cu reduction potential that have not yet been investigated in two-domain laccases so far, Ssl1 variants were created by site-directed mutagenesis focusing on the first and second coordination sphere of the T1 Cu. The T1 Cu reduction potential and the correlation with the substrate spectrum and catalytic activity were analyzed for a series of mutants.
- 2) Due to the major influence of the T1 Cu axial ligand on the reduction potential further structural and spectroscopic characterization was carried out. To the best of our knowledge, such a systematic spectroscopic and structural investigation of a two-domain laccase with different axial ligands is still missing.
- 3) The intramolecular electron transfer (IET) from the T1 Cu to the TNC is an integral part of the laccase reaction mechanism and is among other factors also dependent on the T1 Cu reduction potential. To better understand the influence of the T1 Cu reduction potential a ruthenated Ssl1 variant was produced and its suitability for IET measurements was examined.

4 Manuscript 1: Correlation between the T1 copper reduction potential and catalytic activity of a small laccase

Title: Correlation between the T1 copper reduction potential and catalytic activity of a small laccase

Authors: Anna C. Olbrich, Jan N. Schild, Vlada B. Urlacher

Published in: Journal of Inorganic Biochemistry Volume 201, 2019

DOI: 10.1016/j.jinorgbio.2019.110843

Contribution: Site-directed mutagenesis

Expression and purification of Ss11 variants

Determination of reduction potentials, kinetic constants, conversion of substituted phenols, decolorization assays

Supervision of bachelor thesis of Jan N. Schild (development of phenol conversion reaction set up, method development for HPLC analysis of phenol conversion)

Writing the manuscript

The publisher (Elsevier) allows to include the article in a dissertation without explicit written permission.



Contents lists available at ScienceDirect

Journal of Inorganic Biochemistry

journal homepage: www.elsevier.com/locate/jinorgbio

Correlation between the T1 copper reduction potential and catalytic activity of a small laccase



Anna C. Olbrich, Jan N. Schild, Vlada B. Urlacher*

Institute of Biochemistry, Heinrich-Heine-University Düsseldorf, Universitätsstr. 1, 40225 Düsseldorf, Germany

ARTICLE INFO

Keywords:

Small laccase
Type 1 (T1) copper
Reduction potential
Axial ligand
Substituted phenols

ABSTRACT

Laccases are multicopper enzymes that catalyze oxidation of electron-rich substrates coupled to reduction of molecular oxygen to water. Since the Type 1 copper (T1 Cu) is the site where electrons are withdrawn from the substrate, it is assumed that the reduction potential of this copper correlates with enzyme activity. Herein, we studied the correlation of the T1 Cu reduction potential and the enzymatic activity of the small two-domain laccase Ssl1 from *Streptomyces sviveus*. For a systematic approach, we aimed to minimize any effects other than the reduction potential difference. To this end, we constructed a series of Ssl1 mutants with reduction potentials varying from < 290 to 560 mV. Along with the hydrophobicity of the axial ligand of the T1 Cu also structural changes in the substrate binding site and additional hydrogen bonding increased the reduction potential. Enzyme activity experiments demonstrated that the T1 Cu reduction potential has a different effect on oxidation of different substrates. Whereas there was no obvious correlation between the T1 Cu reduction potential and kinetic parameters for the oxidation of syringaldazine (with a reduction potential of 390 mV), a good correlation was observed between the T1 Cu reduction potential and the conversion of substituted phenols with reduction potentials between 660 and 820 mV. This correlation was pronounced for the Ssl1 variants with reduction potentials above 470 mV, which demonstrated increased activities also during the oxidation of two dyes, alizarin red S and indigo carmine.

1. Introduction

Laccases (EC 1.10.3.2) are multicopper oxidases that catalyze the one-electron oxidation of substrates coupled with the four-electron reduction of molecular oxygen to water. Known laccase substrates include phenols, aryl amines, anilines, benzenethiols, and metal ions [1–3]. Laccases contain four Cu ions and commonly consist of three cupredoxin-like domains formally numbered 1, 2, and 3. Domain 3 contains one Type 1 (blue) copper site (T1 Cu). Between domains 1 and 3 a trinuclear cluster (TNC) is located that is formed by one Type 2 copper and two Type 3 copper ions [4]. Domain 2 is not involved in the copper binding. The copper sites of laccases are distinguished by their spectroscopic and paramagnetic properties [5]. Along with typical three-domain laccases the so-called small laccases exist that are composed of two domains. These two-domain small laccases form functional homotrimers with the TNC located at the interface of neighboring monomers [6–8].

Although the T1 Cu coordination is similar among the multicopper proteins and involves at least two histidines and one cysteine, the coordination spheres in various enzymes are different [9]. The T1 Cu in

plant laccases is coordinated by two histidines, one cysteine, and one methionine as coordinating axial ligand [10]. Fungal laccases possess a non-coordinating residue like leucine or phenylalanine instead of the axial methionine. These differences in coordination geometry were shown to influence electronic structure and electron transfer to the T1 Cu. Among others, the axial ligand of the T1 copper, and particularly presence or absence of the coordinating methionine, is known to determine the T1 Cu reduction potential (E°) [11]. Thus, low-potential laccases with reduction potentials between 340 and 490 mV versus NHE commonly have methionine as the axial ligand of the T1 Cu. Medium-potential laccases have reduction potentials in the range between 470 and 710 mV and non-coordinating leucine in the axial position. Laccases with reduction potentials of 720 to 780 mV are classified as high-potential laccases, which carry in most cases a non-coordinating phenylalanine residue as the axial ligand [12]. Besides metal-ligand interactions, other factors including the hydrophobicity of the residues within 6 Å of the T1 Cu, H-bonding to the coordinating cysteine-sulfur atom, protein constraints, and electrostatic interactions in the protein have been identified as the main determinants of the T1 Cu reduction potential [13–15]. Thus, among laccases with identical ligand sets, E°

* Corresponding author.

E-mail address: Vlada.Urlacher@uni-duesseldorf.de (V.B. Urlacher).<https://doi.org/10.1016/j.jinorgbio.2019.110843>

Received 4 June 2019; Received in revised form 22 August 2019; Accepted 7 September 2019

Available online 09 September 2019

0162-0134/ © 2019 Elsevier Inc. All rights reserved.

can differ substantially [10].

During laccase-mediated catalysis, four substrate molecules undergo one electron abstractions at the T1 Cu. The electrons abstracted from substrates are subsequently transferred from the T1 Cu to the TNC via the approximately 13 Å long conserved His-Cys-His path - the super-exchange pathway. In the fully reduced form (4 Cu^I) of the enzyme, molecular oxygen is reduced at the TNC [16]. A peroxide intermediate is formed after two two-electron reduction steps and finally water is released [17].

The intermolecular electron transfer from the substrate to the T1 Cu is considered the rate-limiting step of laccase activity [18,19]. According to the Marcus theory the rate constant of the intermolecular electron transfer (k_{ET}) is mainly influenced by the electronic driving force, ΔG° (i.e. the difference in the reduction potential) and the reorganization energy [20]. The reorganization energy is the energy required for substrate and protein rearrangements between initial and final states upon electron transfer [10].

For many substrates catalytic activity of laccases correlates with the difference in half reduction potentials between the T1 Cu and the substrate (ΔE°) [2,21,22]. Laccases can oxidize also the substrates with E° exceeding their T1 Cu E° . The endergonic oxidation of the substrate may be compensated by the exergonic reduction of O₂ to H₂O [23]. Thus, understanding the correlation between the T1 Cu reduction potential and the catalytic activity of laccases has been of great interest [1], and remains a topic of current research [15,24,25]. High-potential laccases have been reported to oxidize recalcitrant dyes and to possess higher activities as compared to middle- and low-potential laccases [23]. Respectively, increasing the T1 Cu E° by protein engineering could not only enhance substrate oxidation rate but also extend laccases' substrate spectra. However, ΔE° does not always clearly correlate with laccase activity. Studies on four laccases from basidiomycetes revealed that for monophenolic substrates with low E° , ΔE° between the T1 Cu and the substrate did not directly influence the laccase activity [24]. Replacement of the axial phenylalanine by methionine in a *Trametes villosa* laccase resulted in an expected decrease of the reduction potential by 110 mV but in increased k_{cat} during the oxidation of phenolic substrates [26]. Obviously, E° is not the only determining factor of laccase activity. Along with the above mentioned reorganization energy, also the electrostatic environment of the substrate [27] and steric hindrances associated with substrates' size [21] affect laccase activity. Furthermore, the substrate binding mode influences the donor-acceptor distance between the substrate donor atom and the T1 Cu; as the electron transfer rate decays exponentially with the donor-acceptor distance it significantly affects k_{cat} [28].

So far, studies on the correlation between laccase activity and the difference in half potentials of the T1 Cu and the substrate (ΔE°) have been conducted mainly on high- and middle-potential fungal laccases and the reported results demonstrate the complexity of this aspect. Since the past decade, bacterial laccases have gained research interest because of their comparably easy heterologous production, lack of glycosylation, activity and stability at alkaline pH and high tolerance towards Cl⁻ as compared to fungal laccases [29,30]. However, bacterial laccases possess lower activity as compared to fungal laccases. Even though some mutants with changed reduction potential have been reported for bacterial laccases [31–33], the correlation between the T1 Cu reduction potentials of bacterial laccases and their activity remains much less investigated. As small two-domain laccases have been discovered only relatively recently, a respective systematic investigation is still missing.

Thus, the aim of this work was firstly to investigate the factors contributing to the reduction potential of the small two-domain laccase Ssl1 from *Streptomyces sviveus*, and secondly to study the correlation between the T1 Cu reduction potential and the enzyme activity. To this end, we constructed a series of Ssl1 mutants with reduction potentials spanning a range of at least 270 mV and investigated their ability to oxidize several laccase substrates with various sizes and half potentials.

2. Experimental

2.1. Site-directed mutagenesis

Site-directed mutagenesis of *ssl1* was performed using the QuikChange protocol (Stratagene) with primers containing the desired mutation (Table S1) and pET22H_ssl1 or variants thereof as template. Correct sequences of *ssl1* genes were verified by Sanger sequencing (GATC Biotech, Konstanz, Germany).

2.2. Expression and purification of Ssl1

Ssl1 laccase from *S. sviveus* (UniProtKB B5HSR1) and Ssl1 variants were expressed without the natural N-terminal *tat*-signal sequence. Residue numbering follows the sequence containing the natural signal sequence [34]. For expression of *ssl1*, *E. coli* BL21-CodonPlus(DE3)-RP was transformed with pET22H_ssl1 or variants thereof. Cells were grown in 200 mL terrific broth (TB)-medium in 2 L flasks supplemented with 100 µg/mL ampicillin and 34 µg/mL chloramphenicol at 37 °C and 180 rpm to an OD₆₀₀ of 1.5. Expression was induced with 20 µM isopropyl β-D-1-thiogalactopyranoside (IPTG) and 2 mM CuSO₄. After expression for 20 h at 19 °C and 140 rpm, cells were harvested by centrifugation (11,000 ×g, 30 min, 4 °C), resuspended in 15 mL potassium phosphate buffer (50 mM, pH 7.5) and centrifuged (3082 ×g, 30 min, 4 °C). Cell pellets were stored at -20 °C.

For lysis cells were resuspended in chilled potassium phosphate buffer (50 mM, pH 7.5) containing 0.3 mM copper(II) sulfate and 0.1 mM phenylmethanesulfonyl fluoride. Cells were lysed by sonication on a Branson Sonifier 250 with three cycles of 60 s (40% duty cycle, output control 4) with at least 60 s incubation on ice between cycles. Cell debris was separated by centrifugation (30,000 ×g) and 1.0 mM CuSO₄ was added to the soluble fraction. After incubation for 2 h at room temperature or until no further increase in activity was observed, the lysate was subjected to a heat precipitation (20 min, 65 °C). Precipitated proteins were removed by centrifugation (50,000 ×g, 30 min, 4 °C).

After heat precipitation of most endogenous *E. coli* proteins, further purification of Ssl1 was achieved by immobilized metal ion affinity chromatography (IMAC) using a HiTrap TALON crude 5 mL column (GE Healthcare, München) on an ÄKTApurifier 100 fast performance liquid chromatography (FPLC) system (GE Healthcare, München). The column was equilibrated with five column volumes (CV) binding buffer (50 mM potassium phosphate buffer, 500 mM sodium chloride, pH 7.5) and the filtered (0.45 µm) supernatant from the heat precipitation was applied with 1 mL/min. The column was washed with two CV binding buffer, five CV washing buffer (5 mM imidazole) and Ssl1 was eluted with five CV of elution buffer (150 mM imidazole). The elution of proteins was monitored by absorption at 280, 330, and 600 nm. Ssl1 containing fractions were pooled, concentrated (Vivaspin Turbo 15, MWCO of 10 kDa, Sartorius, Göttingen) and the elution buffer was replaced by 50 mM potassium phosphate buffer (pH 7.5) using PD miditrap G-25 columns (GE Healthcare, München). Protein concentrations were determined using the Bradford method [35].

2.3. Determination of reduction potentials

The reduction potentials were determined by redox titrations with the redox couple potassium hexacyanoferrate(III)/potassium hexacyanoferrate(II) ($E^\circ = 0.433$ V) as mediator under nitrogen atmosphere. Reduced Ssl1 (50 µM) in 10 mM 4-(2-hydroxyethyl)-1-piperazineethanesulfonic acid (HEPES, pH 7.0) and 10 mM potassium hexacyanoferrate(II) was gradually oxidized by adding a solution containing 50 µM Ssl1 and potassium hexacyanoferrate(III) (10–900 mM) in 10 mM HEPES (pH 7.0). Oxidation of the T1 Cu was followed spectrophotometrically on a TIDAS E photo diode array spectrophotometer (J&M Analytik, Essingen, Germany) using the

increase in absorption at ~ 600 nm (Figs. S4, S5). After each step, a spectrum from 340 to 1000 nm was recorded. Reduction potentials were calculated according to the Nernst equation. The absorption at ~ 600 nm (y) was plotted against the reduction potential (x) and fitted to the Nernst equation $y = A_2 + \frac{A_1 - A_2}{1 + \exp\left(\frac{x - x_0}{dx}\right)}$ with $dx = \frac{RT}{nF} = 0.02526$ J/C for one electron oxidations/reductions in OriginPro 9G (OriginLab Corporation, Northampton, MA, USA). The fit parameter x_0 represents the midpoint potential of the laccase (Figs. S6-S13).

2.4. Determination of catalytic constants for syringaldazine conversion

Kinetic constants of Ssl1 variants were determined with the typical laccase substrate syringaldazine (SGZ). Reactions were performed at 25 °C in 50 mM potassium phosphate buffer (pH 8.0) and 10% (v/v) dimethyl sulfoxide (DMSO) for substrate solubilization. SGZ concentrations of 0.4–400 μ M were used. Product formation was followed spectrophotometrically at 525 nm ($65 \text{ mM}^{-1} \text{ cm}^{-1}$) on a Tecan Infinite PRO 200 (Tecan, Männedorf, Switzerland) reader. Initial reaction rates were determined in triplicate according to the Lambert-Beer law and were fitted by non-linear regression to the Michaelis-Menten equation $v = v_{\text{max}}[S]/(K_M + [S])$ in OriginPro 9G (Fig. S3). k_{cat} values were calculated based on the protein concentration determined by the Bradford method.

2.5. Decolorization of dyes

The decolorization of alizarin red S and indigo carmine by Ssl1 variants was analyzed as previously described [7]. Conversion rates were determined by comparing the residual absorption at 608 nm for indigo carmine and 513 nm for alizarin red S, respectively, with the absorption of the control reactions without enzyme.

2.6. Conversion of substituted phenols

Phenol oxidation reactions contained 1 mM substrate, 1 μ M enzyme, and 1% (v/v) ethanol for substrate solubilization in 1 mL potassium phosphate buffer (50 mM, pH 8.0). After incubation for 24 h at 25 °C with overhead rotation (15 rpm) reactions were stopped by addition of 30 μ L 6 M hydrochloric acid. Denatured protein was separated by centrifugation (12,300 g, 5 min). The reactions were analyzed using high-performance liquid chromatography (HPLC) on a Shimadzu HPLC system (Shimadzu, Duisburg, Germany) equipped with a Chromolith Performance RP-18e column (100 \times 4.6 mm, Merck, Darmstadt, Germany). The injection volume was 5 μ L. A solvent gradient of acetonitrile and 0.1% formic acid was applied at a flow rate of 1 mL/min. The acetonitrile concentration was increased from 5 to 100% in 10 min, held at 100% for 3 min, followed by re-equilibration of the column with 5% acetonitrile for 4 min. A photodiode array was used for detection of compounds by monitoring absorption between 190 and 800 nm. Remaining substrate concentrations were calculated from the substrate peak areas at 280 nm using calibration curves determined from 50 to 1000 μ M. The substrate concentration in control reactions after 24 h was used as reference for calculation of conversion rates.

2.7. Calculation of ClogP

ClogP values were calculated as described by Garner et al. [36] using the Bio-Loom program available at <http://www.biobyte.com/bb/prod/bioloom.html> that is based on the fragment method by Abraham and Leo [37].

3. Results

3.1. Correlation between the axial ligand hydrophobicity and the reduction potential

In our previous work on the two-domain laccase Ssl1 from *S. sviveus* we demonstrated that replacement of the axial T1 Cu ligand methionine by leucine (M295L) increased E° [7]. In the present study, we tested the effect of the axial ligand by introducing not only phenylalanine, the third naturally occurring axial ligand in laccases, but also tyrosine, valine, isoleucine, alanine, and threonine. Substitution of the axial methionine by alanine in *Alcaligenes xylosoxidans* nitrite reductase increased E° from 240 to 314 mV [38,39]. Threonine was chosen, because the exchange of the axial methionine with threonine in *Rhodobacter sphaeroides* nitrite reductase led to great changes in the electronic structure [40]. Valine, isoleucine, and tyrosine were identified as interesting candidates for axial ligands with increased E° due to their similarities to leucine and phenylalanine, respectively.

All mutants were expressed in *E. coli* and purified to homogeneity yielding up to 300 mg Ssl1 per liter of culture and their Cu loading was analyzed (see Supporting Information). The correlation between reduction potential and the side chain hydrophobicity of the axial ligand was linear with an R^2 of 0.84 (Fig. 1) with the highest potentials for M295I and M295L. The potential decreased in the row M295F, M295V, M295Y and WT with methionine 295. The reduction potentials of M295A and M295T could not be determined using the ferro/ferricyanide redox couple. They were lower than 290 mV. These results confirm the axial ligand hydrophobicity as an essential contribution to the increase of E° .

3.2. Combination of mutations can further increase reduction potential

However, the axial ligand hydrophobicity is not the only factor influencing the T1 Cu reduction potential. We therefore sought to examine, if the reduction potential of Ssl1 can further be increased by introducing additional mutations in the second sphere of the T1 Cu. In our previous study we found that mutation of M195 and M293 (both located in the putative substrate binding site and in close proximity to the T1 Cu) influenced the reduction potential of Ssl1 (Fig. 2A) [7]. Starting from Ssl1 M295L (456 mV) we first added the M293G mutation and thereby another 40 mV to the T1 Cu reduction potential (Fig. 3).

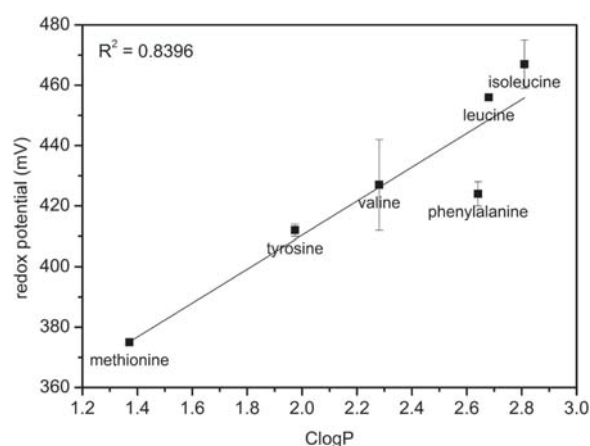


Fig. 1. Correlation of the T1 Cu reduction potential and the ClogP as measure of hydrophobicity of the amino acid residue at the axial position. Values for wildtype (methionine) and M295L (leucine) are from Gunne et al. [7]. The correlation can be described with the following equation: $E^\circ = 298 + 56 \times \text{ClogP}$. Error bars represent SD of triplicates.

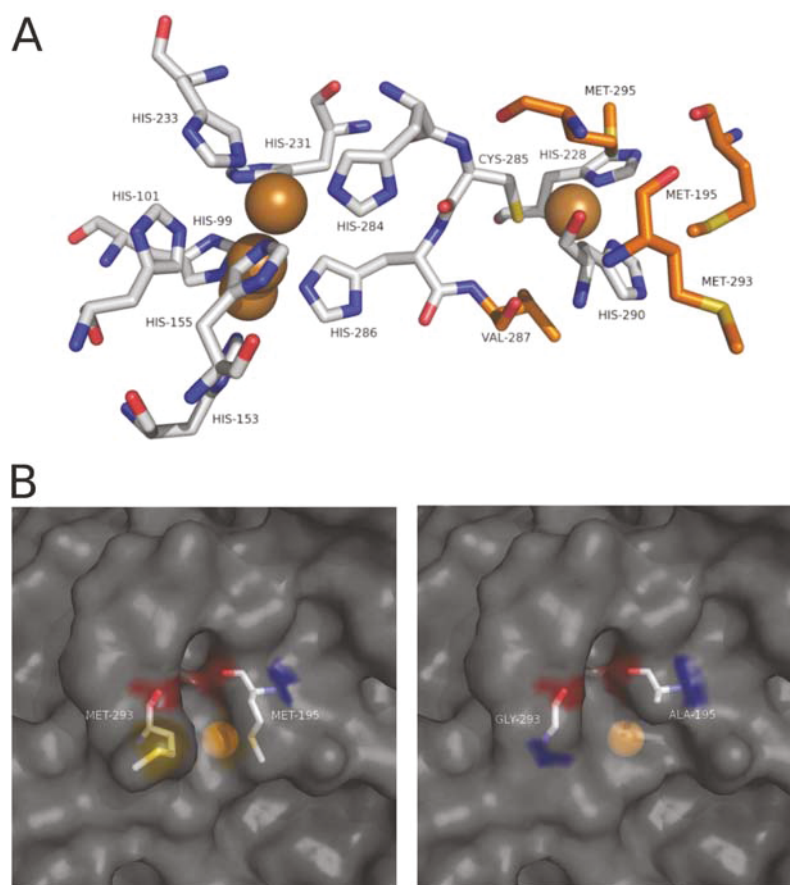


Fig. 2. A) Structure of the Ssl1 active site (PDB 4M3H). Copper ions are depicted as spheres. Positions subjected to mutagenesis are highlighted in orange. B) Location of the M195A and M293G mutations in the putative substrate binding site of Ssl1. The orange sphere represents the T1 Cu ion. Mutations were modeled using the PyMol mutagenesis tool.

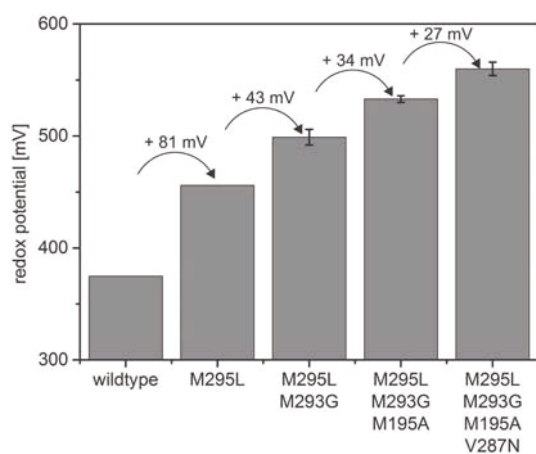


Fig. 3. Increasing T1 Cu reduction potential in Ssl1 mutants. Error bars represent SD of triplicates. Values for wildtype and M295L are from Gunne et al. [7].

The M195A substitution contributed another 30 mV. Both the M195A and M293G mutations should enlarge the putative substrate binding site (Fig. 2B) as previously described for another small laccase SLAC [41].

Electron density near the T1 Cu favors Cu^{II} over Cu^{I} through ionic interactions, thereby lowering E° [14,42]. In Ssl1 the carbonyl oxygen of Y227 is located 4.1 Å away from the T1 Cu (see Fig. S1), possibly contributing electron density to the T1 Cu site. The protein backbone cannot be addressed directly through mutations, but introduction of a hydrogen bond donor in the carbonyl-O vicinity can redirect electron density. Based on the previous mutational studies on azurin [42] and the two-domain small laccase from *Streptomyces coelicolor* (SLAC) [33] we identified V287 as a suitable residue for hydrogen bond formation with the carbonyl-O of Tyr227 and introduced asparagine (Fig. 2A and Fig. S1). The T1 Cu reduction potential in Ssl1 V287N increased by 139 mV to 514 mV, the highest potential measured for single mutants of Ssl1 so far. The Ssl1 reduction potential was increased by another 30 mV after adding the V287N mutation to the triple mutant. The quadruple Ssl1 mutant M195A/V287N/M293G/M295L has a T1 Cu reduction potential of 560 mV, making it a medium-potential laccase (Fig. 3).

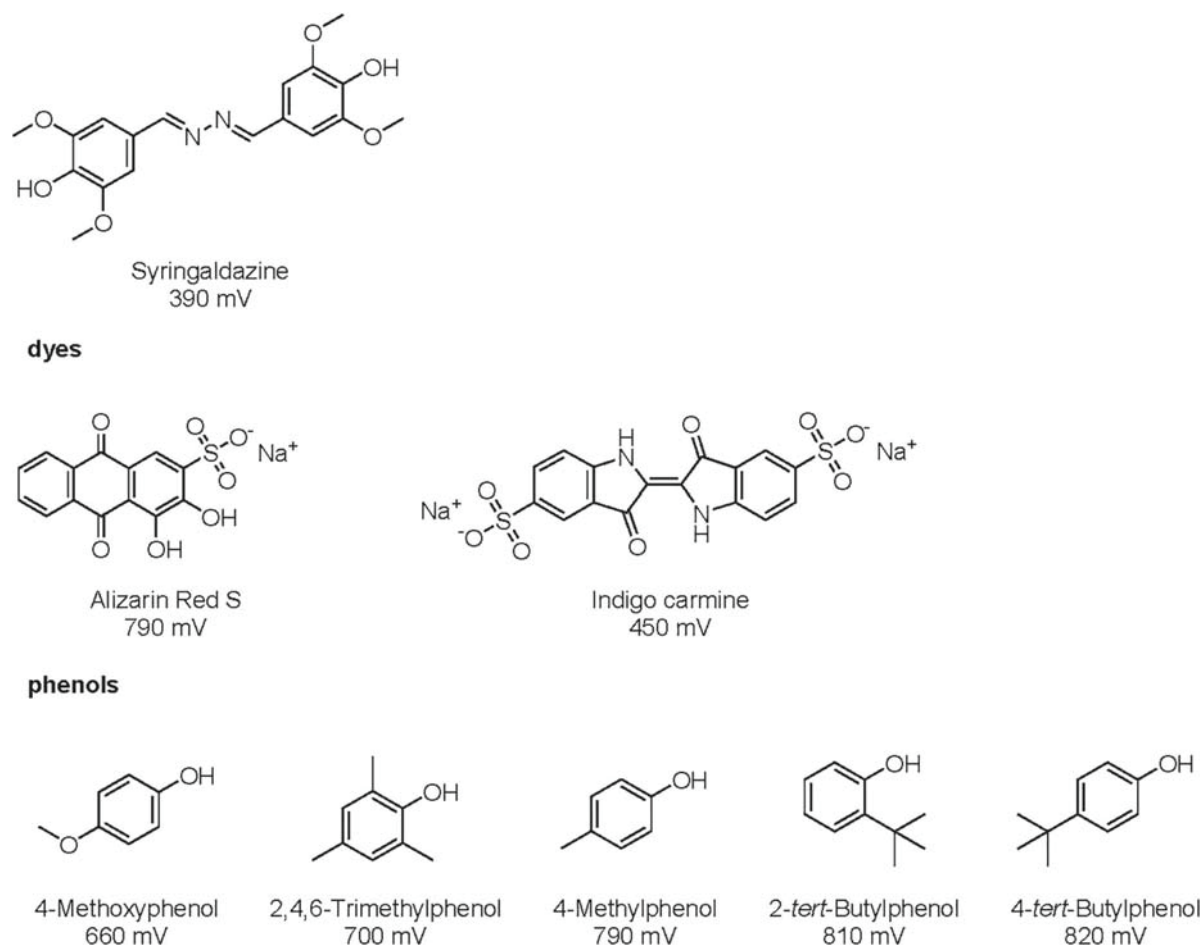


Fig. 4. Tested laccase substrates and the reduction potentials for syringaldazine [43], alizarin red S [45], indigo carmine [46] and phenols [21].

3.3. Activity of Ssl1 variants towards different substrates

For evaluation of the effect of the T1 Cu reduction potential on enzyme activity we tested the typical laccase substrate syringaldazine with a reduction potential of 390 mV at pH 7 [1,43,44], high-potential substrates like the dyes alizarin red S [45] and indigo carmine [46] as well as substituted phenols [21] (Fig. 4). Kinetic constants for syringaldazine oxidation correlated with the difference between the half potentials of T1 Cu and substrate (ΔE°) only partially (Table 1 and Fig. S2). The two mutants M295A and M295T with lower E° as compared to the wild type indeed displayed decreased k_{cat} and increased K_M values and therefore a 100–600-fold decreased catalytic efficiency. The amino acid substitutions M295L, M293G, M195A alone had no or only small effect on K_M . But when included in double or triple mutants, resulted in decreased K_M values which suggests altered substrate binding modes (Table 1).

Although the k_{cat} values decreased for all mutants, two mutants were able to oxidize syringaldazine with increased catalytic efficiency due to lower K_M , namely V287N ($1233 \text{ mM}^{-1} \text{ min}^{-1}$) and M195A/M293G/M295L ($2000 \text{ mM}^{-1} \text{ min}^{-1}$). Surprisingly, the quadruple mutant M195A/V287N/M293G/M295L demonstrated a very low activity, probably due to incomplete copper loading with only 2 Cu per monomer (Table S2). Copper content determination using the bicinchoninic acid method (see Supplemental Information) only gives an

average value for the Cu content and does not provide any information regarding the distribution of Cu ions and the amount of fully Cu loaded and active enzyme in the sample. Changes in the oxidative activity of this mutant cannot be directly attributed to the effects of mutations and the increased reduction potential and we therefore excluded this mutant from further experiments.

Further, the activity tests were performed with the dyes alizarin red S and indigo carmine, which are more difficult to oxidize [7,24]. Our results demonstrated that despite their increasing effect on E° , the mutations M295Y, M295V, and M295F impaired decolorization (Fig. 5). The effect was more pronounced for alizarin red S, where conversion decreased from 55% (with WT) to 10–20%. Variants with isoleucine and leucine in the axial position (M295I, M295L) converted both dyes similarly to the wildtype enzyme. This is in accordance with the previously reported values for wildtype and M295L [7]. For mutants with T1 Cu reduction potential of at least 499 mV, higher activities were observed with both dyes. Out of the mutants with lower E° than that of wild type, only Ssl1 M295A ($< 290 \text{ mV}$) was able to convert indigo carmine (6% in 24 h) but not alizarin red S. Generally, for dye decolorization substitutions enlarging the putative substrate binding site of Ssl1 were more beneficial (Fig. 5).

For a more systematical analysis of the correlation between ΔE° and laccase activity we searched for compounds differing in their potentials but with only small structural differences. Five substituted phenols with

Table 1

Kinetic constants for syringaldazine conversion and T1 Cu redox potentials of Ssl1 variants. Values are given as means of triplicates \pm SD.

	Kinetic constants for syringaldazine			Redox potential [mV]
	K_M [μ M]	k_{cat} [min^{-1}]	k_{cat}/K_M [$\text{mM}^{-1} \text{min}^{-1}$]	
M295A	100 \pm 2.2	0.1 \pm 0.03	1	< 290
M295T	52 \pm 4.1	0.3 \pm 0.07	6	< 290
wildtype	30 \pm 2.7	19 \pm 2.5	633	375 [7]
M293G	43 \pm 8.5	13 \pm 2.3	302	387 \pm 6
M195A	19 \pm 4.4	16 \pm 1.6	842	408 \pm 3
M295Y	190 \pm 53.0	3.7 \pm 1.0	20	412 \pm 2
M295F	37 \pm 2.2	4.9 \pm 0.5	132	424 \pm 4
M295V	80 \pm 3.8	7.6 \pm 1.7	95	427 \pm 15
M295L	27 \pm 1.9	13 \pm 1.1	481	456 [7]
M295I	45 \pm 8.8	7.5 \pm 1.5	167	467 \pm 8
M293G/ M295L	9.0 \pm 0.5	2.8 \pm 0.3	278	499 \pm 7
V287N	3.0 \pm 0.1	3.7 \pm 0.5	1233	514 \pm 7
M195A/ M293G/ M295L	3.7 \pm 0.2	7.4 \pm 1.5	2000	533 \pm 3
M195A/ V287N/ M293G/ M295L	7.5 \pm 1.1	0.004 \pm 0.001	0.533	560 \pm 6

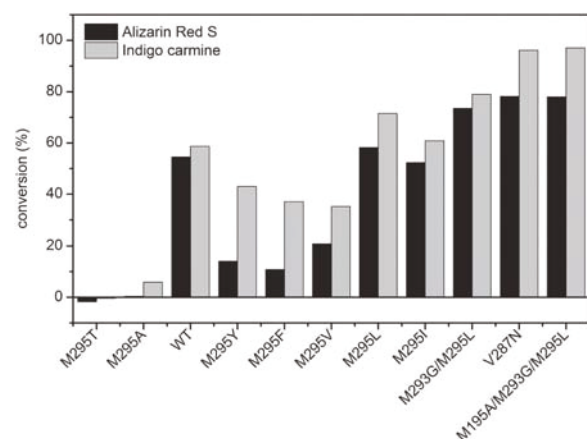


Fig. 5. Conversion of alizarin red S after 4 h (black columns) and indigo carmine after 24 h (grey columns) by Ssl1 wildtype (WT) and variants. Conversion rates are given as means of triplicates. The standard deviation was always < 1.1%.

E° ranging from 660 to 820 mV (Fig. 4) were then tested with the Ssl1 variants.

Although the exact reduction potential of the M295A and M295T mutants could not be determined so far, for ease of comparison these mutants were included in the analysis using a $E^\circ = 290$ mV, because it is the highest possible reduction potential for these variants (Fig. 6 and Fig. S14). Ssl1 M295A and Ssl1 M295T only converted 8 and 5% of 4-methoxyphenol (660 mV) in 24 h but no further substituted phenols. With increasing T1 Cu E° , the conversion rates generally increased and with increasing substrate E° they decreased. While conversions of 4-methoxyphenol (660 mV) were between 59 and 99%, the maximum conversion for 4-*tert*-butylphenol (820 mV) was 29%. For variants with $E^\circ < 500$ mV conversion of 4-*tert*-butylphenol was < 15% (Fig. S14).

It is worth to emphasize that the half potentials of all substituted phenols were higher than the half potentials of all Ssl1 mutants, so that ΔE° in Fig. 6 is negative. Generally, the correlation between ΔE° and

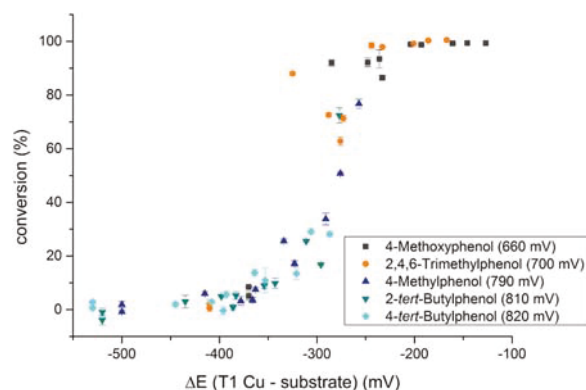


Fig. 6. Correlation between conversion of phenolic compounds and ΔE° . Conversion of 4-methoxyphenol (grey square), 2,4,6-trimethylphenol (orange dot), 4-methylphenol (dark blue triangle), 2-*tert*-butylphenol (cyan triangle), and 4-*tert*-butylphenol (light blue diamond) by laccase variants with different E° was determined after 24 h. Error bars represent SD. (For interpretation of the references to colour in this figure legend, the reader is referred to the web version of this article.)

laccases' activities has a sigmoidal shape with an inflection point at approximately -275 mV (Fig. 6). A detailed analysis reveals that substituted phenols with reduction potential of < 700 mV were oxidized by all Ssl1 mutants (except for the M295A and M295T with the lowest reduction potential) and the phenols with reduction potentials of ≥ 790 mV were oxidized by the Ssl1 variants with reduction potential of ≥ 456 mV.

4. Discussion

4.1. Redox potentials

Replacement of the axial coordinating methionine by a non-coordinating residue like leucine or phenylalanine has been identified as a factor significantly influencing reduction potentials of multicopper oxidases [10]. Further, the hydrophobicity of the axial ligand has been described as the major determinant of the reduction potential for several T1 Cu containing proteins, including azurin, three-domain laccase, nitrite reductase, rusticyanin, and stellacyanin [36]. In our previous work we demonstrated that the T1 Cu reduction potential increased by 81 mV through mutation of the axial methionine to leucine in the small laccase Ssl1 [7]. We now extended our studies towards axial ligands other than the wild-type methionine and leucine. The observed linear correlation between E° and ClogP value confirmed that the hydrophobicity of a non-coordinating axial ligand is the dominant factor for the reduction potential changes also in two-domain laccases. Extrapolation of the reduction potentials for Ssl1 M295A and M295T from the ClogP values (alanine: 1.103; threonine: -0.235) gives theoretical E° values of 360 mV and 285 mV, respectively. That the reduction potential of the M295A mutant is in fact lower than the theoretical value indicates that the amino acid hydrophobicity is not the only contribution to the reduction potential decrease in this case. The axial position of the T1 Cu might become accessible to a water molecule when residues with smaller side chains are introduced. Based on spectroscopic analysis, presence of a water molecule in the axial position was proposed for the M510A and M510T mutants of the cuprous oxidase CueO from *E. coli* [32]. These two mutants also possess lower reduction potentials as compared to the wildtype CueO.

Even though phenylalanine is the axial ligand of T1 Cu sites in high-potential fungal laccases, E° of the Ssl1 M295F mutant was lower (424 mV) than of the M295L mutant (456 mV). Similar effects were observed in the three-domain laccase CotA from *Bacillus subtilis* when

the axial methionine was mutated to leucine or phenylalanine [31]. The M502L mutation increased the T1 Cu reduction potential of CotA from *B. subtilis* by 93 mV (and by 81 mV induced through the homologous mutation in Ssl1), whereas the introduction of phenylalanine led to a smaller reduction potential increase (60 mV in CotA, 49 mV in Ssl1).

Decreasing E° by reverse mutations in fungal laccases has also been described. In the *T. villosa* laccase, the wildtype with phenylalanine as axial ligand had the highest E° (790 mV). Mutation to leucine decreased the reduction potential by 50 mV, and to methionine by 110 mV. Mutation of the leucine to methionine in the high-potential *B. aclada* laccase (720 mV) lowered the T1 Cu reduction potential to 580 mV [47]. In *M. thermophila* and *R. solani* laccases mutation of leucine to phenylalanine had no impact on E° at all [48].

The reduction potential of the Ssl1 variants could further be increased by adding mutations in the second sphere of the T1 Cu, however the observed effect was generally weaker (Fig. 3). By replacing M195 and M293 by a smaller residue like alanine and glycine for enlarging the substrate binding site (Fig. 2B) in the Ssl1 M295L mutant, we achieved further 30–40 mV increases of E° . In contrast to the M195L and M293L mutations, that we previously described [7], this enhancement cannot be attributed to the increased hydrophobicity in the second sphere, because alanine and glycine are less hydrophobic than methionine based on their side chain ClogP values (1.103 and -1.316 , respectively). These alterations might be due to the structural changes of the protein backbone that influence the T1 Cu site. Confirmation of this hypothesis requires structural information from crystallization experiments, which are in progress. By introducing the additional mutation V287N (+27 mV) we created a quadruple mutant with a reduction potential of 560 mV. Our results demonstrate that the M195A, M293G, V287N, and M295L mutations affected the reduction potential not independently, because their individual effects were not additive in the multiple mutants. For example, the M293G mutation led to a +12 mV increase in the wildtype Ssl1 and a +43 mV increase in the M295L mutant. In contrast, the M195A mutation had the same effect in various multiple mutants. The M195A single mutant has a reduction potential of 408 mV (+33 mV compared to the wildtype) and the difference between the M293G/M295L double and the M195A/M293G/M295L triple mutant was +34 mV. Introduction of the fourth mutation V287N to this triple mutant increased the potential by only 27 mV, whereas it led to the largest increase observed for a single mutant (+139 mV compared to the wildtype). Differently, in azurin individual effects of three mutations influencing different aspects of the T1 Cu were additive [42]. However, effects observed in blue copper proteins like azurin containing only one reduction active copper ion are not directly transferrable to multicopper proteins like laccases, where other factors like the presence of the trinuclear cluster also play a role [49]. Possibly, the +139 mV increase in reduction potential of Ssl1 achieved through insertion of asparagine instead of valine 287 might act via the redirection of electron density from a backbone carbonyl through hydrogen bond formation as was described for the azurin mutant F114N (+129 mV) (Fig. S1) [42].

4.2. Laccase activity

Increasing reduction potential and thereby laccase activity has long been of research interest, and the correlation between laccase activity and the reduction potential of the electron accepting copper ion in the active site has been intensively studied [1,21,32,50].

In our study, the Ssl1 activity only partly correlated with the T1 Cu reduction potentials (Fig. S2). For syringaldazine oxidation, replacement of the axial methionine resulted in reduced k_{cat} values. Decrease in k_{cat} was more pronounced for the phenylalanine mutant as shown also for the laccase CotA from *B. subtilis* [31]. However, along with T1

Cu reduction potential, other factors have been described to influence laccase activity and should also be considered during protein engineering for higher laccase activity [51,52]. In some studies, the electronic coupling and the reorganization energy associated with electron transfer were suggested to have a stronger effect on the catalytic activity than ΔE° between the T1 Cu and the substrate [26]. For instance, the M298F mutation of the axial ligand in the SLAC laccase from *S. coelicolor* resulted in increased reduction potential but decreased oxidation activity towards 2,2'-azino-bis(3-ethylbenzothiazoline-6-sulphonic acid (ABTS) and 2,6-dimethoxyphenol (2,6-DMP) [33]. A similar effect was described for the F463M mutant of *T. villosa* laccase with decreased T1 Cu reduction potential which unexpectedly demonstrated increased oxidative activity as compared to the wild type. This was explained by a stronger effect of the changed electronic coupling and/or the reorganization energy as compared to a decreased thermodynamic driving force (ΔG°) and thus a lower k_{ET} [26]. The effect of electronic coupling and reorganization energy associated with electron transfer in Ssl1 should be elucidated in further spectroscopic studies of Ssl1 variants.

Often substrate binding event has a greater effect on activity than the reduction potential, as shown for *M. thermophila* laccase (460 mV) and *P. cinnabarinus* laccase (790 mV) in computational studies [53]. K_{M} values have been shown to correlate with the affinity of the substrates for the T1 binding pocket. Christensen and Kepp developed a model in which active poses should represent short donor-acceptor distances from substrate donor atom to T1 Cu [28]. In our study in the reaction with syringaldazine the amino acid substitutions M295L, M293G, M195A had a small effect on K_{M} , but when combined in the triple mutant (with E° of > 500 mV), resulted in a 3–10-fold decreased K_{M} values and as consequence in increased catalytic efficiencies (Table 1). These strong alterations might result from different syringaldazine binding modes, due to the binding pocket enlarging mutations M195A and M293G. Another effect to be considered for the mutants containing smaller residues in the substrate binding pocket of Ssl1 (M195A and M293G) is a decreased hydrophobic interaction with the substrate as observed in *T. versicolor* laccase mutants F265A and F332A [54].

For oxidation of alizarin red S and indigo carmine we observed the influence of several factors on laccase activity as well. Whereas alizarin red S has a higher potential of 790 mV, indigo carmine with a potential of 450 mV is bulkier and less flexible. Conversions of indigo carmine were unexpectedly lower than those of alizarin red S, which confirms the observation made with other laccases that not only redox features of the substrate (contributing to potential differences), but also substrate structure is important for the effective oxidation by laccase [21]. Apart from steric hindrance that diminishes laccase activity, the substrate geometry that influences the donor-acceptor distance, and the reorganization energy influence laccase activity [55]. In case of alizarin red S, ΔE° is negative for all Ssl1 variants. Our results indicate that the oxidation of alizarin red S may be endergonic by 300–400 mV, because this substrate (790 mV) was oxidized (though with a rather low efficiency) by the wild type Ssl1 (375 mV) and all variants with higher E° (Fig. 5). As activity profiles for alizarin red S and indigo carmine oxidations are similar, and the Ssl1 variants with the enlarged putative binding site were more active (Fig. 5), the steric hindrance issue cannot be excluded for alizarin red S as well.

For the substituted phenols indeed a correlation between activity and E° of the Ssl1 laccases was observed. Similarly to alizarin red S, ΔE° is negative for all Ssl1 variants and the tested phenolic compounds. Our results (Fig. 6) indicate that the oxidation of substituted phenols may be endergonic by no more than 300 mV, similar to previous observations by Tadesse et al., who investigated *M. thermophila* laccase (460 mV) and *T. villosa* laccase (790 mV) [21]. They also found a correlation between the conversion of substituted phenols and the laccase reduction

potential. While *T. villosa* laccase was able to oxidize substrates with E° up to 1.2 V, *M. thermophila* laccase only oxidized substrates with $E^\circ < 800$ mV. For the phenolic compounds we expected the same or at least a very similar binding modes, resulting in similar donor-acceptor distances, and therefore ΔE° as the major factor contributing to the enzyme activity. However, the Ssl1 variants with the highest E° (≥ 514 mV) did not convert 4-methylphenol, 2-*tert*-butylphenol and 4-*tert*-butylphenol (with very similar E° values of 790, 810, and 820 mV, respectively) to the same extent (Fig. S14). The decreased activity towards 2-*tert*-butylphenol and 4-*tert*-butylphenol can be explained by the fact that although *tert*-butyl is electron donating, this bulky alkyl group has a strong steric effect which obviously influences substrate affinity and thus laccase activity.

In summary, in this study we demonstrated that that hydrophobicity of the axial ligand is the major determinant for the reduction potential changes observed in mutants of the small two-domain laccase Ssl1 from *S. sviveus*. By combining substitutions of the axial ligand with mutations in the second sphere of the T1 Cu we developed a middle-potential bacterial laccase with a reduction potential of 560 mV. The Ssl1 variants with $E^\circ \geq 500$ mV enabled oxidation of 4-methylphenol, 2-*tert*-butylphenol and 4-*tert*-butylphenol, which were not accepted as substrates by the wild type enzyme (375 mV). Laccase activity towards substituted phenols correlated with the difference in reduction potentials of the substrates and T1 Cu. For the dyes alizarin red S and indigo carmine such correlation was observed for the Ssl1 variants with $E^\circ > 450$ mV. Our results demonstrate that the difference in reduction potentials of the substrate and the T1 Cu is not the only factor that influence the activity of Ssl1 variants. For indigo carmine, alizarin red S and the *tert*-butyl substituted phenols steric hindrance/substrate affinity have a strong effect on laccase activity.

Abbreviations

CV	column volume
FPLC	fast performance liquid chromatography
HPLC	high performance liquid chromatography
IMAC	immobilized metal ion affinity chromatography
IPTG	isopropyl β -D-1-thiogalactopyranoside
SGZ	syringaldazine
T1 Cu	Type 1 copper
T2 Cu	Type 2 copper
T3 Cu	Type 3 copper
TNC	trinuclear cluster

Declaration of competing interest

The authors declare no competing interest.

Acknowledgments

We thank the Heinrich Heine University Düsseldorf for financial support.

Funding

This research did not receive any specific grant from funding agencies in the public, commercial, or not-for-profit sectors.

Appendix A. Supplementary data

Supplementary data to this article can be found online at <https://doi.org/10.1016/j.jinorgbio.2019.110843>.

References

- [1] F. Xu, *Biochemistry* 35 (1996) 7608–7614.
- [2] F. Xu, W. Shin, S.H. Brown, J.A. Wahleithner, U.M. Sundaram, E.I. Solomon, *Biochim. Biophys. Acta* 1292 (1996) 303–311.
- [3] C.F. Thurston, *Microbiology* 140 (1994) 19–26.
- [4] N. Hakulinen, J. Rouvinen, *Cell. Mol. Life Sci.* 72 (2015) 857–868.
- [5] B. Reinhammar, B. Malmström, "Blue" copper-containing oxidases, in: T.G. Spiro (Ed.), *Copper Proteins*, 3 Wiley, New York, 1981, pp. 109–149.
- [6] S. Tishchenko, A. Gabdulkhakov, L. Trubitsina, A. Lisov, M. Zakharova, A. Leontievsky, *Acta Crystallogr. Sect. F Struct. Biol. Cryst. Commun.* 71 (2015) 1200–1204.
- [7] M. Gunne, A. Höppner, P.L. Hagedoorn, V.B. Urlacher, *FEBS J.* 281 (2014) 4307–4318.
- [8] T. Skállová, J. Dohnálek, L.H. Østergaard, P.R. Østergaard, P. Kolenko, J. Dušková, A. Štěpánková, J. Hašek, *J. Mol. Biol.* 385 (2009) 1165–1178.
- [9] H.B. Gray, B.G. Malmstrom, R.J. Williams, *J. Biol. Inorg. Chem.* 5 (2000) 551–559.
- [10] S.M. Jones, E.I. Solomon, *Cell. Mol. Life Sci.* 72 (2015) 869–883.
- [11] T. Sakurai, K. Kataoka, *Cell. Mol. Life Sci.* 64 (2007) 2642–2652.
- [12] S. Shleev, J. Tkac, A. Christenson, T. Ruzgas, A.I. Yaropolov, J.W. Whittaker, L. Gorton, *Biosens. Bioelectron.* 20 (2005) 2517–2554.
- [13] L. Hu, M. Farrokhnia, J. Heimdal, S. Shleev, L. Rulisek, U. Ryde, *J. Phys. Chem. B* 115 (2011) 13111–13126.
- [14] H. Li, S.P. Webb, J. Ivanic, J.H. Jensen, *J. Am. Chem. Soc.* 126 (2004) 8010–8019.
- [15] N.J. Fowler, C.F. Blanford, J. Warwicker, S.P. de Visser, *Chem. Eur. J.* 23 (2017) 15436–15445.
- [16] E.I. Solomon, D.E. Heppner, E.M. Johnston, J.W. Ginsbach, J. Cirera, M. Qayyum, M.T. Kieber-Emmons, C.H. Kjaergaard, R.G. Hadt, L. Tian, *Chem. Rev.* 114 (2014) 3659–3853.
- [17] E.I. Solomon, P. Chen, M. Metz, S.-K. Lee, A.E. Palmer, *Angew. Chem. Int. Ed.* 40 (2001) 4570–4590.
- [18] E.I. Solomon, C.H. Kjaergaard, D.E. Heppner, Molecular properties and reaction mechanism of multicopper oxidases related to their use in biofuel cells, in: A. Lewenstam, L. Gorton (Eds.), *Electrochemical Processes in Biological Systems*, Vol. 248, John Wiley & Sons, Hoboken, NJ, 2015, pp. 169–212.
- [19] E.I. Solomon, U.M. Sundaram, T.E. Machonkin, *Chem. Rev.* 96 (1996) 2563–2606.
- [20] R.A. Marcus, N. Sutin, *Biochim. Biophys. Acta* 811 (1985) 265–322.
- [21] M.A. Tadesse, A. D'Annibale, C. Galli, P. Gentili, F. Sergi, *Org. Biomol. Chem.* 6 (2008) 868–878.
- [22] F. Xu, J.J. Kulyts, K. Duke, K. Li, K. Krikstopaitis, H.J. Deussen, E. Abbate, V. Galinyte, P. Schneider, *Appl. Environ. Microbiol.* 66 (2000) 2052–2056.
- [23] F. Xu, T. Damhus, S. Danielsen, L.H. Østergaard, Catalytic applications of laccase, in: R.D. Schmid, V.B. Urlacher (Eds.), *Modern Biooxidation: Enzymes, Reactions and Applications*, Wiley-VCH, Weinheim, 2007, pp. 43–75.
- [24] O. Glazunova, N. Trushkin, K. Moiseenko, I. Filimonov, T. Fedorova, *Catalysts* 8 (2018) 152.
- [25] G. Hong, D.M. Ivnitki, G.R. Johnson, P. Atanassov, R. Pachter, *J. Am. Chem. Soc.* 133 (2011) 4802–4809.
- [26] F. Xu, A.E. Palmer, D.S. Yaver, R.M. Berka, G.A. Gambetta, S.H. Brown, E.I. Solomon, *J. Biol. Chem.* 274 (1999) 12372–12375.
- [27] A. Warshel, P.K. Sharma, M. Kato, Y. Xiang, H. Liu, M.H. Olsson, *Chem. Rev.* 106 (2006) 3210–3235.
- [28] N.J. Christensen, K.P. Kepp, *J. Mol. Catal. B-Enzym* 100 (2014) 68–77.
- [29] Z.B. Guan, Q. Luo, H.R. Wang, Y. Chen, X.R. Liao, *Cell. Mol. Life Sci.* 75 (2018) 3569–3592.
- [30] D.M. Mate, M. Alcalde, *Microb. Biotechnol.* 10 (2017) 1457–1467.
- [31] P. Durao, I. Bento, A.T. Fernandes, E.P. Melo, P.F. Lindley, L.O. Martins, *J. Biol. Inorg. Chem.* 11 (2006) 514–526.
- [32] S. Kurose, K. Kataoka, N. Shinohara, Y. Miura, M. Tsutsumi, S. Tsujimura, K. Kano, T. Sakurai, *Bull. Chem. Soc. Jpn.* 82 (2009) 504–508.
- [33] A. Prins, L. Kleinsmidt, N. Khan, B. Kirby, T. Kudanga, J. Vollmer, J. Pleiss, S. Burton, M. Le Roes-Hill, *Enzym. Microb. Technol.* 68 (2015) 23–32.
- [34] M. Gunne, V.B. Urlacher, *PLoS One* 7 (2012) e52360.
- [35] M.M. Bradford, *Anal. Biochem.* 72 (1976) 248–254.
- [36] D.K. Garner, M.D. Vaughan, H.J. Hwang, M.G. Savelieff, S.M. Berry, J.F. Honek, Y. Lu, *J. Am. Chem. Soc.* 128 (2006) 15608–15617.
- [37] D.J. Abraham, A.J. Leo, *Proteins: Structure, Function, and Bioinformatics* 2 (1987) 130–152.
- [38] M.J. Ellis, M. Prudencio, F.E. Dodd, R.W. Strange, G. Sawers, R.R. Eady, S.S. Hasnain, *J. Mol. Biol.* 316 (2002) 51–64.
- [39] O. Farver, R.R. Eady, G. Sawers, M. Prudencio, I. Pecht, *FEBS Lett.* 561 (2004) 173–176.
- [40] L. Basumallick, R.K. Szilagy, Y. Zhao, J.P. Shapleigh, C.P. Scholes, E.I. Solomon, *J. Am. Chem. Soc.* 125 (2003) 14784–14792.
- [41] M.D. Toscano, L. De Maria, S. Lobedanz, L.H. Østergaard, *ChemBioChem* 14 (2013) 1209–1211.
- [42] N.M. Marshall, D.K. Garner, T.D. Wilson, Y.-G. Gao, H. Robinson, M.J. Nilges, Y. Lu, *Nature* 462 (2009) 113–116.
- [43] P. Hapiot, J. Pinson, P. Neta, C. Rolando, *J. Electroanal. Chem. (Lausanne Switz.)* 353 (1993) 225–235.
- [44] M. Frasconi, G. Favero, H. Boer, A. Koivula, F. Mazzei, *Biochim. Biophys. Acta* 1804 (2010) 899–908.
- [45] H.-P. Dai, K.-K. Shiu, *Electrochim. Acta* 43 (1998) 2709–2715.
- [46] J. Carretero-Gonzalez, E. Castillo-Martinez, M. Armand, *Energy Environ. Sci.* 9 (2016) 3521–3530.

- [47] E. Osipov, K. Polyakov, R. Kittl, S. Shleev, P. Dorovatovsky, T. Tikhonova, S. Hann, R. Ludwig, V. Popov, *Acta Crystallogr. Sect. D. Biol. Crystallogr.* 70 (2014) 2913–2923.
- [48] F. Xu, R.M. Berka, J.A. Wahleithner, B.A. Nelson, J.R. Shuster, S.H. Brown, A.E. Palmer, E.I. Solomon, *Biochem. J.* 334 (1998) 63–70.
- [49] A.J. Augustine, M.E. Kragh, R. Sarangi, S. Fujii, B.D. Liboiron, C.S. Stoj, D.J. Kosman, K.O. Hodgson, B. Hedman, E.I. Solomon, *Biochemistry* 47 (2008) 2036–2045.
- [50] I. Mateljak, E. Monza, M.F. Lucas, V. Guallar, O. Aleksejeva, R. Ludwig, D. Leech, S. Shleev, M. Alcalde, *ACS Catal.* 9 (2019) 4561–4572.
- [51] E. Monza, M.F. Lucas, S. Camarero, L.C. Alejaldre, A.T. Martinez, V. Guallar, *J. Phys. Chem. Lett.* 6 (2015) 1447–1453.
- [52] G. Santiago, F. de Salas, M.F. Lucas, E. Monza, S. Acebes, A.T. Martinez, S. Camarero, V. Guallar, *ACS Catal.* 6 (2016) 5415–5423.
- [53] M.F. Lucas, E. Monza, L.J. Jørgensen, H.A. Ernst, K. Piontek, M.J. Bjerrum, A.T. Martinez, S. Camarero, V. Guallar, *J. Chem. Theory Comput.* 13 (2017) 1462–1467.
- [54] C. Galli, P. Gentili, C. Jolivald, C. Madzak, R. Vadalà, *Appl. Microbiol. Biotechnol.* 91 (2011) 123–131.
- [55] R. Mehra, K.P. Kepp, *Phys. Chem. Chem. Phys.* 21 (2019) 15805–15814.

Supplementary Information

Correlation between the T1 copper reduction potential and catalytic activity of a small laccase

Anna C. Olbrich, Jan N. Schild, Vlada B. Urlacher*

Institute of Biochemistry, Heinrich-Heine-University Düsseldorf, Universitätsstr. 1, 40225 Düsseldorf, Germany

*Corresponding author: Vlada B. Urlacher

phone: +49-211-811-3889, email: Vlada.Urlacher@uni-duesseldorf.de

Experimental

Determination of copper concentration using bicinchoninic acid

The copper content of Ssl1 variants was determined using bicinchoninic acid following the method of Brenner & Harris [1]. 150 μ L of 15 μ M Ssl1 solutions were mixed with 50 μ L of trichloroacetic acid (0.3 g/mL). Precipitated proteins were separated by centrifugation and 100 μ L of the supernatant were transferred to microtiter plates, mixed with 20 μ L of freshly prepared ascorbic acid (2 mM), followed by 80 μ L of BCA reagent. After incubation for 10 min at room temperature, the absorption at 354 and 562 nm were measured on a Tecan Infinite PRO 200 (Tecan, Männedorf, Switzerland) microplate reader. Copper concentrations from 0 to 80 μ M were used as standard.

Site-directed mutagenesis

Table S1. Oligonucleotides used for QuikChange mutagenesis

mutation	sequence
M295F	forward C TCC GAC ATG GGG <u>TTT</u> GTG GGC CTG TTC reverse GAA CAG GCC CAC <u>AAA</u> CCC CAT CTC GGA G
M295A	forward C TCC GAC ATG GGG <u>GCG</u> GTG GGC CTG TTC reverse GAA CAG GCC CAC <u>CGC</u> CCC CAT CTC GGA G
M295T	forward C TCC GAC ATG GGG <u>ACC</u> GTG GGC CTG TTC reverse GAA CAG GCC CAC <u>GGT</u> CCC CAT CTC GGA G
M295V	forward C TCC GAC ATG GGG <u>GTG</u> GTG GGC CTG TTC reverse GAA CAG GCC CAC <u>CAC</u> CCC CAT CTC GGA G
M295Y	forward C TCC GAC ATG GGG <u>TAT</u> GTG GGC CTG TTC reverse GAA CAG GCC CAC <u>ATA</u> CCC CAT CTC GGA G
M295I	forward C TCC GAC ATG GGG <u>ATC</u> GTG GGC CTG TTC reverse GAA CAG GCC CAC <u>GAT</u> CCC CAT CTC GGA G
M293G/M295L	forward GC CAC TCC GAC <u>GGC</u> GGG <u>CTG</u> GTG GG reverse CC CAC <u>CAG</u> CCC <u>GCC</u> GTC GGA GTG GC
M195A	forward ATC GTC TTC AAC GAC <u>GCG</u> CTC ATC AAC AAC AGG reverse CCT GTT GTT GAT GAG <u>CGC</u> GTC GTT GAA GAC GAT
M293G	forward GC CAC TCC GAC <u>GGC</u> GGG ATG GTG GG reverse CC CAC CAT CCC <u>GCC</u> GTC GGA GTG GC
V287N	forward G TAC CAC TGC CAT <u>AAC</u> CAG AGC CAC TCC reverse GGA GTG GCT CTG <u>GTT</u> ATG GCA GTG GTA C

Results

Copper content

Table S2. Copper contents of purified Ssl1 variants

	copper content
	[Cu/laccase]
wildtype	3.9
M295L	3.1
M295F	2.9
M295A	5.0
M295T	3.7
M295V	3.9
M295Y	3.2
M295I	2.9
M195A	3.0
M293G	3.4
M293G/M295L	3.0
M195A/M293G/M295L	3.4
M195A/V287N/M293G/M295L	2.0
V287N	3.0

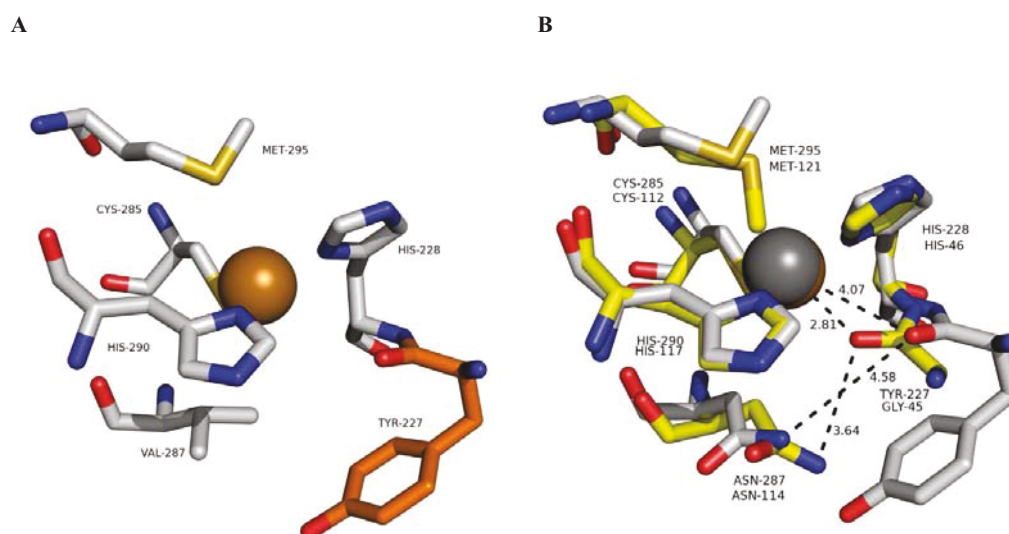


Figure S1. **A)** The carbonyl-O of Tyr227 is located close (4.07 Å distance) to the T1 Cu (PDB 4M3H). **B)** Comparison of the T1 Cu site of the azurin mutant N47S F114N (PDB 3JTB) and a model for the Ssl1 V287N mutant created from 4M3H using the Pymol mutagenesis tool. Dashed lines give distances in Å.

Determination of catalytic constants for syringaldazine conversion

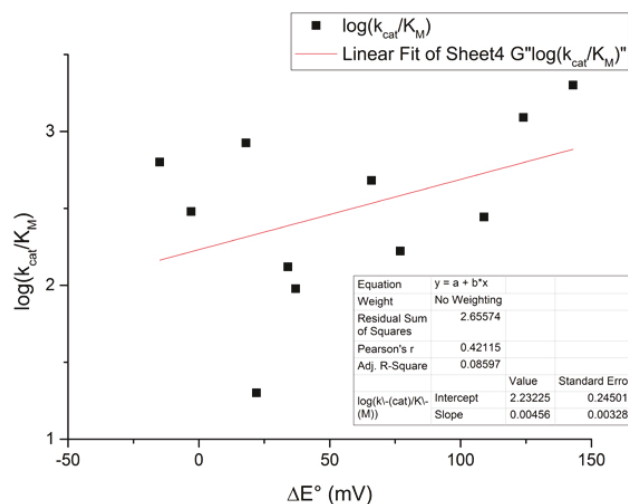


Figure S2: The rate constant k_{cat}/K_M does not correlate with the potential difference between T1 Cu and substrate.

Table S3: Kinetic constants for syringaldazine conversion by SslI variants and the protein concentrations used for calculation of k_{cat} . Concentrations were determined using the Bradford assay.

	K_M [μ M]					v_{max} [μ M]					protein concentration [μ M]		k_{cat} [min^{-1}]	
	1	2	3	mean	SD	1	2	3	mean	SD	SD	SD	mean	SD
M295A	97	100	102	100	2.2	2.07	2.33	2.45	2.28	0.20	18.01	2.01	0.1	0.03
M295T	55	47	53	52	4.1	1.70	1.82	2.24	1.92	0.28	6.72	0.69	0.3	0.07
wildtype	30	28	33	30	2.7	7.48	7.70	8.44	7.87	0.50	0.41	0.03	19	2.5
M295Y	225	129	216	190	53.0	5.13	3.83	4.84	4.60	0.68	1.23	0.13	3.7	1.0
M295V	77	84	79	80	3.8	4.78	5.04	4.73	4.85	0.16	0.64	0.12	7.6	1.7
M295F	35	37	39	37	2.2	5.72	5.94	6.25	5.97	0.26	1.22	0.06	4.9	0.5
M295L	29	27	25	27	1.9	6.90	7.07	7.13	7.04	0.12	0.54	0.04	13	1.1
M295I	51	50	35	45	8.8	4.90	4.97	4.08	4.65	0.50	0.62	0.06	7.5	1.5
M293G/ M295L	8.9	9.6	8.6	9.0	0.5	1.76	1.82	1.77	1.78	0.03	0.64	0.06	2.8	0.3
V287N	3.0	3.1	2.9	3.0	0.1	1.88	1.86	1.87	1.87	0.01	0.51	0.07	3.7	0.5
M195A/ M293G/ M295L	3.8	3.7	3.4	3.7	0.2	3.02	3.10	3.12	3.08	0.06	0.41	0.08	7.4	1.5
M195A/ V287N/ M293G/ M295L	8.8	7.1	6.8	7.5	1.1	0.34	0.28	0.26	0.29	0.04	73.69	2.11	0.004	0.0007
M293G	35	44	52	44	8.5	5.09	5.71	6.53	5.78	0.72	0.45	0.02	13	2.3
M195A	24	19	15	19	4.4	9.65	9.65	9.54	9.61	0.07	0.60	0.05	16	1.6

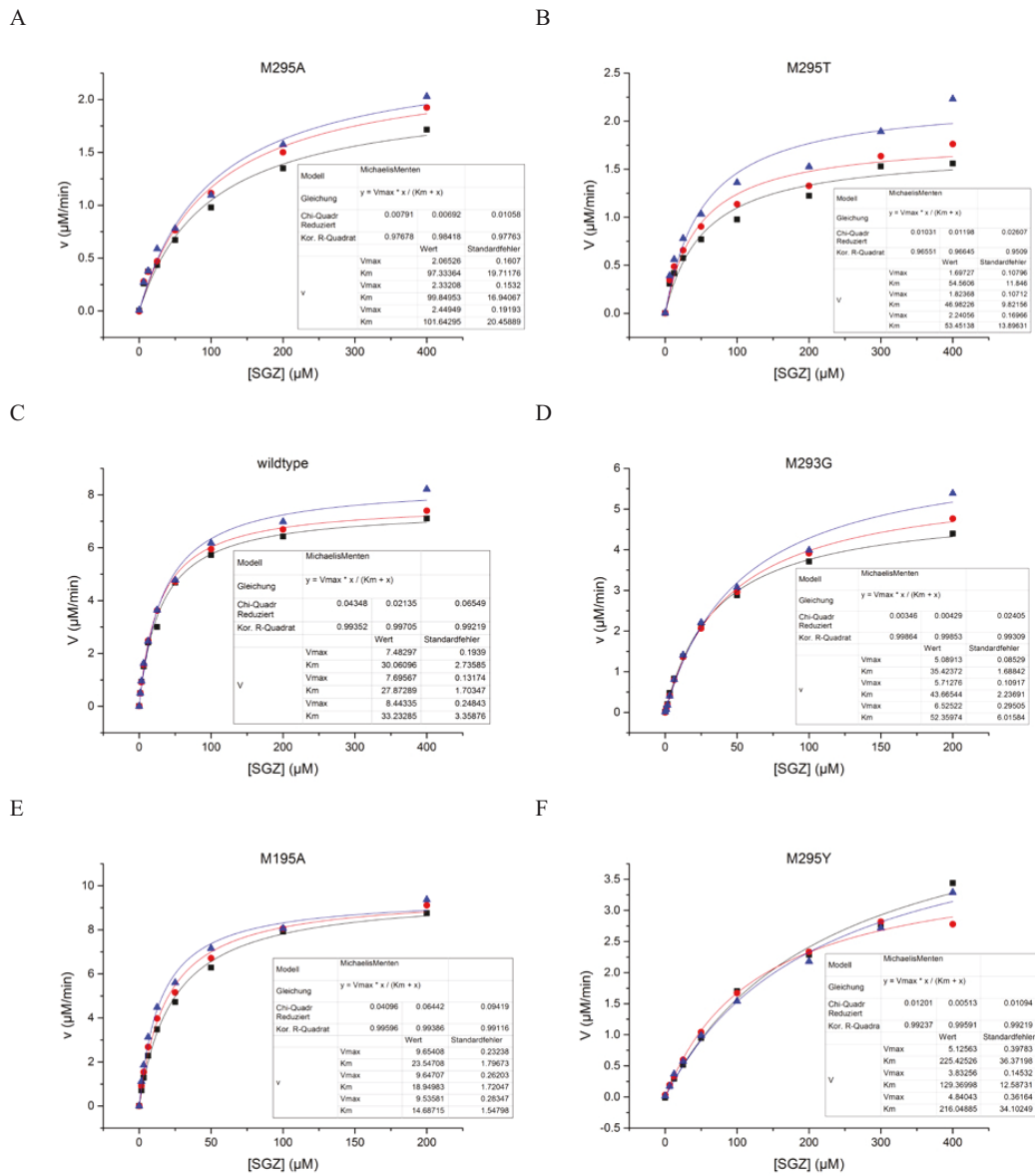
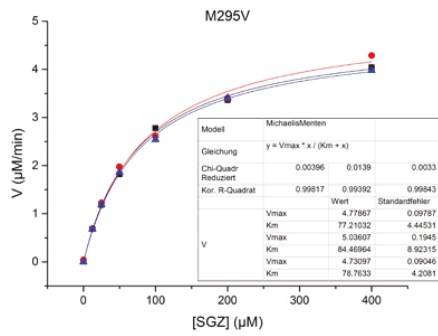
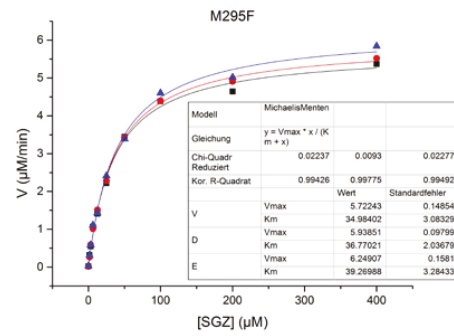


Figure S3: Syringaldazine oxidation by SslI variants. Data points were fitted to the Michaelis-Menten-Equation in Origin.

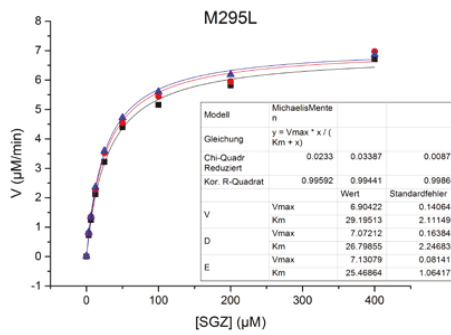
G



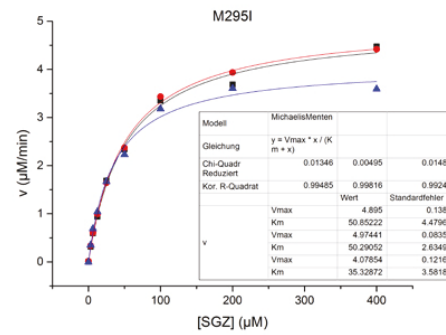
H



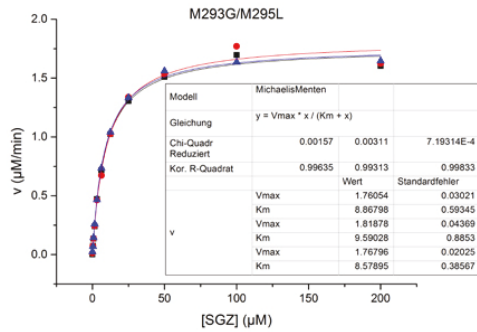
I



J



K



L

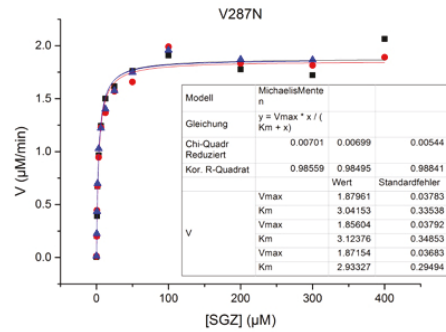
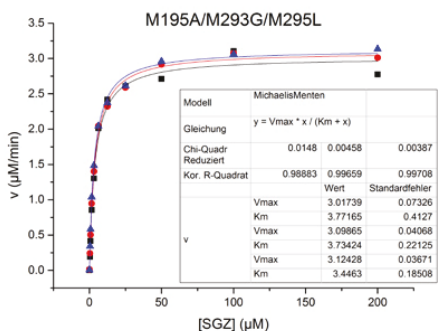


Figure S3 continued.

M



N

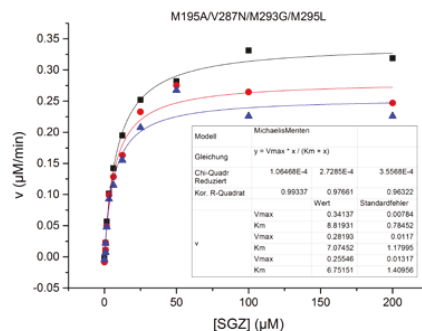
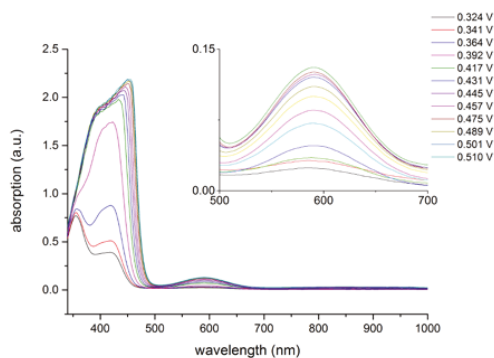


Figure S3 continued.

Redox titrations

Example spectra M295F

A



B

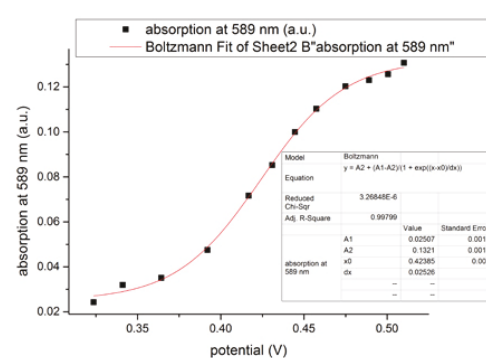
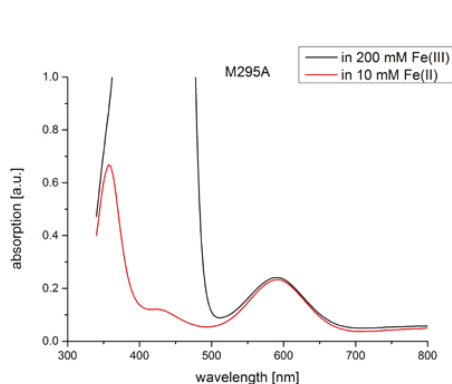


Figure S4. Determination of the T1 Cu redox potential using spectrophotometric redox titrations. (A) Spectra recorded after each titration step. Inset shows decreasing absorption of the T1 Cu at 600 nm upon reduction. (B) Absorption of the T1 Cu at 589 nm as a function of the potential.

The T1 Cu of M295A and M295T was not reduced in the presence of 10 mM potassium hexacyanidoferrate(II) their redox potentials must be less than 290 mV, the lowest potential we set using a mixture of Fe(III) and Fe(II) during titrations.

A



M295T

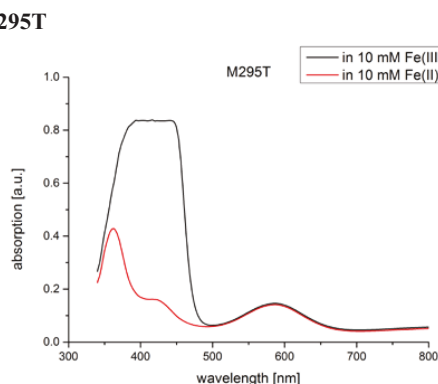
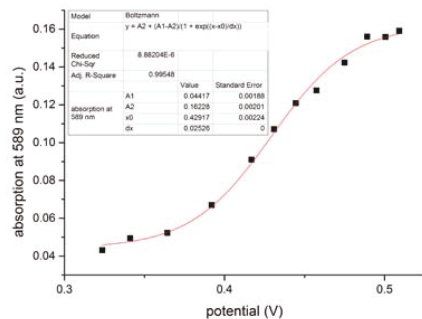


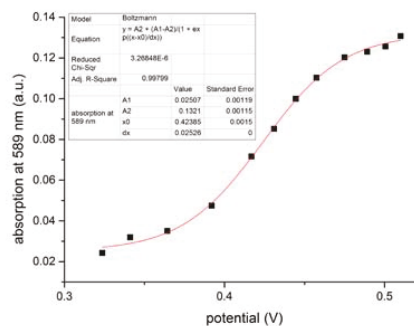
Figure S5: Absorption spectra of 50 µM M295A (A) and M295T (B) in 10 mM HEPES (pH 7.0) and potassium hexacyanidoferrate(II) or potassium hexacyanoferrate(III).

M295F

A



B



C

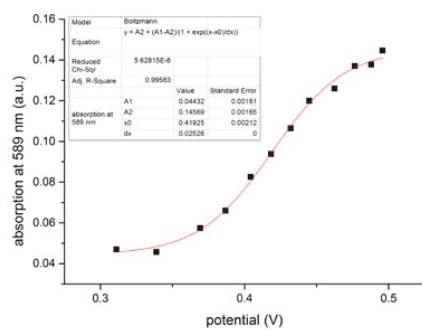
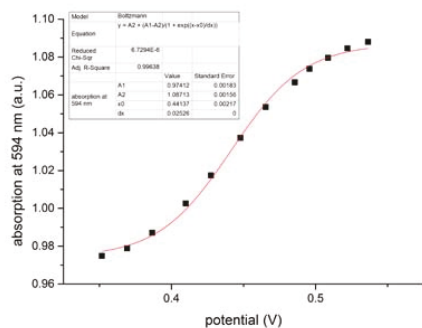


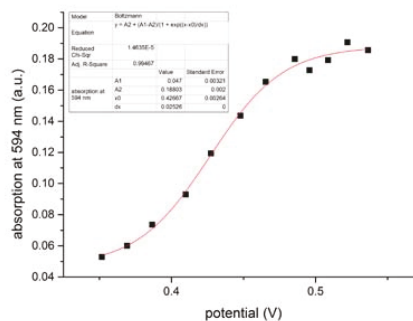
Figure S6: Titration curves for Ssl1 M295F. The potentials obtained from fitting to the Nernst equation in origin were (A) 429 mV, (B) 424 mV, and (C) 419 mV, respectively.

M295V

A



B



C

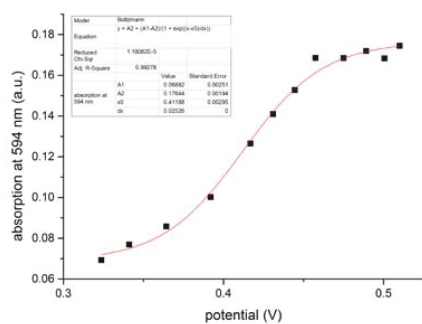
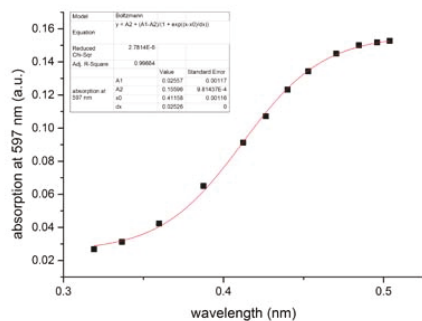


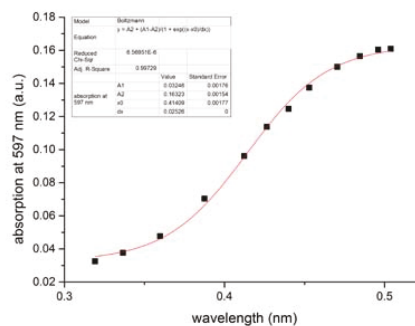
Figure S7: Titration curves for Ssl1 M295V. The potentials obtained from fitting to the Nernst equation in origin were (A) 441 mV, (B) 427 mV, and (C) 412 mV, respectively.

M295Y

A



B



C

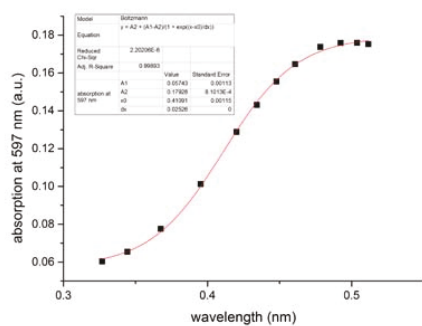


Figure S8: Titration curves for Ssl1 M295Y. The potentials obtained from fitting to the Nernst equation in origin were (A) 412 mV, (B) 414 mV, and (C) 411 mV, respectively.

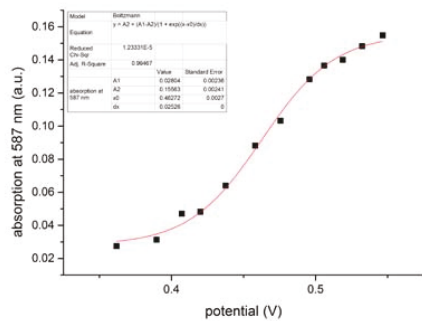
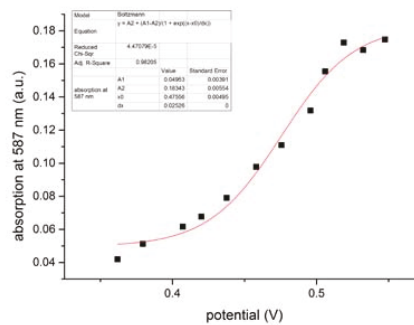
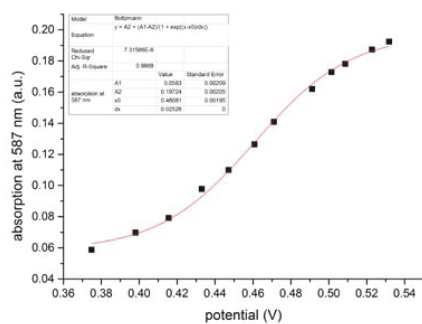
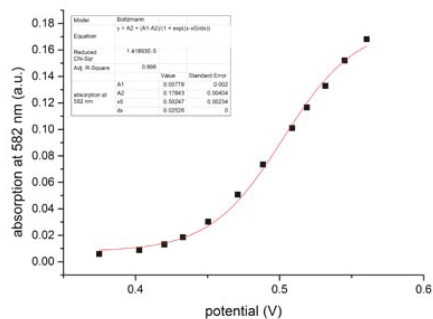
M295I
A

B

C


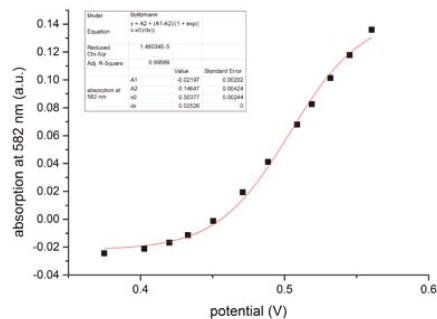
Figure S9: Titration curves for Ssl1 M295I. The potentials obtained from fitting to the Nernst equation in origin were (A) 463 mV, (B) 476 mV, and (C) 461 mV, respectively.

M293G/M295L

A



B



C

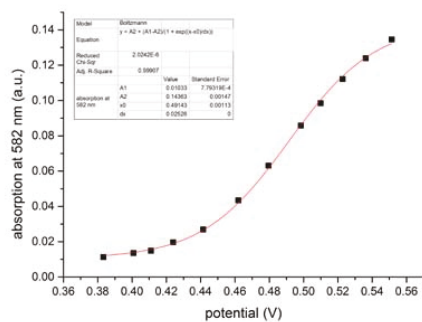
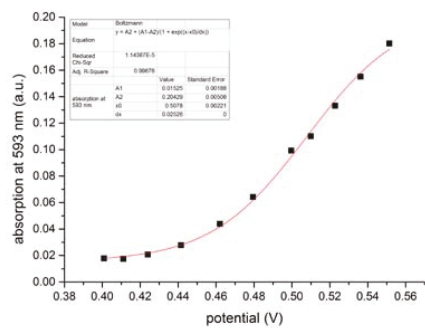


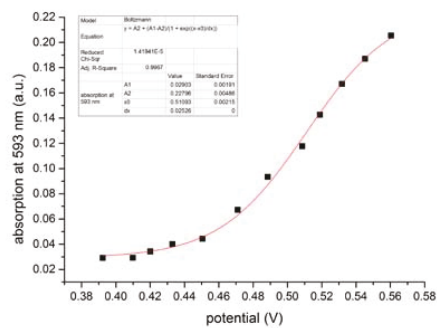
Figure S10: Titration curves for Ssl1 M293G/M295L. The potentials obtained from fitting to the Nernst equation in origin were (A) 502 mV, (B) 504 mV, and (C) 491 mV, respectively.

V287N

A



B



C

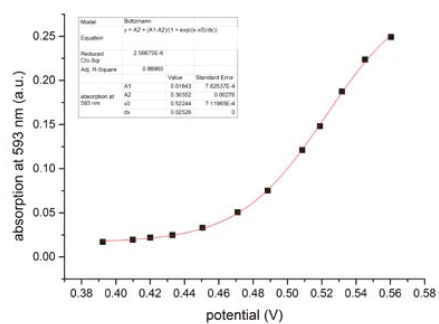
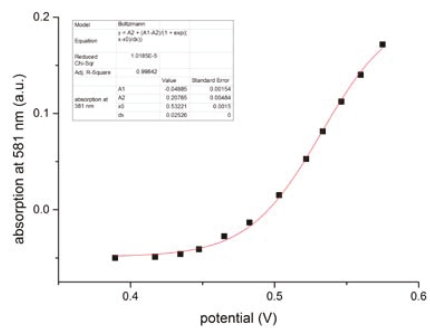


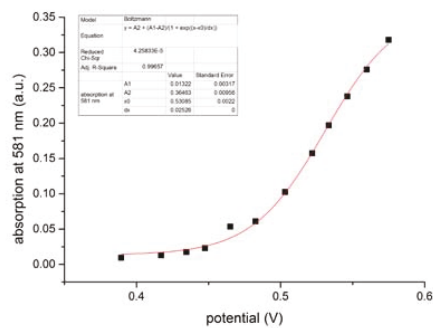
Figure S11: Titration curves for Ssl1 V287N. The potentials obtained from fitting to the Nernst equation in origin were (A) 508 mV, (B) 511 mV, and (C) 522 mV, respectively.

M195A/M293G/M295L

A



B



C

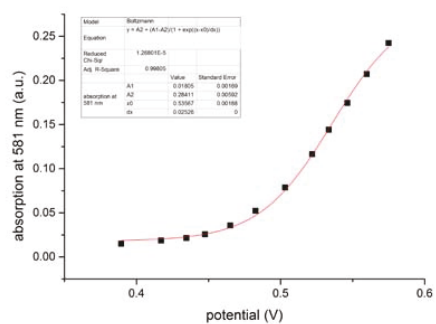
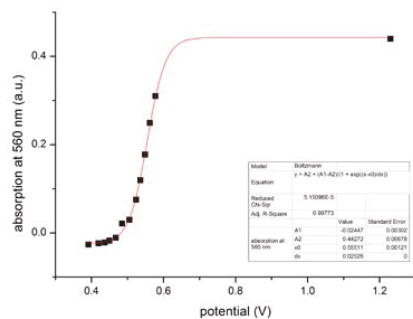


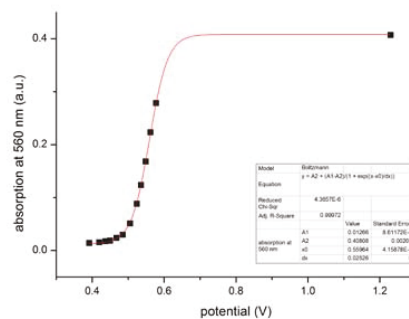
Figure S12: Titration curves for Ssl1 M195A/M293G/M295L. The potentials obtained from fitting to the Nernst equation in origin were (A) 532 mV, (B) 531 mV, and (C) 536 mV, respectively.

M195A/V287N/M293G/M295L

A



B



C

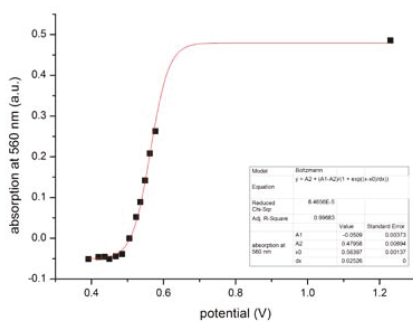


Figure S13: Titration curves for Ssl1 M195A/M293G/M295L. The absorption of the fully oxidized enzyme was set to 1.23 V. The potentials obtained from fitting to the Nernst equation in origin were (A) 555 mV, (B) 560 mV, and (C) 564 mV, respectively.

Conversion of phenolic compounds

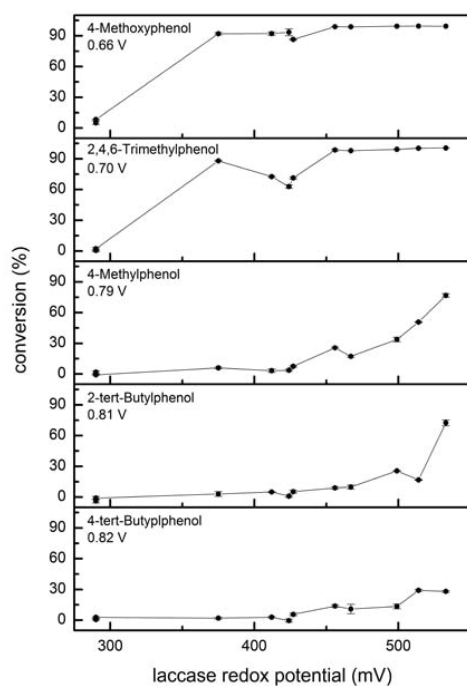


Figure S14: Conversion of phenolic compounds by laccase variants with different T1 Cu reduction potentials. Error bars represent SD.

References

- [1] A.J. Brenner, E.D. Harris, *Anal. Biochem.* 226 (1995) 80-84.

5 Manuscript 2: Influence of the T1 Cu axial ligand on kinetic, spectral, and structural properties of the laccase Ssl1 from *Streptomyces sviveus*

Title: Influence of the T1 Cu axial ligand on kinetic, spectral, and structural properties of the laccase Ssl1 from *Streptomyces sviveus*

Authors: Anna C. Olbrich, Steffen Mielenbrink, Vivian P. Willers, George E. Cutsail III, James A. Birrell, Ingrid Span, Vlada B. Urlacher

Contribution: Expression and purification of Ssl1 variants for CD, UV/Vis and crystallization
Collection of UV/Vis spectra
Analysis and interpretation of CD and UV/Vis spectra and the stopped-flow data
Supervision of master thesis of Vivian P. Willers (Production of T2D variants and their characterization, stopped-flow measurements, and evaluation of the data)
Writing the manuscript except for X-ray crystallography and EPR-related parts

Influence of the T1 Cu axial ligand on kinetic, spectral, and structural properties of the laccase Ssl1 from *Streptomyces sviveus*

Authors

Anna C. Olbrich^{a†}, Steffen Mielenbrink^{b†}, Vivian P. Willers^a, George E. Cutsail III^c, James A. Birrell^c,
Ingrid Span^{b*}, Vlada B. Urlacher^{a*}

*corresponding authors: Vlada.Urlacher@hhu.de, Ingrid.Span@hhu.de

† These authors contributed equally.

^a Institut für Biochemie, Heinrich-Heine-Universität Düsseldorf, Universitätsstr. 1, 40225 Düsseldorf, Germany

^b Institut für Physikalische Biologie, Heinrich-Heine-Universität Düsseldorf, Universitätsstr. 1, 40225 Düsseldorf, Germany

^c Max Planck Institute for Chemical Energy Conversion, Stiftstr. 34-36, 45470 Mülheim an der Ruhr, Germany

Abstract

Laccases are multicopper oxidases which couple the oxidation of substrates at a type 1 (T1) copper site to the reduction of O₂ to H₂O. The T1 Cu in bacterial two-domain laccases has four ligands, a cysteine, two histidines and a methionine as the axial ligand. The axial ligand of the T1 Cu has a major influence on the reduction potential which affects the substrate scope and catalytic activity of laccases. To explore the impact of the ligand on the T1 Cu of the two-domain laccase Ssl1 from *Streptomyces sviveus* we analyzed the spectral and structural characteristics of Ssl1 variants in which the axial methionine was replaced by valine, isoleucine, alanine, phenylalanine, threonine, and tyrosine. All these variants displayed perturbed spectral features with an increased absorption of the N(His)→ Cu charge transfer at 430 nm and a more rhombic signal in EPR spectroscopy. These are typical for T1 Cu sites with an axial oxygen ligand. Indeed, the crystal structures of the Ssl1 variants M295A/V/I/Y/F revealed a water molecule coordinating the T1 Cu. The influence of the mutations on reorganization energy and/or substrate-T1 Cu electronic coupling became apparent from kinetic measurements of the T1 Cu reduction.

Keywords

Laccase, Multicopper oxidase, Type 1 Cu, Axial Ligand, EPR, X-ray crystallography

Abbreviations

CD: Circular dichroism; CT: Charge transfer; λ : Reorganization energy; HQ: Hydroquinone; k_{ET} : Electron transfer rate; T1: Type 1; T2: Type 2; T2D: Type 2 depleted; T3: Type 3; TNC: Trinuclear cluster

Introduction

Laccases (EC 1.10.3.2) are multi-copper oxidases that catalyze the one-electron oxidation of various aromatic compounds¹⁻³ coupled to the reduction of molecular oxygen to water. Laccases are widely distributed in nature and were found in fungi⁴, higher plants⁵, insects⁶, and bacteria⁷. Their physiological functions include lignification in plants⁸ and delignification in white-rot fungi³, cuticle sclerotization in insects^{6,9}, and spore pigmentation¹⁰ and copper homeostasis¹¹ in bacteria. Laccases are considered attractive “green” catalysts¹² since they do not rely on expensive cofactors, only need oxygen as co-substrate, and produce water as the only by-product. Due to their broad substrate scope they are potential candidates for various biotechnological applications like the detoxification of pollutants and bioremediation of phenolic compounds¹³⁻¹⁴, the delignification of lignocellulose in biorefineries¹⁵ and pulp bio-bleaching¹⁶.

Typically, laccases consist of three cupredoxin-like domains. Each domain contains two beta-sheets with seven β -strands arranged in a Greek-key- β -barrel. This architecture is closely related to that of small copper proteins like azurin or plastocyanin and typical for all multi-copper oxidases¹⁷. Laccases contain a total of four copper ions, organized in one mononuclear type 1 copper site in domain 3 and an interdomain trinuclear cluster (TNC) with one type 2 (T2) and two type 3 (T3) copper ions which is located at the interface between domain 1 and 3. Domain 2 assists in the positioning of the two other domains and is involved in formation of the substrate pocket¹⁸. In addition, bacterial two-domain laccases were identified¹⁹⁻²¹ which lack domain 2. To compensate for the lack of domain 2, two-domain laccases require trimerization to form a functional TNC between two neighboring monomers. These two-domain laccases contain the required characteristics of a common ancestor in the evolution of multicopper oxidases with three and six domains²²⁻²³.

The type 1 (T1) Cu is strongly coordinated by at least three ligands, one cysteine and two histidine residues in a pseudo-trigonal manner²⁴. The variations in T1 Cu sites that are observed in different proteins arise from different axial interactions. Methionine is a common axial ligand, e.g. in azurin and bacterial laccases, while fungal laccases have non-coordinating leucine or phenylalanine in the axial position instead. Stellacyanin has a glutamine axial ligand and azurin has an additional ligand beneath the S(Cys)-N(His)-N(His) plane, a backbone carbonyl oxygen. Valine²⁵⁻²⁶ and arginine²⁷ were also found in the position of the axial ligand. The arginine residue was found to rotate away from the Cu so that a water is bound in the axial position of the T1 Cu²⁷.

The T1 Cu is responsible for electron shuttling between the reducing substrate and the TNC where oxygen is reduced to water. Thus, it participates in two electron transfer (ET) steps, the intermolecular ET from the substrate to the T1 Cu and the intramolecular ET from the T1 Cu to the TNC. It has an intense charge transfer (CT) transition at 600 nm in the ultraviolet-visible (UV/Vis) spectrum and a small parallel hyperfine coupling constant in electron paramagnetic resonance (EPR) ($A_{\parallel} = 40-90 \times 10-$

4 cm⁻¹)²⁸. These spectroscopic characteristics are a result of the high covalency of the Cu^{II}-S(Cys) bond²⁹ which provides strong electronic coupling into the superexchange pathway to the TNC³⁰.

The three copper ions of the TNC are coordinated by eight histidine residues from two different domains. The T2 Cu has a square planar coordination by two histidine residues and one water molecule³¹. It has no absorption feature and a parallel hyperfine coupling constant which is characteristic for tetragonal copper centers ($A_{\parallel} = 140\text{-}200 \cdot 10^{-4} \text{ cm}^{-1}$)²⁸. The T3 Cu pair is coordinated by six N_ε atoms of histidine side chains in two-domain laccases. The T3 Cu's are antiferromagnetically coupled through a bridging hydroxide ligand, thus not observable in EPR spectroscopy. They contribute to the absorption spectrum with charge transfer (CT) transition from the bridging OH⁻ ligand at ~330 nm. Each of the copper ions in the TNC has an open coordination position oriented into the cluster resulting in an unsaturated coordination that is necessary for the bridged intermediates in the reduction of O₂ to H₂O³².

Fungal laccases exhibit high activities and broad substrate spectra attributed to the high reduction potentials of up to 800 mV of the electron accepting T1 Cu, but applications are limited due to the restriction to acidic reaction conditions and relatively low stability towards inhibitors⁴. Due to their higher stabilities, bacterial laccases including two-domain laccases like “small laccase” (SLAC) from *Streptomyces coelicolor* and Ssl1 from *Streptomyces sviveus* have gained research interest. Ssl1 displays phenol oxidase activity at alkaline pH and tolerance towards detergents, organic co-solvents, and elevated temperatures³³. The reduction potential of Ssl1 (375 mV)³⁴ is comparable to other bacterial laccases but low compared to fungal laccases. In our previous studies axial ligand was mutated to increase the T1 Cu reduction potential for increasing oxidation rates and extending substrate spectra³⁴⁻³⁵. To this end, the axial ligand of the T1 Cu in Ssl1 was mutated to leucine, phenylalanine, alanine, threonine, valine, isoleucine, and tyrosine. The mutation of an axial methionine to phenylalanine, leucine, and alanine were previously reported to increase the reduction potential³⁶⁻³⁹. Due to their structural similarity to leucine and phenylalanine the amino acids valine, isoleucine, and tyrosine were identified as additional promising candidates to increase the reduction potential. On the other hand, threonine was chosen because it was expected to decrease the reduction potential and the methionine to threonine mutation in nitrite reductase led to great changes in the electronic structure of the T1 Cu site⁴⁰.

Our previous results demonstrated that the hydrophobicity of the axial ligand was determining the reduction potential changes in axial ligand mutants³⁵. To gain a deeper understanding of how various axial ligands influence the T1 Cu reduction rate (k_{ET}) as well as the spectral and structural properties of a two-domain laccase, herein we systematically investigated a series of Ssl1 mutants. To the best of our knowledge a systematic spectroscopic and structural investigation of a two-domain laccase where different axial ligands were introduced at the T1 Cu site is still missing. For this purpose, we used electronic absorption, circular dichroism (CD) and electron paramagnetic resonance (EPR) spectroscopy and X-ray crystallography. The kinetics of the T1 Cu reduction were measured using a stopped-flow method.

Methods

Mutagenesis

The axial Ssl1 mutants were constructed as previously described³⁵. T2 copper depleted (T2D) Ssl1 variants were created by introducing the H99Y mutation using the Quik-Change mutagenesis protocol (Stratagene). The primer sequences were 5'-GG GCG AGC CTG TAC GTC CAC GGC CTG-3' and 5'-CC GTG GAC GTA CAG GCT CGC CCG GAC-3'. Mutated *ssl1* sequences were confirmed by Sanger sequencing.

Expression and purification of Ssl1 and spectrophotometric redox titrations

Expression and purification of Ssl1 and variants thereof as well as the spectrophotometric redox titrations were performed as described previously³⁵. Briefly, Ssl1 laccase from *S. sviveus* (UniProtKB B5HSR1) and Ssl1 variants carrying a N-terminal hexahistidine tag were expressed in *E. coli* BL21-CodonPlus(DE3)-RP. The soluble fraction obtained after sonication of the cells was incubated with CuSO₄ at room temperature for 2 h or until no further increase in activity was observed to increase copper loading. Purification was carried out using heat precipitation at 65 °C and immobilized metal ion affinity chromatography (IMAC). Finally, the buffer was exchanged to 50 mM potassium phosphate buffer (pH 7.5) and the protein concentrations were determined using the Bradford method⁴¹. The reduction potentials were determined by spectrophotometric redox titrations using the redox couple potassium hexacyanoferrate(III)/potassium hexacyanidoferrate(II) as mediator. The oxidation of the T1 Cu was followed spectrophotometrically using the increase in absorption at ~600 nm and plotted against the reduction potential established by the mediator. The midpoint potential of the laccase was obtained from fitting the data to the Nernst equation.

Stopped-Flow measurements

The reduction of the T1 Cu by hydroquinone (benzene-1,4-diol, HQ) under anaerobic conditions was measured using a SX20 Stopped-Flow System (Applied Photophysics Limited, Leatherhead, United Kingdom) equipped with a photodiode array detector. To ensure an anaerobic environment a constant flow of nitrogen was maintained at the sample handling unit and through the thermostat water. Additionally, 1 g of sodium dithionite were added to the thermostat water to eliminate any adsorbed or dissolved oxygen. All samples and buffers were prepared in a Glovebox under nitrogen atmosphere and contained 180 mU glucose oxidase and 100 mM glucose to maintain oxygen free conditions. Equal volumes of 20 μM laccase in 50 mM potassium phosphate buffer (pH 7.5) and 20 mM HQ in water (both solutions also containing glucose and glucose oxidase) were rapidly mixed. The exponential decay

rates were obtained by fitting the absorbance decrease at the ~592 nm to a first order exponential decay using Origin pro 9.0G (OriginLab Corporation, Northampton, MA, USA).

Electronic absorption spectroscopy

Electronic absorption spectra of Ssl1 were recorded on a Lambda35 spectrophotometer (Perkin Elmer, Rodgau, Germany) in 1 nm intervals in the range of 300-1000 nm with a slit width of 1 nm and a scan speed of 480 nm/min. For each variant 3 cycles were accumulated. The solution contained purified Ssl1 variants in 50 mM potassium phosphate buffer (pH 7.5). Molar extinction coefficients for Ssl1 variants were calculated using the Lambert-Beer law and protein concentrations determined by the Bradford method⁴¹.

Circular dichroism spectroscopy

Circular dichroism (CD) spectroscopy was performed on a Jasco J-815 CD Spectrometer (Jasco Germany, Pfungstadt, Germany). An average of 20 scans was collected at 20°C with a scanning speed of 100 nm/min and a bandwidth of 5 nm in a quartz glass high precision cell with a 1 mm path length. Samples contained 500 μM Ssl1 WT or M295I/V/F, 1148 μM Ssl1 M295A, 1189 μM Ssl1 M295T, or 287 μM Ssl1 M295Y in 50 mM potassium phosphate buffer (pH 7.5).

Electron paramagnetic resonance

Continuous-wave (CW) X-band (~9.63 GHz) EPR spectra were collected on a Bruker E500 spectrometer equipped with an Oxford liquid helium flow cryostat operated at 30 K. The spectra were collected with 100 kHz field modulation at 6 G amplitude, a 163.84 ms time constant, and a 40.96 ms conversion time for the 4096 point spectrum. Data were simulated in Matlab 2017a using the EasySpin software package (v 5.2)⁴².

Crystallization

Crystals were obtained using sitting drop vapor diffusion method with a 1:1 mixture of the protein solution at a concentration of 10 mg/ml in 50 mM potassium phosphate buffer (pH 7.5) and a reservoir solution at room temperature. M295A crystals were obtained with a reservoir solution consisting of 50 mM HEPES at pH 7.0, 1.1 M (NH₄)₂SO₄, and 5 mM [Co(NH₃)₆]Cl₃. M295F crystals were obtained with a reservoir solution consisting of 50 mM HEPES at pH 7.0, 1.1 M (NH₄)₂SO₄, and 20 mM [Co(NH₃)₆]Cl₃. M295I crystals were obtained with a reservoir solution consisting of 50 mM HEPES at

pH 7.0, 1.4 M $(\text{NH}_4)_2\text{SO}_4$, and 10 mM $[\text{Co}(\text{NH}_3)_6]\text{Cl}_3$. M295V crystals were obtained with a reservoir solution consisting of 50 mM HEPES at pH 7.0, 1.3 M $(\text{NH}_4)_2\text{SO}_4$, and 20 mM $[\text{Co}(\text{NH}_3)_6]\text{Cl}_3$. M295Y crystals were obtained with a reservoir solution consisting of 50 mM HEPES at pH 7.0, 1.2 M $(\text{NH}_4)_2\text{SO}_4$, and 15 mM $[\text{Co}(\text{NH}_3)_6]\text{Cl}_3$. Blue-colored and rod-shaped crystals were observed within 14 days, flash frozen immediately after soaking for 60 s in cryo-protecting solution (saturated LiSO_4), mounted into MiTeGen MicroMounts/MicroLoops, and stored in liquid nitrogen.

Data collection and structure determination

Data sets were collected at 100 K using synchrotron radiation at P11 beamline, PETRA III, Hamburg, Germany. High-resolution native data sets for structure refinement were collected at 12.4 keV. For the anomalous scattering contribution of copper atoms, a second, high-multiplicity data set was collected at 9 keV for each Ssl1 variant. The data was processed using the program package XDS⁴³. Molecular replacement and structure refinement were performed using the software package ccp4⁴⁴ starting from *Streptomyces sviveus* Ssl1 (PDB ID 4M3H) as the starting model. More detailed, data reduction was performed with AIMLESS⁴⁵, phasing was done by PHASER⁴⁶. Coot⁴⁷ was used for model building and validation, and REFMAC5⁴⁸ was employed for structure refinement. Maps were calculated using FFT⁴⁹.

PyMOL⁵⁰ was used to prepare the figures and to calculate the root-mean-square deviation (RMSD) of the $\text{C}\alpha$ atoms using the align command with the number of cycles set to 0, thus, not including outlier rejection. The structures were visualized using PyMol and the atomic coordinates have been deposited with the Protein Data Bank, Research Collaboratory for Structural Bioinformatics at Rutgers University (PDB ID: 6YZD, 6YZY, 6YZF, 6Y4A, 6YO5).

The final models of M295A, M295F, M295I, and M295Y contained 98.00 % in the favored region and 0.00 % in outlier regions of the Ramachandran plot as defined by MolProbity⁵¹. The final model of M295V has 94.00 % in the favored and 0.00 % in the outlier regions of the Ramachandran plot.

Results

The axial ligand is a major determinant for the T1 Cu reduction potential E° as we have previously confirmed in Ssl1 variants³⁵. Exchange of the axial ligand M295 with the less hydrophobic amino acids alanine and threonine led to a decrease of the reduction potential, while the variants M295Y, M295V, M295I, and M295F with more hydrophobic axial ligands possess increased reduction potentials³⁵. Following the Marcus theory, the electron transfer rate k_{ET} is directly related to the reduction potential difference between the electron donor (laccase substrate) and acceptor (T1 Cu)⁵². Additionally, effects from reorganization energy⁵³, substrate binding⁵⁴, and substrate structure⁵⁵ need to be considered while analyzing the experimentally observed changes in k_{ET} .

In this work, we first investigated the relation between k_{ET} and E° in Ssl1 variants differing in their axial ligands and reduction potentials. The first reaction step in Ssl1, the transfer of one electron from the common low-potential laccase substrate hydroquinone (HQ)⁵⁶ to the T1 Cu was analyzed using a stopped-flow approach. To disrupt the intramolecular electron flow from the T1 Cu to the TNC we constructed the corresponding T2 Cu depleted Ssl1 variants. The T2 Cu coordinating His99 was mutated to tyrosine to prevent T2 Cu coordination. A similar approach was previously described in the production of T2 copper depleted Fet3⁵⁷. Further, the T2 copper depleted variants (T2D) bearing various axial residues at the T1 Cu site were analyzed regarding their reduction potentials (Table 1), which were in good agreement with values previously reported³⁴⁻³⁵ for the corresponding Ssl1 variants with the intact T2 copper site.

The decrease in absorption at ~600 nm that accompanies the reduction of the T1 Cu followed a first order exponential decay in T2D Ssl1 variants. This is in accordance with results obtained for *Rhus vernicifera* laccase using either a T2D variant⁵⁸⁻⁵⁹ or fluoride mediated inhibition of the T2 Cu⁶⁰. The k_{ET} values varied over two orders of magnitude between the fastest reduction in the T2D variant with the wild-type axial methionine with $k_{ET} = 2.01 \text{ s}^{-1}$ and the slowest measured with Ssl1 T2D M295A (0.02 s^{-1}) (Table 1). While decreased T1 Cu reduction potentials indeed resulted in lower k_{ET} , increased T1 Cu reduction potentials did not necessarily lead to increased values for k_{ET} . This underlines the importance of further contributions, e.g., from changes in the reorganization energy λ . To assess those contributions, the spectroscopic and structural properties of the Ssl1 variants were investigated.

Table 1: Reduction potentials of T2D Ssl1 variants and reduction rates k_{ET} for the reduction of the T1 Cu by HQ. Values are given as mean \pm standard deviation of at least triplicates.

Ssl1 variant	reduction potential [mV]	reduction rate k_{ET} [s ⁻¹]
H99Y/		
M295A	<290	0.02 \pm 0.008
M295T	306 \pm 13	0.07 \pm 0.005
M295Y	396 \pm 9	0.37 \pm 0.19
M295 (wt)	404 \pm 9	2.01 \pm 0.31
M295F	430 \pm 9	0.99 \pm 0.26
M295V	432 \pm 3	0.93 \pm 0.17
M295I	442 \pm 11	1.40 \pm 0.13

X-ray crystallography

To obtain high-resolution structural information of the T1 Cu site in Ssl1, we performed crystallization experiments and were able to obtain crystals for the five Ssl1 variants M295A, M295Y, M295F, M295V, and M295I. The structure of the wild-type and the variant Ssl1 M295L were previously reported (PDB ID 4M3H and PDB ID 4WTO, respectively). All crystals showed an intense blue color, indicating the presence of copper at the T1 Cu site. The Ssl1 variants crystallized in the orthorhombic space group $P2_12_12_1$, and the asymmetric unit contains one biological assembly consisting of a protein trimer. The poor diffraction of the Ssl1 M295T variant did not lead to high quality data suitable for structure solution. Native and anomalous data for all Ssl1 variants were collected and their crystal structures were solved using molecular replacement with the structure published by Gunne *et al.*³⁴ (PDB ID 4M3H) as a starting model. A summary of the data collection and refinement statistics can be found in the crystallographic table (Supplementary Table S1).

The overall architecture of all Ssl1 variants is very similar to the wild-type structure³⁴ with root mean square deviations (RMSD) in the range of 0.330 – 0.599 Å (calculated for all C α atoms of residues 43-311 without outlier rejection).

The electron density at the T1 Cu site revealed that none of the amino acids introduced as axial ligand at position 295 is directly interacting with the copper but influences the stability of this region. The side chains of alanine, isoleucine, and valine in their respective variants (M295A, M295I, M295V) are well-defined, which is probably due to the short side chain of these residues. The larger residues Phe295 and Tyr295 are not well defined. This indicates that the Ssl1 variants have a higher degree of flexibility in the vicinity of larger residues at position 295. Notably, the residues 203-205 that are located close to residue 295 could also be affected in their flexibility. The disorder in the region 203-205 may be caused by the disorder of large residues at position 295. Both the phenylalanine and tyrosine residues are flipped away from the Cu coordination site towards the region of residues 203-205 while the alanine, isoleucine,

and valine residues point towards the Cu coordination site. M295 in the wild-type protein reaches far into the metal-binding site of Ssl1 and coordinates to the T1 copper, while all introduced mutations are not capable of filling this space and interacting with the copper. We assume that the side chains of phenylalanine and tyrosine are too large to reach into the pocket, while isoleucine, valine, and alanine are smaller than methionine and do not occupy the entire space in the pocket. As a result, water molecules can occupy the open coordination site in the variants.

In chain A of the structures of the variants M295A, M295I, and M295F two water molecules are occupying the space between the residues at position 295 and the T1 Cu. The chain A of M295Y shows three water molecules between the residues at position 295 and the T1 copper, whereas the M295V variant shows one water molecule at this position.

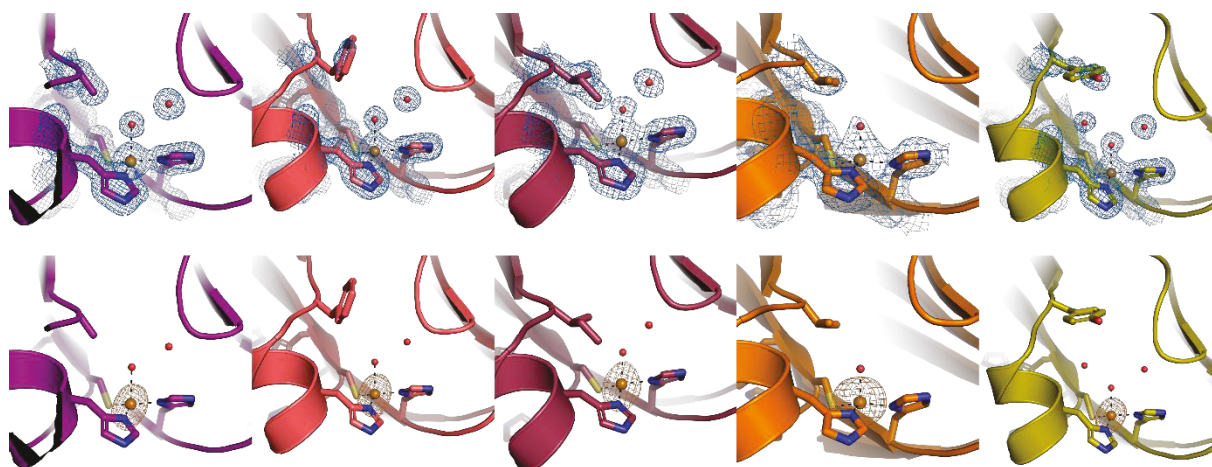


Figure 1: Structure of the T1 Cu sites of the Ssl1 variants M295A (purple), M295F (red), M295I (dark red), M295V (orange), and M295Y (green). T1 Cu is shown in brown spheres. Red spheres show oxygen atoms representing water molecules. Dashed black lines show bonds between atoms of Cu-coordinating molecules. The coordinating amino acid residues and the side chain of the axial ligand of T1 Cu are shown as sticks. The blue mesh in the top row shows the native electron density map measured at 12 keV (contoured at 1.0 σ). The brown mesh in the bottom row shows the Cu electron density map measured at 9 keV (contoured at 1.0 σ).

CD & UV/Vis

Wild-type Ssl1 is characterized by a deep blue color and its absorption spectrum in the UV/Vis region is characteristic for laccases (Figure 2)³⁴. Due to the high Cu-S(Cys) bond covalency there is an intense S(Cys) $\pi \rightarrow \text{Cu}^{\text{II}}$ $3d_{x^2-y^2}$ CT transition at 592 nm. The shoulder at 330 nm corresponds to the T3 Cu site and originates from an OH $^- \rightarrow \text{Cu}^{\text{II}}$ CT. The d-d transitions form a shoulder to the 592 nm maximum and are centered around 730 nm in the wild-type's spectrum. The T2 Cu does not contribute to the absorption spectrum.

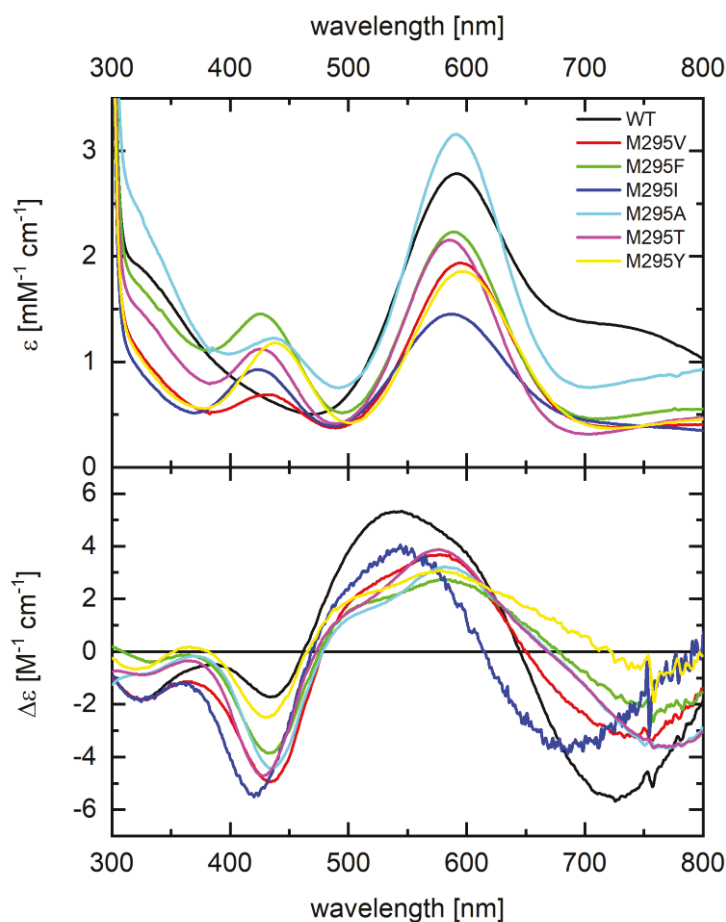


Figure 2: Electronic absorption (top) and CD (bottom) spectra of wild-type *Ssl1* (black curves) and the variants M295V (red), M295F (green), M295I (dark blue), M295A (light blue), M295T (pink), and M295Y (yellow).

The most intriguing effect of the mutation of M295 on the absorption spectrum (Figure 2) is the presence of an additional band at ~430 nm assigned to the His(N) \rightarrow Cu^{II} charge transfer based on its negative feature in the CD spectrum. This band is usually weak for multicopper oxidases⁶¹ and also not recognized from the absorption spectrum of wild-type *Ssl1*. The increase in absorption indicates an increased overlap of the N(His) π -orbitals with the Cu $d_{x^2-y^2}$ orbital and is indicative of a tetrahedral distortion. The intensity of the 430 nm transition varies between mutants (Figure 2 and Table 2) and is always less intense than the ~590 nm feature in the absorption spectra. The strongest absorption at ~430 nm was observed in the M295F mutant ($\epsilon_{427} = 1.454 \text{ mM}^{-1}\text{cm}^{-1}$).

The S(Cys) π \rightarrow Cu^{II} CT transition at ~590 nm is the most prominent feature in the absorption spectrum whereas the S(Cys) σ \rightarrow Cu^{II} CT (500-530 nm) is only resolved in CD spectroscopy. The intensity of the 600 nm absorption decreased in all mutants except for M295A ($\epsilon_{590} = 3.158 \text{ mM}^{-1}\text{cm}^{-1}$). The S(Cys) σ \rightarrow Cu^{II} CT forms a pronounced shoulder to the ~600 nm transition in CD spectra of M295Y, M295V, M295F, M295A, and M295T. In spectra of M295I and wild-type *Ssl1* the S(Cys) σ \rightarrow Cu^{II} CT is more intense and there is one broad intense feature between 500 and 600 nm.

The transition at 330 nm that is observed both in the absorption and CD spectrum is a OH \rightarrow Cu^{II} CT from the T3 Cu site. Compared to the wild-type ($1.835 \text{ mM}^{-1}\text{cm}^{-1}$) the intensity of the absorption at

330 nm increased in the M295A variant ($2.245 \text{ mM}^{-1}\text{cm}^{-1}$) (Table 2). In spectra of M295V, M295Y and M295I a transition at 330 nm is not resolved, but it is present in the CD spectra of the respective mutants.

Mutation of the T1 Cu axial ligand impacted the d-d transitions (mostly $d_{xz}/d_{yz} \rightarrow d_{x^2-y^2}$ from the T1) between 700 and 800 nm. They are shifted to higher wavelength/lower energy and are less intense in the M295F, M295V, M295Y, M295A, and M295T mutants as compared to the wild-type (Table 3) reflecting a weaker ligand field and indicating tetrahedral distortion of the T1 Cu site. For the M295I mutant the d-d transition feature shifted to lower wavelength/higher energies compared to Ssl1 wild-type. This would indicate a larger ligand field splitting, increasing the energy of the $d_{x^2-y^2}$, possibly reflecting a tetragonal distortion relative to the T1 site with an axial methionine.

Table 2: Electronic absorption transitions and their molar extinction coefficients.

Ssl1 variant	$\text{OH}^- \rightarrow \text{Cu}^{\text{II}}$ CT	$\text{S}(\text{Cys})\pi \rightarrow \text{Cu}^{\text{II}}$ CT		$\text{N}(\text{His}) \rightarrow \text{Cu}^{\text{II}}$ CT	
	$\epsilon_{330} [\text{mM}^{-1}\text{cm}^{-1}]$	wavelength [nm]	$\epsilon [\text{mM}^{-1}\text{cm}^{-1}]$	wavelength [nm]	$\epsilon [\text{mM}^{-1}\text{cm}^{-1}]$
WT	1.835	591	2.785	-	-
M295F	1.636	589	2.232	427	1.454
M295V	0.990	594	1.938	428	0.687
M295Y	0.950	597	1.859	438	1.182
M295I	0.830	587	1.451	423	0.927
M295A	2.245	590	3.158	436	1.225
M295T	1.409	585	2.154	425	0.120

Table 3: Circular dichroism transitions of Ssl1 mutants. Wavelengths in nm were obtained from Gaussian fits using MagicPlot. Details and plots for Gaussian fits are given in the supplementary information.

Ssl1 variant	$\text{OH}^- \rightarrow \text{Cu}^{\text{II}}$	$\text{N}(\text{His}) \rightarrow \text{Cu}^{\text{II}}$ CT	$\text{S}(\text{Cys})\sigma \rightarrow \text{Cu}^{\text{II}}$	$\text{S}(\text{Cys})\pi \rightarrow \text{Cu}^{\text{II}}$	d-d (-)
	CT (-) [nm]	(-) [nm]	CT (+) [nm]	CT (+) [nm]	centered at [nm]
WT	326	441	535	615	725
M295F	335	434	498	582	761
M295V	328	437	507	589	738
M295Y	321	432	492	577	760
M295I	326	422	523	570	687
M295A	322	435	498	583	767
M295T	322	428	492	576	770

EPR

Continuous wave (cw) X-band (9.64 GHz) EPR spectra were measured for wild-type and all mutants. Experimental spectra along with spectral simulations are shown in Figure 3 and the simulation parameters are shown in Table 4. The EPR spectrum of the wild-type protein is reminiscent of typical laccases with two components. The first is an axial spectrum ($g_{\parallel} = g_{\parallel} = 2.230$ and $g_2 = g_3 = g_{\perp} = 2.046$) with a small anisotropic Cu hyperfine coupling ($A_{\parallel} = 221.8$ MHz and $A_{\perp} = 35$ MHz) that splits the g_{\parallel} into four lines. This is typical for distorted tetrahedral T1 copper sites where the singly occupied molecular orbital (SOMO) has $d_{x^2-y^2}$ character, where a large amount of covalency lowers the hyperfine coupling relative to that observed for the square planar CuCl_4^{2-} complex. The second component is also axial ($g_{\parallel} = 2.215$ and $g_{\perp} = 2.05$) but with a much larger anisotropic Cu hyperfine ($A_{\parallel} = 599.6$ MHz and $A_{\perp} = 3$ MHz). This is typical of tetragonal T2 copper sites with a highly ionic Cu center (low covalency).

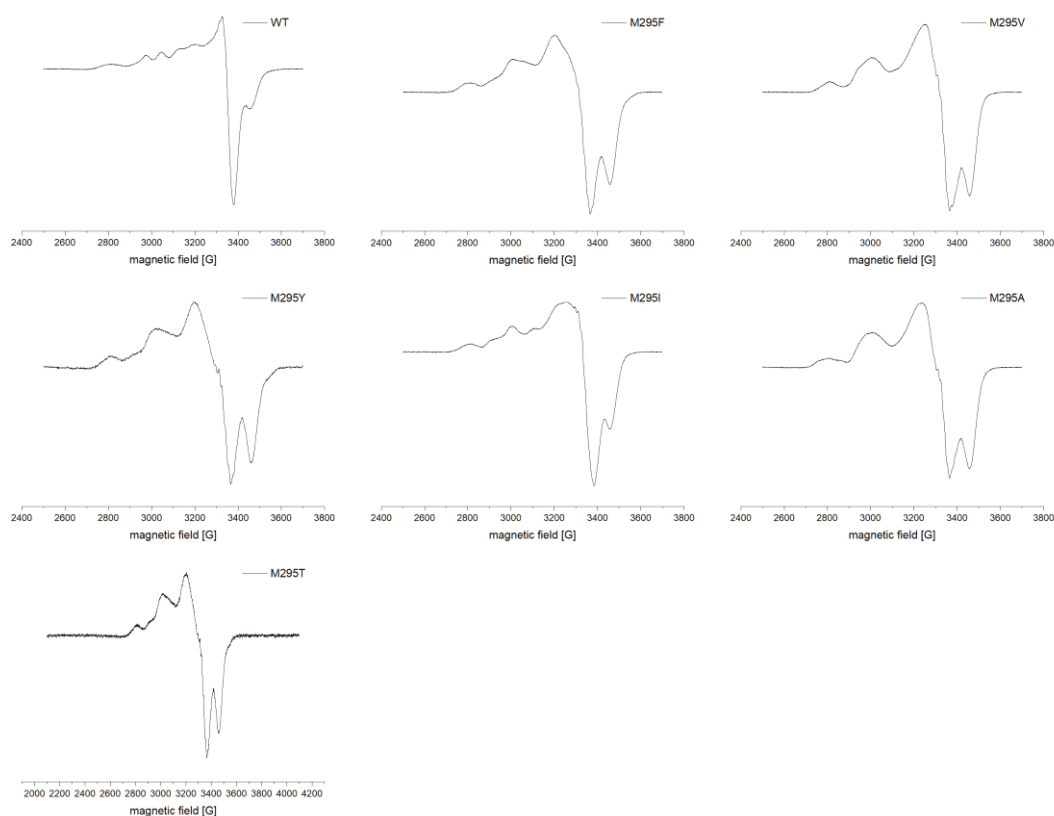


Figure 3: Experimental EPR spectra of *SslI* variants.

Table 4. EPR parameters of SslI variants.

SslI variant	T1								T2					
	g1	g2	g3	g-perp	rhombicity	A1	A2	A3	g1	g2	g3	A1	A2	A3
WT	2.23	2.059	2.033	2.046	2.6	221.8	40	30	2.215	2.05	2.05	599.6	3	3
M295F	2.298	2.108	2.04	2.074	6.8	180	100	60	2.216	2.05	2.05	599.6	40	40
M295V	2.298	2.075	2.05	2.0625	2.5	130	120	60	2.214	2.05	2.05	595	40	40
M295Y	2.3	2.12	2.05	2.085	7	200	40	40	2.215	2.05	2.05	599.6	40	40
M295I	2.255	2.075	2.045	2.06	3	280	90	40	2.215	2.05	2.05	599.6	40	40
M295A	2.298	2.075	2.05	2.0625	2.5	130	100	40	2.215	2.05	2.05	599.6	3	3
M295T	2.298	2.12	2.05	2.085	7	180	85	40	2.215	2.05	2.05	599.6	40	40

Interestingly, the methionine variants all show drastically different EPR spectra where the characteristic T1 copper site is significantly altered with higher g_{\parallel} -values (ca. 2.3), much smaller A_{\parallel} values (ca. 100 MHz), and a slightly rhombic line shape (i.e. $g_2 \neq g_3$). The hyperfine coupling has three components: 1) The Fermi contact interaction relates to the s -electron density at the nucleus, which is indirectly affected by the d -electrons (through spin polarization of $3s$ and $2s$ electrons) and contributes to the isotropic part ($A_{\text{iso}} = (A_{\parallel} + 2A_{\perp})/2$) of the hyperfine coupling tensor, 2) spin dipolar coupling between the electron spin and the nuclear spin, which contributes to the anisotropic part. This A_{\parallel} is usually large and negative. Lastly, the orbital dipolar coupling, between the magnetic field experienced by the electron as it orbits the nucleus and its intrinsic spin, is also anisotropic, and is proportional to the g -values. Components 1 and 2 are reduced by covalency – electron delocalization from the $d_{x^2-y^2}$ onto the ligands. The small values of A_{\parallel} and A_{iso} are both due to the high covalency of the T1 site with Cu-S/N bonding. Interestingly, removing the axial methionine ligand generally gives even smaller A_{\parallel} indicating increased covalency (stronger Cu-S/N bonding). In general, the rhombicity of the EPR spectrum is increased in the mutants, indicative of some d_{z^2} mixing into the $d_{x^2-y^2}$ ground state, in agreement with the lower energy ligand field transitions observed in UV/Vis. Also, the g_1 value increases, indicating larger spin-orbit coupling through mixing of excited states into the $d_{x^2-y^2}$ ground state.

Discussion

The T1 or blue copper sites in numerous proteins have been extensively studied including mutants of the axial ligands due to the major influence of the axial ligand on the reduction potential and electronic structure. One of the best studied proteins in this regard is azurin. The axial methionine of azurin has been mutated to every other natural amino acid⁶²⁻⁶⁶ as well as non-natural amino acids⁶⁶⁻⁶⁸. Axial ligand mutations have also been studied in other cupredoxins⁶⁹⁻⁷² and multicopper oxidases, including nitrite reductase^{36,40,73}, bilirubin oxidase⁷⁴⁻⁷⁵ and laccases^{34-35,38,76-81}. Thus, there are already detailed descriptions of the electronic structures available for many T1 Cu containing proteins and variants thereof with different axial ligands of the T1 Cu.

Herein we provide structural and spectroscopic data for axial ligand variants of a two-domain laccase, Ssl1 from *S. sviveus*. Ssl1 WT has spectral characteristics of a classic blue Cu/T1 Cu site like plastocyanin with two N(His), a highly covalent S(Cys), and an axial S(Met) ligand⁸²⁻⁸³. There is an intense S(Cys) π \rightarrow Cu^{II} CT at 591 nm and only little absorption at ~450 nm in the absorption spectrum. Additionally, there is the contribution of a OH \rightarrow Cu^{II} CT from the T3 Cu pair in the TNC. A contribution from the S(Met) \rightarrow Cu^{II} CT transition at 390 nm that is observed e.g. in nitrite reductase⁴⁰ and is sometimes noticeable when performing curve analysis⁶¹ was not recognized from the UV/Vis and CD spectra of wild-type Ssl1.

The overall architecture of all Ssl1 variants is very similar to the wild-type structure and there were no significant effects on the TNC observed in the crystal structures. Removing the axial methionine in Ssl1 resulted in a water molecule occupying the open axial coordination site of the T1 Cu and perturbed spectroscopic features. Both the increased covalency of the N(His) \rightarrow Cu^{II} bond and the decreased ligand field strength indicate a tetrahedral distortion of the T1 Cu site⁸⁴. The weak S(Cys) pseudo- σ CT in all Ssl1 variants investigated in this study also indicates that there is no tetragonal distortion of the T1 Cu site but instead a tetrahedral geometry⁶⁹. This distorted tetrahedral geometry is characteristic for T1 Cu sites with an oxygen bound to the T1 Cu in the axial position such as stellacyanin⁸⁴ and the M121Q mutant of azurin⁸⁵. Analogous to the Ssl1 wild-type, the Q99M mutant of stellacyanin has no tetragonal distortion and a more trigonal site⁶⁹. Even though the origin of the coordinating oxygen differs, the effects on the T1 Cu site are similar. Spectroscopic perturbations consistent with oxygen coordinating the axial position of the T1 Cu (increased absorption of the His(N) \rightarrow Cu^{II} CT at 450 nm, red-shifted d-d transitions) were also observed in the *E. coli* CueO mutants M510Q/A/T⁷⁷. This led the authors to the conclusion that the axial position in these three mutants is occupied by an oxygen ligand, presumably originating from the respective side chains in the M510Q and M510T mutants and a water molecule in M510A⁷⁷. In bilirubin oxidase from *Myrothecium verrucaria* the open coordination site in the axial ligand mutants M467F and M467L became occupied by the amide oxygen of an adjacent asparagine⁷⁵. This resulted in spectral features similar to the M467Q mutant of bilirubin oxidase⁸⁶⁻⁸⁸.

EPR data supports the crystallographic results and gives further insights into effects of the mutations on the geometry of the T1 Cu site. Unsurprisingly, the mutations have an effect on the covalency in the active site, as the loss of the axial donor might be compensated by interactions to His(N) and Cys(S), which is supported by the presence of a 430 nm band in the UV/Vis spectrum. Also the strength of the axial ligand interaction influences the Cu-S(Cys) covalency⁶⁹ and is thereby also influencing the electronic coupling into the superexchange pathway to the TNC²⁶. On the other hand, values for the electronic coupling matrix element (H_{DA}) for the superexchange pathway in different MCOs are not significantly different^{29,89-90}. Interestingly this is underlined by our results for Cu-N(His) interactions. The His(N) \rightarrow Cu²⁺ band is considerably stronger for blue copper proteins showing the rhombic EPR signal⁶¹ which we also observed in the M295Y, M295F, M295T (w/o structure), M295V, and M295A mutants of Ssl1 inferring an increased rhombicity for this mutants.

An interesting feature of the axial position of the T1 Cu in the mutants is that water is occupying this space and takes the role of the axial ligand, which also influences the geometry, supported by the EPR spectra, considering a small parallel hyperfine coupling constant ($A_{\parallel} = 40-90 \cdot 10^{-4} \text{ cm}^{-1}$) of the T1 Cu. Due to more space at the axial position of the T1 Cu the coordination site can form a more tetrahedral geometry. This is also reported for a Cu-containing nitrite reductase. In this Cu-containing nitrite reductase from *Achromobacter cycloclastes* the mutation M150Q of the axial ligand changed the type of Cu coordination geometry and led to CD and UV/Vis spectral features like stellacyanin, but still axial symmetry in EPR instead of the rhombic signal observed for stellacyanin, which is in agreement with a symmetrical tetrahedron⁷³. Considering a parallel hyperfine coupling constant characteristic for tetragonal copper centers ($A_{\parallel} = 200 \cdot 10^{-4} \text{ cm}^{-1}$) for the T2 Cu ion, no absorption features or alterations can be detected for the T2 Cu site.

The side chains of phenylalanine and tyrosine as axial ligands at position 295 flipped away from the T1 Cu and increased the exposure of the T1 Cu to the solvent. The analogous M502F mutation of the axial ligand in CotA from *B. subtilis* only led to a slight movement of the mutated residue towards the protein surface and the phenylalanine residue was still oriented towards the Cu ion³⁸. In a purple cupredoxin from *Nitrosopumilus maritimus* arginine in axial position rotates away from the T1 Cu and there is a water bound to the Cu²⁷. Since spectroscopy supports the presence of oxygen bound as the axial ligand to the T1 Cu in Ssl1 M295Y and M295F, we assume that this movement is not a crystallographic artifact. Unfortunately, we were unable to solve a structure for M295T, but based on spectroscopy we can assume an oxygen coordinating the T1 Cu in this mutant but cannot state if this originates from the threonine hydroxyl group or a water molecule.

The spectral perturbations observed in Ssl1 mutants need to be distinguished from another type of distorted T1 Cu sites (green Cu sites), which are present e.g. in *Rhodobacter sphaeroides* nitrite reductase with an axial methionine⁸⁴. Relative to the classical blue copper site in plastocyanin the Cu-S(Cys) bond is longer and weaker, the geometry is tetragonally distorted, and the Cu $3d_{x^2-y^2}$ rotates⁴⁰.

This results in intense σ and weak π S(Cys) \rightarrow Cu^{II} charge-transfer transitions at ~450 nm and ~600nm, respectively⁴⁰. These kinds of perturbations are also associated with mutation of the axial ligand of the T1 Cu. Exchanging the axial Leu513 with His in *Myceliophthora thermophila* laccase changed the T1 Cu site to a green Cu site⁷⁶.

The absorption intensity of the OH⁻ \rightarrow Cu CT at 330 nm displayed a two-fold decrease in Ssl1 M295V, M295Y, and M295I. Possible explanations for this are a depletion of T3 Cu, absence of the bridging hydroxide, or (partly) reduced T3 Cu ions. The M502L and M502F mutants of CotA have a dioxygen and a peroxide moiety, respectively, bound at the TNC and therefore no absorption shoulder at 330 nm³⁸. The lower absorption intensities of the OH⁻ \rightarrow Cu^{II} CT in both M467F and M467L mutants of bilirubin oxidase were due to the TNC being in a partly reduced state and an unbridged form⁷⁵. Depletion of the T2 Cu as observed in the Ssl1 crystal structures can result in partly reduced T3 Cu sites as it was shown for T2D *Rhus vernicifera* laccase, that the T2D variant contains a reduced type 3 site and does not show significant absorption at 330 nm⁹¹⁻⁹².

Our previous study revealed that the increase of the T1 Cu reduction potential in Ssl1 was not necessarily accompanied with an increase in activity towards syringaldazine, indigo carmine, and alizarin red S³⁵. This observation was also confirmed in this study when T2 Cu depleted Ssl1 variants with various axial ligands to the T1 Cu were investigated in the stopped-flow experiments with HQ as reducing substrate. Herein we observed no direct correlation between the T1 Cu reduction potential and the rate of reduction of the T1 Cu. Decreasing the reduction potential led to lower values for k_{ET} as expected and increasing the reduction potential from the M295V/F to M295I also increased k_{ET} . However, in all three variants k_{ET} was lower than k_{ET} measured for the T2 depleted wild-type with a lower reduction potential (Table 1).

According to the Marcus theory⁵² for electron transfer, the electron transfer rate k is determined by three contributions: the free energy difference ΔG° which is directly related to the reduction potential difference ΔE , the reorganization energy (λ), and the electronic coupling matrix element H_{DA} ⁸⁹. The absence of a direct correlation between k_{ET} and ΔE implies changes in the reorganization energy and/or electronic coupling accompanying the mutation of the axial ligand.

An increase in reorganization energy for the Cu(II) to Cu(I) reduction is supported by the spectroscopic data which indicate a tetrahedral distortion of the T1 Cu site in Ssl1 variants with axial ligands other than methionine. Removal of the axial methionine allows the Cu center to relax into a state with locally lower energy but with a larger reorganization energy. Following the Rack/entatic state⁹³⁻⁹⁵ theory, the protein environment, specifically, the axial ligand enforces a slightly unfavorable conformation of the Cu ion, but one that is close to the transition state structure during reduction/oxidation. The impact of the axial ligand on the reorganization energy was previously demonstrated for several T1 Cu sites^{26,53,96}. The reorganization energy of the T1 Cu was 0.3 eV (30 kJ mol⁻¹) higher in the M150G, M150H, and M150T mutants of nitrite reductase (M150 is the axial ligand in the wild-type protein)⁵³. In umecyanin

the introduction of an axial methionine instead of the wild-type glutamine was also preferable for fast electron transfer which was attributed to a smaller inner sphere reorganization energy in the Gln95Met variant^{26,96}. While this seems indeed to be an important factor, because it leads to the two-fold lower reduction rates in the case of the Ssl1 M295V/F variants, it is not the dominant factor in the Ssl1 M295A and M295T variants, which appear to have much lower redox potentials, and consequently up to 100-fold decreases in reduction rates (Table 1). Structurally, the M295A and M295V variants are very similar, yet they have huge differences in both their T1 Cu center redox potentials as well as their reduction rates. It seems likely that this would be due to electrostatic effects, i.e., differences in the hydrophobicity of the local T1 Cu environment. Similar observations have been made previously with azurin⁶⁸. However, it is noteworthy to mention that the M295A variant shows a much larger decrease in energy for the ligand-field transition (absorption at 767 nm) than the M295V variant (absorption at 738 nm), indicating a larger tetrahedral distortion for the former. The crystal structures also support higher solvent access to the T1 Cu site in M295A compared to M295V (see Figure 1). This can be due to more accessible space around the axial position of the T1 Cu site. Alanine offers more space for the solvent as it is the amino acid with the smallest side chain pointing towards the T1 Cu. Due to the orientation of the isoleucine side chain there is space for two water molecules, while valine seems to occupy more space than isoleucine. Solvent accessibility also influences the reorganization energy as was recently demonstrated by the correlation between the solvent accessible surface area and the reorganization energy using a series of engineered T1 Cu sites⁹⁷.

For the Ssl1 variant M295A we have previously hypothesized that water might occupy the axial position of the T1 Cu as its reduction potential is considerably lower (<290 mV) than anticipated from the correlation between reduction potential and axial ligand hydrophobicity³⁵. Usually, the T1 Cu reduction potential decreases when oxygen binds at the axial position due to stabilization of the Cu^{II} state⁹⁸. Consequently, the reduction potential of the T1 Cu sites decreases in going from an axial Met to Gln, e.g. from 240 mV to 113 mV in nitrite reductase⁷³ or from 470 to 270 mV in bilirubin oxidase⁸⁸. The mutation that led to a water molecule bound to the T1 Cu in CotA also decreased the reduction potential⁹⁹. Thus, the presence of a water molecule and the increased reduction potentials of the M295Y/V/F/L/I³⁵ mutants seem to contradict each other. On the other hand, only M295 was found to be able to exclude water from the axial T1 Cu position so far in Ssl1 and a more polar environment of the T1 Cu makes it even more sensitive to the hydrophobicity of the axial ligand. For both stellacyanin¹⁰⁰ which has a greater active site solvent exposure and azurin with an additional axial carbonyl ligand display a higher sensitivity for the hydrophobicity of the axial ligand compared to other T1 Cu sites was observed⁶⁸.

Conclusion

In this study we provided the structural and spectroscopic description of the T1 Cu site of the two-domain laccase Ssl1 with various axial ligands. Replacement of the axial ligand methionine by valine, isoleucine, alanine, phenylalanine, threonine, and tyrosine in Ssl1 influences the T1 Cu reduction potential and results in perturbed spectral features which are often found in four-coordinate T1 Cu sites with an axial oxygen ligand, i.e., the carbonyl oxygen of the glutamine side chain or a water molecule. Indeed, the crystal structures of the Ssl1 variants M295A/V/I/Y/F contain a water molecule bound to the T1 Cu instead of the methionine thioether in wildtype Ssl1. Stopped-flow measurements of the T1 Cu reduction kinetics indicated that mutation of the axial ligand not only influences the T1 Cu reduction potential but also the reorganization energy and/or the electronic coupling between substrate and the T1 Cu. Changes in reorganization energy upon mutation of the axial ligand were supported by the observed tetrahedral distortion of the T1 Cu site which increases the reorganization energy for the $\text{Cu}^{\text{II}}/\text{Cu}^{\text{I}}$ reduction. Additionally, the changes in solvent accessibility of the T1 Cu site in axial ligand mutants might increase the contribution of the solvent to the reorganization energy. Overall, this work underlines the importance of the axial ligand for the T1 Cu site in two-domain laccases and the complex interactions between the factors determining electron transfer rates, namely reduction potential, reorganization energy, and donor-acceptor electronic coupling.

Acknowledgements

We acknowledge DESY (Hamburg, Germany), a member of the Helmholtz Association HGF, for the provision of experimental facilities. Parts of this research were carried out at PETRA III and we would like to thank Anja Burkhardt, Olga Lorbeer, and Eva Crosas for assistance in using the Bioimaging and diffraction beamline P11.

References

- 1 Xu, F., Oxidation of phenols, anilines, and benzenethiols by fungal laccases: Correlation between activity and redox potentials as well as halide inhibition. *Biochemistry* **1996**, *35* (23), 7608-7614. doi:10.1021/bi952971a
- 2 Xu, F.; Shin, W.; Brown, S. H.; Wahleithner, J. A.; Sundaram, U. M.; Solomon, E. I., A study of a series of recombinant fungal laccases and bilirubin oxidase that exhibit significant differences in redox potential, substrate specificity, and stability. *BBA - Protein Struct. M.* **1996**, *1292* (2), 303-311. doi:10.1016/0167-4838(95)00210-3
- 3 Thurston, C. F., The structure and function of fungal laccases. *Microbiology* **1994**, *140* (1), 19-26. doi:10.1099/13500872-140-1-19
- 4 Baldrian, P., Fungal laccases—occurrence and properties. *FEMS Microbiol. Rev.* **2006**, *30* (2), 215-242. doi:10.1111/j.1574-4976.2005.00010.x
- 5 Mayer, A. M.; Staples, R. C., Laccase: new functions for an old enzyme. *Phytochemistry* **2002**, *60* (6), 551-565. doi:10.1016/S0031-9422(02)00171-1
- 6 Dittmer, N. T.; Kanost, M. R., Insect multicopper oxidases: Diversity, properties, and physiological roles. *Insect Biochem. Mol. Biol.* **2010**, *40* (3), 179-188. doi:10.1016/j.ibmb.2010.02.006
- 7 Claus, H., Laccases and their occurrence in prokaryotes. *Arch. Microbiol.* **2003**, *179* (3), 145-150. doi:10.1007/s00203-002-0510-7
- 8 Schuetz, M.; Benske, A.; Smith, R. A.; Watanabe, Y.; Tobimatsu, Y.; Ralph, J.; Demura, T.; Ellis, B.; Samuels, A. L., Laccases Direct Lignification in the Discrete Secondary Cell Wall Domains of Protoxylem. *Plant Physiol.* **2014**, *166* (2), 798-807. doi:10.1104/pp.114.245597
- 9 Arakane, Y.; Muthukrishnan, S.; Beeman, R. W.; Kanost, M. R.; Kramer, K. J., Laccase 2 is the phenoxidase gene required for beetle cuticle tanning. *Proc. Natl. Acad. Sci. U. S. A.* **2005**, *102* (32), 11337-11342. doi:10.1073/pnas.0504982102
- 10 Hullo, M.-F.; Moszer, I.; Danchin, A.; Martin-Verstraete, I., CotA of *Bacillus subtilis* Is a Copper-Dependent Laccase. *J. Bacteriol.* **2001**, *183* (18), 5426-5430. doi:10.1128/jb.183.18.5426-5430.2001
- 11 Outten, F. W.; Huffman, D. L.; Hale, J. A.; O'Halloran, T. V., The independent *cue* and *cus* Systems confer copper tolerance during aerobic and anaerobic growth in *Escherichia coli*. *J. Biol. Chem.* **2001**, *276* (33), 30670-30677. doi:10.1074/jbc.M104122200
- 12 Riva, S., Laccases: blue enzymes for green chemistry. *Trends Biotechnol.* **2006**, *24* (5), 219-226. doi:10.1016/j.tibtech.2006.03.006
- 13 Singh, G.; Bhalla, A.; Kaur, P.; Capalash, N.; Sharma, P., Laccase from prokaryotes: A new source for an old enzyme. *Rev. Environ. Sci. Biotechnol.* **2011**, *10* (4), 309-326. doi:10.1007/s11157-011-9257-4
- 14 Zerva, A.; Simić, S.; Topakas, E.; Nikodinovic-Runic, J., Applications of Microbial Laccases: Patent Review of the Past Decade (2009–2019). *Catalysts* **2019**, *9* (12), 1023. doi:10.3390/catal9121023
- 15 Osma, J. F.; Toca-Herrera, J. L.; Rodríguez-Couto, S., Uses of laccases in the food industry. *Enzyme Res.* **2010**, *2010*, 918761-918761. doi:10.4061/2010/918761
- 16 Mate, D. M.; Alcalde, M., Laccase: a multi-purpose biocatalyst at the forefront of biotechnology. *Microb. Biotechnol.* **2016**, *10* (6), 1457-1467. doi:10.1111/1751-7915.12422
- 17 Giardina, P.; Faraco, V.; Pezzella, C.; Piscitelli, A.; Vanhulle, S.; Sannia, G., Laccases: a never-ending story. *Cell. Mol. Life Sci.* **2010**, *67* (3), 369-385. doi:10.1007/s00018-009-0169-1
- 18 Hakulinen, N.; Rouvinen, J., Three-dimensional structures of laccases. *Cell. Mol. Life Sci.* **2015**, *72* (5), 857-868. doi:10.1007/s00018-014-1827-5
- 19 Endo, K.; Hosono, K.; Beppu, T.; Ueda, K., A novel extracytoplasmic phenol oxidase of *Streptomyces*: its possible involvement in the onset of morphogenesis. *Microbiology* **2002**, *148* (6), 1767-1776. doi:10.1099/00221287-148-6-1767
- 20 Machczynski, M. C.; Vijgenboom, E.; Samyn, B.; Canters, G. W., Characterization of SLAC: a small laccase from *Streptomyces coelicolor* with unprecedented activity. *Protein Sci.* **2004**, *13* (9), 2388-2397. doi:10.1110/ps.04759104

- 21 Lawton, T. J.; Sayavedra-Soto, L. A.; Arp, D. J.; Rosenzweig, A. C., Crystal structure of a two-domain multicopper oxidase: implications for the evolution of multicopper blue proteins. *J. Biol. Chem.* **2009**, *284* (15), 10174-10180. doi:10.1074/jbc.M900179200
- 22 Nakamura, K.; Kawabata, T.; Yura, K.; Go, N., Novel types of two-domain multi-copper oxidases: possible missing links in the evolution. *FEBS Lett.* **2003**, *553* (3), 239-244. doi:10.1016/S0014-5793(03)01000-7
- 23 Komori, H.; Miyazaki, K.; Higuchi, Y., X-ray structure of a two-domain type laccase: A missing link in the evolution of multi-copper proteins. *FEBS Lett.* **2009**, *583* (7), 1189-1195. doi:10.1016/j.febslet.2009.03.008
- 24 Warren, J. J.; Lancaster, K. M.; Richards, J. H.; Gray, H. B., Inner-and outer-sphere metal coordination in blue copper proteins. *J. Inorg. Biochem.* **2012**, *115*, 119-126. doi:10.1016/j.jinorgbio.2012.05.002
- 25 Dennison, C.; Harrison, M. D.; Lawler, A. T., Alkaline transition of phytocyanins: a comparison of stellacyanin and umecyanin. *Biochem. J.* **2003**, *371* (2), 377-383. doi:10.1042/bj20021869
- 26 Yanagisawa, S.; Dennison, C., Reduction Potential Tuning at a Type 1 Copper Site Does Not Compromise Electron Transfer Reactivity. *J. Am. Chem. Soc.* **2005**, *127* (47), 16453-16459. doi:10.1021/ja054426v
- 27 Hosseinzadeh, P.; Tian, S.; Marshall, N. M.; Hemp, J.; Mullen, T.; Nilges, M. J.; Gao, Y.-G.; Robinson, H.; Stahl, D. A.; Gennis, R. B.; Lu, Y., A Purple Cupredoxin from *Nitrosopumilus maritimus* Containing a Mononuclear Type 1 Copper Center with an Open Binding Site. *J. Am. Chem. Soc.* **2016**, *138* (20), 6324-6327. doi:10.1021/jacs.5b13128
- 28 Solomon, E. I., Spectroscopic methods in bioinorganic chemistry: blue to green to red copper sites. *Inorg. Chem.* **2006**, *45* (20), 8012-8025. doi:10.1021/ic060450d
- 29 Solomon, E. I.; Szilagy, R. K.; DeBeer George, S.; Basumallick, L., Electronic Structures of Metal Sites in Proteins and Models: Contributions to Function in Blue Copper Proteins. *Chem. Rev.* **2004**, *104* (2), 419-458. doi:10.1021/cr0206317
- 30 Lowery, M. D.; Guckert, J. A.; Gebhard, M. S.; Solomon, E. I., Active-Site Electronic Structure Contributions to Electron-Transfer Pathways in Rubredoxin and Plastocyanin: Direct versus Superexchange. *J. Am. Chem. Soc.* **1993**, *115* (7), 3012-3013. doi:10.1021/ja00060a074
- 31 Enguita, F. J.; Martins, L. O.; Henriques, A. O.; Carrondo, M. A., Crystal structure of a bacterial endospore coat component. A laccase with enhanced thermostability properties. *J. Biol. Chem.* **2003**, *278* (21), 19416-19425. doi:10.1074/jbc.M301251200
- 32 Solomon, E. I.; Augustine, A. J.; Yoon, J., O₂ reduction to H₂O by the multicopper oxidases. *Dalton Trans.* **2008**, (30), 3921-3932. doi:10.1039/b800799c
- 33 Gunne, M.; Urlacher, V. B., Characterization of the Alkaline Laccase Ssl1 from *Streptomyces sviveus* with Unusual Properties Discovered by Genome Mining. *PLoS One* **2012**, *7* (12), e52360. doi:10.1371/journal.pone.0052360
- 34 Gunne, M.; Höppner, A.; Hagedoorn, P. L.; Urlacher, V. B., Structural and redox properties of the small laccase Ssl1 from *Streptomyces sviveus*. *FEBS J.* **2014**, *281* (18), 4307-4318. doi:10.1111/febs.12755
- 35 Olbrich, A. C.; Schild, J. N.; Urlacher, V. B., Correlation between the T1 copper reduction potential and catalytic activity of a small laccase. *J. Inorg. Biochem.* **2019**, *201*, 110843. doi:10.1016/j.jinorgbio.2019.110843
- 36 Ellis, M. J.; Prudêncio, M.; Dodd, F. E.; Strange, R. W.; Sawers, G.; Eady, R. R.; Hasnain, S. S., Biochemical and crystallographic studies of the Met144Ala, Asp92Asn and His254Phe mutants of the nitrite reductase from *Alcaligenes xylosoxidans* provide insight into the enzyme mechanism. *J. Mol. Biol.* **2002**, *316* (1), 51-64. doi:10.1006/jmbi.2001.5304
- 37 Farver, O.; Eady, R. R.; Sawers, G.; Prudêncio, M.; Pecht, I., Met144Ala mutation of the copper-containing nitrite reductase from *Alcaligenes xylosoxidans* reverses the intramolecular electron transfer. *FEBS Lett.* **2004**, *561* (1-3), 173-176. doi:10.1016/S0014-5793(04)00171-1
- 38 Durao, P.; Bento, I.; Fernandes, A. T.; Melo, E. P.; Lindley, P. F.; Martins, L. O., Perturbations of the T1 copper site in the CotA laccase from *Bacillus subtilis*: structural, biochemical, enzymatic and stability studies. *J. Biol. Inorg. Chem.* **2006**, *11* (4), 514-526. doi:10.1007/s00775-006-0102-0

- 39 Marshall, N. M.; Garner, D. K.; Wilson, T. D.; Gao, Y.-G.; Robinson, H.; Nilges, M. J.; Lu, Y., Rationally tuning the reduction potential of a single cupredoxin beyond the natural range. *Nature* **2009**, *462* (7269), 113-116. doi:10.1038/nature08551
- 40 Basumallick, L.; Szilagyi, R. K.; Zhao, Y.; Shapleigh, J. P.; Scholes, C. P.; Solomon, E. I., Spectroscopic Studies of the Met182Thr Mutant of Nitrite Reductase: Role of the Axial Ligand in the Geometric and Electronic Structure of Blue and Green Copper Sites. *J. Am. Chem. Soc.* **2003**, *125* (48), 14784-14792. doi:10.1021/ja037232t
- 41 Bradford, M. M., A rapid and sensitive method for the quantitation of microgram quantities of protein using the principles of protein-dye binding. *Anal. Biochem.* **1976**, *72* (1-2), 248-254. doi:10.1016/0003-2697(76)90527
- 42 Stoll, S.; Schweiger, A., EasySpin, a comprehensive software package for spectral simulation and analysis in EPR. *J. Magn. Reson.* **2006**, *178* (1), 42-55. doi:10.1016/j.jmr.2005.08.013
- 43 Kabsch, W., XDS. *Acta Crystallogr. D* **2010**, *66* (Pt 2), 125-132. doi:10.1107/S0907444909047337
- 44 Winn, M. D.; Ballard, C. C.; Cowtan, K. D.; Dodson, E. J.; Emsley, P.; Evans, P. R.; Keegan, R. M.; Krissinel, E. B.; Leslie, A. G.; McCoy, A., Overview of the CCP4 suite and current developments. *Acta Crystallogr. D* **2011**, *67* (4), 235-242. doi:10.1107/S0907444910045749
- 45 Evans, P. R.; Murshudov, G. N., How good are my data and what is the resolution? *Acta Crystallogr. D* **2013**, *69* (Pt 7), 1204-1214. doi:10.1107/S0907444913000061
- 46 McCoy, A. J.; Grosse-Kunstleve, R. W.; Adams, P. D.; Winn, M. D.; Storoni, L. C.; Read, R. J., *Phaser* crystallographic software. *J. Appl. Crystallogr.* **2007**, *40* (4), 658-674. doi:10.1107/S0021889807021206
- 47 Emsley, P.; Cowtan, K., *Coot*: model-building tools for molecular graphics. *Acta Crystallogr. D* **2004**, *60* (12), 2126-2132. doi:10.1107/S0907444904019158
- 48 Murshudov, G. N.; Skubák, P.; Lebedev, A. A.; Pannu, N. S.; Steiner, R. A.; Nicholls, R. A.; Winn, M. D.; Long, F.; Vagin, A. A., *REFMAC5* for the refinement of macromolecular crystal structures. *Acta Crystallogr. D* **2011**, *67* (4), 355-367. doi:10.1107/S0907444911001314
- 49 Immirzi, A., Crystallographic Computing Techniques (Ahmed FR, editor., ed) p. 399. *Munksgaard, Copenhagen* **1966**,
- 50 Schrodinger, LLC, The PyMOL Molecular Graphics System, Version 2.0. 2015.
- 51 Chen, V. B.; Arendall, W. B.; Headd, J. J.; Keedy, D. A.; Immormino, R. M.; Kapral, G. J.; Murray, L. W.; Richardson, J. S.; Richardson, D. C., *MolProbity*: all-atom structure validation for macromolecular crystallography. *Acta Crystallogr. D* **2010**, *66* (1), 12-21. doi:10.1107/S0907444909042073
- 52 Marcus, R. A.; Sutin, N., Electron transfers in chemistry and biology. *BBA - Rev. Bioenergetics* **1985**, *811* (3), 265-322. doi:10.1016/0304-4173(85)90014-X
- 53 Wijma, H. J.; MacPherson, I.; Farver, O.; Tocheva, E. I.; Pecht, I.; Verbeet, M. P.; Murphy, M. E. P.; Canters, G. W., Effect of the Methionine Ligand on the Reorganization Energy of the Type-1 Copper Site of Nitrite Reductase. *J. Am. Chem. Soc.* **2007**, *129* (3), 519-525. doi:10.1021/ja064763j
- 54 Christensen, N. J.; Kepp, K. P., Setting the stage for electron transfer: Molecular basis of ABTS-binding to four laccases from *Trametes versicolor* at variable pH and protein oxidation state. *J. Mol. Catal. B Enzym.* **2014**, *100*, 68-77. doi:10.1016/j.molcatb.2013.11.017
- 55 Tadesse, M. A.; D'Annibale, A.; Galli, C.; Gentili, P.; Sergi, F., An assessment of the relative contributions of redox and steric issues to laccase specificity towards putative substrates. *Org. Biomol. Chem.* **2008**, *6* (5), 868-878. doi:10.1039/b716002j
- 56 Steenken, S.; Neta, P., One-Electron Redox Potentials of Phenols. Hydroxy- and Aminophenols and Related Compounds of Biological Interest. *J. Phys. Chem.* **1982**, *86* (18), 3661-3667. doi:10.1021/j100215a033
- 57 Blackburn, N. J.; Ralle, M.; Hassett, R.; Kosman, D. J., Spectroscopic Analysis of the Trinuclear Cluster in the Fet3 Protein from Yeast, a Multinuclear Copper Oxidase. *Biochemistry* **2000**, *39* (9), 2316-2324. doi:10.1021/bi992334a
- 58 Reinhammar, B.; Oda, Y., Spectroscopic and Catalytic Properties of *Rhus vernicifera* Laccase Depleted in Type 2 Copper. *J. Inorg. Biochem.* **1979**, *11* (2), 115-127. doi:10.1016/S0162-0134(00)80177-4

- 59 Wynn, R. M.; Knaff, D. B.; Holwerda, R. A., Reactivity, Electrochemical, and Spectroscopic Studies of Type 2 Copper-Depleted *Rhus vernicifera* Laccase. *Biochemistry* **1984**, *23* (2), 241-247. doi:10.1021/bi00297a011
- 60 Andréasson, L.-E.; Reinhammar, B., Kinetic studies of *Rhus vernicifera* laccase: Role of the metal centers in electron transfer. *BBA - Enzymol.* **1976**, *445* (3), 579-597. doi:10.1016/0005-2744(76)90112-1
- 61 Sakurai, T.; Kataoka, K., Structure and function of type I copper in multicopper oxidases. *Cell. Mol. Life Sci.* **2007**, *64* (19-20), 2642-2652. doi:10.1007/s00018-007-7183-y
- 62 Karlsson, B. G.; Aasa, R.; Malmström, B. G.; Lundberg, L. G., Rack-induced bonding in blue copper proteins: Spectroscopic properties and reduction potential of the azurin mutant Met-121 → Leu. *FEBS Lett.* **1989**, *253* (1), 99-102. doi:10.1016/0014-5793(89)80938-X
- 63 Karlsson, B. G.; Nordling, M.; Pascher, T.; Tsai, L.-C.; Sjölin, L.; Lundberg, L. G., Cassette mutagenesis of Met121 in azurin from *Pseudomonas aeruginosa*. *Protein Eng. Des. Sel.* **1991**, *4* (3), 343-349. doi:10.1093/protein/4.3.343
- 64 Pascher, T.; Karlsson, B. G.; Nordling, M.; Malmstrom, B. G.; Vanngard, T., Reduction potentials and their pH dependence in site-directed-mutant forms of azurin from *Pseudomonas aeruginosa*. *Eur. J. Biochem.* **1993**, *212* (2), 289-296. doi:10.1111/j.1432-1033.1993.tb17661.x
- 65 Kroes, S. J.; Hoitink, C. W. G.; Andrew, C. R.; Ai, J.; Sanders-Loehr, J.; Messerschmidt, A.; Hagen, W. R.; Canters, G. W., The Mutation Met121→His Creates a Type-1.5 Copper Site in *Alcaligenes denitrificans* Azurin. *Eur. J. Biochem.* **1996**, *240* (2), 342-351. doi:10.1111/j.1432-1033.1996.0342h.x
- 66 Clark, K. M.; Yu, Y.; Marshall, N. M.; Sieracki, N. A.; Nilges, M. J.; Blackburn, N. J.; van der Donk, W.; Lu, Y., Transforming a Blue Copper into a Red Copper Protein: Engineering Cysteine and Homocysteine into the Axial Position of Azurin using Site-Directed Mutagenesis and Expressed Protein Ligation. *J. Am. Chem. Soc.* **2010**, *132* (29), 10093-10101. doi:10.1021/ja102632p
- 67 Berry, S. M.; Ralle, M.; Low, D. W.; Blackburn, N. J.; Lu, Y., Probing the Role of Axial Methionine in the Blue Copper Center of Azurin with Unnatural Amino Acids. *J. Am. Chem. Soc.* **2003**, *125* (29), 8760-8768. doi:10.1021/ja029699u
- 68 Garner, D. K.; Vaughan, M. D.; Hwang, H. J.; Savelieff, M. G.; Berry, S. M.; Honek, J. F.; Lu, Y., Reduction Potential Tuning of the Blue Copper Center in *Pseudomonas aeruginosa* Azurin by the Axial Methionine as Probed by Unnatural Amino Acids. *J. Am. Chem. Soc.* **2006**, *128* (49), 15608-15617. doi:10.1021/ja062732i
- 69 DeBeer George, S.; Basumallick, L.; Szilagy, R. K.; Randall, D. W.; Hill, M. G.; Nersissian, A. M.; Valentine, J. S.; Hedman, B.; Hodgson, K. O.; Solomon, E. I., Spectroscopic Investigation of Stellacyanin Mutants: Axial Ligand Interactions at the Blue Copper Site. *J. Am. Chem. Soc.* **2003**, *125* (37), 11314-11328. doi:10.1021/ja035802j
- 70 Kataoka, K.; Kondo, A.; Yamaguchi, K.; Suzuki, S., Spectroscopic and electrochemical properties of the Met86Gln mutant of *Achromobacter cycloclastes* pseudoazurin. *J. Inorg. Biochem.* **2000**, *82* (1), 79-84. doi:10.1016/S0162-0134(00)00146-X
- 71 Carrell, C. J.; Ma, J. K.; Antholine, W. E.; Hosler, J. P.; Mathews, F. S.; Davidson, V. L., Generation of Novel Copper Sites by Mutation of the Axial Ligand of Amicyanin. Atomic Resolution Structures and Spectroscopic Properties. *Biochemistry* **2007**, *46* (7), 1900-1912. doi:10.1021/bi0619674
- 72 Hall, J. F.; Kanbi, L. D.; Strange, R. W.; Hasnain, S. S., Role of the Axial Ligand in Type 1 Cu Centers Studied by Point Mutations of Met148 in Rusticyanin. *Biochemistry* **1999**, *38* (39), 12675-12680. doi:10.1021/bi990983g
- 73 Kataoka, K.; Yamaguchi, K.; Sakai, S.; Takagi, K.; Suzuki, S., Characterization and function of Met150Gln mutant of copper-containing nitrite reductase from *Achromobacter cycloclastes* IAM1013. *Biochem. Biophys. Res. Commun.* **2003**, *303* (2), 519-524. doi:10.1016/s0006-291x(03)00381-4
- 74 Kamitaka, Y.; Tsujimura, S.; Kataoka, K.; Sakurai, T.; Ikeda, T.; Kano, K., Effects of axial ligand mutation of the type I copper site in bilirubin oxidase on direct electron transfer-type bioelectrocatalytic reduction of dioxygen. *J. Electroanal. Chem.* **2007**, *601* (1), 119-124. doi:10.1016/j.jelechem.2006.10.035

- 75 Kataoka, K.; Tsukamoto, K.; Kitagawa, R.; Ito, T.; Sakurai, T., Compensatory binding of an asparagine residue to the coordination-unsaturated type I Cu center in bilirubin oxidase mutants. *Biochem. Biophys. Res. Commun.* **2008**, *371* (3), 416-419. doi:10.1016/j.bbrc.2008.04.096
- 76 Palmer, A. E.; Szilagyi, R. K.; Cherry, J. R.; Jones, A.; Xu, F.; Solomon, E. I., Spectroscopic Characterization of the Leu513His Variant of Fungal Laccase: Effect of Increased Axial Ligand Interaction on the Geometric and Electronic Structure of the Type 1 Cu Site. *Inorg. Chem.* **2003**, *42* (13), 4006-4017. doi:10.1021/ic026099n
- 77 Kurose, S.; Kataoka, K.; Shinohara, N.; Miura, Y.; Tsutsumi, M.; Tsujimura, S.; Kano, K.; Sakurai, T., Modification of Spectroscopic Properties and Catalytic Activity of *Escherichia coli* CueO by Mutations of Methionine 510, the Axial Ligand to the Type I Cu. *Bull. Chem. Soc. Jpn.* **2009**, *82* (4), 504-508. doi:10.1246/bcsj.82.504
- 78 Osipov, E.; Polyakov, K.; Kittl, R.; Shleev, S.; Dorovatovsky, P.; Tikhonova, T.; Hann, S.; Ludwig, R.; Popov, V., Effect of the L499M mutation of the ascomycetous *Botrytis aclada* laccase on redox potential and catalytic properties. *Acta Crystallogr. D* **2014**, *70* (11), 2913-2923. doi:10.1107/s1399004714020380
- 79 Prins, A.; Kleinsmidt, L.; Khan, N.; Kirby, B.; Kudanga, T.; Vollmer, J.; Pleiss, J.; Burton, S.; Le Roes-Hill, M., The effect of mutations near the T1 copper site on the biochemical characteristics of the small laccase from *Streptomyces coelicolor* A3 (2). *Enzyme Microb. Technol.* **2015**, *68*, 23-32. doi:10.1016/j.enzmictec.2014.10.003
- 80 Xu, F.; Palmer, A. E.; Yaver, D. S.; Berka, R. M.; Gambetta, G. A.; Brown, S. H.; Solomon, E. I., Targeted mutations in a *Trametes villosa* laccase - Axial perturbations of the T1 copper. *J. Biol. Chem.* **1999**, *274* (18), 12372-12375. doi:10.1074/jbc.274.18.12372
- 81 Xu, F.; Berka, R. M.; Wahleithner, J. A.; Nelson, B. A.; Shuster, J. R.; Brown, S. H.; Palmer, A. E.; Solomon, E. I., Site-directed mutations in fungal laccase: effect on redox potential, activity and pH profile. *Biochem. J.* **1998**, *334*, 63-70. doi:10.1042/bj3340063
- 82 Solomon, E. I.; Penfield, K. W.; Gewirth, A. A.; Lowery, M. D.; Shadle, S. E.; Guckert, J. A.; LaCroix, L. B., Electronic structure of the oxidized and reduced blue copper sites: contributions to the electron transfer pathway, reduction potential, and geometry. *Inorg. Chim. Acta* **1996**, *243* (1), 67-78. doi:10.1016/0020-1693(95)04893-6
- 83 Gewirth, A. A.; Solomon, E. I., Electronic structure of plastocyanin: excited state spectral features. *J. Am. Chem. Soc.* **1988**, *110* (12), 3811-3819. doi:10.1021/ja00220a015
- 84 LaCroix, L. B.; Randall, D. W.; Nersissian, A. M.; Hoitink, C. W. G.; Canters, G. W.; Valentine, J. S.; Solomon, E. I., Spectroscopic and Geometric Variations in Perturbed Blue Copper Centers: Electronic Structures of Stellacyanin and Cucumber Basic Protein. *J. Am. Chem. Soc.* **1998**, *120* (37), 9621-9631. doi:10.1021/ja980606b
- 85 Romero, A.; Hoitink, C. W. G.; Nar, H.; Huber, R.; Messerschmidt, A.; Canters, G. W., X-ray Analysis and Spectroscopic Characterization of M121Q Azurin: A Copper Site Model for Stellacyanin. *J. Mol. Biol.* **1993**, *229* (4), 1007-1021. doi:10.1006/jmbi.1993.1101
- 86 Shimizu, A.; Kwon, J.-H.; Sasaki, T.; Satoh, T.; Sakurai, N.; Sakurai, T.; Yamaguchi, S.; Samejima, T., *Myrothecium verrucaria* Bilirubin Oxidase and Its Mutants for Potential Copper Ligands. *Biochemistry* **1999**, *38* (10), 3034-3042. doi:10.1021/bi9819531
- 87 Kataoka, K.; Tanaka, K.; Sakai, Y.; Sakurai, T., High-level expression of *Myrothecium verrucaria* bilirubin oxidase in *Pichia pastoris*, and its facile purification and characterization. *Protein Expr. Purif.* **2005**, *41* (1), 77-83. doi:10.1016/j.pep.2005.02.001
- 88 Kataoka, K.; Kitagawa, R.; Inoue, M.; Naruse, D.; Sakurai, T.; Huang, H. W., Point mutations at the type I Cu ligands, Cys457 and Met467, and at the putative proton donor, Asp105, in *Myrothecium verrucaria* bilirubin oxidase and reactions with dioxygen. *Biochemistry* **2005**, *44* (18), 7004-7012. doi:10.1021/bi0476836
- 89 Hadt, R. G.; Gorelsky, S. I.; Solomon, E. I., Anisotropic Covalency Contributions to Superexchange Pathways in Type One Copper Active Sites. *J. Am. Chem. Soc.* **2014**, *136* (42), 15034-15045. doi:10.1021/ja508361h
- 90 Sekretaryova, A.; Jones, S. M.; Solomon, E. I., O₂ Reduction to Water by High Potential Multicopper Oxidases: Contributions of the T1 Copper Site Potential and the Local Environment of the Trinuclear Copper Cluster. *J. Am. Chem. Soc.* **2019**, *141* (28), 11304-11314. doi:10.1021/jacs.9b05230

- 91 LuBien, C. D.; Winkler, M. E.; Thamann, T. J.; Scott, R. A.; Co, M. S.; Hodgson, K. O.; Solomon, E. I., Chemical and Spectroscopic Properties of the Binuclear Copper Active Site in *Rhus* Laccase: Direct Confirmation of a Reduced Binuclear Type 3 Copper Site in Type 2 Depleted Laccase and Intramolecular Coupling of the Type 3 to the Type 1 and Type 2 Copper Sites. *J. Am. Chem. Soc.* **1981**, *103* (23), 7014-7016. doi:10.1021/ja00413a063
- 92 Kau, L. S.; Spira-Solomon, D. J.; Penner-Hahn, J. E.; Hodgson, K. O.; Solomon, E. I., X-ray absorption Edge Determination of the Oxidation State and Coordination Number Of Copper. Application to the Type 3 Site in *Rhus vernicifera* laccase and Its Reaction with Oxygen. *J. Am. Chem. Soc.* **1987**, *109* (21), 6433-6442. doi:10.1021/ja00255a032
- 93 LaCroix, L. B.; Shadle, S. E.; Wang, Y. N.; Averill, B. A.; Hedman, B.; Hodgson, K. O.; Solomon, E. I., Electronic Structure of the Perturbed Blue Copper Site in Nitrite Reductase: Spectroscopic Properties, Bonding, and Implications for the Entatic/Rack State. *J. Am. Chem. Soc.* **1996**, *118* (33), 7755-7768. doi:10.1021/ja961217p
- 94 Vallee, B. L.; Williams, R. J. P., Metalloenzymes: the entatic nature of their active sites. *Proc. Natl. Acad. Sci. U. S. A.* **1968**, *59* (2), 498-505. doi:10.1073/pnas.59.2.498
- 95 Guckert, J. A.; Lowery, M. D.; Solomon, E. I., Electronic Structure of the Reduced Blue Copper Active Site: Contributions to Reduction Potentials and Geometry. *J. Am. Chem. Soc.* **1995**, *117* (10), 2817-2844. doi:10.1021/ja00115a016
- 96 Harrison, M. D.; Dennison, C., An Axial Met Ligand at a Type 1 Copper Site is Preferable for Fast Electron Transfer. *Chembiochem* **2004**, *5* (11), 1579-1581. doi:10.1002/cbic.200400152
- 97 Szuster, J.; Zitare, U. A.; Castro, M. A.; Leguto, A. J.; Morgada, M. N.; Vila, A. J.; Murgida, D. H., Cu A-based chimeric T1 copper sites allow for independent modulation of reorganization energy and reduction potential. *Chemical science* **2020**, *11* (24), 6193-6201. doi:10.1039/D0SC01620A
- 98 Lowery, M. D.; Solomon, E. I., Axial ligand bonding in blue copper proteins. *Inorg. Chim. Acta* **1992**, *198*, 233-243. doi:10.1016/S0020-1693(00)92365-X
- 99 Durao, P.; Chen, Z.; Silva, C. S.; Soares, C. M.; Pereira, M. M.; Todorovic, S.; Hildebrandt, P.; Bento, I.; Lindley, P. F.; Martins, L. O., Proximal mutations at the type 1 copper site of CotA laccase: spectroscopic, redox, kinetic and structural characterization of I494A and L386A mutants. *Biochem. J.* **2008**, *412* (2), 339-346. doi:10.1042/bj20080166
- 100 Nersissian, A. M.; Immoos, C.; Hill, M. G.; Hart, P. J.; Williams, G.; Herrmann, R. G.; Valentine, J. S., Uclacyanins, stellacyanins, and plantacyanins are distinct subfamilies of phytocyanins: Plant-specific mononuclear blue copper proteins. *Protein Sci.* **1998**, *7* (9), 1915-1929. doi:10.1002/pro.5560070907

Supplementary information

Influence of the T1 Cu axial ligand on kinetic, spectral, and structural properties of the laccase Ssl1 from *Streptomyces sviveus*

Authors:

Anna C. Olbrich^{a†}, Steffen Mielenbrink^{b†}, Vivian P. Willers^a, George E. Cutsail III^c, James A. Birrell^c, Ingrid Span^{b*}, Vlada B. Urlacher^{a*}

*corresponding authors: Vlada.Urlacher@hhu.de, Ingrid.Span@hhu.de

† These authors contributed equally.

^a Institut für Biochemie, Heinrich-Heine-Universität Düsseldorf, Universitätsstr. 1, 40225 Düsseldorf, Germany

^b Institut für Physikalische Biologie, Heinrich-Heine-Universität Düsseldorf, Universitätsstr. 1, 40225 Düsseldorf, Germany

^c Max Planck Institute for Chemical Energy Conversion, Stiftstr. 34-36, 45470 Mülheim an der Ruhr, Germany

Crystallography Analysis

Table S1: Data collection and refinement statistics.

	M295A	M295F	M295I	M295V	M295Y
Data collection					
Space group	P2 ₁ 2 ₁ 2 ₁	P222	P2 ₁ 2 ₁ 2 ₁	P2 ₁ 2 ₁ 2 ₁	P222
Cell dimensions					
<i>a</i> , <i>b</i> , <i>c</i> (Å)	51.440, 104.100, 163.130	51.41, 104.46, 162.21	51.38, 104.32, 162.33	51.35, 103.96, 161.67	51.40, 104.24, 162.06
α , β , γ (°)	90, 90, 90	90, 90, 90	90, 90, 90	90, 90, 90	90, 90, 90
Resolution (Å)	30.36-1.41 (1.43-1.41)*	50.00-1.5 (1.59-1.5)*	50.00-1.79 (1.89-1.79)*	50.00-2.28 (2.42-2.28)*	50.00-1.68 (1.79-1.68)*
<i>R</i> _{merge}	0.093 (1.852)	0.082 (1.160)	0.185 (1.910)	0.344 (1.686)	0.1395 (1.913)
<i>I</i> / σ <i>I</i>	13.0 (1.2)	13.05 (1.34)	7.64 (0.88)	4.96 (0.96)	8.87 (0.90)
Completeness (%)	99.9 (99.9)	99.9 (70.4)	99.8 (99.0)	98.7 (96.8)	99.3 (97.3)
Redundancy	12.9 (11.8)	?(?)	?(?)	?(?)	?(?)
Refinement					
Resolution (Å)	30.36-1.41	48.06-1.5	48.08-1.79	48.99-2.28	49.00-1.68
No. reflections	168969	138706	83649	39762	98712
<i>R</i> _{work} / <i>R</i> _{free}	0.200/0.225	0.176/0.199	0.186/0.228	0.227/0.285	0.191/0.232
No. atoms					
Protein	12295	12309	12230	12256	12212
Ligand/ion	24	34	9	30	25
Water	225	516	641	60	675
<i>B</i> -factors					
Protein	21	21	26	36	24
Ligand/ion	32,375	28,444	27,556	46,214	31,462
Water			?		
R.m.s. deviations					
Bond lengths (Å)	0.012	0.013	0.009	0.006	0.012
Bond angles (°)	1.657	1.750	1.559	1.411	1.625

*Values in parentheses are for highest-resolution shell.

Gaussian Fits of CD transitions

Five transitions in the CD spectra of Ssl1 variants were fitted to the Gaussian function (Equation S1) using MagicPlot.

$$y(x) = a \cdot \exp\left(-\ln(2) \cdot \frac{(x-x_0)^2}{dx^2}\right)$$

Equation S1

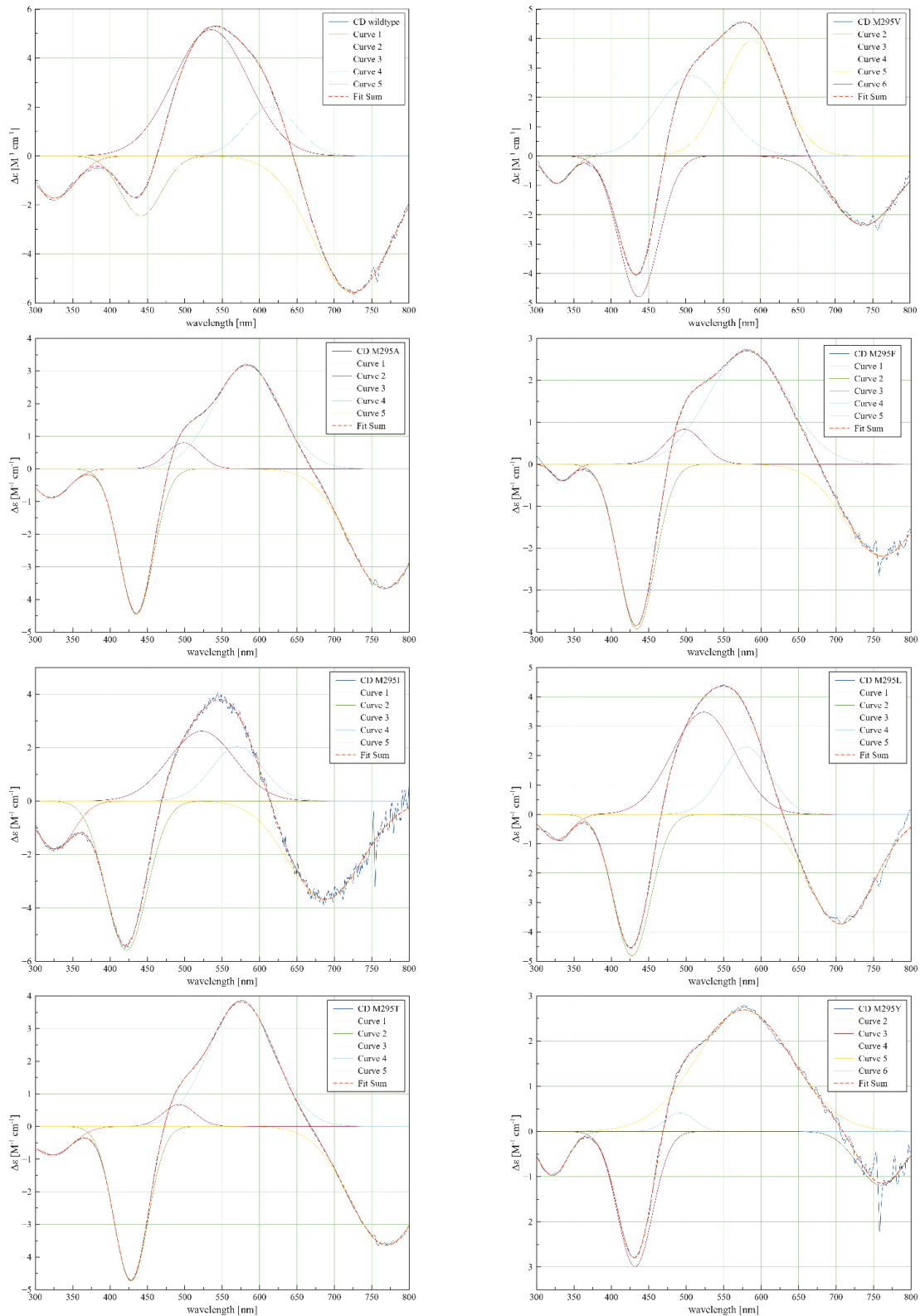


Figure S1: CD spectra of Ssl1 variants and Gaussian fits.

Table S2: Parameters for Gaussian fits of CD spectra. For M295A the fitting interval was decreased to 315–800 nm. For M295V and M295Y the baseline was adjusted before fitting.

		WT	M295L	M295F	M295I	M295V	M295A	M295T	M295Y
Data Intervals		300-800 nm	315-800 nm	300-800 nm	300-800 nm				
Results						baseline adj.			
Iterations		26	36	13	81	26	8	11	26
Convergence		7.9549e-11	5.6997e-12	6.8812e-11	3.9181e-11	1.2954e-10	8.855e-11	4.2317e-11	2.3316e-10
Residual Sum of Squares (RSS, χ^2)		4.889	10.6039	3.4948	33.4236	4.7035	0.4479	0.5544	6.8686
Reduced RSS		0.005	0.0108	0.0035	0.0339	0.0048	9.5088e-4	0.0011	0.0141
Residual Standard Deviation		0.0704	0.1037	0.0595	0.1841	0.0691	0.0308	0.0338	0.1189
Coefficient of Determination R ²		0.9996	0.9985	0.999	0.9949	0.9992	0.9998	0.9998	0.9942
Adjusted R ²		0.9996	0.9985	0.9989	0.9948	0.9992	0.9998	0.9998	0.9941
Fitted Curves									
		mean	mean	mean	mean	mean	mean	mean	mean
		SD	SD	SD	SD	SD	SD	SD	SD
1	a	-1.7254	-0.8697	-0.3961	-1.7899	-0.9292	-0.8885	-0.8824	-0.9743
	x ₀	325.7978	327.0553	335.4111	326.3158	328.1317	321.7466	321.7566	321.3436
	dx	33.1767	22.42	15.1802	29.8439	21.0523	27.7231	32.5222	23.572
2	a	-2.4495	-4.8128	-3.9324	-5.5955	-4.7992	-4.4557	-4.7372	-2.9904
	x ₀	441.4332	427.5006	433.9072	421.9121	436.936	435.2726	428.0259	431.6022
	dx	31.8317	29.2017	28.9543	32.294	31.291	26.6997	26.7521	27.4957
3	a	5.1572	3.479	0.8314	2.6148	2.7271	0.7985	0.6707	0.4098
	x ₀	535.1472	523.4546	497.5506	522.711	507.1585	498.1159	492.24	491.7864
	dx	58.905	49.6307	29.4674	51.9099	62.6685	25.9621	25.3435	23.1099
4	a	2.0096	2.2979	2.7029	2.0425	3.9183	3.174	3.8212	2.6883
	x ₀	614.9903	579.447	582.211	570.2139	588.8048	582.9857	575.6339	577.0859
	dx	40.3176	38.1602	2.7392	40.4149	46.1747	52.0463	52.1524	74.9042
5	a	-5.5913	-3.7264	-2.1929	-3.6867	-2.3609	-3.6711	-3.6383	-1.1918
	x ₀	724.62	706.0978	761.2911	687.3692	737.9399	767.2824	770.0185	760.3123
	dx	62.8539	53.2864	58.6757	58.144	51.1038	56.6424	58.6872	36.7188

Stopped Flow

The absorption of the T1 Cu at 592 nm was plotted against time for all mutants and fitted to a first order exponential decay (Equation S2) in origin. All plots and fit parameters are given in the following figures (Figure 2 to Figure 8) and tables (Table 3 to Table 9).

$$y = A1 \cdot \exp\frac{-x}{t1} + y0 \text{ and } k = \frac{1}{t1} \quad \text{Equation S2}$$

H99Y:

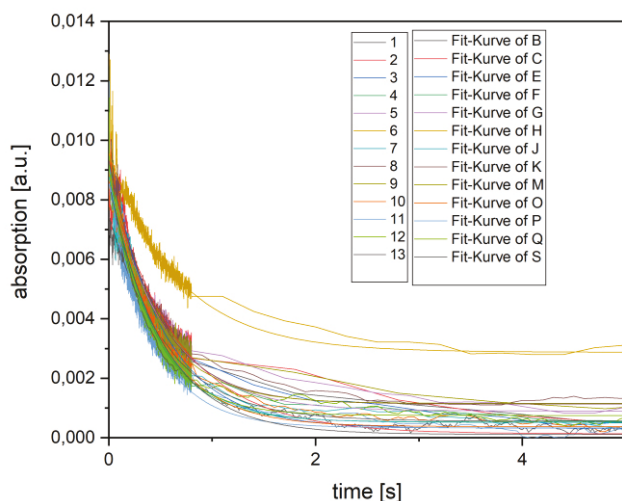


Figure S2: Absorption traces for the reduction of the T1 Cu in Ssl1 H99Y by hydroquinone followed at ~592 nm. The traces were fitted to a first order exponential decay using Origin pro 9.0G.

Table S3: Fit parameters for H99Y obtained from fitting absorption traces to a first order exponential decay.

	y0	y0	A1	A1	t1	t1	k	k	statistics	statistics
	value	standard error	value	standard error	value	standard error	value	standard error	reduced Chi-Sqr	Adj. R-Square
1	5.59E-04	2.00E-05	0.00691	3.23E-05	0.55435	0.0051	1.80393	0.01659	8.18E-08	0.97964
2	1.31E-04	3.09E-05	0.00844	4.88E-05	0.67162	0.00785	1.48894	0.01741	1.92E-07	0.96963
3	3.21E-04	1.93E-05	0.00899	3.13E-05	0.52256	0.00357	1.91366	0.01309	7.58E-08	0.98857
4	5.34E-04	1.96E-05	0.00841	3.29E-05	0.43519	0.00335	2.29783	0.01767	8.03E-08	0.98563
5	8.98E-04	2.19E-05	0.00766	3.52E-05	0.54389	0.00493	1.8386	0.01666	9.68E-08	0.98024
6	0.00288	2.82E-05	0.00669	4.41E-05	0.67153	0.009	1.48914	0.01995	1.57E-07	0.96061
7	5.16E-04	2.53E-05	0.00827	4.12E-05	0.46154	0.00456	2.16664	0.02139	1.28E-07	0.97671
8	0.00114	1.97E-05	0.0082	3.20E-05	0.47234	0.00365	2.1171	0.01636	7.77E-08	0.98559
9	0.00116	2.27E-05	0.00774	3.78E-05	0.46046	0.0044	2.17174	0.02074	1.07E-07	0.9778
10	3.75E-04	2.29E-05	0.00856	3.62E-05	0.47885	0.00407	2.08833	0.01774	9.96E-08	0.983
11	3.35E-04	2.35E-05	0.0082	3.86E-05	0.41726	0.00395	2.3966	0.02267	1.09E-07	0.97921
12	7.50E-04	1.74E-05	0.00828	2.90E-05	0.40306	0.00284	2.48101	0.0175	6.12E-08	0.9884
13	1.12E-04	8.45E-06	0.00847	1.04E-04	0.51582	0.009	1.93867	0.03382	6.40E-08	0.92957

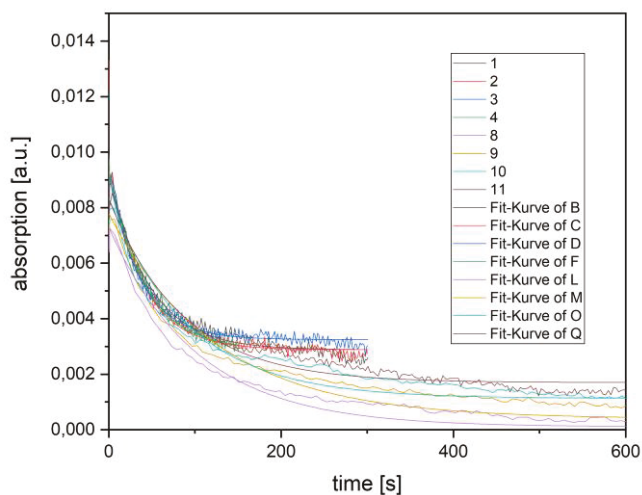
H99Y/M295A

Figure S3: Absorption traces for the reduction of the T1 Cu in Ssl1 H99Y/M295A by hydroquinone followed at ~592 nm. The traces were fitted to a first order exponential decay using Origin pro 9.0G.

Table S4: Fit parameters for H99Y/M295A obtained from fitting absorption traces to a first order exponential decay.

	y0	y0	A1	A1	t1	t1	k	k	statistics	statistics
	value	standard error	value	standard error	value	standard error	value	standard error	Reduced Chi-Sqr	Adj. R-Square
B	0.00288	5.01E-05	0.00637	5.16E-05	46.60806	1.65316	0.02146	7.61E-04	2.17E-07	0.95841
C	0.00288	4.42E-05	0.00644	4.59E-05	39.92022	1.36261	0.02505	8.55E-04	1.99E-07	0.96394
D	0.00325	4.05E-05	0.00596	4.23E-05	36.51943	1.30457	0.02738	9.78E-04	1.81E-07	0.96251
F	0.00288	5.10E-05	0.00637	5.07E-05	41.80462	1.01052	0.02392	5.78E-04	7.97E-08	0.98019
L	1.02E-04	3.43E-05	0.00719	3.67E-05	102.8565	3.15028	0.00972	2.98E-04	1.60E-07	0.97839
M	3.94E-04	3.33E-05	0.00739	3.54E-05	123.77332	3.21853	0.00808	2.10E-04	1.37E-07	0.98198
O	0.00113	3.57E-05	0.00722	3.81E-05	91.7743	2.80517	0.0109	3.33E-04	1.68E-07	0.9773
Q	0.0017	3.42E-05	0.00661	3.56E-05	85.46526	2.09781	0.0117	2.87E-04	1.11E-07	0.98043

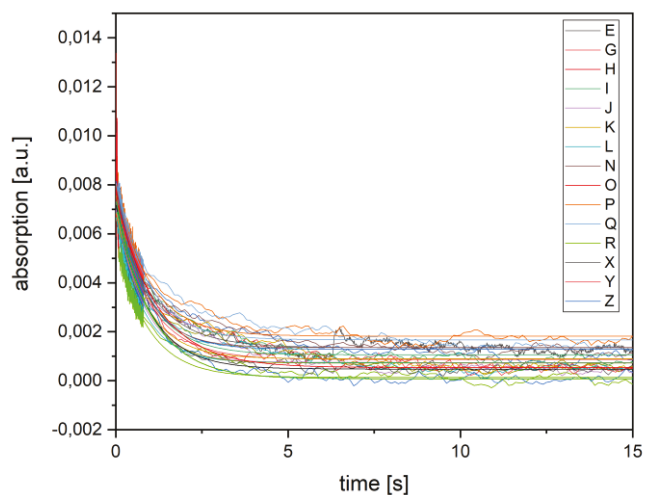
H99Y/M295F

Figure S4: Absorption traces for the reduction of the T1 Cu in Ssl1 H99Y/M295F by hydroquinone followed at ~592 nm. The traces were fitted to a first order exponential decay using Origin pro 9.0G.

Table S5: Fit parameters for H99Y/M295F obtained from fitting absorption traces to a first order exponential decay.

	y0	y0	A1	A1	t1	t1	k	k	statistics	statistics
	value	standard error	value	standard error	value	standard error	value	standard error	Reduced Chi-Sqr	Adj. R-Square
B	5.86E-04	1.10E-05	0.00618	4.96E-05	1.673	0.02239	0.59773	0.008	6.75E-08	0.96048
C	8.72E-04	1.15E-05	0.00579	4.43E-05	1.96899	0.02634	0.50787	0.00679	6.35E-08	0.96213
D	3.54E-04	8.48E-06	0.00587	2.77E-05	2.46497	0.02134	0.40568	0.00351	2.56E-08	0.98539
E	0.00135	9.16E-06	0.0056	5.81E-05	1.08755	0.01738	0.9195	0.0147	5.96E-08	0.94165
G	8.69E-04	2.34E-05	0.00617	3.32E-05	0.9968	0.01277	1.00321	0.01285	9.22E-08	0.97373
H	0.00129	2.54E-05	0.00693	3.75E-05	0.83108	0.0099	1.20326	0.01433	1.14E-07	0.97337
I	0.00106	2.14E-05	0.00631	3.07E-05	0.95394	0.01083	1.04829	0.0119	7.82E-08	0.9784
J	7.49E-04	2.59E-05	0.0063	3.83E-05	0.81793	0.01088	1.22259	0.01626	1.18E-07	0.96663
K	8.97E-04	2.49E-05	0.00601	3.64E-05	0.87627	0.01195	1.1412	0.01556	1.08E-07	0.9668
L	7.39E-04	2.33E-05	0.00599	3.48E-05	0.7838	0.00982	1.27584	0.01598	9.68E-08	0.96936
N	0.00136	2.08E-05	0.00667	3.14E-05	0.80572	0.00821	1.24112	0.01264	7.91E-08	0.97987
O	7.23E-04	2.56E-05	0.00692	3.87E-05	0.80792	0.00979	1.23774	0.015	1.20E-07	0.97181
P	0.00182	1.82E-05	0.00626	2.67E-05	0.9522	0.00941	1.0502	0.01038	5.89E-08	0.98354
Q	0.00167	2.35E-05	0.00646	3.47E-05	0.9214	0.01129	1.08531	0.0133	9.88E-08	0.97416
R	1.39E-04	1.70E-05	0.00554	2.95E-05	0.92814	0.0111	1.07743	0.01289	5.14E-08	0.97998
X	5.50E-04	1.86E-05	0.00667	2.87E-05	0.93622	0.00915	1.06812	0.01044	6.73E-08	0.9838
Y	6.42E-04	1.76E-05	0.00684	3.00E-05	1.19503	0.01348	0.8368	0.00944	5.91E-08	0.98681
Z	1.77E-04	1.88E-05	0.00699	3.09E-05	1.02623	0.01072	0.97444	0.01018	6.82E-08	0.98492

H99Y/M295I

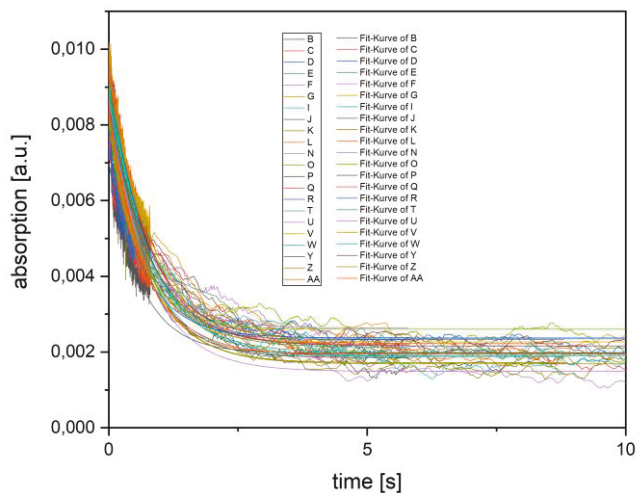


Figure S5: Absorption traces for the reduction of the T1 Cu in Ssl1 H99Y/M295I by hydroquinone followed at ~592 nm. The traces were fitted to a first order exponential decay using Origin pro 9.0G.

Table S6: Fit parameters for H99Y/M295I obtained from fitting absorption traces to a first order exponential decay.

	y0	y0	A1	A1	t1	t1	k	k	statistics	statistics
	value	standard error	Reduced Chi-Sqr	Adj. R-Square						
B	0.00185	1.90E-05	0.00728	2.55E-05	0.68205	0.00525	1.46616	0.01128	5.16E-08	0.98797
C	0.00219	1.91E-05	0.00747	2.46E-05	0.75317	0.00563	1.32772	0.00992	4.85E-08	0.98928
D	0.00232	2.06E-05	0.00661	2.81E-05	0.63926	0.00588	1.56432	0.0144	6.25E-08	0.98234
E	0.00212	2.34E-05	0.00679	2.99E-05	0.76554	0.00769	1.30628	0.01312	7.17E-08	0.98099
F	0.00264	2.52E-05	0.00607	3.39E-05	0.6716	0.00821	1.48899	0.01821	9.12E-08	0.9699
G	0.00224	2.11E-05	0.00637	2.83E-05	0.67165	0.00654	1.48888	0.0145	6.37E-08	0.9807
I	0.00188	2.09E-05	0.00695	2.97E-05	0.70584	0.00646	1.41676	0.01296	7.14E-08	0.98246
J	0.00233	2.05E-05	0.00695	2.85E-05	0.75809	0.0068	1.31911	0.01183	6.64E-08	0.9838
K	0.00172	1.96E-05	0.00731	2.77E-05	0.71426	0.00581	1.40005	0.0114	6.22E-08	0.98614
L	0.00222	2.00E-05	0.00725	2.77E-05	0.78046	0.00658	1.28129	0.01081	6.30E-08	0.9859
N	0.00235	1.89E-05	0.00614	2.74E-05	0.69949	0.00661	1.42961	0.01351	6.11E-08	0.98096
O	0.0026	2.04E-05	0.00543	3.07E-05	0.59883	0.00694	1.66993	0.01936	7.48E-08	0.96981
P	0.00197	2.57E-05	0.00504	3.84E-05	0.61306	0.0096	1.63117	0.02554	1.17E-07	0.94664
Q	0.0019	2.01E-05	0.00533	2.84E-05	0.79044	0.00923	1.26512	0.01477	6.67E-08	0.97322
R	0.00238	2.25E-05	0.005	3.31E-05	0.6669	0.00923	1.49948	0.02075	8.83E-08	0.95914
T	0.00199	2.09E-05	0.00689	3.07E-05	0.78035	0.00749	1.28148	0.0123	7.79E-08	0.98137
U	0.00149	2.35E-05	0.00722	3.48E-05	0.74583	0.00763	1.34079	0.01371	9.94E-08	0.97827
V	0.00226	2.07E-05	0.00707	2.99E-05	0.83532	0.0078	1.19714	0.01118	7.51E-08	0.98317
W	0.0019	1.72E-05	0.00721	2.51E-05	0.79954	0.00604	1.25072	0.00944	5.22E-08	0.98858
Y	0.00216	1.84E-05	0.00637	2.73E-05	0.79754	0.00736	1.25385	0.01158	6.19E-08	0.98293
Z	0.00169	1.83E-05	0.00651	2.73E-05	0.76025	0.00678	1.31536	0.01173	6.16E-08	0.98352
AA	0.00195	1.58E-05	0.00655	2.42E-05	0.65479	0.00495	1.5272	0.01153	4.72E-08	0.98711

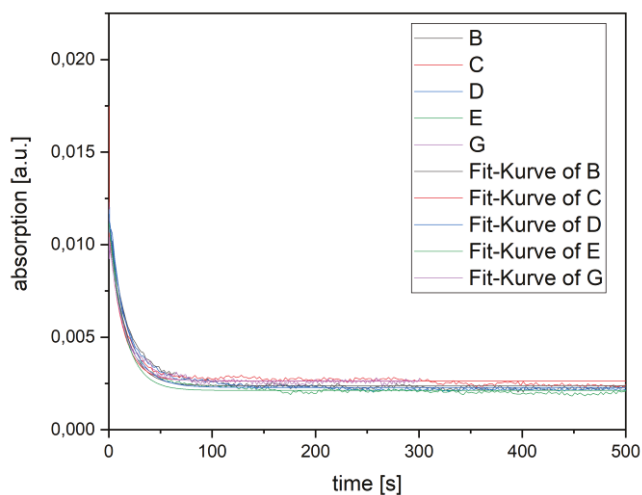
H99Y/M295T

Figure S6: Absorption traces for the reduction of the T1 Cu in Ssl1 H99Y/M295T by hydroquinone followed at ~592 nm. The traces were fitted to a first order exponential decay using Origin pro 9.0G.

Table S7: Fit parameters for H99Y/M295T obtained from fitting absorption traces to a first order exponential decay.

	y0	y0	A1	A1	t1	t1	k	k	statistics	statistics
	value	standard error	value	standard error	value	standard error	value	standard error	Reduced Chi-Sqr	Adj. R-Square
B	0.00238	3.20E-05	0.00896	3.60E-05	15.00463	0.59851	0.06665	0.00266	1.83E-07	0.98547
C	0.00264	2.10E-05	0.00805	2.40E-05	13.34813	0.40722	0.07492	0.00229	7.99E-08	0.99209
D	0.00229	2.28E-05	0.0094	2.54E-05	16.66595	0.43079	0.06	0.00155	9.17E-08	0.99335
E	0.00213	2.04E-05	0.00908	2.30E-05	14.77484	0.37213	0.06768	0.0017	7.43E-08	0.99422
G	0.00263	2.04E-05	0.00783	2.23E-05	14.66074	0.33406	0.06821	0.00155	6.84E-08	0.99265

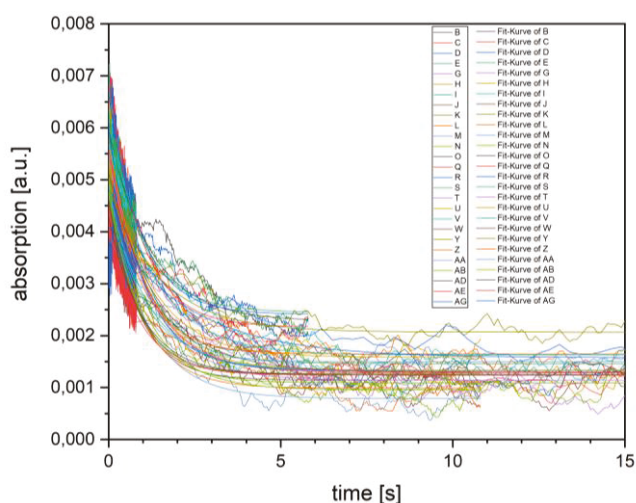
H99Y/M295V

Figure S7: Absorption traces for the reduction of the T1 Cu in Ssl1 H99Y/M295V by hydroquinone followed at ~592 nm. The traces were fitted to a first order exponential decay using Origin pro 9.0G.

Table S8: Fit parameters for H99Y/M295V obtained from fitting absorption traces to a first order exponential decay.

	y0	y0	A1	A1	t1	t1	k	k	statistics	statistics
	value	standard error	value	standard error	value	standard error	value	standard error	Reduced Chi-Sqr	Adj. R-Square
B	0.00228	3.18E-05	0.00368	3.24E-05	1.2343	0.03025	0.81018	0.01986	7.76E-08	0.93151
C	0.00217	2.12E-05	0.00469	2.48E-05	0.94032	0.0123	1.06347	0.01391	4.93E-08	0.97288
D	0.00241	2.15E-05	0.00423	2.51E-05	0.94676	0.01397	1.05624	0.01559	5.05E-08	0.96594
E	0.00245	2.37E-05	0.0036	2.66E-05	1.02577	0.01952	0.97487	0.01855	5.60E-08	0.94855
G	0.00131	2.00E-05	0.00438	2.57E-05	1.12625	0.01688	0.8879	0.01331	5.77E-08	0.96745
H	0.00158	2.07E-05	0.00378	2.56E-05	1.24348	0.02271	0.80419	0.01468	5.82E-08	0.95672
I	0.00133	1.80E-05	0.00345	2.28E-05	1.16063	0.02001	0.8616	0.01485	4.59E-08	0.95859
J	0.00114	2.01E-05	0.00354	2.76E-05	0.8782	0.01565	1.13869	0.02029	6.42E-08	0.94396
K	0.00127	1.65E-05	0.0033	2.28E-05	0.86142	0.01348	1.16087	0.01817	4.38E-08	0.95558
L	9.87E-04	1.92E-05	0.00375	2.57E-05	0.97158	0.01585	1.02926	0.01679	5.65E-08	0.95625
M	7.87E-04	1.80E-05	0.00392	2.31E-05	1.12967	0.01707	0.88521	0.01338	4.67E-08	0.96703
N	9.54E-04	1.89E-05	0.00381	2.41E-05	1.1338	0.01844	0.88199	0.01434	5.09E-08	0.96215
O	0.00125	1.92E-05	0.00332	2.64E-05	0.88429	0.01606	1.13085	0.02054	5.87E-08	0.94219
Q	0.00129	2.00E-05	0.00432	2.71E-05	1.145	0.01831	0.87337	0.01397	6.51E-08	0.9638
R	0.00133	2.09E-05	0.00465	2.91E-05	1.01926	0.01533	0.9811	0.01476	7.33E-08	0.96401
S	0.00147	2.10E-05	0.00482	2.92E-05	1.00966	0.01466	0.99044	0.01438	7.40E-08	0.9661
T	0.00114	2.35E-05	0.00435	3.14E-05	1.19823	0.02262	0.83457	0.01576	8.83E-08	0.95242
U	0.00134	2.20E-05	0.00438	2.99E-05	1.12865	0.01953	0.88601	0.01533	7.92E-08	0.95728
V	0.00163	1.79E-05	0.00409	2.33E-05	1.33306	0.02101	0.75016	0.01182	4.93E-08	0.96981
W	0.0013	2.28E-05	0.00382	2.90E-05	1.4234	0.03112	0.70254	0.01536	7.80E-08	0.94717
Y	0.00207	1.89E-05	0.0028	2.47E-05	1.50892	0.0397	0.66273	0.01744	5.75E-08	0.93105
Z	0.00165	1.86E-05	0.00361	2.68E-05	0.97837	0.01699	1.0221	0.01775	6.17E-08	0.95093
AA	0.0015	1.71E-05	0.00339	2.46E-05	0.95876	0.01613	1.04302	0.01755	5.18E-08	0.95292
AB	0.00109	1.74E-05	0.00362	2.51E-05	0.9614	0.01553	1.04014	0.0168	5.42E-08	0.95656
AD	0.00125	1.54E-05	0.00303	2.32E-05	0.98277	0.01749	1.01753	0.01811	4.60E-08	0.94941
AE	0.00124	1.52E-05	0.00285	2.31E-05	0.90588	0.01641	1.1039	0.02	4.51E-08	0.94342
AG	0.00158	2.96E-05	0.00252	3.91E-05	2.37501	0.14976	0.42105	0.02655	1.56E-07	0.82475

H99Y/M295Y

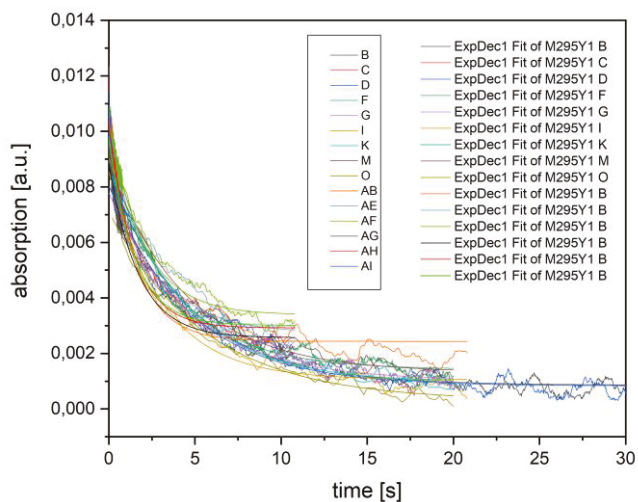


Figure S8: Absorption traces for the reduction of the T1 Cu in Ssl1 H99Y/M295Y by hydroquinone followed at ~592 nm. The traces were fitted to a first order exponential decay using Origin pro 9.0G.

Table S9: Fit parameters for H99Y/M295Y obtained from fitting absorption traces to a first order exponential decay.

	y0	y0	A1	A1	t1	t1	k	k	statistics	statistics
	value	standard error	value	standard error	value	standard error	value	standard error	Reduced Chi-Sqr	Adj. R-Square
B	8.59E-04	1.70E-05	0.00763	5.43E-05	4.6744	0.06222	0.21393	0.00285	1.13E-07	0.96484
C	8.27E-04	1.72E-05	0.00722	5.51E-05	4.66636	0.06654	0.2143	0.00306	1.17E-07	0.95983
D	8.29E-04	1.74E-05	0.00723	5.57E-05	4.65442	0.06687	0.21485	0.00309	1.19E-07	0.95919
F	0.00142	1.76E-05	0.00762	4.30E-05	3.82705	0.04515	0.2613	0.00308	8.72E-08	0.97523
G	0.00102	2.19E-05	0.00679	4.05E-05	4.61298	0.0655	0.21678	0.00308	9.23E-08	0.96934
I	0.00106	4.48E-05	0.0075	6.36E-05	3.12802	0.09407	0.31969	0.00961	1.83E-07	0.97906
K	9.30E-04	5.72E-05	0.00779	1.19E-04	4.3888	0.15123	0.22785	0.00785	7.06E-08	0.98108
M	0.00132	6.66E-05	0.00751	1.32E-04	4.53044	0.18359	0.22073	0.00894	8.92E-08	0.97472
O	2.98E-04	7.89E-05	0.00683	1.13E-04	5.49134	0.24622	0.1821	0.00817	7.78E-08	0.97456
AB	0.00244	3.03E-05	0.00725	3.85E-05	1.64995	0.02753	0.60608	0.01011	1.43E-07	0.97374
AE	0.00276	4.20E-05	0.0074	3.89E-05	2.43469	0.04436	0.41073	0.00748	1.06E-07	0.97795
AF	0.00339	3.36E-05	0.00693	3.32E-05	2.04679	0.03338	0.48857	0.00797	9.23E-08	0.97887
AG	0.00257	3.89E-05	0.00628	4.17E-05	1.71296	0.03635	0.58379	0.01239	1.57E-07	0.95794
AH	0.00292	3.25E-05	0.00734	3.76E-05	1.45771	0.02201	0.68601	0.01036	1.28E-07	0.97441
AI	0.00301	3.54E-05	0.00681	4.06E-05	1.48702	0.0264	0.67249	0.01194	1.50E-07	0.96564

Redox titrations of T2D Ssl1 variants

Titration curves were fitted to the Nernst equation (Equation S3) in Origin 9.0G. The fit parameter x_0 represents the midpoint potential of the laccase.

$$y = A_2 + \frac{A_1 - A_2}{1 + \exp\left(\frac{x - x_0}{dx}\right)} \text{ with } dx = \frac{RT}{nF} = 0.02526 \text{ J/C} \quad \text{Equation S3}$$

H99Y

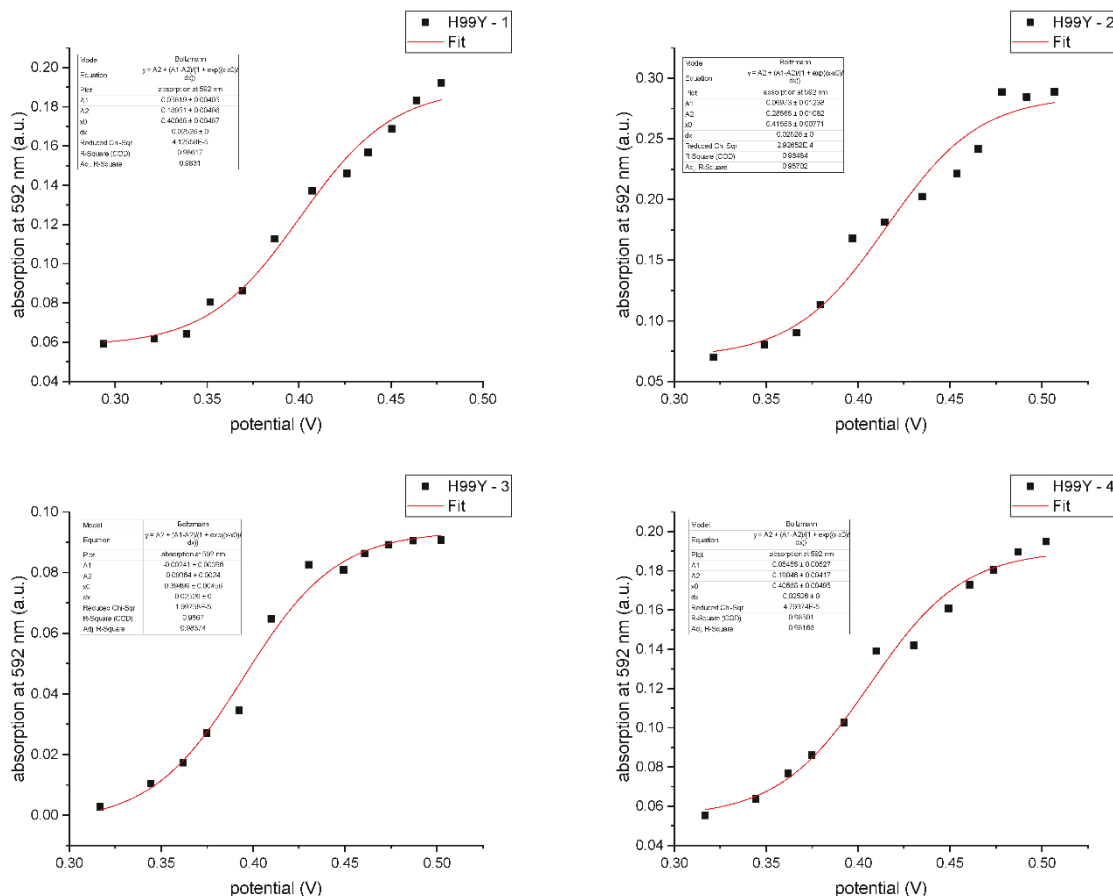


Figure S9: Titration curves for Ssl1 H99Y. Curves were fitted to the Nernst equation in Origin 9.0G.

Table S10: Fit parameters obtained from fitting titration curves to the Nernst equation in Origin 9.0G.

H99Y				
	1	2	3	4
A1	0.05819 ± 0.00405	0.06973 ± 0.01238	-0.00241 ± 0.00396	0.05455 ± 0.00527
A2	0.18951 ± 0.00486	0.28565 ± 0.01082	0.09364 ± 0.0024	0.19046 ± 0.00417
x_0	0.40068 ± 0.00487	0.41553 ± 0.00771	0.39499 ± 0.00456	0.40668 ± 0.00495
dx	0.02526 ± 0	0.02526 ± 0	0.02526 ± 0	0.02526 ± 0
Reduced Chi-Sqr	4.13E+00	2.93E+01	2.00E+00	4.79E+00
R-Square (COD)	0.98617	0.96484	0.9867	0.98501
Adj. R-Square	0.9831	0.95702	0.98374	0.98168

H99Y/M295F

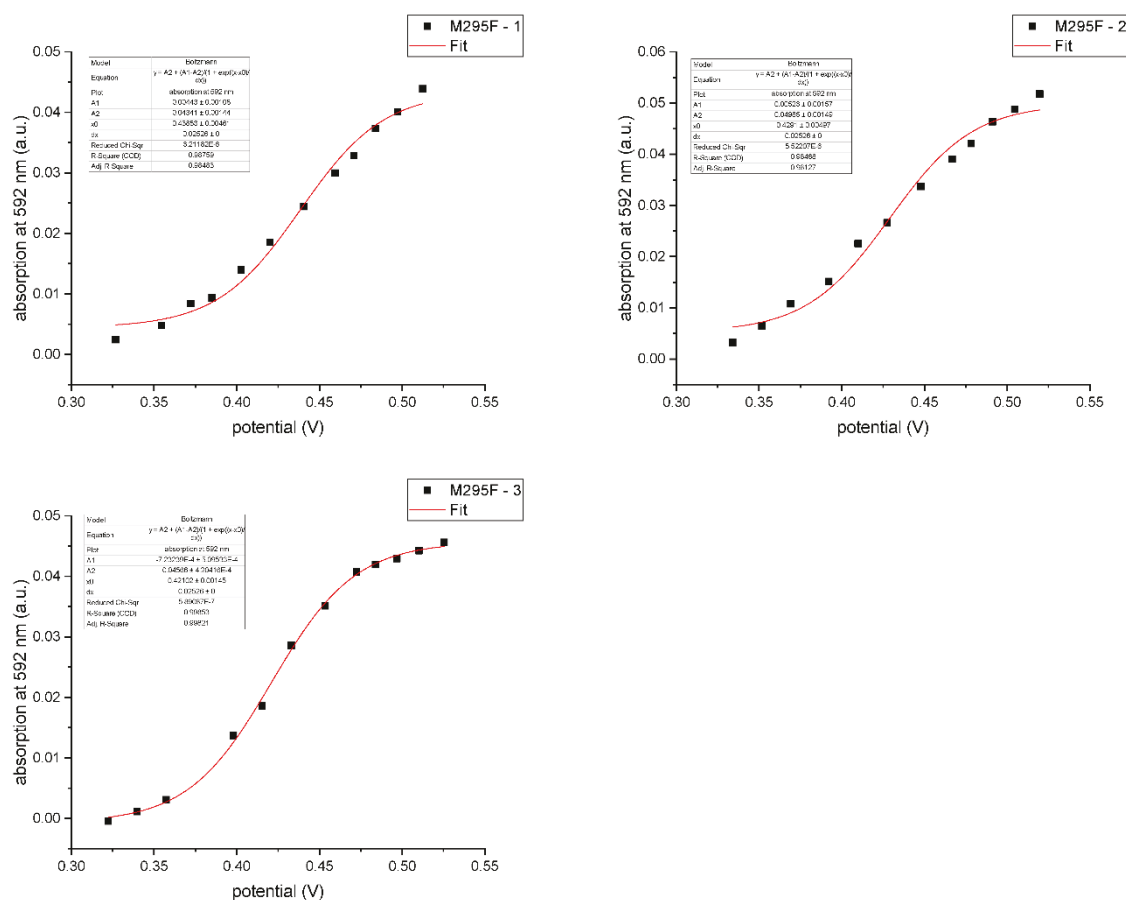


Figure S10: Titration curves of H99Y/M295F. Curves were fitted to the Nernst equation in Origin 9.0G.

Table S11: Fit parameters obtained from fitting titration curves to the Nernst equation in Origin 9.0G.

H99Y/M295F			
	1	2	3
A1	0.00443 ± 0.00108	0.00523 ± 0.00157	-7.23239E-4 ± 5.09533E-4
A2	0.04341 ± 0.00144	0.04985 ± 0.00149	0.04566 ± 4.20416E-4
x0	0.43853 ± 0.00461	0.4291 ± 0.00497	0.42102 ± 0.00145
dx	0.02526 ± 0	0.02526 ± 0	0.02526 ± 0
Reduced Chi-Sqr	3.21E-01	5.52E-01	5.89E-02
R-Square (COD)	0.98759	0.98468	0.99853
Adj. R-Square	0.98483	0.98127	0.99821

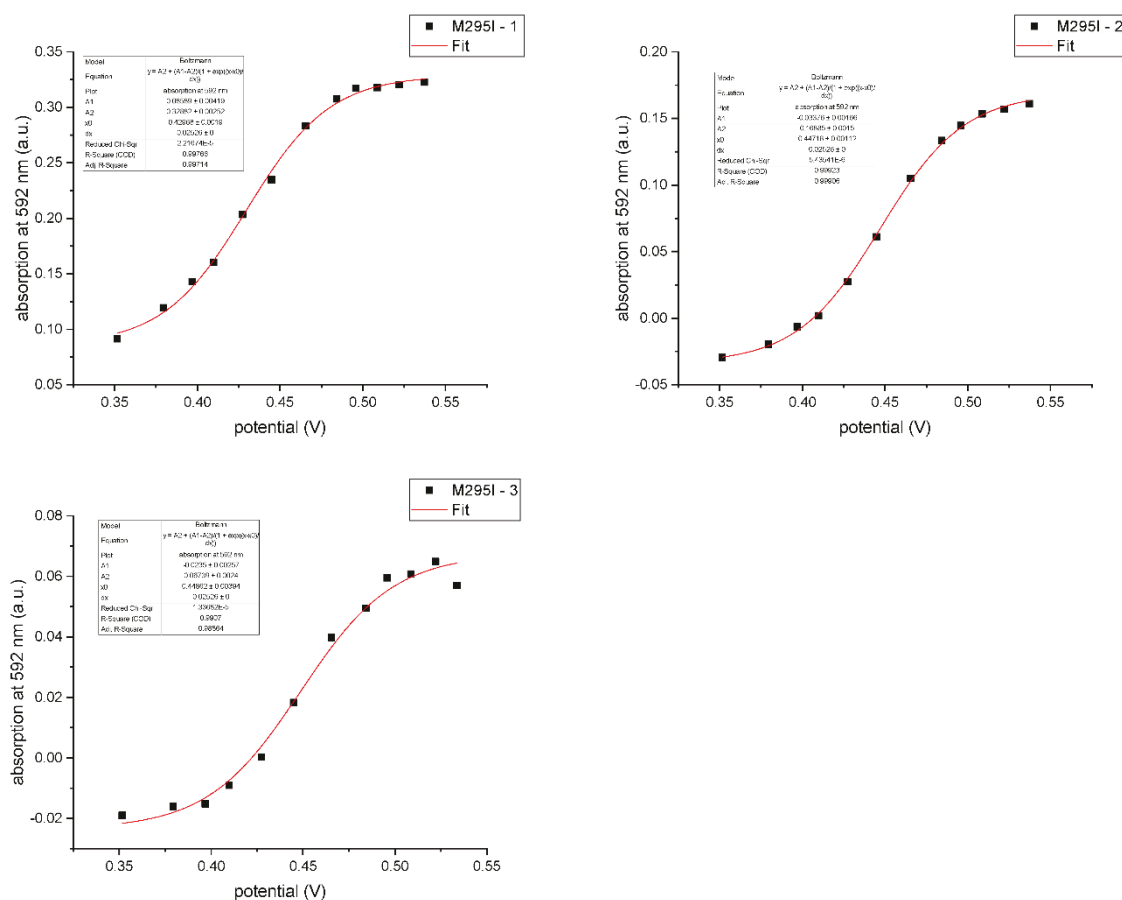
H99Y/M295I


Figure S11: Titration curves for H99Y/M295I. Curves were fitted to the Nernst equation in Origin 9.0G.

Table S12: Fit parameters obtained from fitting titration curves for H99Y/M295I to the Nernst equation in Origin 9.0G.

H99Y/M295I			
	1	2	3
A1	0.08589 ± 0.00419	-0.03376 ± 0.00166	-0.0235 ± 0.00257
A2	0.32882 ± 0.00252	0.16885 ± 0.0015	0.06739 ± 0.0024
x0	0.42968 ± 0.0019	0.44718 ± 0.00112	0.44862 ± 0.00394
dx	0.02526 ± 0	0.02526 ± 0	0.02526 ± 0
Reduced Chi-Sqr	2.22E+00	5.44E-01	1.34E+00
R-Square (COD)	0.99766	0.99923	0.9907
Adj. R-Square	0.99714	0.99906	0.98864

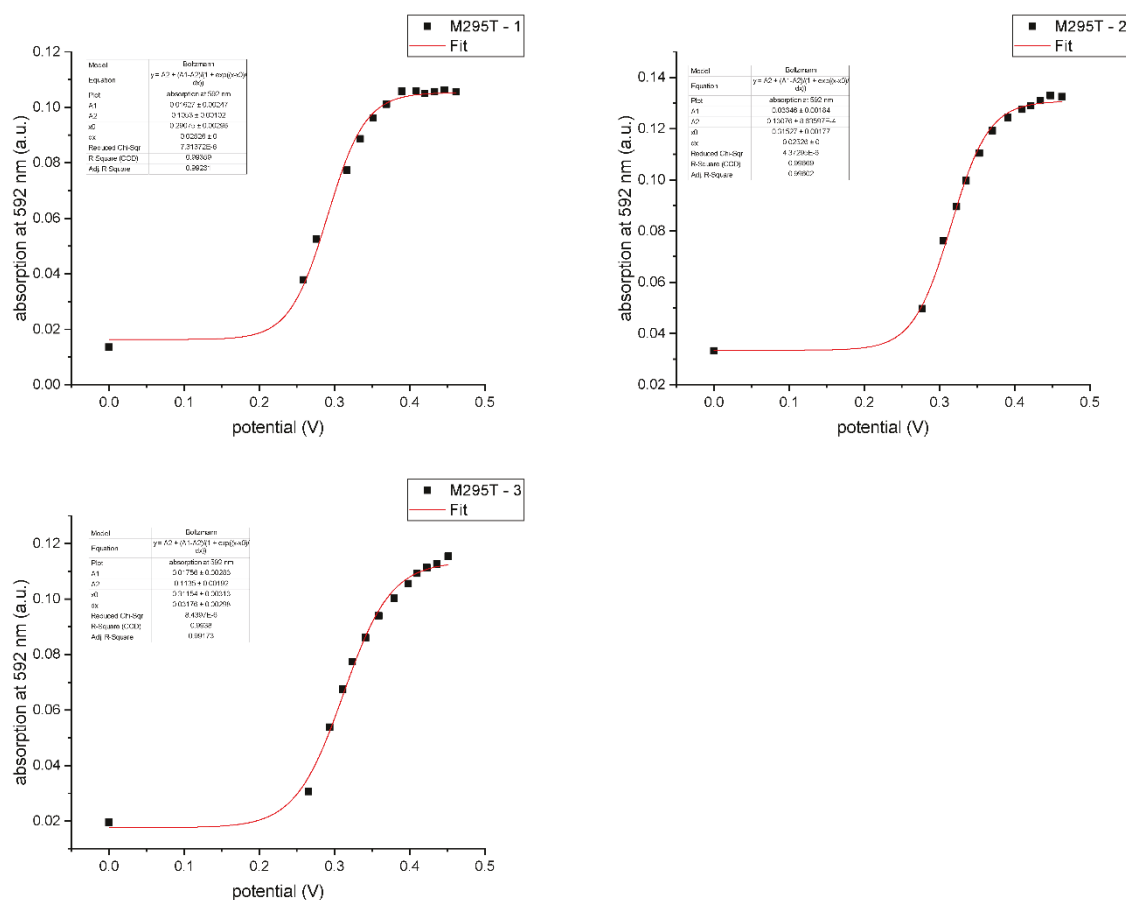
H99Y/M295T


Figure S12: Titration curves for H99Y/M295T. Curves were fitted to the Nernst equation in Origin 9.0G. The absorption of reduced SslI H99Y/M295T in 10 mM Fe(II) was used for fitting with arbitrary potential of 0 V.

Table S13: Fit parameters obtained from fitting titration curves to the Nernst equation in Origin 9.0G.

	H99Y/M295T		
	1	2	3
A1	0.01627 ± 0.00247	0.03346 ± 0.00184	0.01756 ± 0.00283
A2	0.1053 ± 0.00102	0.13076 ± 8.63597E-4	0.1135 ± 0.00192
x0	0.29075 ± 0.00296	0.31527 ± 0.00177	0.31154 ± 0.00313
dx	0.02526 ± 0	0.02526 ± 0	0.03176 ± 0.00298
Reduced Chi-Sqr	7.31E-01	4.37E-01	8.44E-02
R-Square (COD)	0.99359	0.99669	0.9938
Adj. R-Square	0.99231	0.99602	0.99173

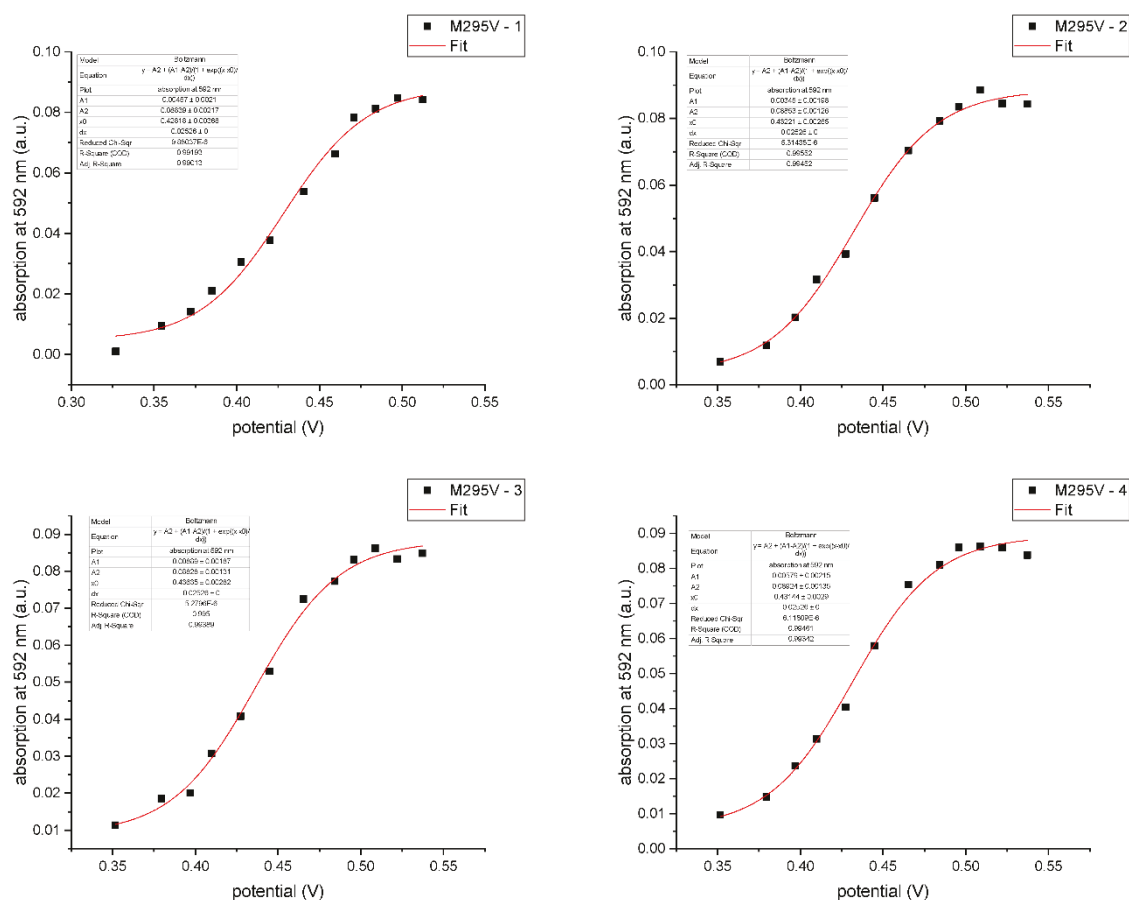
H99Y/M295V


Figure S13: Titration curves for H99Y/M295V. Curves were fitted to the Nernst equation in Origin 9.0G.

Table S14: Fit parameters obtained from fitting titration curves to the Nernst equation in Origin 9.0G.

H99Y/M295V				
	1	2	3	4
A1	0.00457 ± 0.0021	0.00345 ± 0.00198	0.00889 ± 0.00187	0.00579 ± 0.00215
A2	0.08839 ± 0.00217	0.08853 ± 0.00126	0.08828 ± 0.00131	0.08924 ± 0.00135
x0	0.42818 ± 0.00368	0.43221 ± 0.00265	0.43635 ± 0.00282	0.43144 ± 0.0029
dx	0.02526 ± 0	0.02526 ± 0	0.02526 ± 0	0.02526 ± 0
Reduced Chi-Sqr	9.88E-01	5.31E-01	5.28E-02	6.12E-01
R-Square (COD)	0.99193	0.99552	0.995	0.99461
Adj. R-Square	0.99013	0.99452	0.99389	0.99342

H99Y/M295Y

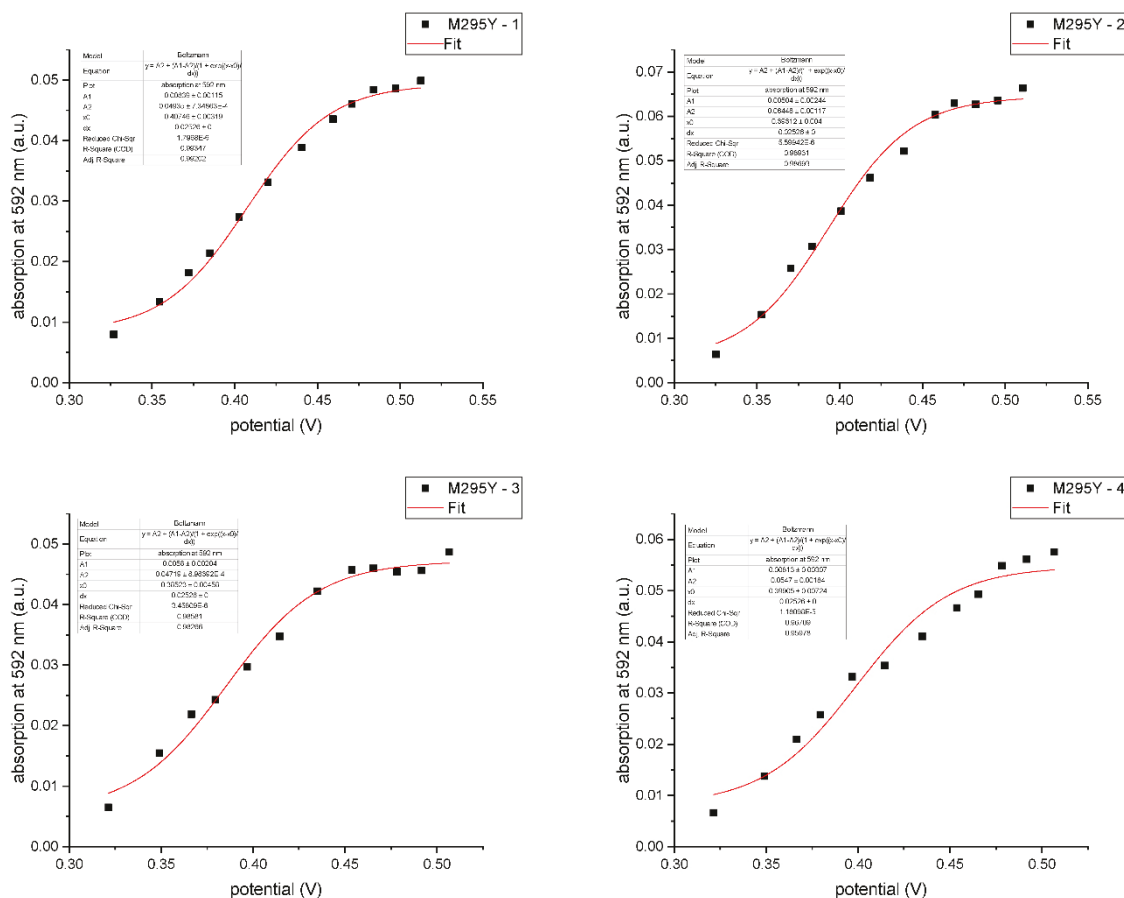


Figure S14: Titration curves for H99Y/M295Y. Curves were fitted to the Nernst equation in Origin 9.0G.

Table S15: Fit parameters obtained from fitting titration curves to the Nernst equation in Origin 9.0G.

H99Y/M295Y				
	1	2	3	4
A1	0.00839 ± 0.00115	0.00504 ± 0.00244	0.0058 ± 0.00204	0.00813 ± 0.00307
A2	0.04935 ± 7.34863E-4	0.06448 ± 0.00117	0.04719 ± 8.98392E-4	0.0547 ± 0.00184
x0	0.40746 ± 0.00319	0.39312 ± 0.004	0.38523 ± 0.00458	0.39905 ± 0.00724
dx	0.02526 ± 0	0.02526 ± 0	0.02526 ± 0	0.02526 ± 0
Reduced Chi-Sqr	1.80E-02	5.60E-01	3.46E-01	1.18E+00
R-Square (COD)	0.99347	0.98931	0.98581	0.96709
Adj. R-Square	0.99202	0.98693	0.98266	0.95978

H99Y/M295A

The T1 Cu of H99Y/M295A was fully oxidized at 0.29 V thus the T1 Cu reduction potential of H99Y/M295A is less than 290 mV.

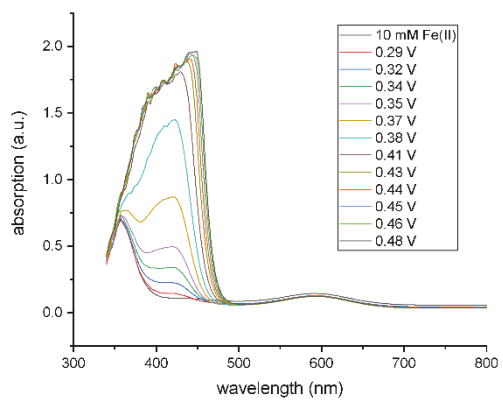


Figure S15: Absorption spectra of H99Y/M295A recorded after each titration step.

6 Ruthenation of Ssl1: First steps towards measurements of the T1 to TNC electron transfer kinetics

The intramolecular electron transfer (IET) from the T1 Cu to the TNC in laccases has been studied since the early 1990s¹⁴⁶ using different approaches and has increased our understanding of the reaction mechanism. The method mostly employed for IET studies has been pulse radiolysis. This method is based on subjecting solvent molecules to short (0.1-1 μ s) pulses of high energy accelerated electrons (\sim 2-10 MeV) producing OH radicals and hydrated electrons from water molecules⁴⁷. In subsequent reactions these can be converted to more selective reducing agents like CO_2^- radicals and the uncharged 1-methylnicotinamide (1-MNA*) radical that reduce the T1 Cu^{II} of laccases⁴⁷. The reoxidation of the T1 Cu^{I} and the concomitant reduction of the T3 Cu^{II} following an IET process can be observed through the absorption increase at \sim 600 nm (T1 Cu^{II}) and absorption decrease at \sim 330 nm (T3 Cu^{II}) and the rate constants for the intramolecular T1 \rightarrow TNC electron transfer can be determined. An overview about the IET rate constants ($k_{\text{T1} \rightarrow \text{TNC}}$) of laccases determined by pulse radiolysis is given in Table 2. It is noteworthy that $k_{\text{T1} \rightarrow \text{TNC}}$ increased more than 10-fold when SLAC from *S. coelicolor* was subjected to sequential pulses and gradually reduced¹⁶⁹.

Table 2: Kinetic parameters for the T1 \rightarrow TNC ET in laccases as determined by pulse radiolysis.

Laccase	Type	$k_{\text{T1} \rightarrow \text{TNC}}$	Reference
SLAC (<i>S. coelicolor</i>)	2dMCO, type B, homotrimer	“cycled” initial 15 s^{-1} final 186 s^{-1}	169
mgLAC	2dMCO, type C, homotrimer	fast: 110 s^{-1} slow: 3 s^{-1}	170
Ascorbate oxidase (<i>C. pepo</i>)	3dMCO, homodimer	fast: 201 s^{-1} slow: 2.3 s^{-1}	171
Laccase (<i>Trametes hirsuta</i>)	3dMCO	$k = 25 \text{ s}^{-1}$	172

More recently a method using fluorescence-based detection of protein redox state(s), named FluRedox¹⁷³, has been applied to study the IET in SLAC¹⁷⁴. SLAC variants with one surface-exposed cysteine (K204C or R203C) were prepared and selectively labeled with Atto647N-maleimide. The emission of the fluorescence dye Atto647N overlaps with the 590 nm absorption of the S(Cys)- Cu^{II} CT band of SLAC. Thus, in the SLAC-Atto647N-conjugate the fluorescence is quenched by Förster resonance energy transfer (FRET) from the dye to the S(Cys)- Cu^{II} CT absorption. Since the 590 nm absorption is not present in the reduced state (T1 Cu^{I}) there is no fluorescence quenching, and the fluorescence emission is present. Thus, the Atto647N-fluorescence of the protein-dye conjugate can be

used to probe the T1 Cu redox state¹⁷⁴. The SLAC-Atto647N-conjugate was further immobilized on glass coverslips and single molecule fluorescence measurements were performed on a confocal microscope. The rate constants for the T1→TNC ET step determined for 720 individual SLAC molecules followed a log-normal distribution with an arithmetic mean of $k_{\text{T1} \rightarrow \text{TNC}} = 460 \text{ s}^{-1}$. This is higher than the previously reported value of 186 s^{-1} obtained from pulse radiolysis experiments¹⁶⁹. The explanation for this difference given by the authors¹⁷⁴ is the partial decay of the native intermediate (NI) to the resting oxidized (RO) form that might occur during pulse radiolysis measurements. The RO form can transfer electrons from the T1 to the TNC only at a slower rate than the NI and therefore the NI is the catalytically relevant state in the catalytic cycle of laccases¹⁴⁰ (see also Chapter 3.2.1).

According to the Marcus theory (see Chapter 3.1.4) $k_{\text{T1} \rightarrow \text{TNC}}$ depends on the reduction potential difference between donor and acceptor. Increasing the donor (here T1 Cu) reduction potential while the acceptor (here TNC) remains unchanged decreases $k_{\text{T1} \rightarrow \text{TNC}}$. This effect of a higher T1 Cu reduction potential on the T1 → TNC ET has been recently studied with stopped-flow measurements on *T. versicolor* laccase (TvL, 780 mV) and *R. vernicifera* laccase (RvL, 430 mV)¹⁷⁵. The increase of the T1 Cu reduction potential by 350 mV in TvL compared to RvL reduced the driving force for IET to the native intermediate (NI) by 8 kcal/mol. Consequently, the rate-determining step in the laccase reaction differs between RvL and TvL. Whereas the T1 Cu reduction is rate-limiting in the medium-redox potential laccase RvL, in high-potential MCOs⁶¹ like TvL it is the first IET step.

Low-spin, pseudo-octahedral Ru complexes have suitable properties for the investigation of ET reactions. Small structural changes accompanying the reduction/oxidation result in a low inner-sphere reorganization energy and thus fast ET reactions. Additionally, the reduction potential of the Ru^{III}/Ru^{II} redox couple can vary between <0 and >1.5 V vs. normal hydrogen electrode (NHE) depending on the choice of ligands¹⁷⁶. The modification of proteins with Ru complexes for electron transfer measurements is well established and different ruthenium complexes have been used to modify proteins since 1978 when Matthews *et al.*¹⁷⁷ first reported modification of ribonuclease A with $[\text{Ru}(\text{NH}_3)_5(\text{OH}_2)]^{2+}$. Ruthenium complexes bind specifically to surface histidine residues and the imidazole side chain constitutes one of the metal ligands (Figure 10). In the early 1980s the first long-range electron transfer from Ru^{II} to the heme Fe^{III} over a distance of 15 Å in $[\text{Ru}(\text{NH}_3)_5(\text{His}33)]$ -cytochrome *c* was measured¹⁷⁸. In addition to the above-mentioned characteristics, ruthenium bipyridine complexes, e.g. $[\text{Ru}(\text{bpy})_2(\text{Im})(\text{His})]^{2+}$ (bpy = 2,2'-bipyridine; Im = imidazole), have long-lived, luminescent metal-to-ligand charge transfer (MLCT) excited states and a Ru^{III}/Ru^{II} reduction potential of >1 V vs. NHE¹⁷⁶. Ruthenium complexes have been used to modify and study IET processes not only in heme containing proteins, e.g., myoglobin¹⁷⁹ and cytochrome *c*¹⁸⁰⁻¹⁸³, but also in blue copper proteins, e.g., azurin^{70,184} (Figure 10) and plastocyanin¹⁸⁵.

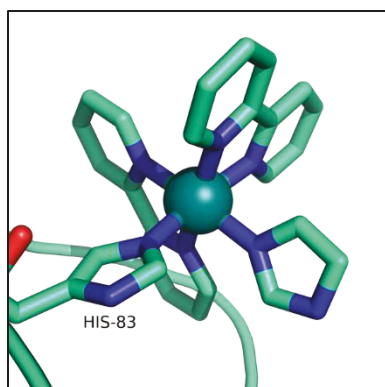


Figure 10: $[\text{Ru}(\text{bpy})_2(\text{Im})(\text{His}83)]\text{-azurin}$ (PDB code 1JZE). The ruthenium ion (teal colored sphere) is coordinated by two 2,2'-bipyridine ligands, and two imidazole ligands, one of which belongs to H83 of azurin.

To study the IET in Ssl1 the protein was modified with a ruthenium bipyridine complex bound to a surface-exposed histidine residue ($[\text{Ru}(\text{bpy})_2(\text{Im})(\text{His})]\text{-Ssl1}$). Since ET rates are depending on the distance between the participating electron donor and acceptor it is necessary to modify Ssl1 site-specifically and in the vicinity of the T1 Cu and to avoid labeling at multiple sites.

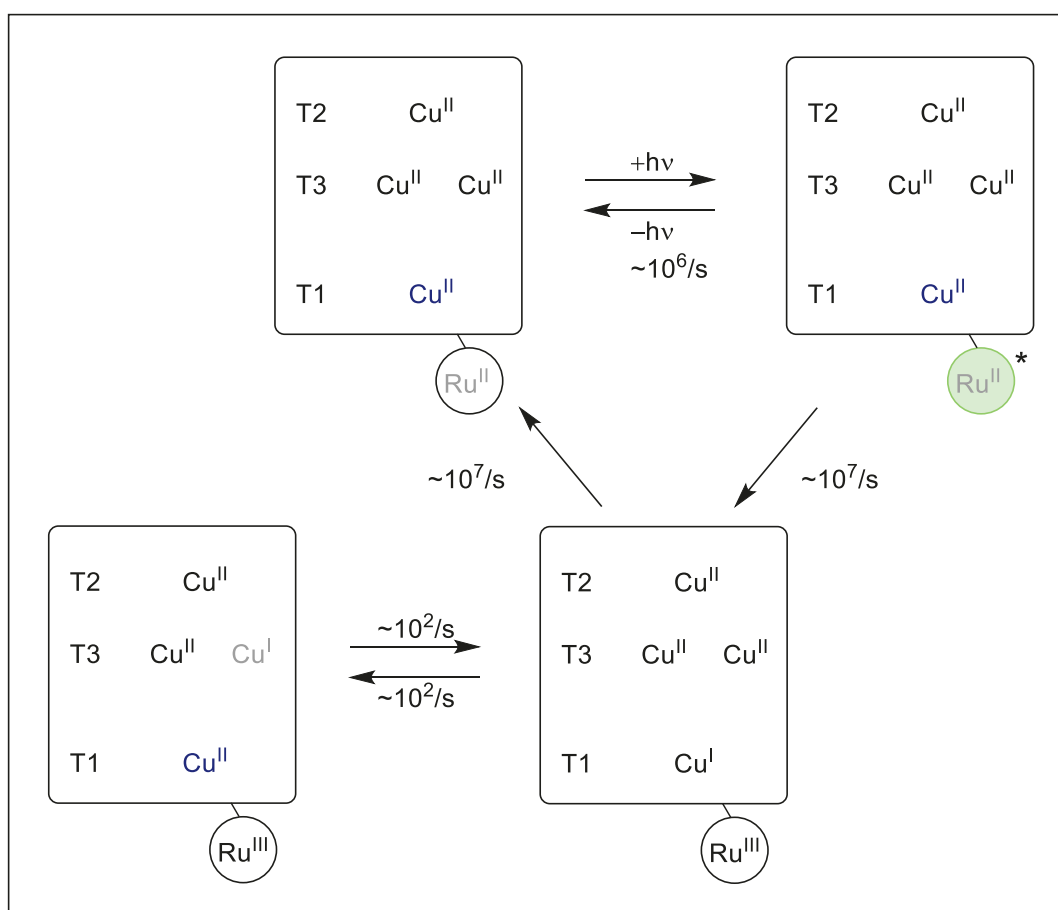


Figure 11: Mechanism of redox reactions in ruthenated laccase. Upon photoexcitation $\text{Ru}^{\text{II}*}$ can transfer one electron to the T1 Cu ion of the enzyme which quenches the fluorescence of the Ru^{II} species.

Figure 11 shows a proposed reaction mechanism for the redox reactions in ruthenated Ssl1. The photoexcited ruthenium complex can transfer one electron to the T1 Cu, which is then further transferred to the TNC. The oxidized Ru^{III} species is non-fluorescent. Thus, electron transfer from the photoexcited

$\text{Ru}^{\text{II}*}$ to the T1 Cu^{II} is also a fluorescence quenching process. Reduction of the laccase, e.g., by ascorbate, hinders this fluorescence quenching mechanism as there is no ET from the $\text{Ru}^{\text{II}*}$ to the T1 Cu^{I} . This should be observable through an increased fluorescence lifetime and thereby fluorescence intensity upon reduction of the laccase by addition of ascorbate. Evidence for the T1 \rightarrow TNC electron transfer and how this varies with the oxidation state and the presence or absence of oxygen is presumably observable through the fluorescence lifetimes. Under anaerobic conditions the enzyme can be reduced by adding ethylenediaminetetraacetic acid (EDTA) as a scavenger that reduces Ru^{III} to Ru^{II} leaving an electron in the enzyme (Prof. Scot Wherland, personal communication).

The overall goal is to study the IET in Ssl1 variants with reduction potentials in the range between 290 and 560 mV. Compared to the previous studies on ET that compared different wildtype MCOs, we can study the influence of the T1 Cu reduction potential on the IET in a single laccase, thus with only minor differences in the surrounding protein matrix. The availability of several Ssl1 mutant structures (see Chapter 5) allows the interpretation of the IET rates with respect to the structure of the T1 Cu center. This chapter reports on the modification of a Ssl1 variant with the fluorescent $[\text{Ru}(\text{bpy})_2(\text{Im})_2]^{2+}$ complex. We also present the characterization of the fluorescence properties of the labeled Ssl1 variant and evidence for electron transfer between the Ru complex and the T1 Cu.

Materials and Methods

Chemicals, enzymes, buffers

All chemicals were purchased from Sigma Aldrich, VWR, Carl Roth, AppliChem, and Merck unless stated otherwise. *DpnI* was purchased from New England Biolabs (Frankfurt am Main, Germany), Phusion Polymerase, *NheI*, and *HindIII* were obtained from Thermo Fisher Scientific (Braunschweig, Germany), and thrombin from bovine plasma was purchased from Sigma Aldrich (Steinheim, Germany). $[\text{Ru}(\text{bpy})_2]\text{CO}_3$ was provided by Professor Scot Wherland, Department of Chemistry, Washington State University, Pullman, WA.

Strains, plasmids, oligonucleotides

Table 3: *E. coli* strains.

Strain	Genotype	Supplier
DH5 α	F ⁻ ϕ 80dlacZ Δ M15 Δ (lacZYA-argF)U169 <i>deoR recA1 endA1 hsdR17</i> (r _K ⁻ m _K ⁺) <i>phoA supE44</i> λ ⁻ <i>thi-1 gyrA96 relA1</i>	Clontech, Saint-Germain-en-Laye, France
BL21-CodonPlus(DE3)-RP	F ⁻ <i>ompT hsdS</i> (r _B ⁻ m _B ⁻) <i>dcm</i> ⁺ Tet ^r <i>gal</i> λ (DE3) <i>endA Hte</i> [<i>argU proL Cam</i> ^r]	New England Biolabs, Frankfurt am Main, Germany

Table 4: Plasmids used in this study.

Plasmid	Properties	Reference
pET22H_ssl1	<i>S. sviveus</i> Ssl1 with N-terminal His ₆ -tag, without natural <i>tat</i> signal sequence	⁴⁵
pET22H_His(6x)_thrombin↓_ssl1_H85Q/H132Q/ Δ C	<i>S. sviveus</i> Ssl1 H85Q/H132Q/ Δ C without natural <i>tat</i> signal sequence but with N-terminal His ₆ -tag followed by a thrombin recognition sequence	this study

Oligonucleotides for site-directed mutagenesis and cloning of *ssl1* were obtained from Eurofins Genomics, Ebersberg, Germany (HPSF purified) and are listed in Table 5. Sequencing primers were provided by GATC Biotech, Konstanz, Germany.

Table 5: Oligonucleotide primers for site-directed mutagenesis, cloning, and Sanger sequencing of *ssl1*. Codon exchanges are underlined. Restriction sites are shown in italics.

		Sequence	Reference
Site-directed mutagenesis			
H85Q	forward	GGC GAC ACC CTG <u>CAG</u> ATC GAG TTC GAG	this study
H85Q	reverse	CTC GAA CTC GAT <u>CTG</u> CAG GGT GTC GCC	this study
H132Q	forward	CC TGG CGC ACC <u>CAG</u> GCG CCG GGC C	this study
H132Q	reverse	G GCC CGG CGC <u>CTG</u> GGT GCG CCA GG	this study
$\Delta C_{313-325}$	forward	CCG GGG TAC GAG <u>TAG</u> CAC GAG CAC AGC	⁴⁵
$\Delta C_{313-325}$	reverse	GCT GTG CTC GTG <u>CTA</u> CTC GTA CCC CGG	⁴⁵
Cloning			
forward; contains sequences for His ₆ tag and thrombin recognition site		CTT <i>GCT AGC</i> ATG CAT CAT CAT CAT CAT CTG GTG CCA CGC GGT TCT GCC CCG GGC GGC GAG GTC AG	this study
reverse		GGC <i>AAG CTT</i> TCA GTG GTG GTG TTC GGC CCG C	¹⁶⁵
Sanger sequencing			
T7		TAATACGACTCACTATAGGG	GATC Biotech, Konstanz, Germany
pET-RP		CTAGTTATTGCTCAGCGG	GATC Biotech, Konstanz, Germany

Cloning of *ssl1* gene variants

Ssl1 genes variants with an N-terminal His₆ tag followed by a thrombin recognition site were amplified from pET22H_*ssl1*¹⁶⁵ using the primers listed in Table 5 and subsequently cloned into the vector pET22H¹⁸⁶ via *Nhe*I and *Hind*III restriction sites. Site-directed mutagenesis was performed as described previously¹⁶⁴ (Chapter 4) using the primer sequences given in Table 5. Correct sequences were verified by Sanger sequencing (GATC Biotech, Konstanz, Germany).

Expression and purification of Ssl1 for site-specific labeling

Expression and purification of Ssl1 variants with an N-terminal His₆-tag followed by a thrombin recognition site were carried out as described previously¹⁶⁴ (Chapter 4). The N-terminal His₆-tag was removed by thrombin cleavage. Thrombin (0.5 mg (18.5 U) per g cell wet weight) was added to the purified fusion protein (in 50 mM potassium phosphate buffer, pH 7.5) and incubated for 2-3.5 h at room temperature with overhead rotation at 5 rpm. Isolation of the cleavage product of interest was performed using affinity chromatography.

Uncleaved His₆-Ssl1, the His₆-tag, and thrombin were removed by affinity chromatography. A 5 mL HiTrap Talon crude column and a 1 mL HiTrap Benzamidine FF (high sub) column were placed in

series on an Äkta purifier 100 system and equilibrated with binding buffer (50 mM potassium phosphate buffer, 500 mM sodium chloride, pH 7.5). The sample was applied to the columns at a flow rate of 1 mL min^{-1} and Ssl1 without the tag was washed out in the flow through and afterwards with binding buffer (1 mL min^{-1}) until the absorption at 280, 330, and 600 nm reached the baseline level. Ssl1 containing fractions – identified by absorption at 600 nm or laccase activity – were pooled, concentrated (Vivaspin Turbo 15, 10 kDa MWCO, Sartorius, Göttingen), and the buffer was changed to potassium phosphate buffer, (50 mM, pH 7.5) using PD MidiTrap G-25 columns (GE Healthcare, München).

The HiTrap Talon crude and HiTrap Benzamidine FF (high sub) columns were then treated separately. Thrombin was eluted from the HiTrap Benzamidine FF column with 10 CV of 50 mM glycine-HCl buffer pH 3.0. The HiTrap Talon crude column was washed with 5 CV 500 mM imidazole in binding buffer (50 mM potassium phosphate buffer, 500 mM sodium chloride, pH 7.5), to elute bound proteins.

Determination of total protein concentrations

Protein concentrations were determined using the Bradford method¹⁸⁷. 40 μL of 5x RotiQuant (Carl Roth, Karlsruhe, Germany) were added to 160 μL of protein solutions and incubated for 5 min at room temperature before determining the absorption at 595 nm. Standard solutions with 0 – 50 $\mu\text{g/mL}$ bovine serum albumin were used for calibration. Molar concentrations of purified Ssl1 solutions were calculated using the theoretically (ExPASy ProtParam) determined molecular weight, which has been experimentally confirmed previously for wildtype Ssl1¹⁶⁵.

Spectrophotometric redox titrations and determination of catalytic constants for syringaldazine conversion

The T1 Cu reduction potentials and kinetic constants for syringaldazine conversion were determined as described previously¹⁶⁴ (Chapter 4).

Ruthenation of Ssl1

Based on the procedure for labeling of cytochrome c with $[\text{Ru}(\text{bpy})_2(\text{Im})_2]^{2+}$ reported elsewhere¹⁸¹, we established a protocol for ruthenation of Ssl1. To prepare $[\text{Ru}(\text{bpy})_2(\text{H}_2\text{O})(\text{His})]$ -Ssl1, 100 μM of Ssl1 variants were mixed with 250 or 500 μM $[\text{Ru}(\text{bpy})_2]\text{CO}_3$ to test the influence of the concentration. The reaction was buffered with 50 mM potassium phosphate buffer (pH 7.5) and left at room temperature in the dark under a nitrogen atmosphere for 19 h. Excess $[\text{Ru}(\text{bpy})_2]\text{CO}_3$ was removed by gel filtration using a PD MidiTrap G-25 column (GE Healthcare Europe, Freiburg) or an Econo-Pac 10DG Desalting

column (BioRad, München) depending on the sample size. Absorption spectra were recorded with a TIDAS E photo diode array spectrophotometer (J&M Analytik, Essingen).

To obtain [Ru(bpy)₂(Im)(His)]-Ssl1 the reaction buffer was exchanged to 50 mM potassium phosphate buffer (pH 7.5) containing 200 mM imidazole and 200 mM NaCl, via a PD MidiTrap G-25 column. The reaction mixture was kept at room temperature in the dark for several days. Exchange of the water ligand with imidazole was followed by measuring the fluorescence of the resulting [Ru(bpy)₂(Im)(His)]-Ssl1 species. Fluorescence emission and excitation spectra of 200 µL samples in black microtiter plates were recorded on a Tecan infinite M200 pro (Tecan, Männedorf, Switzerland). Imidazole and sodium chloride were removed via PD MidiTrap G-25 columns if necessary.

Results and discussion

Cloning, expression, and purification of a Ssl1 variant for site-specific ruthenation

To allow for electron transfer between Ru^{II} and the T1 Cu, the labeling of Ssl1 with the ruthenium complex must be done site-specifically in the vicinity of the T1 Cu via a histidine residue. In this respect, the first step was to create a Ssl1 variant that has only one surface exposed histidine residue in a suitable position. Examination of the sequence and 3D-structure of Ssl1 revealed five histidine residues in the flexible C-terminal region and three surface-exposed histidine residues, H85, H132, H203 (Figure 12a and b). Of these, H203, was found to be suitable as labeling site being close enough to the T1 Cu (~13 Å).

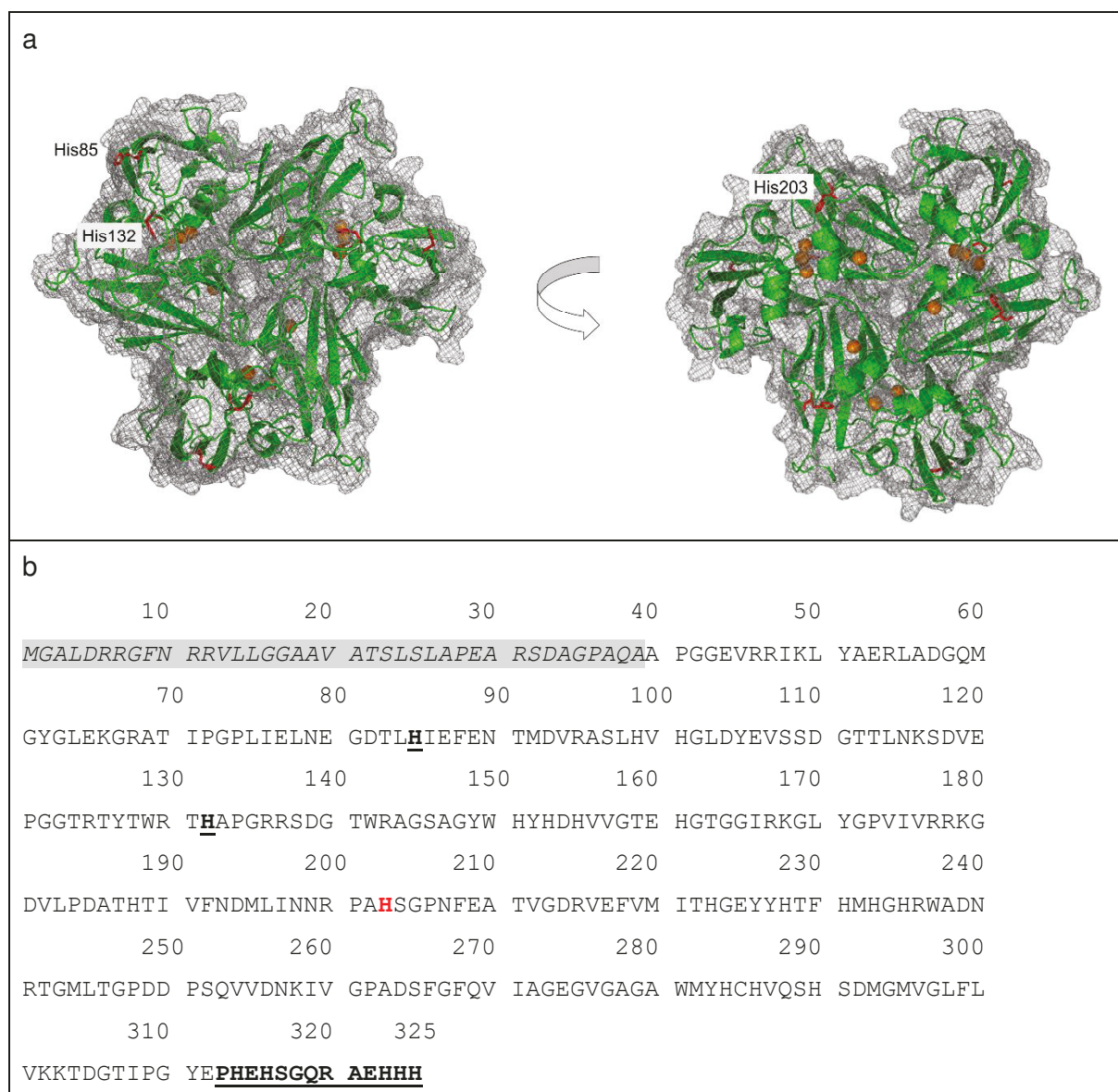


Figure 12: (a) Structure (PDB code 4M3H) and (b) sequence of wildtype Ssl1. Histidine residues on the enzyme surface are depicted as red sticks, copper ions as orange spheres. For ruthenation Ssl1 was expressed without its natural signal sequence (grey background) but with a His₆-tag followed by a thrombin cleavage sequence (MHHHHHHLVPRGS). Mutated residues are shown in bold and underlined. H203 is highlighted in red.

A Ssl1 mutant lacking the 13 C-terminal residues and therefore the above mentioned five C-terminal histidine residues has been previously described⁴⁵ and was also used in this study. The N-terminal His₆-

tag enhances the expression level of Ssl1 and enables easy purification but hinders site-specific ruthenation. Thus, we decided to use a Ssl1_ΔC variant with a thrombin cleavage site between the N-terminal His₆-tag and the protein. The surface exposed histidine residues H85 and H132 were mutated to glutamine. Mutation of a T2 Cu coordinating histidine to glutamine has been successfully applied for the creation of T2 Cu depleted Ssl1 (see chapter 5) and Fet3¹⁸⁸. Glutamine presumably also does not coordinate the ruthenium complex and the mutation does not affect the enzyme structure. The thrombin-catalyzed cleavage leaves a glycine and serine residue at the N-terminus of the Ssl1 originating from the thrombin recognition sequence. In this chapter Ssl1 H85Q/H132Q/ΔC always refers to the untagged protein. Presence of a hexahistidine tag will be explicitly indicated, e.g. His₆-Ssl1. To elucidate the influence of the mutations and the affinity tag we also produced an Ssl1 wildtype variant without the His₆-tag.

Intact copper centers and catalytic activity of the Ssl1 variants are a prerequisite for IET measurements. We observed no differences in the absorption spectrum of Ssl1 H85Q/H132Q/ΔC (Figure 13) compared to the wildtype spectrum¹⁶⁵. Therefore, we assume that the mutations do not alter the electronic structure of the copper sites. Ssl1 H85Q/H132Q/ΔC is catalytically active as was determined with reactions using syringaldazine as substrate ($k_{\text{cat}} = 68 \text{ min}^{-1}$, $K_M = 49 \text{ μM}$, Figure S2 and Table S3). Since we ultimately wanted to study Ssl1 variants with different T1 Cu reduction potentials, we also performed spectrophotometric redox titrations. The T1 E° of Ssl1 H85Q/H132Q/ΔC was determined to be 432 mV. This is in accordance with an increase of E° due to deletion of the 13 C-terminal amino acids as previously described⁴⁵ and the increase observed upon the removal of the His₆-tag. When comparing wildtype Ssl1 variants with and without the hexahistidine tag, we found a 13 mV increase of the T1 Cu E° from 375 mV¹⁶⁵ for His₆-Ssl1 to $388 \pm 2 \text{ mV}$ for the untagged Ssl1 wildtype variant (see Figure S1 and Table S2). It is unlikely that ruthenation of Ssl1 changes the T1 Cu reduction potential any further since ruthenation did not influence the T1 Cu reduction potential of azurin¹⁸⁹.

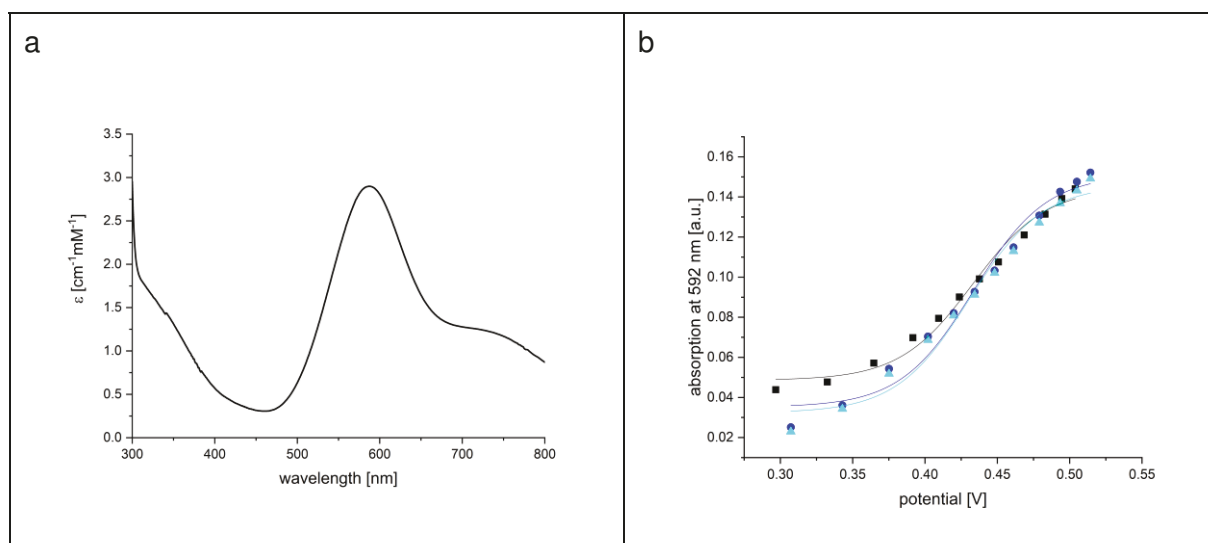


Figure 13: (a) Absorption spectrum of Ssl1 H85Q/H132Q/ΔC. The molar extinction coefficient at 592 nm was determined to be $2.83 \text{ mM}^{-1} \text{ cm}^{-1}$. (b) Spectrophotometric titration curves of Ssl1 H85Q/H132Q/ΔC. The T1 Cu reduction potential was determined to be $432 \pm 1 \text{ mV}$. Details are given in Table S1.

Ruthenation of Ssl1

The first reaction step towards ruthenation of Ssl1 was the reaction of Ssl1 with $[\text{Ru}(\text{bpy})_2]\text{CO}_3$, which is present as $[\text{Ru}(\text{bpy})_2(\text{H}_2\text{O})_2]^{2+}$ in solution¹⁹⁰. Exchange of one water ligand with the imidazole of a histidine residue from Ssl1 results in the reaction product $[\text{Ru}(\text{bpy})_2(\text{H}_2\text{O})(\text{His})]\text{-Ssl1}$. We tested two different reactant ratios using either a 2.5-fold or a 5-fold molar excess of the ruthenium complex. Additionally, we included the reaction of 100 μM His₆-Ssl1 with 250 μM $[\text{Ru}(\text{bpy})_2]\text{CO}_3$ as a control reaction. As previously mentioned, His₆-Ssl1 has numerous histidine residues available for complex formation with $[\text{Ru}(\text{bpy})_2]$.

$[\text{Ru}(\text{bpy})_2]\text{CO}_3$ has two absorption maxima at 370 and 490 nm (Figure 14) when dissolved in potassium phosphate buffer under anaerobic conditions. The 490 nm absorption is attributed to the MLCT band ($d\pi(\text{Ru}) \rightarrow \pi^*(\text{bpy})$)¹⁹¹. Absence of changes in the absorption spectrum after incubation for 19 h at room temperature indicated that the complex remained stable during the reaction (Figure 14).

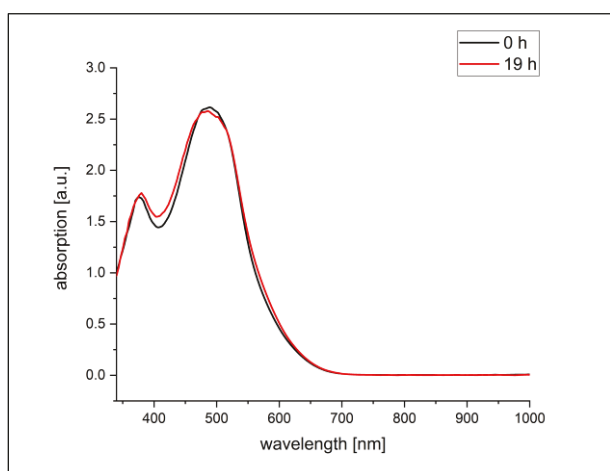


Figure 14: Absorption spectrum of 250 μM $[\text{Ru}(\text{bpy})_2]\text{CO}_3$ dissolved in 50 mM potassium phosphate buffer (pH 7.5) under N_2 atmosphere before (black curve) and after (red curve) incubation at room temperature for 19 h.

$[\text{Ru}(\text{bpy})_2(\text{Im})_2]^{2+}$ was shown to have the same UV/Vis absorption and emission properties as $[\text{Ru}(\text{bpy})_2(\text{Im})(\text{His})]\text{-protein complexes}$ ¹⁹¹. Therefore, we concluded that $[\text{Ru}(\text{bpy})_2(\text{Im})(\text{H}_2\text{O})]^{2+}$ is a suitable model complex for $[\text{Ru}(\text{bpy})_2(\text{H}_2\text{O})(\text{His})]\text{-Ssl1}$. The absorption spectrum of $[\text{Ru}(\text{bpy})_2(\text{Im})(\text{H}_2\text{O})]^{2+}$ includes two MLCT bands at 486 nm ($d\pi(\text{Ru})\text{-}\pi^*(\text{bpy})$; $1.21 \times 10^{-4} \text{ M}^{-1} \text{ cm}^{-1}$) and 340 nm ($d\pi(\text{Ru})\text{-}\pi_2^*(\text{bpy})$; $0.963 \times 10^{-4} \text{ M}^{-1} \text{ cm}^{-1}$), as well as two $\pi\text{-}\pi^*$ transitions of the bipyridine ligands at 242 nm ($2.93 \times 10^{-4} \text{ M}^{-1} \text{ cm}^{-1}$) and 290 nm ($7.50 \times 10^{-4} \text{ M}^{-1} \text{ cm}^{-1}$)¹⁹¹. Presence of these transitions in the absorption spectrum of the reaction product would indicate formation of $[\text{Ru}(\text{bpy})_2(\text{H}_2\text{O})(\text{His})]\text{-Ssl1}$.

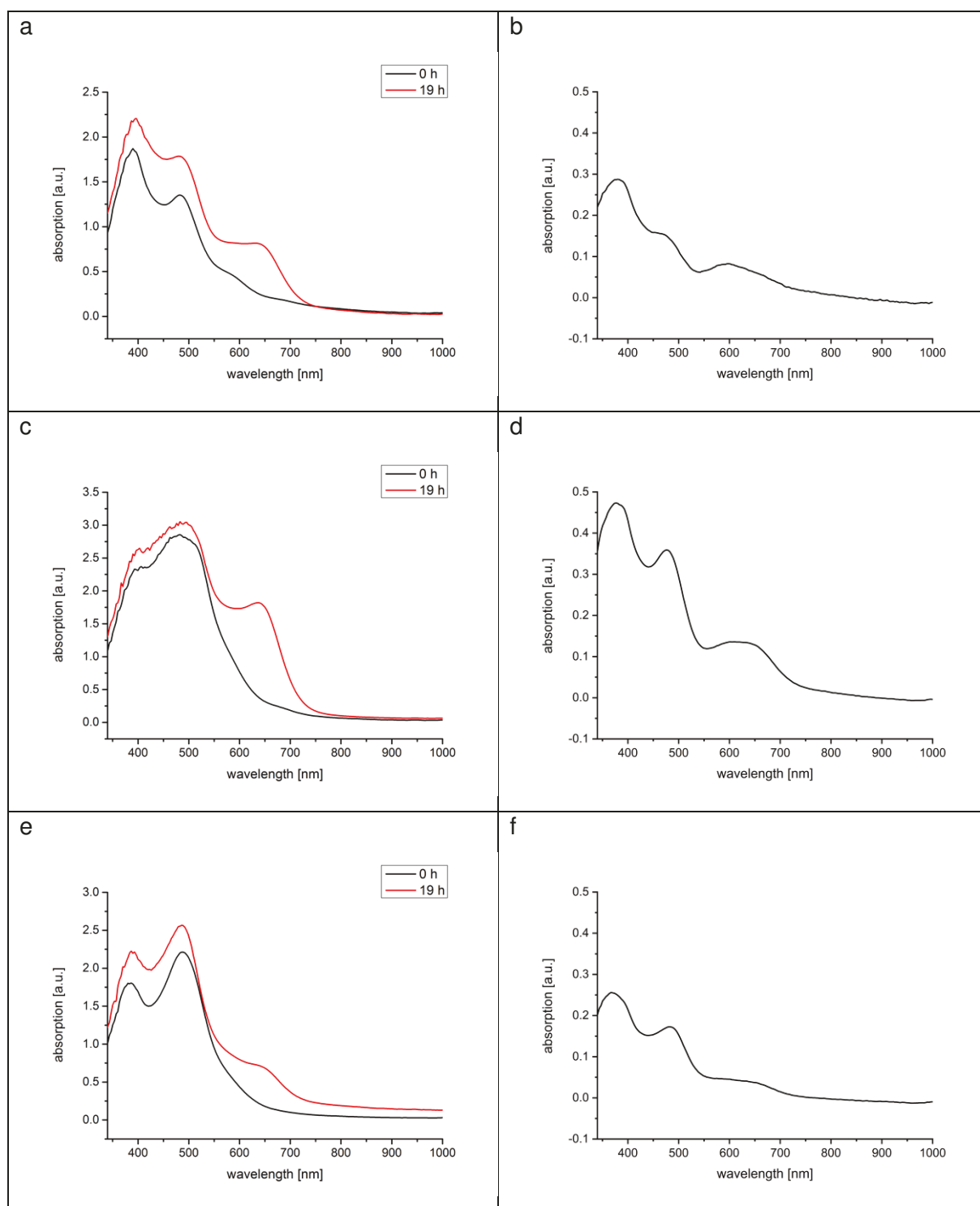


Figure 15: Reaction of Ssl1 H85Q/H132Q/ΔC and Ssl1 with $[\text{Ru}(\text{bpy})_2]\text{CO}_3$. (a) $100 \mu\text{M}$ Ssl1 H85Q/H132Q/ΔC + $250 \mu\text{M}$ $[\text{Ru}(\text{bpy})_2]\text{CO}_3$; (c) $100 \mu\text{M}$ Ssl1 H85Q/H132Q/ΔC + $500 \mu\text{M}$ $[\text{Ru}(\text{bpy})_2]\text{CO}_3$; (e) $100 \mu\text{M}$ His₆-Ssl1 + $250 \mu\text{M}$ $[\text{Ru}(\text{bpy})_2]\text{CO}_3$; (b,d,f) respective reactions after removal of excess $[\text{Ru}(\text{bpy})_2]\text{CO}_3$.

Absorption spectra of the reaction mixtures containing Ssl1 and $[\text{Ru}(\text{bpy})_2]\text{CO}_3$ (black curves in Figure 15a, c, e) include the expected contributions from the ruthenium complex (absorption bands at 370 and 490 nm) and from Ssl1. The 590 nm CT band of the laccase is visible as a shoulder of the 490 nm absorption of the ruthenium complex. During the reaction, an additional absorption at 650 nm developed. It was most intense in the reaction of Ssl1 H85Q/H132Q/ΔC with a 5-fold molar excess of the ruthenium reagent (Figure 15c). The reactions were transferred from the N_2 atmosphere and

unreacted $[\text{Ru}(\text{bpy})_2]\text{CO}_3$ was removed. The absorption spectra of the reaction products are shown in Figure 15 (b, d, and f). The presence of the absorption bands characteristic for $[\text{Ru}(\text{bpy})_2(\text{Im})(\text{H}_2\text{O})]^{2+}$ at 380 nm and 475–485 nm after the removal of free $[\text{Ru}(\text{bpy})_2]\text{CO}_3$ through gel filtration indicated the formation of $[\text{Ru}(\text{bpy})_2(\text{H}_2\text{O})(\text{His})]\text{-Ssl1}$.

In the next step, the water ligand was exchanged by imidazole to obtain a $[\text{Ru}(\text{bpy})_2(\text{Im})(\text{His})]\text{-Ssl1}$ complex. The reaction products described above (Figure 15) were transferred into buffer containing 200 mM imidazole. Additionally, 100 μM $[\text{Ru}(\text{bpy})_2(\text{H}_2\text{O})_2]^{2+}$ were incubated with 200 mM imidazole as a control reaction. In contrast to $[\text{Ru}(\text{bpy})_2(\text{H}_2\text{O})(\text{Im})]^{2+}$ the complex $[\text{Ru}(\text{bpy})_2(\text{Im})_2]^{2+}$ is fluorescent with an emission maximum at 662 nm ($\lambda_{\text{ex}} = 436 \text{ nm}$)¹⁹¹. The substitution process is known to be slow, e.g. substitution of the water ligand by imidazole in $[\text{Ru}(\text{bpy})_2(\text{H}_2\text{O})(\text{His33})]\text{-cyt } c$ required 6 days while reacting with 1 M imidazole¹⁸¹. Thus, we followed the formation of $[\text{Ru}(\text{bpy})_2(\text{Im})(\text{His})]\text{-Ssl1}$ or $[\text{Ru}(\text{bpy})_2(\text{Im})_2]^{2+}$, respectively, by the increase in fluorescence emission at 667 nm ($\lambda_{\text{ex}} = 436 \text{ nm}$) over six days (Figure 16).

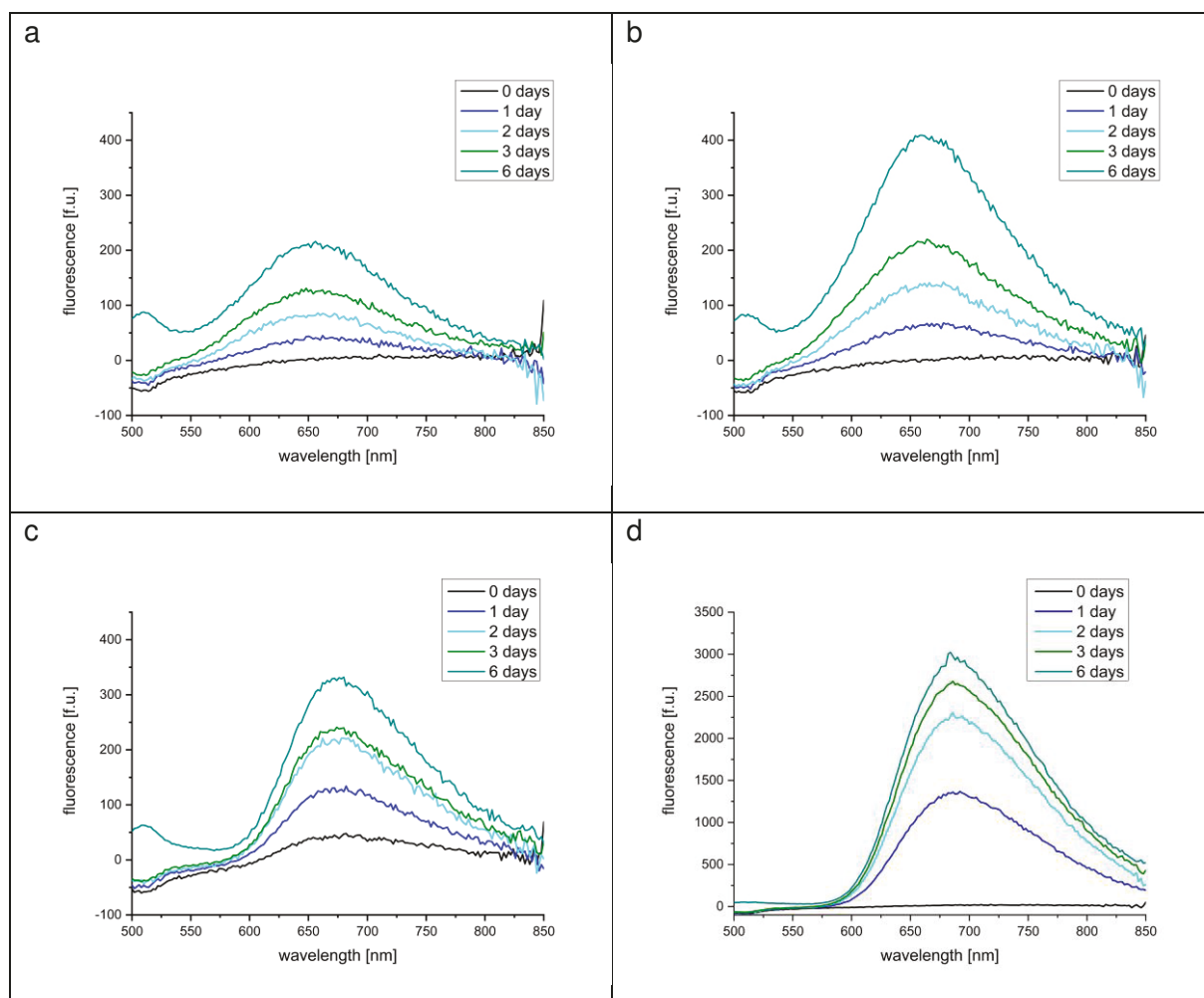


Figure 16: Substitution of the water ligand in (a-c) $[\text{Ru}(\text{bpy})_2(\text{H}_2\text{O})(\text{His})]\text{-Ssl1}$ and (d) $[\text{Ru}(\text{bpy})_2(\text{H}_2\text{O})_2]^{2+}$ with imidazole (200 mM imidazole in 50 mM potassium phosphate pH 7.5, 200 mM sodium chloride) as followed by fluorescence spectroscopy. (a) $[\text{Ru}(\text{bpy})_2(\text{H}_2\text{O})(\text{His})]\text{-Ssl1}$ H85Q/H132Q/ ΔC from reaction with 2.5-fold excess of $[\text{Ru}(\text{bpy})_2]\text{CO}_3$; (b) $[\text{Ru}(\text{bpy})_2(\text{H}_2\text{O})(\text{His})]\text{-Ssl1}$ H85Q/H132Q/ ΔC from reaction with 5-fold excess of $[\text{Ru}(\text{bpy})_2]\text{CO}_3$; (c) $[\text{Ru}(\text{bpy})_2(\text{H}_2\text{O})(\text{His})]\text{-His6-Ssl1}$ from reaction with 2.5-fold excess of $[\text{Ru}(\text{bpy})_2]\text{CO}_3$; (d) $[\text{Ru}(\text{bpy})_2(\text{H}_2\text{O})_2]^{2+}$ is formed from $[\text{Ru}(\text{bpy})_2]\text{CO}_3$ when dissolved in water. Emission 500–850 nm, excitation at 436 nm.

The fluorescence intensity after six days correlated both with the amount of $[\text{Ru}(\text{bpy})_2]\text{CO}_3$ used in the first reaction and the amount of histidine residues accessible for reaction with $[\text{Ru}(\text{bpy})_3]\text{CO}_3$. In the reaction of $[\text{Ru}(\text{bpy})_2(\text{H}_2\text{O})(\text{His})]\text{-Ssl1 H85Q/H132Q}/\Delta\text{C}$ obtained from the previous reaction with 2.5-fold excess of $[\text{Ru}(\text{bpy})_2]\text{CO}_3$ the fluorescence intensity at 660 nm increased to 200 f.u. Using the Ssl1 wildtype variant with more accessible histidine residues or a 5-fold excess of $[\text{Ru}(\text{bpy})_2]\text{CO}_3$ in the first reaction step led to higher fluorescence intensities (300 and 400 f.u., respectively) in the subsequent reaction with imidazole (Figure 16b and c). In the control reaction of $[\text{Ru}(\text{bpy})_2]\text{CO}_3$ with imidazole the fluorescence intensity increased to 3000 f.u. in six days (Figure 16d). Unlike Luo *et al.* who described complete exchange of the water ligand with imidazole after six days¹⁸¹, ligand exchange in $[\text{Ru}(\text{bpy})_2(\text{H}_2\text{O})]\text{-His-Ssl1}$ was probably not complete after six days. In contrast to the control reaction (Figure 16d) and reactions described in the literature¹⁸¹ the fluorescence intensity did not reach a plateau (Figure 16a-c). For higher yields of $[\text{Ru}(\text{bpy})_2(\text{Im})(\text{His})]\text{-Ssl1}$ it might be necessary to prolong incubation times.

Further fluorescence experiments on $[\text{Ru}(\text{bpy})_2(\text{Im})(\text{His})]\text{-Ssl1 H85Q/H132Q}/\Delta\text{C}$ also support successful ruthenation of His203. The excitation and emission spectra of the $[\text{Ru}(\text{bpy})_2(\text{Im})(\text{His})]\text{-Ssl1 H85Q/H132Q}/\Delta\text{C}$ are consistent with literature data¹⁹¹ reported for $[\text{Ru}(\text{bpy})_2(\text{Im})_2]^{2+}$. The excitation spectrum has three maxima at 290, 340 and 490 nm. The maximum of the fluorescence emission was observed at 666 nm.

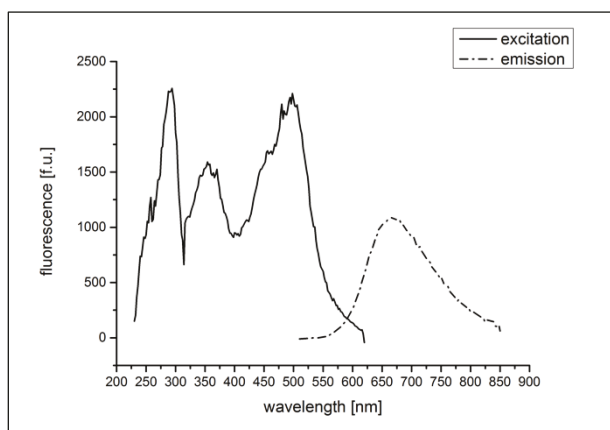


Figure 17: Excitation and emission spectra of $[\text{Ru}(\text{bpy})_2(\text{Im})(\text{His})]\text{-Ssl1 H85Q/H132Q}/\Delta\text{C}$. Excitation 230-620 nm, emission 650 nm. Emission 510-850 nm, excitation 470 nm.

The oxidation state of the T1 Cu effects the ruthenium complex fluorescence. When the T1 Cu was reduced by ascorbate an increase of the fluorescence intensity was observed (Figure 18a). Reoxidation of the laccase by molecular oxygen following aeration by shaking the solution every ten minutes reversed this effect in 20 min (Figure 18b). This can be explained by fluorescence quenching through ET from the excited Ru^{II} to the T1 Cu^{II} which is not possible when the T1 Cu is reduced to the Cu^{I} state. Consequently, the fluorescence lifetime and thereby fluorescence intensity increased. This is an indicator for the ruthenation of Ssl1 in proximity to the T1 Cu. Fluorescence being an artefact due to presence of $[\text{Ru}(\text{bpy})_2(\text{Im})_2]^{2+}$ originating from the reaction of residual $[\text{Ru}(\text{bpy})_2]\text{CO}_3$ with imidazole

is unlikely due to at least two gel filtration steps removing small molecules during the labeling procedure.

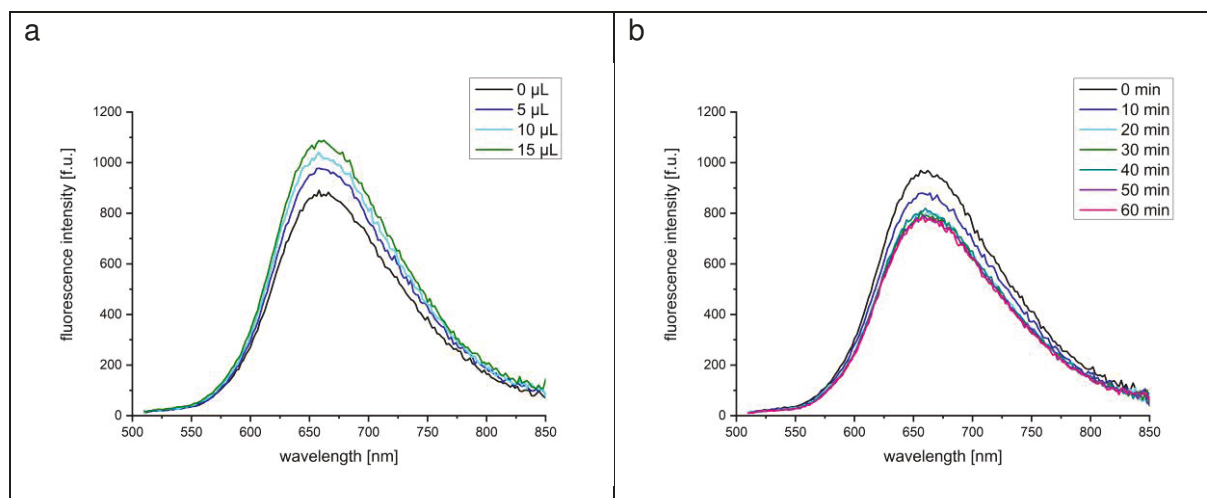


Figure 18: Fluorescence emission spectra of $[\text{Ru}(\text{bpy})_2(\text{Im})(\text{His})]\text{-Ssl1 H85Q/H132Q}/\Delta\text{C}$ after (a) reduction of Ssl1 with ascorbate and (b) reoxidation by aeration. Ssl1 was reduced by addition of $5 \mu\text{L}$ of 13 mM ascorbate three times. Reoxidation was achieved by 5 s of orbital shaking in a microplate reader every 10 min .

Samples of ruthenated Ssl1 H85Q/H132Q/ ΔC were shipped to Prof. Israel Pecht (Weizmann Institute of Science, Rehovot, Israel) where further measurements were performed. The fluorescence lifetimes observed for oxidized and reduced Ssl1 (see Table S4) were rather short and problematic (Prof. Israel Pecht, personal communication). Due to these difficulties this approach was not pursued any further.

Other sites for labeling cannot be ruled out because there are four remaining histidine residues (H188, H151, H161, H223) that are not coordinated to a copper ion. To determine the site of labeling it would be necessary to perform mass spectrometry analysis. One must also take into account that there are possibly multiple stereoisomeric species as reported for the reaction of $[\text{Ru}(\text{bpy})_2(\text{L}=\text{Im or H}_2\text{O})(\text{H}_2\text{O})]$ with horse heart cytochrome c ^{181,192}.

Problems with the fluorescence measurements can also arise because there are at least two fluorescence quenching mechanisms with relation to the oxidized T1 Cu. First, the excited Ru^{II} species can transfer an electron to the T1 Cu. Second, the absorption of the T1 Cu at 600 nm overlaps with the fluorescence emission of the ruthenium imidazole complex and therefore quenching by non-radiative FRET is possible. The presence of several quenching mechanisms might be an explanation for the observed short fluorescence lifetimes of ruthenated Ssl1. On the other hand, the non-radiative FRET was negligible in a photocatalytic system with laccase and $[\text{Ru}(\text{bpy})_3]^{2+}$ ¹⁹³.

For further studies pursuing intramolecular electron transfer measurements it might be worth to try a single molecule approach using fluorescence-based detection of protein redox state described by Gupta *et al.*¹⁷⁴ for SLAC. Using a cysteine for labeling chemistry would be also feasible for Ssl1 since the enzyme contains only one natural cysteine residue. This cysteine is ligating the T1 Cu ion and therefore

not accessible for reactions. After establishing a suitable method for IET measurements in Ssl1 variants, these should be extended to Ssl1 variants with varying T1 Cu reduction potentials.

7 Conclusions

In the framework of this study, molecular factors contributing to the T1 Cu reduction potential in two-domain laccases were elucidated. In addition to mutations of the axial ligand in the laccase Ssl1 from *S. sviveus*, mutations in the second coordination sphere of the T1 Cu were identified which increased the T1 Cu reduction potential and were not described for two-domain laccases yet. The hydrophobicity of the axial ligand was found to be a major determinant for the reduction potential changes observed in the respective mutants. The correlation between the laccase activity and the reduction potential difference between substrate and T1 Cu was demonstrated for substituted phenols and variants with increased reduction potentials displayed a larger substrate scope. However, the oxidation of syringaldazine, alizarin red S, indigo carmine and hydroquinone was not directly dependent on the difference in reduction potentials of the mutated laccases. These observations indicated that not only the reduction potential, but also the reorganization energy and electronic coupling for the electron transfer processes changed in the axial ligand Ssl1 mutants. This was confirmed in further investigations of the structural and spectroscopic properties of the T1 Cu site in Ssl1 variants with different axial ligands. Removing the coordinating methionine residue in Ssl1 variants resulted in perturbed spectral features. Structural studies revealed a water molecule replacing the methionine residue in the axial position of the T1 Cu in all mutants. Moreover, a tetrahedral distortion of the coordination geometry occurred as well. The intramolecular electron transfer (IET) from the T1 Cu to the TNC is an integral part of the laccase reaction mechanism and a proof of concept for site-specific ruthenation of Ssl1 for potential electron transfer measurements was provided. Since the intended measurements of the intramolecular electron transfer were not feasible due to short fluorescence lifetimes other approaches for future studies were suggested.

Overall, this work highlights the importance of the axial ligand for the T1 Cu site in two-domain laccases. Mutation of the axial ligand in Ssl1 appears to influence all three factors which determine the electron transfer rates: reduction potential, reorganization energy, and donor-acceptor electronic coupling. Due to these effects of axial ligand mutations, residues in the second coordination sphere of the T1 Cu might be a promising target for further protein engineering of two-domain laccases with increased reduction potentials and activities.

9 Abbreviations

1-MNA*	1-methylnicotinamide radical
2dMCO	two-domain multicopper oxidase
3dMCO	three-domain multicopper oxidase
ABTS	2,2'-azino-bis(3-ethylbenzthiazoline-6-sulfonic acid)
BCO	blue copper oxidase
bpy	2,2'-bipyridine
CD	circular dichroism
CT	charge transfer
CuNiR	copper nitrite reductase
E°	reduction potential vs. SHE
EDTA	ethylenediaminetetraacetic acid
EPR	electron paramagnetic resonance
ET	electron transfer
EXAFS	extended X-ray absorption fine structure
FRET	Förster resonance energy transfer
h	Planck constant
H_{DA}	electronic coupling matrix element
HPLC	high performance liquid chromatography
IET	intramolecular electron transfer
Im	imidazole
k_B	Boltzmann constant
k_{ET}	electron transfer rate
$k_{T1 \rightarrow TNC}$	rate constant for IET from the T1 to the TNC
LMCT	ligand-to-metal charge transfer
MCO	multicopper oxidase

MLCT	metal-to-ligand charge transfer
N ₂ OR	nitrous oxide reductase
NHE	normal hydrogen electrode
NI	native intermediate
PDB	Protein Data Bank
PI	peroxide intermediate
QM/MM	quantum mechanics/molecular mechanics
RO	resting oxidized
RvL	<i>Rhus vernicifera</i> laccase
S	steric term in Marcus theory
SHE	standard hydrogen electrode
T1 Cu	type 1 copper
T2 Cu	type 2 copper
T3 Cu	type 3 copper
TNC	trinuclear cluster
TvL	<i>Trametes versicolor</i> laccase
UV/Vis	ultraviolet-visible
ΔG°	free energy difference
λ	reorganization energy

10 References

- 1 Andreini, C.; Bertini, I.; Cavallaro, G.; Holliday, G. L.; Thornton, J. M., Metal ions in biological catalysis: from enzyme databases to general principles. *J. Biol. Inorg. Chem.* **2008**, *13* (8), 1205-1218. doi:10.1007/s00775-008-0404-5
- 2 Lu, Y.; Yeung, N.; Sieracki, N.; Marshall, N. M., Design of functional metalloproteins. *Nature* **2009**, *460* (7257), 855-862. doi:10.1038/nature08304
- 3 Holm, R. H.; Kennepohl, P.; Solomon, E. I., Structural and Functional Aspects of Metal Sites in Biology. *Chem. Rev.* **1996**, *96* (7), 2239-2314. doi:10.1021/cr9500390
- 4 Solomon, E. I.; Szilagy, R. K.; DeBeer George, S.; Basumallick, L., Electronic Structures of Metal Sites in Proteins and Models: Contributions to Function in Blue Copper Proteins. *Chem. Rev.* **2004**, *104* (2), 419-458. doi:10.1021/cr0206317
- 5 Solomon, E. I.; Heppner, D. E.; Johnston, E. M.; Ginsbach, J. W.; Cirera, J.; Qayyum, M.; Kieber-Emmons, M. T.; Kjaergaard, C. H.; Hadt, R. G.; Tian, L., Copper active sites in biology. *Chem. Rev.* **2014**, *114* (7), 3659-3853. doi:10.1021/cr400327t
- 6 Brown, K.; Djinic-Carugo, K.; Haltia, T.; Cabrito, I.; Saraste, M.; Moura, J. G.; Moura, I.; Tegoni, M.; Cambillau, C., Revisiting the Catalytic CuZ Cluster of Nitrous Oxide (N₂O) Reductase: Evidence of a Bridging Inorganic Sulfur. *J. Biol. Chem.* **2000**, *275* (52), 41133-41136. doi:10.1074/jbc.M008617200
- 7 Murphy, M. E. P.; Lindley, P. F.; Adman, E. T., Structural comparison of cupredoxin domains: domain recycling to construct proteins with novel functions. *Protein Sci.* **1997**, *6* (4), 761-770. doi:10.1002/pro.5560060402
- 8 Kosman, D. J., Multicopper oxidases: a workshop on copper coordination chemistry, electron transfer, and metallophysiology. *J. Biol. Inorg. Chem.* **2010**, *15* (1), 15-28. doi:10.1007/s00775-009-0590-9
- 9 Sakurai, T.; Kataoka, K., Basic and Applied Features of Multicopper Oxidases, CueO, Bilirubin Oxidase, and Laccase. *Chem. Rec.* **2007**, *7* (4), 220-229. doi:10.1002/tcr.20125
- 10 Majumdar, S.; Lukk, T.; Solbiati, J. O.; Bauer, S.; Nair, S. K.; Cronan, J. E.; Gerlt, J. A., Roles of Small Laccases from *Streptomyces* in Lignin Degradation. *Biochemistry* **2014**, *53* (24), 4047-4058. doi:10.1021/bi500285t
- 11 Endo, K.; Hosono, K.; Beppu, T.; Ueda, K., A novel extracytoplasmic phenol oxidase of *Streptomyces*: its possible involvement in the onset of morphogenesis. *Microbiology* **2002**, *148* (6), 1767-1776. doi:10.1099/00221287-148-6-1767
- 12 Tanaka, N.; Mura, S., Purification and Some Properties of Bilirubin Oxidase of *Myrothecium verrucaria* MT-1. *Agric. Biol. Chem.* **1982**, *46* (10), 2499-2503. doi:10.1271/bbb1961.46.2499
- 13 Hullo, M.-F.; Moszer, I.; Danchin, A.; Martin-Verstraete, I., CotA of *Bacillus subtilis* Is a Copper-Dependent Laccase. *J. Bacteriol.* **2001**, *183* (18), 5426-5430. doi:10.1128/jb.183.18.5426-5430.2001
- 14 Thurston, C. F., The structure and function of fungal laccases. *Microbiology* **1994**, *140* (1), 19-26. doi:10.1099/13500872-140-1-19
- 15 Sakuraba, H.; Koga, K.; Yoneda, K.; Kashima, Y.; Ohshima, T., Structure of a multicopper oxidase from the hyperthermophilic archaeon *Pyrobaculum aerophilum*. *Acta Crystallogr. F* **2011**, *67* (Pt 7), 753-757. doi:10.1107/s1744309111018173
- 16 Fernandes, A. T.; Damas, J. M.; Todorovic, S.; Huber, R.; Baratto, M. C.; Pogni, R.; Soares, C. M.; Martins, L. O., The multicopper oxidase from the archaeon *Pyrobaculum aerophilum* shows nitrous oxide reductase activity. *FEBS J.* **2010**, *277* (15), 3176-3189. doi:10.1111/j.1742-4658.2010.07725.x
- 17 Arakane, Y.; Muthukrishnan, S.; Beeman, R. W.; Kanost, M. R.; Kramer, K. J., Laccase 2 is the phenoloxidase gene required for beetle cuticle tanning. *Proc. Natl. Acad. Sci. U. S. A.* **2005**, *102* (32), 11337-11342. doi:10.1073/pnas.0504982102

- 18 Dittmer, N. T.; Kanost, M. R., Insect multicopper oxidases: Diversity, properties, and physiological roles. *Insect Biochem. Mol. Biol.* **2010**, *40* (3), 179-188. doi:10.1016/j.ibmb.2010.02.006
- 19 Roberts, S. A.; Weichsel, A.; Grass, G.; Thakali, K.; Hazzard, J. T.; Tollin, G.; Rensing, C.; Montfort, W. R., Crystal structure and electron transfer kinetics of CueO, a multicopper oxidase required for copper homeostasis in *Escherichia coli*. *Proc. Natl. Acad. Sci. U. S. A.* **2002**, *99* (5), 2766-2771. doi:10.1073/pnas.052710499
- 20 Roberts, S. A.; Wildner, G. F.; Grass, G.; Weichsel, A.; Ambrus, A.; Rensing, C.; Montfort, W. R., A Labile Regulatory Copper Ion Lies Near the T1 Copper Site in the Multicopper Oxidase CueO. *J. Biol. Chem.* **2003**, *278* (34), 31958-31963. doi:10.1074/jbc.M302963200
- 21 Grass, G.; Rensing, C., CueO is a Multi-copper Oxidase that Confers Copper Tolerance in *Escherichia coli*. *Biochem. Biophys. Res. Commun.* **2001**, *286* (5), 902-908. doi:10.1006/bbrc.2001.5474
- 22 Messerschmidt, A.; Rossi, A.; Ladenstein, R.; Huber, R.; Bolognesi, M.; Gatti, G.; Marchesini, A.; Petruzzelli, R.; Finazzi-Agró, A., X-ray crystal structure of the blue oxidase ascorbate oxidase from zucchini: analysis of the polypeptide fold and a model of the copper sites and ligands. *J. Mol. Biol.* **1989**, *206* (3), 513-529. doi:10.1016/0022-2836(89)90498-1
- 23 Messerschmidt, A.; Huber, R., The blue oxidases, ascorbate oxidase, laccase and ceruloplasmin. Modelling and structural relationships. *Eur. J. Biochem.* **1990**, *187* (2), 341-352. doi:10.1111/j.1432-1033.1990.tb15311.x
- 24 Taylor, A. B.; Stoj, C. S.; Ziegler, L.; Kosman, D. J.; Hart, P. J., The copper-iron connection in biology: structure of the metallo-oxidase Fet3p. *Proc. Natl. Acad. Sci. U. S. A.* **2005**, *102* (43), 15459-15464. doi:10.1073/pnas.0506227102
- 25 Askwith, C.; Eide, D.; Van Ho, A.; Bernard, P. S.; Li, L.; Davis-Kaplan, S.; Sipe, D. M.; Kaplan, J., The *FET3* Gene of *S. cerevisiae* Encodes a Multicopper Oxidase Required for Ferrous Iron Uptake. *Cell* **1994**, *76* (2), 403-410. doi:10.1016/0092-8674(94)90346-8
- 26 De Silva, D. M.; Askwith, C. C.; Eide, D.; Kaplan, J., The *FET3* Gene Product Required for High Affinity Iron Transport in Yeast Is a Cell Surface Ferroxidase. *J. Biol. Chem.* **1995**, *270* (3), 1098-1101. doi:10.1074/jbc.270.3.1098
- 27 Rouch, D. A.; Brown, N. L., Copper-inducible transcriptional regulation at two promoters in the *Escherichia coli* copper resistance determinant *pco*. *Microbiology* **1997**, *143* (4), 1191-1202. doi:10.1099/00221287-143-4-1191
- 28 Brown, N. L.; Barrett, S. R.; Camakaris, J.; Lee, B. T. O.; Rouch, D. A., Molecular genetics and transport analysis of the copper-resistance determinant (*pco*) from *Escherichia coli* plasmid pRJ1004. *Mol. Microbiol.* **1995**, *17* (6), 1153-1166. doi:10.1111/j.1365-2958.1995.mmi_17061153.x
- 29 Brouwers, G.-J.; de Vrind, J. P. M.; Corstjens, P. L. A. M.; Cornelis, P.; Baysse, C.; de Vrind-de Jong, E. W., *cumA*, a Gene Encoding a Multicopper Oxidase, Is Involved in Mn²⁺ Oxidation in *Pseudomonas putida* GB-1. *Appl. Environ. Microbiol.* **1999**, *65* (4), 1762-1768. doi:10.1128/AEM.65.4.1762-1768.1999
- 30 Smith, A. W.; Camara-Artigas, A.; Wang, M.; Allen, J. P.; Francisco, W. A., Structure of Phenoxazinone Synthase from *Streptomyces antibioticus* Reveals a New Type 2 Copper Center. *Biochemistry* **2006**, *45* (14), 4378-4387. doi:10.1021/bi0525526
- 31 Le Roes-Hill, M.; Goodwin, C.; Burton, S., Phenoxazinone synthase: what's in a name? *Trends Biotechnol.* **2009**, *27* (4), 248-258. doi:10.1016/j.tibtech.2009.01.001
- 32 Fujii, I.; Iijima, H.; Tsukita, S.; Ebizuka, Y.; Sankawa, U., Purification and Properties of Dihydrogeodin Oxidase from *Aspergillus terreus*. *J. Biochem.* **1987**, *101* (1), 11-18. doi:10.1093/oxfordjournals.jbchem.a121881
- 33 Huang, K.; Yoshida, Y.; Mikawa, K.; Fujii, I.; Ebizuka, Y.; Sankawa, U., Purification and Characterization of Sulochrin Oxidase from *Penicillium frequentans*. *Biol. Pharm. Bull.* **1996**, *19* (1), 42-46. doi:10.1248/bpb.19.42

- 34 Nordlöv, H.; Gatenbeck, S., Enzymatic Synthesis of (+)- and (-)-Bisdechlorogeodin with Sulochrin Oxidase from *Penicillium frequentans* and *Oospora sulphurea-ochracea*. *Arch. Microbiol.* **1982**, *131* (3), 208-211. doi:10.1007/bf00405880
- 35 Zaitseva, I.; Zaitsev, V.; Card, G.; Moshkov, K.; Bax, B.; Ralph, A.; Lindley, P., The X-ray structure of human serum ceruloplasmin at 3.1 Å: nature of the copper centres. *J. Biol. Inorg. Chem.* **1996**, *1* (1), 15-23. doi:10.1007/s007750050018
- 36 Bielli, P.; Calabrese, L., Structure to function relationships in ceruloplasmin: a 'moonlighting' protein. *Cell. Mol. Life Sci.* **2002**, *59* (9), 1413-1427. doi:10.1007/s00018-002-8519-2
- 37 Petrak, J.; Vyoral, D., Hephaestin—a ferroxidase of cellular iron export. *Int. J. Biochem. Cell Biol.* **2005**, *37* (6), 1173-1178. doi:10.1016/j.biocel.2004.12.007
- 38 Li, L.; Vulpe, C. D.; Kaplan, J., Functional studies of hephaestin in yeast: evidence for multicopper oxidase activity in the endocytic pathway. *Biochem. J.* **2003**, *375* (3), 793-798. doi:10.1042/bj20030866
- 39 Nakamura, K.; Kawabata, T.; Yura, K.; Go, N., Novel types of two-domain multi-copper oxidases: possible missing links in the evolution. *FEBS Lett.* **2003**, *553* (3), 239-244. doi:10.1016/S0014-5793(03)01000-7
- 40 Rydén, L. G.; Hunt, L. T., Evolution of protein complexity: the blue copper-containing oxidases and related proteins. *J. Mol. Evol.* **1993**, *36* (1), 41-66. doi:10.1007/bf02407305
- 41 Komori, H.; Miyazaki, K.; Higuchi, Y., X-ray structure of a two-domain type laccase: A missing link in the evolution of multi-copper proteins. *FEBS Lett.* **2009**, *583* (7), 1189-1195. doi:10.1016/j.febslet.2009.03.008
- 42 Lawton, T. J.; Sayavedra-Soto, L. A.; Arp, D. J.; Rosenzweig, A. C., Crystal structure of a two-domain multicopper oxidase: implications for the evolution of multicopper blue proteins. *J. Biol. Chem.* **2009**, *284* (15), 10174-10180. doi:10.1074/jbc.M900179200
- 43 Machczynski, M. C.; Vijgenboom, E.; Samyn, B.; Canters, G. W., Characterization of SLAC: a small laccase from *Streptomyces coelicolor* with unprecedented activity. *Protein Sci.* **2004**, *13* (9), 2388-2397. doi:10.1110/ps.04759104
- 44 Skálová, T.; Dohnálek, J.; Østergaard, L. H.; Østergaard, P. R.; Kolenko, P.; Dušková, J.; Štěpánková, A.; Hašek, J., The Structure of the Small Laccase from *Streptomyces coelicolor* Reveals a Link between Laccases and Nitrite Reductases. *J. Mol. Biol.* **2009**, *385* (4), 1165-1178. doi:10.1016/j.jmb.2008.11.024
- 45 Gunne, M.; Höppner, A.; Hagedoorn, P. L.; Urlacher, V. B., Structural and redox properties of the small laccase Ssl1 from *Streptomyces sviveus*. *FEBS J.* **2014**, *281* (18), 4307-4318. doi:10.1111/febs.12755
- 46 Solomon, E. I., Spectroscopic methods in bioinorganic chemistry: blue to green to red copper sites. *Inorg. Chem.* **2006**, *45* (20), 8012-8025. doi:10.1021/ic060450d
- 47 Farver, O.; Pecht, I., Electron transfer in blue copper proteins. *Coord. Chem. Rev.* **2011**, *255* (7-8), 757-773. doi:10.1016/j.ccr.2010.08.005
- 48 Sakurai, T.; Kataoka, K., Structure and function of type I copper in multicopper oxidases. *Cell. Mol. Life Sci.* **2007**, *64* (19-20), 2642-2652. doi:10.1007/s00018-007-7183-y
- 49 DeBeer George, S.; Basumallick, L.; Szilagy, R. K.; Randall, D. W.; Hill, M. G.; Nersissian, A. M.; Valentine, J. S.; Hedman, B.; Hodgson, K. O.; Solomon, E. I., Spectroscopic Investigation of Stellacyanin Mutants: Axial Ligand Interactions at the Blue Copper Site. *J. Am. Chem. Soc.* **2003**, *125* (37), 11314-11328. doi:10.1021/ja035802j
- 50 Lowery, M. D.; Guckert, J. A.; Gebhard, M. S.; Solomon, E. I., Active-Site Electronic Structure Contributions to Electron-Transfer Pathways in Rubredoxin and Plastocyanin: Direct versus Superexchange. *J. Am. Chem. Soc.* **1993**, *115* (7), 3012-3013. doi:10.1021/ja00060a074
- 51 Xie, X.; Hadt, R. G.; Pauleta, S. R.; González, P. J.; Un, S.; Moura, I.; Solomon, E. I., A variable temperature spectroscopic study on *Paracoccus pantotrophus* pseudoazurin: Protein constraints

- on the blue Cu site. *J. Inorg. Biochem.* **2009**, *103* (10), 1307-1313. doi:10.1016/j.jinorgbio.2009.04.012
- 52 Ghosh, S.; Xie, X.; Dey, A.; Sun, Y.; Scholes, C. P.; Solomon, E. I., Thermodynamic equilibrium between blue and green copper sites and the role of the protein in controlling function. *Proc. Natl. Acad. Sci. U. S. A.* **2009**, *106* (13), 4969-4974. doi:10.1073/pnas.0900995106
- 53 Hadt, R. G.; Gorelsky, S. I.; Solomon, E. I., Anisotropic Covalency Contributions to Superexchange Pathways in Type One Copper Active Sites. *J. Am. Chem. Soc.* **2014**, *136* (42), 15034-15045. doi:10.1021/ja508361h
- 54 Basumallick, L.; Szilagyi, R. K.; Zhao, Y.; Shapleigh, J. P.; Scholes, C. P.; Solomon, E. I., Spectroscopic Studies of the Met182Thr Mutant of Nitrite Reductase: Role of the Axial Ligand in the Geometric and Electronic Structure of Blue and Green Copper Sites. *J. Am. Chem. Soc.* **2003**, *125* (48), 14784-14792. doi:10.1021/ja037232t
- 55 Enguita, F. J.; Martins, L. O.; Henriques, A. O.; Carrondo, M. A., Crystal structure of a bacterial endospore coat component. A laccase with enhanced thermostability properties. *J. Biol. Chem.* **2003**, *278* (21), 19416-19425. doi:10.1074/jbc.M301251200
- 56 Quintanar, L.; Yoon, J.; Aznar, C. P.; Palmer, A. E.; Andersson, K. K.; Britt, R. D.; Solomon, E. I., Spectroscopic and Electronic Structure Studies of the Trinuclear Cu Cluster Active Site of the Multicopper Oxidase Laccase: Nature of Its Coordination Unsaturation. *J. Am. Chem. Soc.* **2005**, *127* (40), 13832-13845. doi:10.1021/ja0421405
- 57 Solomon, E. I.; Augustine, A. J.; Yoon, J., O₂ reduction to H₂O by the multicopper oxidases. *Dalton Trans.* **2008**, (30), 3921-3932. doi:10.1039/b800799c
- 58 Marcus, R. A.; Sutin, N., Electron transfers in chemistry and biology. *BBA - Rev. Bioenergetics* **1985**, *811* (3), 265-322. doi:10.1016/0304-4173(85)90014-X
- 59 Kosman, D. J., Substrate entasis and electronic coupling elements in electron transfer from Fe^{II} in a multicopper ferroxidase. *Inorg. Chim. Acta* **2008**, *361* (4), 844-849. doi:10.1016/j.ica.2007.10.013
- 60 Jones, S. M.; Solomon, E. I., Electron transfer and reaction mechanism of laccases. *Cell. Mol. Life Sci.* **2015**, *72* (5), 869-883. doi:10.1007/s00018-014-1826-6
- 61 Sekretaryova, A.; Jones, S. M.; Solomon, E. I., O₂ Reduction to Water by High Potential Multicopper Oxidases: Contributions of the T1 Copper Site Potential and the Local Environment of the Trinuclear Copper Cluster. *J. Am. Chem. Soc.* **2019**, *141* (28), 11304-11314. doi:10.1021/jacs.9b05230
- 62 Warren, J. J.; Lancaster, K. M.; Richards, J. H.; Gray, H. B., Inner-and outer-sphere metal coordination in blue copper proteins. *J. Inorg. Biochem.* **2012**, *115*, 119-126. doi:10.1016/j.jinorgbio.2012.05.002
- 63 Mehra, R.; Kepp, K. P., Contribution of substrate reorganization energies of electron transfer to laccase activity. *Phys. Chem. Chem. Phys.* **2019**, *21* (28), 15805-15814. doi:10.1039/c9cp01012b
- 64 Olsson, M. H.; Ryde, U.; Roos, B. O., Quantum chemical calculations of the reorganization energy of blue-copper proteins. *Protein Sci.* **1998**, *7* (12), 2659-2668. doi:10.1002/pro.5560071220
- 65 Ryde, U.; Olsson, M. H., Structure, strain, and reorganization energy of blue copper models in the protein. *Int. J. Quantum Chem.* **2001**, *81* (5), 335-347. doi:10.1002/1097-461x(2001)81:5<335::Aid-Qua1003>3.0.Co;2-Q
- 66 Nielsen, M. T.; Moltved, K. A.; Kepp, K. P., Electron Transfer of Hydrated Transition-Metal Ions and the Electronic State of Co³⁺(aq). *Inorg. Chem.* **2018**, *57* (13), 7914-7924. doi:10.1021/acs.inorgchem.8b01011
- 67 Gray, H. B.; Winkler, J. R., Electron tunneling through proteins. *Q. Rev. Biophys.* **2003**, *36* (3), 341-372. doi:10.1017/S0033583503003913

- 68 Stoj, C. S.; Augustine, A. J.; Zeigler, L.; Solomon, E. I.; Kosman, D. J., Structural Basis of the Ferrous Iron Specificity of the Yeast Ferroxidase, Fet3p. *Biochemistry* **2006**, *45* (42), 12741-12749. doi:10.1021/bi061543+
- 69 Gray, H. B.; Winkler, J. R., Long-range electron transfer. *Proc. Natl. Acad. Sci. U. S. A.* **2005**, *102* (10), 3534-3539. doi:10.1073/pnas.0408029102
- 70 Langen, R.; Chang, I.; Germanas, J.; Richards, J.; Winkler; Gray, H., Electron Tunneling in Proteins: Coupling Through a β Strand. *Science* **1995**, *268* (5218), 1733-1735. doi:10.1126/science.7792598
- 71 Beratan, D.; Betts, J.; Onuchic, J., Protein Electron Transfer Rates Set by the Bridging Secondary and Tertiary Structure. *Science* **1991**, *252* (5010), 1285-1288. doi:10.1126/science.1656523
- 72 Zhang, L.; Cui, H.; Dhoke, G. V.; Zou, Z.; Sauer, D. F.; Davari, M. D.; Schwaneberg, U., Engineering of Laccase CueO for Improved Electron Transfer in Bioelectrocatalysis by Semi-Rational Design. *Chemistry (Easton)* **2020**, *26* (22), 4974-4979. doi:10.1002/chem.201905598
- 73 Hong, G.; Ivnitski, D. M.; Johnson, G. R.; Atanassov, P.; Pachter, R., Design Parameters for Tuning the Type 1 Cu Multicopper Oxidase Redox Potential: Insight from a Combination of First Principles and Empirical Molecular Dynamics Simulations. *J. Am. Chem. Soc.* **2011**, *133* (13), 4802-4809. doi:10.1021/ja105586q
- 74 Gray, H. B.; Malmstrom, B. G.; Williams, R. J., Copper coordination in blue proteins. *J. Biol. Inorg. Chem.* **2000**, *5* (5), 551-559. doi:10.1007/s007750000146
- 75 Sailasuta, N.; Anson, F.; Gray, H. B., Studies of the thermodynamics of electron transfer reactions of blue copper proteins. *J. Am. Chem. Soc.* **1979**, *101* (2), 455-458. doi:10.1021/ja00496a031
- 76 Machonkin, T. E.; Zhang, H. H.; Hedman, B.; Hodgson, K. O.; Solomon, E. I., Spectroscopic and Magnetic Studies of Human Ceruloplasmin: Identification of a Redox-Inactive Reduced Type 1 Copper Site. *Biochemistry* **1998**, *37* (26), 9570-9578. doi:10.1021/bi980434v
- 77 Cambria, M. T.; Gullotto, D.; Garavaglia, S.; Cambria, A., In silico study of structural determinants modulating the redox potential of *Rigidoporus lignosus* and other fungal laccases. *J. Biomol. Struct. Dyn.* **2012**, *30* (1), 89-101. doi:10.1080/07391102.2012.674275
- 78 Li, H.; Webb, S. P.; Ivanic, J.; Jensen, J. H., Determinants of the Relative Reduction Potentials of Type-1 Copper Sites in Proteins. *J. Am. Chem. Soc.* **2004**, *126* (25), 8010-8019. doi:10.1021/ja049345y
- 79 Ingledew, W. J.; Cogley, J. G., A potentiometric and kinetic study on the respiratory chain of ferrous-iron-grown *Thiobacillus ferrooxidans*. *BBA - Bioenergetics* **1980**, *590* (2), 141-158. doi:10.1016/0005-2728(80)90020-1
- 80 Jiménez, B.; Piccioli, M.; Moratal, J.-M.; Donaire, A., Backbone Dynamics of Rusticyanin: The High Hydrophobicity and Rigidity of This Blue Copper Protein Is Responsible for Its Thermodynamic Properties. *Biochemistry* **2003**, *42* (35), 10396-10405. doi:10.1021/bi034692q
- 81 Berry, S. M.; Baker, M. H.; Reardon, N. J., Reduction potential variations in azurin through secondary coordination sphere phenylalanine incorporations. *J. Inorg. Biochem.* **2010**, *104* (10), 1071-1078. doi:10.1016/j.jinorgbio.2010.06.004
- 82 Olsson, M. H. M.; Ryde, U., The influence of axial ligands on the reduction potential of blue copper proteins. *J. Biol. Inorg. Chem.* **1999**, *4* (5), 654-663. doi:10.1007/s007750050389
- 83 Guckert, J. A.; Lowery, M. D.; Solomon, E. I., Electronic Structure of the Reduced Blue Copper Active Site: Contributions to Reduction Potentials and Geometry. *J. Am. Chem. Soc.* **1995**, *117* (10), 2817-2844. doi:10.1021/ja00115a016
- 84 Osipov, E.; Polyakov, K.; Kittl, R.; Shleev, S.; Dorovatovsky, P.; Tikhonova, T.; Hann, S.; Ludwig, R.; Popov, V., Effect of the L499M mutation of the ascomycetous *Botrytis aclada* laccase on redox potential and catalytic properties. *Acta Crystallogr. D* **2014**, *70* (11), 2913-2923. doi:10.1107/s1399004714020380

- 85 Xu, F.; Palmer, A. E.; Yaver, D. S.; Berka, R. M.; Gambetta, G. A.; Brown, S. H.; Solomon, E. I., Targeted mutations in a *Trametes villosa* laccase - Axial perturbations of the T1 copper. *J. Biol. Chem.* **1999**, *274* (18), 12372-12375. doi:10.1074/jbc.274.18.12372
- 86 Pascher, T.; Karlsson, B. G.; Nordling, M.; Malmstrom, B. G.; Vanngard, T., Reduction potentials and their pH dependence in site-directed-mutant forms of azurin from *Pseudomonas aeruginosa*. *Eur. J. Biochem.* **1993**, *212* (2), 289-296. doi:10.1111/j.1432-1033.1993.tb17661.x
- 87 Durao, P.; Bento, I.; Fernandes, A. T.; Melo, E. P.; Lindley, P. F.; Martins, L. O., Perturbations of the T1 copper site in the CotA laccase from *Bacillus subtilis*: structural, biochemical, enzymatic and stability studies. *J. Biol. Inorg. Chem.* **2006**, *11* (4), 514-526. doi:10.1007/s00775-006-0102-0
- 88 Nersissian, A. M.; Immoos, C.; Hill, M. G.; Hart, P. J.; Williams, G.; Herrmann, R. G.; Valentine, J. S., Uclacyanins, stellacyanins, and plantacyanins are distinct subfamilies of phytocyanins: Plant-specific mononuclear blue copper proteins. *Protein Sci.* **1998**, *7* (9), 1915-1929. doi:10.1002/pro.5560070907
- 89 Kurose, S.; Kataoka, K.; Shinohara, N.; Miura, Y.; Tsutsumi, M.; Tsujimura, S.; Kano, K.; Sakurai, T., Modification of Spectroscopic Properties and Catalytic Activity of *Escherichia coli* CueO by Mutations of Methionine 510, the Axial Ligand to the Type I Cu. *Bull. Chem. Soc. Jpn.* **2009**, *82* (4), 504-508. doi:10.1246/bcsj.82.504
- 90 Palmer, A. E.; Szilagy, R. K.; Cherry, J. R.; Jones, A.; Xu, F.; Solomon, E. I., Spectroscopic Characterization of the Leu513His Variant of Fungal Laccase: Effect of Increased Axial Ligand Interaction on the Geometric and Electronic Structure of the Type I Cu Site. *Inorg. Chem.* **2003**, *42* (13), 4006-4017. doi:10.1021/ic026099n
- 91 Kroes, S. J.; Hoitink, C. W. G.; Andrew, C. R.; Ai, J.; Sanders-Loehr, J.; Messerschmidt, A.; Hagen, W. R.; Canters, G. W., The Mutation Met121→His Creates a Type-1.5 Copper Site in *Alcaligenes denitrificans* Azurin. *Eur. J. Biochem.* **1996**, *240* (2), 342-351. doi:10.1111/j.1432-1033.1996.0342h.x
- 92 Garner, D. K.; Vaughan, M. D.; Hwang, H. J.; Savelieff, M. G.; Berry, S. M.; Honek, J. F.; Lu, Y., Reduction Potential Tuning of the Blue Copper Center in *Pseudomonas aeruginosa* Azurin by the Axial Methionine as Probed by Unnatural Amino Acids. *J. Am. Chem. Soc.* **2006**, *128* (49), 15608-15617. doi:10.1021/ja062732i
- 93 Berry, S. M.; Ralle, M.; Low, D. W.; Blackburn, N. J.; Lu, Y., Probing the Role of Axial Methionine in the Blue Copper Center of Azurin with Unnatural Amino Acids. *J. Am. Chem. Soc.* **2003**, *125* (29), 8760-8768. doi:10.1021/ja029699u
- 94 Yanagisawa, S.; Banfield, M. J.; Dennison, C., The Role of Hydrogen Bonding at the Active Site of a Cupredoxin: The Phe114Pro Azurin Variant. *Biochemistry* **2006**, *45* (29), 8812-8822. doi:10.1021/bi0606851
- 95 Libeu, C. A. P.; Kukimoto, M.; Nishiyama, M.; Horinouchi, S.; Adman, E. T., Site-Directed Mutants of Pseudoazurin: Explanation of Increased Redox Potentials from X-ray Structures and from Calculation of Redox Potential Differences. *Biochemistry* **1997**, *36* (43), 13160-13179. doi:10.1021/bi9704111
- 96 Machczynski, M. C.; Gray, H. B.; Richards, J. H., An outer-sphere hydrogen-bond network constrains copper coordination in blue proteins. *J. Inorg. Biochem.* **2002**, *88* (3), 375-380. doi:10.1016/S0162-0134(02)00364-1
- 97 Hall, J. F.; Kanbi, L. D.; Harvey, I.; Murphy, L. M.; Hasnain, S. S., Modulating the Redox Potential and Acid Stability of Rusticyanin by Site-Directed Mutagenesis of Ser86. *Biochemistry* **1998**, *37* (33), 11451-11458. doi:10.1021/bi980960m
- 98 Marshall, N. M.; Garner, D. K.; Wilson, T. D.; Gao, Y.-G.; Robinson, H.; Nilges, M. J.; Lu, Y., Rationally tuning the reduction potential of a single cupredoxin beyond the natural range. *Nature* **2009**, *462* (7269), 113-116. doi:10.1038/nature08551
- 99 Vallee, B. L.; Williams, R. J. P., Metalloenzymes: the entatic nature of their active sites. *Proc. Natl. Acad. Sci. U. S. A.* **1968**, *59* (2), 498-505. doi:10.1073/pnas.59.2.498

- 100 Canters, G. W.; Kolczak, U.; Armstrong, F.; Jeuken, L. J.; Camba, R.; Sola, M., The effect of pH and ligand exchange on the redox properties of blue copper proteins. *Faraday Discuss.* **2000**, *116* (116), 205-220. doi:10.1039/b003822i
- 101 Wijma, H. J.; Boulanger, M. J.; Molon, A.; Fittipaldi, M.; Huber, M.; Murphy, M. E. P.; Verbeet, M. P.; Canters, G. W., Reconstitution of the Type-1 Active Site of the H145G/A Variants of Nitrite Reductase by Ligand Insertion. *Biochemistry* **2003**, *42* (14), 4075-4083. doi:10.1021/bi027270+
- 102 Ryde, U.; Olsson, M. H.; Roos, B. O.; De Kerpel, J. O.; Pierloot, K., On the role of strain in blue copper proteins. *J. Biol. Inorg. Chem.* **2000**, *5* (5), 565-574. doi:10.1007/s007750000147
- 103 Ryde, U.; Olsson, M. H. M.; Pierloot, K.; Roos, B. O., The Cupric Geometry of Blue Copper Proteins is not Strained. *J. Mol. Biol.* **1996**, *261* (4), 586-596. doi:10.1006/jmbi.1996.0484
- 104 Olsson, M. H. M.; Ryde, U.; Roos, B. O.; Pierloot, K., On the relative stability of tetragonal and trigonal Cu(II) complexes with relevance to the blue copper proteins. *J. Biol. Inorg. Chem.* **1998**, *3* (2), 109-125. doi:10.1007/s007750050212
- 105 Hurd, C. A.; Besley, N. A.; Robinson, D., A QM/MM study of the nature of the entatic state in plastocyanin. *J. Comput. Chem.* **2017**, *38* (16), 1431-1437. doi:10.1002/jcc.24666
- 106 Hagen, W. R., Hypothesis: entatic *versus* ecstatic states in metalloproteins. *Metallomics* **2019**, *11* (11), 1768-1778. doi:10.1039/c9mt00208a
- 107 Hu, L.; Farrokhnia, M.; Heimdal, J.; Shleev, S.; Rulisek, L.; Ryde, U., Reorganization energy for internal electron transfer in multicopper oxidases. *J. Phys. Chem. B* **2011**, *115* (45), 13111-13126. doi:10.1021/jp205897z
- 108 Fowler, N. J.; Blanford, C. F.; Warwicker, J.; de Visser, S. P., Prediction of Reduction Potentials of Copper Proteins with Continuum Electrostatics and Density Functional Theory. *Chem. Eur. J.* **2017**, *23* (61), 15436-15445. doi:10.1002/chem.201702901
- 109 Varadarajan, R.; Zewert, T.; Gray, H.; Boxer, S., Effects of Buried Ionizable Amino Acids on the Reduction Potential of Recombinant Myoglobin. *Science* **1989**, *243* (4887), 69-72. doi:10.1126/science.2563171
- 110 Battistuzzi, G.; Borsari, M.; Loschi, L.; Righi, F.; Sola, M., Redox Thermodynamics of Blue Copper Proteins. *J. Am. Chem. Soc.* **1999**, *121* (3), 501-506. doi:10.1021/ja982126q
- 111 Dey, A.; Jenney, F. E.; Adams, M. W. W.; Babini, E.; Takahashi, Y.; Fukuyama, K.; Hodgson, K. O.; Hedman, B.; Solomon, E. I., Solvent Tuning of Electrochemical Potentials in the Active Sites of HiPIP Versus Ferredoxin. *Science* **2007**, *318* (5855), 1464-1468. doi:10.1126/science.1147753
- 112 Cascella, M.; Magistrato, A.; Tavernelli, I.; Carloni, P.; Rothlisberger, U., Role of protein frame and solvent for the redox properties of azurin from *Pseudomonas aeruginosa*. *Proc. Natl. Acad. Sci. U. S. A.* **2006**, *103* (52), 19641-19646. doi:10.1073/pnas.0607890103
- 113 Abdelhamid, R. F.; Obara, Y.; Uchida, Y.; Kohzuma, T.; Dooley, D. M.; Brown, D. E.; Hori, H., π - π interaction between aromatic ring and copper-coordinated His81 imidazole regulates the blue copper active-site structure. *J. Biol. Inorg. Chem.* **2007**, *12* (2), 165-173. doi:10.1007/s00775-006-0176-8
- 114 Yanagisawa, S.; Crowley, P. B.; Firbank, S. J.; Lawler, A. T.; Hunter, D. M.; McFarlane, W.; Li, C.; Kohzuma, T.; Banfield, M. J.; Dennison, C., π -Interaction Tuning of the Active Site Properties of Metalloproteins. *J. Am. Chem. Soc.* **2008**, *130* (46), 15420-15428. doi:10.1021/ja8038135
- 115 Yanagisawa, S.; Sato, K.; Kikuchi, M.; Kohzuma, T.; Dennison, C., Introduction of a π - π Interaction at the Active Site of a Cupredoxin: Characterization of the Met16Phe Pseudoazurin Mutant. *Biochemistry* **2003**, *42* (22), 6853-6862. doi:10.1021/bi030030p
- 116 Hosseinzadeh, P.; Marshall, N. M.; Chacón, K. N.; Yu, Y.; Nilges, M. J.; New, S. Y.; Tashkov, S. A.; Blackburn, N. J.; Lu, Y., Design of a single protein that spans the entire 2-V range of physiological redox potentials. *Proc. Natl. Acad. Sci. U. S. A.* **2016**, *113* (2), 262-267. doi:10.1073/pnas.1515897112

- 117 Claus, H., Laccases: structure, reactions, distribution. *Micron* **2004**, *35* (1-2), 93-96. doi:10.1016/j.micron.2003.10.029
- 118 Yoshida, H., LXIII.—Chemistry of lacquer (Urushi). Part I. Communication from the Chemical Society of Tokio. *J. Chem. Soc. Trans.* **1883**, *43* (0), 472-486. doi:10.1039/ct8834300472
- 119 Xu, F., Oxidation of phenols, anilines, and benzenethiols by fungal laccases: Correlation between activity and redox potentials as well as halide inhibition. *Biochemistry* **1996**, *35* (23), 7608-7614. doi:10.1021/bi952971a
- 120 Xu, F.; Shin, W.; Brown, S. H.; Wahleithner, J. A.; Sundaram, U. M.; Solomon, E. I., A study of a series of recombinant fungal laccases and bilirubin oxidase that exhibit significant differences in redox potential, substrate specificity, and stability. *BBA - Protein Struct. M.* **1996**, *1292* (2), 303-311. doi:10.1016/0167-4838(95)00210-3
- 121 Giardina, P.; Faraco, V.; Pezzella, C.; Piscitelli, A.; Vanhulle, S.; Sannia, G., Laccases: a never-ending story. *Cell. Mol. Life Sci.* **2010**, *67* (3), 369-385. doi:10.1007/s00018-009-0169-1
- 122 Tadesse, M. A.; D'Annibale, A.; Galli, C.; Gentili, P.; Sergi, F., An assessment of the relative contributions of redox and steric issues to laccase specificity towards putative substrates. *Org. Biomol. Chem.* **2008**, *6* (5), 868-878. doi:10.1039/b716002j
- 123 Xu, F.; Kulys, J. J.; Duke, K.; Li, K.; Krikstopaitis, K.; Deussen, H.-J. W.; Abbate, E.; Galinyte, V.; Schneider, P., Redox chemistry in laccase-catalyzed oxidation of N-hydroxy compounds. *Appl. Environ. Microbiol.* **2000**, *66* (5), 2052-2056. doi:10.1128/AEM.66.5.2052-2056.2000
- 124 Shleev, S.; Tkac, J.; Christenson, A.; Ruzgas, T.; Yaropolov, A. I.; Whittaker, J. W.; Gorton, L., Direct electron transfer between copper-containing proteins and electrodes. *Biosens. Bioelectron.* **2005**, *20* (12), 2517-2554. doi:10.1016/j.bios.2004.10.003
- 125 Kumar, S. V.; Phale, P. S.; Durani, S.; Wangikar, P. P., Combined Sequence and Structure Analysis of the Fungal Laccase Family. *Biotechnol. Bioeng.* **2003**, *83* (4), 386-394. doi:10.1002/bit.10681
- 126 Brissos, V.; Ferreira, M.; Grass, G.; Martins, L. O., Turning a Hyperthermostable Metallo-Oxidase into a Laccase by Directed Evolution. *ACS Catalysis* **2015**, *5* (8), 4932-4941. doi:10.1021/acscatal.5b00771
- 127 Kataoka, K.; Hirota, S.; Maeda, Y.; Kogi, H.; Shinohara, N.; Sekimoto, M.; Sakurai, T., Enhancement of Laccase Activity through the Construction and Breakdown of a Hydrogen Bond at the Type I Copper Center in *Escherichia coli* CueO and the Deletion Mutant $\Delta\alpha 5-7$ CueO. *Biochemistry* **2011**, *50* (4), 558-565. doi:10.1021/bi101107c
- 128 Quintanar, L.; Gebhard, M.; Wang, T.-P.; Kosman, D. J.; Solomon, E. I., Ferrous Binding to the Multicopper Oxidases *Saccharomyces cerevisiae* Fet3p and Human Ceruloplasmin: Contributions to Ferroxidase Activity. *J. Am. Chem. Soc.* **2004**, *126* (21), 6579-6589. doi:10.1021/ja049220t
- 129 Ducros, V.; Brzozowski, A. M.; Wilson, K. S.; Brown, S. H.; Østergaard, P.; Schneider, P.; Yaver, D. S.; Pedersen, A. H.; Davies, G. J., Crystal structure of the type-2 Cu depleted laccase from *Coprinus cinereus* at 2.2 Å resolution. *Nat. Struct. Biol.* **1998**, *5* (4), 310-316. doi:10.1038/nsb0498-310
- 130 Xie, T.; Liu, Z.; Wang, G., Structural basis for monolignol oxidation by a maize laccase. *Nature Plants* **2020**, *6* (3), 231-237. doi:10.1038/s41477-020-0595-5
- 131 Hakulinen, N.; Rouvinen, J., Three-dimensional structures of laccases. *Cell. Mol. Life Sci.* **2015**, *72* (5), 857-868. doi:10.1007/s00018-014-1827-5
- 132 Toscano, M. D.; De Maria, L.; Lobedanz, S.; Østergaard, L. H., Optimization of a Small Laccase by Active-Site Redesign. *Chembiochem* **2013**, *14* (10), 1209-1211. doi:10.1002/cbic.201300256
- 133 Solomon, E. I.; Sundaram, U. M.; Machonkin, T. E., Multicopper oxidases and oxygenases. *Chem. Rev.* **1996**, *96* (7), 2563-2606. doi:10.1021/cr950046o

- 134 Solomon, E. I.; Chen, P.; Metz, M.; Lee, S. K.; Palmer, A. E., Oxygen Binding, Activation, and Reduction to Water by Copper Proteins. *Angewandte Chemie International Edition* **2001**, *40* (24), 4570-4590. doi:10.1002/1521-3773(20011217)40:24<4570::aid-anie4570>3.0.co;2-4
- 135 Ryde, U.; Hsiao, Y.-W.; Rulišek, L.; Solomon, E. I., Identification of the Peroxy Adduct in Multicopper Oxidases by a Combination of Computational Chemistry and Extended X-ray Absorption Fine-Structure Measurements. *J. Am. Chem. Soc.* **2007**, *129* (4), 726-727. doi:10.1021/ja062954g
- 136 Ferraroni, M.; Myasoedova, N.; Schmatchenko, V.; Leontievsky, A.; Golovleva, L.; Scozzafava, A.; Briganti, F., Crystal structure of a blue laccase from *Lentinus tigrinus*: evidences for intermediates in the molecular oxygen reductive splitting by multicopper oxidases. *BMC Struct. Biol.* **2007**, *7* (1), 60. doi:10.1186/1472-6807-7-60
- 137 Augustine, A. J.; Kjaergaard, C.; Qayyum, M.; Ziegler, L.; Kosman, D. J.; Hodgson, K. O.; Hedman, B.; Solomon, E. I., Systematic Perturbation of the Trinuclear Copper Cluster in the Multicopper Oxidases: The Role of Active Site Asymmetry in Its Reduction of O₂ to H₂O. *J. Am. Chem. Soc.* **2010**, *132* (17), 6057-6067. doi:10.1021/ja909143d
- 138 Lee, S.-K.; George, S. D.; Antholine, W. E.; Hedman, B.; Hodgson, K. O.; Solomon, E. I., Nature of the Intermediate Formed in the Reduction of O₂ to H₂O at the Trinuclear Copper Cluster Active Site in Native Laccase. *J. Am. Chem. Soc.* **2002**, *124* (21), 6180-6193. doi:10.1021/ja0114052
- 139 Yoon, J.; Liboiron, B. D.; Sarangi, R.; Hodgson, K. O.; Hedman, B.; Solomon, E. I., The two oxidized forms of the trinuclear Cu cluster in the multicopper oxidases and mechanism for the decay of the native intermediate. *Proc. Natl. Acad. Sci. U. S. A.* **2007**, *104* (34), 13609-13614. doi:10.1073/pnas.0705137104
- 140 Heppner, D. E.; Kjaergaard, C. H.; Solomon, E. I., Molecular origin of rapid versus slow intramolecular electron transfer in the catalytic cycle of the multicopper oxidases. *J. Am. Chem. Soc.* **2013**, *135* (33), 12212-12215. doi:10.1021/ja4064525
- 141 Augustine, A. J.; Quintanar, L.; Stoj, C. S.; Kosman, D. J.; Solomon, E. I., Spectroscopic and Kinetic Studies of Perturbed Trinuclear Copper Clusters: The Role of Protons in Reductive Cleavage of the O–O Bond in the Multicopper Oxidase Fet3p. *J. Am. Chem. Soc.* **2007**, *129* (43), 13118-13126. doi:10.1021/ja073905m
- 142 Quintanar, L.; Stoj, C.; Wang, T.-P.; Kosman, D. J.; Solomon, E. I., Role of Aspartate 94 in the Decay of the Peroxide Intermediate in the Multicopper Oxidase Fet3p. *Biochemistry* **2005**, *44* (16), 6081-6091. doi:10.1021/bi047379c
- 143 Kataoka, K.; Sugiyama, R.; Hirota, S.; Inoue, M.; Urata, K.; Minagawa, Y.; Seo, D.; Sakurai, T., Four-electron Reduction of Dioxygen by a Multicopper Oxidase, CueO, and Roles of Asp¹¹² and Glu⁵⁰⁶ Located Adjacent to the Trinuclear Copper Center. *J. Biol. Chem.* **2009**, *284* (21), 14405-14413. doi:10.1074/jbc.M808468200
- 144 Brissos, V.; Chen, Z.; Martins, L. O., The kinetic role of carboxylate residues in the proximity of the trinuclear centre in the O₂ reactivity of CotA-laccase. *Dalton Trans.* **2012**, *41* (20), 6247-6255. doi:10.1039/c2dt12067d
- 145 Chen, Z.; Durão, P.; Silva, C. S.; Pereira, M. M.; Todorovic, S.; Hildebrandt, P.; Bento, I.; Lindley, P. F.; Martins, L. O., The role of Glu498 in the dioxygen reactivity of CotA-laccase from *Bacillus subtilis*. *Dalton Trans.* **2010**, *39* (11), 2875-2882. doi:10.1039/b922734b
- 146 Farver, O.; Pecht, I., Long Range Electron Transfer in Blue Copper Proteins. *Mol. Cryst. Liq. Cryst.* **1991**, *194* (1), 215-224. doi:10.1080/00268949108041167
- 147 Kyritsis, P.; Messerschmidt, A.; Huber, R.; Salmon, G. A.; Sykes, A. G., Pulse-radiolysis Studies on the Oxidised Form of the Multicopper Enzyme Ascorbate Oxidase: Evidence for Two Intramolecular Electron-transfer Steps *J. Chem. Soc. Dalton Trans.* **1993**, (5), 731-735. doi:10.1039/dt9930000731

- 148 Beratan, D. N.; Onuchic, J. N.; Betts, J. N.; Bowler, B. E.; Gray, H. B., Electron-Tunneling Pathways in Ruthenated Proteins. *J. Am. Chem. Soc.* **1990**, *112* (22), 7915-7921. doi:10.1021/ja00178a011
- 149 Onuchic, J. N.; Beratan, D. N., A predictive theoretical model for electron tunneling pathways in proteins. *J. Chem. Phys.* **1990**, *92* (1), 722-733. doi:10.1063/1.458426
- 150 Gupta, A.; Nederlof, I.; Sottini, S.; Tepper, A. W.; Groenen, E. J.; Thomassen, E. A.; Canters, G. W., Involvement of Tyr108 in the enzyme mechanism of the small laccase from *Streptomyces coelicolor*. *J. Am. Chem. Soc.* **2012**, *134* (44), 18213-18216. doi:10.1021/ja3088604
- 151 Tepper, A. W. J. W.; Milikisyants, S.; Sottini, S.; Vijgenboom, E.; Groenen, E. J. J.; Canters, G. W., Identification of a Radical Intermediate in the Enzymatic Reduction of Oxygen by a Small Laccase. *J. Am. Chem. Soc.* **2009**, *131* (33), 11680-11682. doi:10.1021/ja900751c
- 152 Riva, S., Laccases: blue enzymes for green chemistry. *Trends Biotechnol.* **2006**, *24* (5), 219-226. doi:10.1016/j.tibtech.2006.03.006
- 153 Osma, J. F.; Toca-Herrera, J. L.; Rodríguez-Couto, S., Uses of laccases in the food industry. *Enzyme Res.* **2010**, *2010*, 918761-918761. doi:10.4061/2010/918761
- 154 Rodríguez Couto, S.; Toca Herrera, J. L., Industrial and biotechnological applications of laccases: A review. *Biotechnol. Adv.* **2006**, *24* (5), 500-513. doi:10.1016/j.biotechadv.2006.04.003
- 155 Kudanga, T.; Le Roes-Hill, M., Laccase applications in biofuels production: current status and future prospects. *Appl. Microbiol. Biotechnol.* **2014**, *98* (15), 6525-6542. doi:10.1007/s00253-014-5810-8
- 156 Kudanga, T.; Nemađziva, B.; Le Roes-Hill, M., Laccase catalysis for the synthesis of bioactive compounds. *Appl. Microbiol. Biotechnol.* **2017**, *101* (1), 13-33. doi:10.1007/s00253-016-7987-5
- 157 Zerva, A.; Simić, S.; Topakas, E.; Nikodinovic-Runic, J., Applications of Microbial Laccases: Patent Review of the Past Decade (2009–2019). *Catalysts* **2019**, *9* (12), 1023. doi:10.3390/catal9121023
- 158 Mate, D. M.; Alcalde, M., Laccase: a multi-purpose biocatalyst at the forefront of biotechnology. *Microb. Biotechnol.* **2016**, *10* (6), 1457-1467. doi:10.1111/1751-7915.12422
- 159 Rodgers, C. J.; Blanford, C. F.; Giddens, S. R.; Skamnioti, P.; Armstrong, F. A.; Gurr, S. J., Designer laccases: a vogue for high-potential fungal enzymes? *Trends Biotechnol.* **2010**, *28* (2), 63-72. doi:10.1016/j.tibtech.2009.11.001
- 160 Baldrian, P., Fungal laccases—occurrence and properties. *FEMS Microbiol. Rev.* **2006**, *30* (2), 215-242. doi:10.1111/j.1574-4976.2005.00010.x
- 161 Nemađziva, B.; Le Roes-Hill, M.; Koorbanally, N.; Kudanga, T., Small laccase-catalyzed synthesis of a caffeic acid dimer with high antioxidant capacity. *Process Biochem.* **2018**, *69*, 99-105. doi:10.1016/j.procbio.2018.03.009
- 162 Ece, S.; Lambertz, C.; Fischer, R.; Commandeur, U., Heterologous expression of a *Streptomyces cyaneus* laccase for biomass modification applications. *AMB Express* **2017**, *7* (1), 86. doi:10.1186/s13568-017-0387-0
- 163 Prins, A.; Kleinsmidt, L.; Khan, N.; Kirby, B.; Kudanga, T.; Vollmer, J.; Pleiss, J.; Burton, S.; Le Roes-Hill, M., The effect of mutations near the T1 copper site on the biochemical characteristics of the small laccase from *Streptomyces coelicolor* A3 (2). *Enzyme Microb. Technol.* **2015**, *68*, 23-32. doi:10.1016/j.enzmictec.2014.10.003
- 164 Olbrich, A. C.; Schild, J. N.; Urlacher, V. B., Correlation between the T1 copper reduction potential and catalytic activity of a small laccase. *J. Inorg. Biochem.* **2019**, *201*, 110843. doi:10.1016/j.jinorgbio.2019.110843
- 165 Gunne, M.; Urlacher, V. B., Characterization of the Alkaline Laccase Ssl1 from *Streptomyces sviveus* with Unusual Properties Discovered by Genome Mining. *PLoS One* **2012**, *7* (12), e52360. doi:10.1371/journal.pone.0052360

- 166 Suljić, S.; Mortzfeld, F. B.; Gunne, M.; Urlacher, V. B.; Pietruszka, J., Enhanced Biocatalytic Performance of Bacterial Laccase from *Streptomyces sviveus*: Application in the Michael Addition Sequence Towards 3-Arylated 4-Oxochromanones. *ChemCatChem* **2015**, *7* (8), 1380-1385. doi:10.1002/cctc.201500142
- 167 Lu, S.; Wang, J.; Chitsaz, F.; Derbyshire, M. K.; Geer, R. C.; Gonzales, N. R.; Gwadz, M.; Hurwitz, D. I.; Marchler, G. H.; Song, J. S.; Thanki, N.; Yamashita, R. A.; Yang, M.; Zhang, D.; Zheng, C.; Lanczycki, C. J.; Marchler-Bauer, A., CDD/SPARCLE: the conserved domain database in 2020. *Nucleic Acids Res.* **2020**, *48* (D1), D265-D268. doi:10.1093/nar/gkz991
- 168 Chapman, J.; Ismail, A.; Dinu, C., Industrial Applications of Enzymes: Recent Advances, Techniques, and Outlooks. *Catalysts* **2018**, *8* (6), 238. doi:10.3390/catal8060238
- 169 Farver, O.; Tepper, A. W. J. W.; Wherland, S.; Canters, G. W.; Pecht, I., Site-Site Interactions Enhances Intramolecular Electron Transfer in *Streptomyces coelicolor* laccase. *J. Am. Chem. Soc.* **2009**, *131* (51), 18226-18227. doi:10.1021/ja908793d
- 170 Wherland, S.; Miyazaki, K.; Pecht, I., Intramolecular Electron Transfer in the Bacterial Two-Domain Multicopper Oxidase mgLAC. *Biochemistry* **2016**, *55* (21), 2960-2966. doi:10.1021/acs.biochem.6b00158
- 171 Farver, O.; Pecht, I., Low activation barriers characterize intramolecular electron transfer in ascorbate oxidase. *Proc. Natl. Acad. Sci. U. S. A.* **1992**, *89* (17), 8283-8287. doi:10.1073/pnas.89.17.8283
- 172 Farver, O.; Wherland, S.; Koroleva, O.; Loginov, D. S.; Pecht, I., Intramolecular electron transfer in laccases. *FEBS J.* **2011**, *278* (18), 3463-3471. doi:10.1111/j.1742-4658.2011.08268.x
- 173 Kuznetsova, S.; Zauner, G.; Schmauder, R.; Mayboroda, O. A.; Deelder, A. M.; Aartsma, T. J.; Canters, G. W., A Förster-resonance-energy transfer-based method for fluorescence detection of the protein redox state. *Anal. Biochem.* **2006**, *350* (1), 52-60. doi:10.1016/j.ab.2005.11.036
- 174 Gupta, A.; Aartsma, T. J.; Canters, G. W., One at a Time: Intramolecular Electron-Transfer Kinetics in Small Laccase Observed during Turnover. *J. Am. Chem. Soc.* **2014**, *136* (7), 2707-2710. doi:10.1021/ja411078b
- 175 Reinhammar, B. R., Oxidation-reduction potentials of the electron acceptors in laccases and stellacyanin. *BBA - Bioenergetics* **1972**, *275* (2), 245-259. doi:10.1016/0005-2728(72)90045-X
- 176 Bjerrum, M. J.; Casimiro, D. R.; Chang, I.-J.; Di Bilio, A. J.; Gray, H. B.; Hill, M. G.; Langen, R.; Mines, G. A.; Skov, L. K.; Winkler, J. R.; Wuttke, D. S., Electron Transfer in Ruthenium-Modified Proteins. *J. Bioenerg. Biomembr.* **1995**, *27* (3), 295-302. doi:10.1007/bf02110099
- 177 Matthews, C.; Erickson, P.; Van Vliet, D.; Petersheim, M., Synthesis of Pentaammineruthenium-Histidine Complexes in Ribonuclease A. *J. Am. Chem. Soc.* **1978**, *100* (7), 2260-2262. doi:10.1021/ja00475a063
- 178 Winkler, J. R.; Nocera, D. G.; Yocom, K. M.; Bordignon, E.; Gray, H. B., Electron-Transfer Kinetics of Pentaammineruthenium(III)(histidine-33)-Ferricytochrome *c*. Measurement of the Rate of Intramolecular Electron Transfer between Redox Centers Separated by 15 Å in a Protein. *J. Am. Chem. Soc.* **1982**, *104* (21), 5798-5800. doi:10.1021/ja00385a047
- 179 Crutchley, R. J.; Ellis, W. R.; Gray, H. B., Long-Distance Electron Transfer in Pentaammineruthenium (Histidine-48)-Myoglobin. Reorganizational Energetics of a High-Spin Heme. *J. Am. Chem. Soc.* **1985**, *107* (17), 5002-5004. doi:10.1021/ja00303a034
- 180 Wuttke, D. S.; Bjerrum, M. J.; Chang, I. J.; Winkler, J. R.; Gray, H. B., Electron tunneling in ruthenium-modified cytochrome *c*. *BBA - Bioenergetics* **1992**, *1101* (2), 168-170. doi:10.1016/0005-2728(92)90204-F
- 181 Luo, J.; Reddy, K. B.; Salameh, A. S.; Wishart, J. F.; Isied, S. S., Ruthenium Bisbipyridine Complexes of Horse Heart Cytochrome *c*: Characterization and Comparative Intramolecular Electron-Transfer Rates Determined by Pulse Radiolysis and Flash Photolysis. *Inorg. Chem.* **2000**, *39* (11), 2321-2329. doi:10.1021/ic9913381

- 182 Casimiro, D. R.; Richards, J. H.; Winkler, J. R.; Gray, H. B., Electron-Transfer in Ruthenium-Modified Cytochromes *c*. σ -Tunneling Pathways through Aromatic Residues. *J. Phys. Chem.* **1993**, *97* (50), 13073-13077. doi:10.1021/j100152a007
- 183 Karpishin, T. B.; Grinstaff, M. W.; Komarpanicucci, S.; Mclendon, G.; Gray, H. B., Electron transfer in cytochrome *c* depends upon the structure of the intervening medium. *Structure* **1994**, *2* (5), 415-422. doi:10.1016/S0969-2126(00)00043-5
- 184 Crane, B. R.; Di Bilio, A. J.; Winkler, J. R.; Gray, H. B., Electron Tunneling in Single Crystals of *Pseudomonas aeruginosa* Azurins. *J. Am. Chem. Soc.* **2001**, *123* (47), 11623-11631. doi:10.1021/ja0115870
- 185 Sigfridsson, K.; Sundahl, M.; Bjerrum, M. J.; Hansson, Ö., Intraprotein electron transfer in a ruthenium-modified Tyr83-His plastocyanin mutant: evidence for strong electronic coupling. *J. Biol. Inorg. Chem.* **1996**, *1* (5), 405-414. doi:10.1007/s007750050072
- 186 Eiben, S.; Bartelmäs, H.; Urlacher, V. B., Construction of a thermostable cytochrome P450 chimera derived from self-sufficient mesophilic parents. *Appl. Microbiol. Biotechnol.* **2007**, *75* (5), 1055-1061. doi:10.1007/s00253-007-0922-z
- 187 Bradford, M. M., A rapid and sensitive method for the quantitation of microgram quantities of protein using the principles of protein-dye binding. *Anal. Biochem.* **1976**, *72* (1-2), 248-254. doi:10.1016/0003-2697(76)90527
- 188 Blackburn, N. J.; Ralle, M.; Hassett, R.; Kosman, D. J., Spectroscopic Analysis of the Trinuclear Cluster in the Fet3 Protein from Yeast, a Multinuclear Copper Oxidase. *Biochemistry* **2000**, *39* (9), 2316-2324. doi:10.1021/bi992334a
- 189 Faham, S.; Day, M. W.; Connick, W. B.; Crane, B. R.; Di Bilio, A. J.; Schaefer, W. P.; Rees, D. C.; Gray, H. B., Structures of ruthenium-modified *Pseudomonas aeruginosa* azurin and [Ru(2,2'-bipyridine)₂(imidazole)₂]SO₄·10H₂O. *Acta Crystallogr. D* **1999**, *55* (2), 379-385. doi:10.1107/s0907444998010464
- 190 Durham, B.; Pan, L. P.; Hahn, S.; Long, J.; Millett, F., Electron-Transfer Kinetics of Singly Labeled Ruthenium(II) Polypyridine Cytochrome *c* Derivatives. In *Electron Transfer in Biology and the Solid State*, American Chemical Society: 1989; Vol. 226, pp 181-193.
- 191 Reddy, K. B.; Cho, M.-o. P.; Wishart, J. F.; Emge, T. J.; Isied, S. S., *cis*-Bis(bipyridine)ruthenium Imidazole Derivatives: A Spectroscopic, Kinetic, and Structural Study. *Inorg. Chem.* **1996**, *35* (25), 7241-7245. doi:10.1021/ic951434b
- 192 Luo, J.; Wishart, J. F.; Isied, S. S., Site-dependent Stereoselective Binding of Ruthenium Aquobipyridine Complexes to Histidine Side Chains in Horse Heart Cytochrome *c*. *J. Am. Chem. Soc.* **1998**, *120* (49), 12970-12971. doi:10.1021/ja9829261
- 193 Simaan, A. J.; Mekmouche, Y.; Herrero, C.; Moreno, P.; Aukauloo, A.; Delaire, J. A.; Réglie, M.; Tron, T., Photoinduced Multielectron Transfer to a Multicopper Oxidase Resulting in Dioxygen Reduction into Water. *Chem. Eur. J.* **2011**, *17* (42), 11743-11746. doi:10.1002/chem.201101282

11 Appendix

Spectrophotometric redox titrations

Ssl1 H85Q/H132Q/ Δ C

Table S1: Fit parameters for spectrophotometric redox titration of Ssl1 H85Q/H132Q/ Δ C.

Model	Boltzmann		
Equation	$y = A2 + (A1-A2)/(1 + \exp((x-x0)/dx))$		
Plot	1 (black)	2 (blue)	3 (cyan)
A1	0.04856 ± 0.00266	0.03516 ± 0.00454	0.03232 ± 0.00449
A2	0.14456 ± 0.00336	0.15112 ± 0.00472	0.14589 ± 0.00444
x0	0.433 ± 0.00413	0.43347 ± 0.0053	0.43067 ± 0.00524
dx	0.02526 ± 0	0.02526 ± 0	0.02526 ± 0
Reduced Chi-Sqr	1.9457E-5	5.00825E-5	4.72013E-5
R-Square (COD)	0.98723	0.97834	0.97879
Adj. R-Square	0.98439	0.97353	0.97408

Ssl1 without a His₆-tag

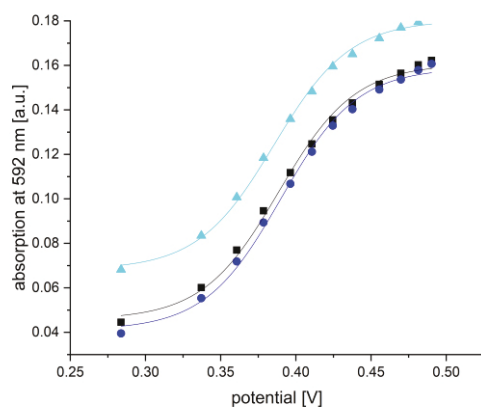


Figure S1: Spectrophotometric titration curves of Ssl1 without a His₆-tag. The T1 Cu reduction potential was determined to be 388 ± 2 mV.

Table S2: Fit parameters for spectrophotometric redox titration of Ssl1 without a His₆-tag. $E^\circ = 388 \pm 2$ mV.

Model	Boltzmann		
Equation	$y = A2 + (A1-A2)/(1 + \exp((x-x0)/dx))$		
Plot	1 (black)	2 (blue)	3 (cyan)
A1	0.04578 ± 0.00228	0.04101 ± 0.00221	0.0682 ± 0.00178
A2	0.16061 ± 0.00148	0.15886 ± 0.00147	0.18031 ± 0.00109
x0	0.38864 ± 0.00215	0.38995 ± 0.00205	0.38546 ± 0.00168
dx	0.02526 ± 0	0.02526 ± 0	0.02526 ± 0
Reduced Chi-Sqr	7.56142E-6	7.27134E-6	4.33225E-6
R-Square (COD)	0.99629	0.99663	0.99773
Adj. R-Square	0.99546	0.99588	0.99722

Determination of catalytic constants for syringaldazine conversion

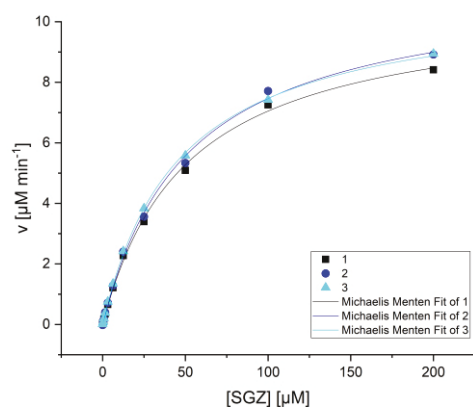


Figure S2: Syringaldazine oxidation by Ssl1 Ssl1 H85Q/H132Q/ΔC. Data points were fitted to the Michaelis-Menten-Equation in Origin.

Table S3: Kinetic constants for syringaldazine conversion by Ssl1 H85Q/H132Q/ΔC obtained from the fitting data points to the Michaelis-Menten-Equation in Origin.

Model	MichaelisMenten		
Equation	$y = Vmax * x / (Km + x)$		
Plot	1 (black)	2 (blue)	3 (cyan)
Vmax	10.61874 ± 0.22286	11.31494 ± 0.27529	10.91985 ± 0.10345
Km	50.64365 ± 2.72757	51.62105 ± 3.20464	46.16796 ± 1.15349
Reduced Chi-Sqr	0.01444	0.0214	0.00356
R-Square (COD)	0.99859	0.99814	0.99969
Adj. R-Square	0.99843	0.99793	0.99965

Fluorescence lifetimes of ruthenated Ssl1 H85Q/H132Q/ Δ C samples

Fluorescence lifetimes of ruthenated Ssl1 H85Q/H132Q/ Δ C as reported by Prof. Israel Pecht (personal communication).

Table S4: Fluorescence lifetimes of ruthenated Ssl1 H85Q/H132Q/ Δ C. Excitation at 470 nm, emission at 670 nm. Coaxial delay 100 ns, Peak Preset 706 counts, repetition rate 100 kHz.

	τ_1 [ns]	τ_2 [ns]	χ^2	τ_1 [ns]	τ_2 [ns]	τ_3 [ns]	χ^2
Ssl1 before adding ascorbic acid	0.3	22.17	1.13	2.4	22.2	0.22	1.097
Ssl1 after adding ascorbic acid	0.25	10.64	1.065	4.15	25.3	0.216	1.024

12 Danksagungen

An dieser Stelle möchte ich mich bei all denjenigen bedanken, ohne deren Unterstützung diese Arbeit nicht möglich gewesen wäre.

Besonders danken möchte ich Prof. Dr. Vlada B. Urlacher für die Überlassung dieses Promotionsthemas und die Betreuung, gute Forschungsbedingungen am Institut sowie für die Übernahme des Gutachtens für diese Arbeit.

Bei Jun.-Prof. Ingrid Span möchte ich mich für die Kristallisation der Mutanten, die Hilfe bei der spektroskopischen Charakterisierung, sowie für die Übernahme des Zweitgutachtens bedanken.

Bei Steffen Mielenbrink bedanke ich mich ebenfalls für die Zusammenarbeit bei der Kristallisation und für das Messen der CD-Spektren.

Dr. George E. Cutsail III und Dr. James A. Birrell danke ich für die EPR-Messungen und deren Auswertung sowie für die Hilfe bei der Auswertung der weiteren spektroskopischen Daten.

Des Weiteren danke ich Prof. Israel Pecht und Prof. Scot Wherland für ihre Bemühungen zur Messung des intramolekularen Elektronentransfers.

Meinen Studenten Manuel Anlauf, Jan N. Schild und Vivian P. Willers danke ich für ihre Unterstützung bei den experimentellen Arbeiten ebenso wie meinem Kollegen Sebastian Hölzel.

Außerdem möchte ich mich herzlich bei allen Kolleg:innen des Instituts für Biochemie für die gemeinsame Zeit im Institut und auch darüber hinaus bedanken. Danke für eure Hilfsbereitschaft und die angenehme Arbeitsatmosphäre.

Meinen Eltern danke ich für ihre Unterstützung während des kompletten Studiums, vom Bachelor bis zur Doktorarbeit.

Zuletzt möchte ich mich bei Robert, Maïke, den Reichs, der 136er WG und ganz besonders bei Arsenij für ihre Unterstützung in den letzten Jahren bedanken.